PMMA Clay Nanocomposites

ELDER, JUDITH

PMMA Clay Nanocomposites

Judith A. Elder

2009

Submitted in conformity with the requirements
for the degree of Doctor of Philosophy

Declaration

The material contained within this thesis has not previously been submitted for a degree at the University of Durham or any other university. The research reported within this thesis has been conducted by the author unless indicated otherwise.

Copyright Notice

PMMA Clay Nanocomposites
Abstract

Polymer clay nanocomposites (PCN) of poly(methyl methacrylate) (PMMA) and clay, were synthesised in-situ using a free radical suspension polymerisation technique. The weight fraction of clay in the PCN was systematically varied in order to understand the effect of clay on the physical properties of the resulting PCNs. However, unexpectedly it was found that the weight fraction of clay had a dramatic impact upon the molecular weight of the polymer matrix and a relationship between clay concentration and polymer molecular weight was established. Furthermore, it was also found that the change in molecular weight was dependent upon the clay type.

Three different clay types were investigated; an organically modified montmorillonite (Cloisite 15a), a synthetic clay (Laponite RD) and a PEO modified Laponite RD. To produce the modified Laponite RD, mono amino PEO was synthesised via anionic polymerisation using dimethyl ethanol amine as an initiator. The modification of the Laponite RD clay took place in the reaction flask prior to the suspension polymerisation of the PCN.

The PCN were characterised using size exclusion chromatography (SEC), X-ray diffraction (XRD), transmission electron microscopy (TEM) and oscillatory shear rheology. Morphological studies of the PCN showed that the extent of clay dispersion depended on the clay type. Within the PMMA/Laponite RD nanocomposites an unusual network structure was formed, which appeared to be continuous throughout the material. Thermal properties of the PCN were investigated using DSC, TGA and Microcalorimetry.

From oscillatory shear rheology, the full master curves for the PCN were obtained by applying the time-temperature superposition (TTS) principle. To quantify the effect of the clay upon the rheology, the experimental data was compared to the time dependent diffusion model of Des Cloizeaux for polydisperse polymer melts, which enables polydispersity to be incorporated through the use of the molecular weight distribution obtained via SEC.

Acknowledgements

I would like to take this opportunity to thank the many people who helped me throughout this project. It would have been difficult to complete without the advice, support and encouragement of colleagues, friends and family. First, I would like to express my gratitude to my supervisors Dr Nigel Clarke and Dr Lian Hutchings for their endless help and support throughout this project. I would also like to thank them for all the valuable discussions on the successes and failures of PMMA clay nanocomposites.

I would like to thank Lucite International for sponsoring this project. Many thanks to my industrial supervisor Dr Ian Robinson who provided advice and support throughout this project. I would also like to thank him for all his trips to Durham with supplies and for meetings. Dr Ian Fraser, Dr Neil Kirtley and Lesley Minto are much appreciated for all their help in setting up this project and for working through all the disastrous suspension polymerisations at the start of the project.

Thanks to Doug Carswell for running the TGA, Helen Riggs for her help with SEM, everyone from the NMR services at Durham and those from Intertek who provided help with micro calorimetry, TEM and the processing of the materials. Thanks to Dr Tim Gough and Dr Ben Whiteside from Bradford University for the use and help with the micro moulding of the materials, and to Tim who helped sit through the long shifts at the ESRF.

I would also like to thank everyone from the MC building, including Stephen, Richard, Sarah, Scott, Simon, Oat, Gavin, Robert, Eduardo, Mireille, Andy, Steven and Stuart, for the random jokes and valuable conversations during my project. Last but not least I would like to thank my friends and family for their valuable support and encouragement throughout this project.

Thank you!

Contents

Chapter 1 Introduction

1.1 Background

In the mid 1800's natural polymers were being modified to tailor their properties for commercial use. One of the most famous examples was the vulcanization of rubber by Charles Goodyear which entailed the crosslinking of natural rubber by sulphur and this improved the elasticity of the rubber. The first commercial synthetic polymer was discovered between 1907-1909 by Leo Bakeland. Bakeland had created a phenol formaldehyde resin which went by the trade name Bakelite[1]. Bakelite was a non-conductive and heat resistant material which had a wide range of applications including radio and telephone cases and even toys. During World War II natural materials became difficult to acquire so more synthetic materials were developed to replace them, including nylon and polyethylene.

Now we are living in a world where plastics play an important role in everyday life. Some of the more common polymers and their uses include; low density polyethylene (LDPE) used in food wrappers and shopping bags, polyethylene teraphthalate (PET) used as soft drinks bottles, Nylon 6,6 used as clothes fibres, polytetrafluroethylene (PTFE) used in non-stick coatings (Teflon) and polystyrene (PS) used for plastic cups. However polymers have their limitations and as they are being used for a wider range of roles and as technology advances, there is an increasing demand for the production of improved materials/plastics. General weaknesses include oxygen permeability (barrier properties), tensile strength and heat resistance. One way of improving the properties of a material is through the development of polymer nanocomposites.

The definition of a nanoparticle is a particle with at least one dimension smaller than 100nm. Examples of nanofillers for polymer nanocomposites include carbon nanotubes[2, 3], silica nanospheres[4] and clays[5]. Polymer clay nanocomposites (PCN) were

believed to be first studied in the Toyota research laboratories where the first commercially available PCN of nylon and montmorillonite was developed[6]. The new material showed improvements in modulus, heat distortion and tensile strength and has been used in the car industry. Since then PCN have become an area of sustained interest and there are several recent reviews on PCN to be found in the literature[7, 8]. Furthermore, it has been reported that increases in thermal stability[9-12], flame retardency[13-15], tensile strength[16-18] and glass transition temperature[19-21] have been achieved in PCN compared to that of pure polymer. One of the advantages of clay is that smaller percentages of clay (<10%), compared to conventional filler, are required to provide improved material properties. For example, Fornes et al[22] compared the Youngs modulus of glass fibre and clay nanocomposites and found that clay provided better reinforcement than the glass fibre with only 7.2 wt.-% of clay needed to double the Youngs modulus, whereas 20 wt.-% of glass fibre was required to obtain a similar effect.

1.2 Aims and Objectives

This project was sponsored by Lucite International. Lucite International produces methyl methacrylate (MMA) and poly(methyl methacrylate) (PMMA). Their materials include Perspex, Lucite and the new alpha MMA. The aim of this project is to produce a PMMA clay nanocomposite which shows an increase in both thermal and mechanical properties but still maintains the optical clarity of the PMMA.

PMMA already has a wide variety of end uses including Perspex^{TM} materials, lighting, dental work, adhesives and impact modified polymers for automotive industry. Improvements in PMMA physical properties would enhance its use in these areas and could also extend its uses further. There have already been a large number of publications on polymer clay nanocomposites and the resulting properties appear to be heavily dependent upon preparation method and the type of clay used. Therefore the underlining objective was to gain a better understanding of the nature of the clay-PMMA interaction and to understand why these interactions cause changes in thermal and mechanical properties.

The PMMA clay nanocomposites will be synthesised in-situ using a free radical suspension polymerisation technique. Both modified and unmodified clays will be used to investigate the effect of modification on the compatibility of the clay and polymer matrix. Also the amount of clay present in the PCN will be systematically varied to gain a better understanding of the effect of the clay on the properties of the polymer matrix. As well as investigating the physical properties, SEC will be used to determine any changes in molecular weight of the matrix PMMA. Through the use of x-ray diffraction and TEM it is hoped that the morphology of the PCN can be studied so that any changes in the morphology can be related back to the physical properties.

1.3 Polymer Synthesis

1.3.1 Introduction

Polymerisation reactions can be divided into two categories, chain growth and step growth. In chain growth an initiator is required to produce the initial active centre, then propagation occurs through successive addition of monomer to the reactive centre. Examples of chain growth reactions include free radical and ionic polymerisations. In step growth polymerisations no initiator is required and the chain will grow in a step-wise manner through successive reactions between two compatible functional groups. For step growth linear polymers to be formed, difunctional monomers are required, as monofunctional monomers will react leaving two unreactive ends as shown in Figure 1.1a. An example of a step growth polymerisation is the formation of polyesters where a diester and a dialcohol react to eliminate water as shown in Figure 1.1b. Monomers with functionalities greater than two can also be used and will result in highly branched or even networked polymers.

a) Monofunctional:

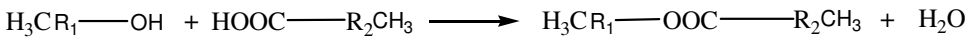

b) Difunctional:

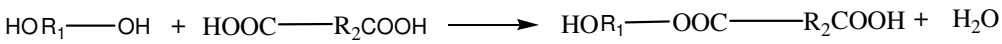

Figure 1.1: a) condensation reaction between a monofunctional alcohol and ester. b) chain growth polymerisation of polyester.

1.3.2 Free Radical Polymerisation

Free radical polymerisation[23] is a form of chain growth polymerisation. As for all chain growth mechanisms, free radical polymerisations have a three step mechanism, initiation, propagation and termination. These steps are outlined in Figure 1.2. Radicals are molecules or atoms with an unpaired electron and are very reactive unless they can be stabilized through resonance. Free radical polymerisation is used to polymerise monomers with the general formula $CH_2=CR_1R_2$, for example styrene ($CH_2=CH(C_6H_5)$), ethylene ($CH_2=CH_2$) and methyl methacrylate ($CH_2=C(CH_3)COOCH_3$).

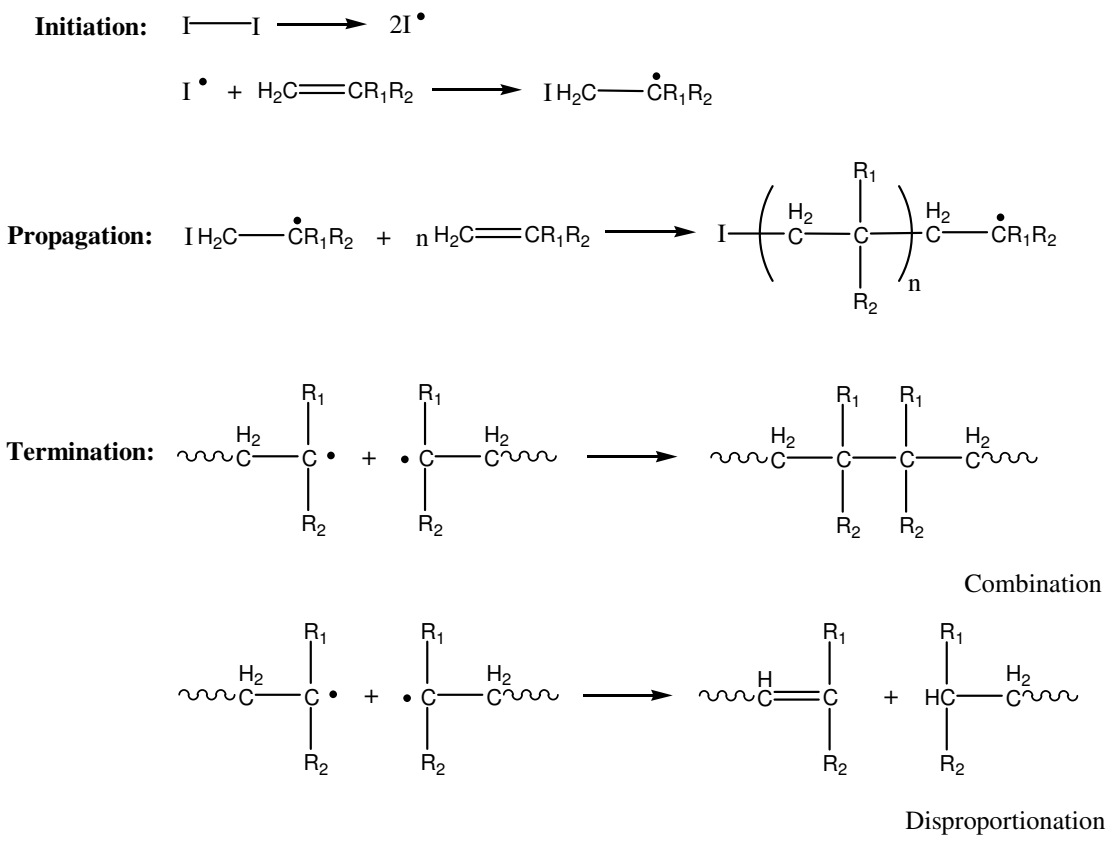

Figure 1.2: A general mechanism of a free radical polymerisation.

The first stage in the initiation process is the homolytic fission of an initiator molecule to produce a radical. Examples of free radical initiators include 2,2 azobisisobutyronitrile (AIBN) and benzoyl peroxide in which the azo (-N=N-) or the peroxide (-O-O-) bond will undergo thermal degradation when heated. The radicals will then proceed to attack the monomer initiating the polymer chain, although some of the radicals may be lost through recombination reactions with other initiating species. Once the initiated chain is formed, the chain will grow quickly through the addition of monomer and the propagation stage will commence. For a generic free radical monomer there are two possible ways in which the monomer can add to the propagating chain as shown in Figure 1.3. The most predominant route will be the one which will provide the lowest steric hindrance for the approaching molecule and will produce the most stable radical. In this case route b will dominate, due to the steric hindrance of the X groups in the head-to-head addition and the stability of the radical produced in the head-to-tail addition, although head-to-head linkages may still occur.

a) Head-to-Head:

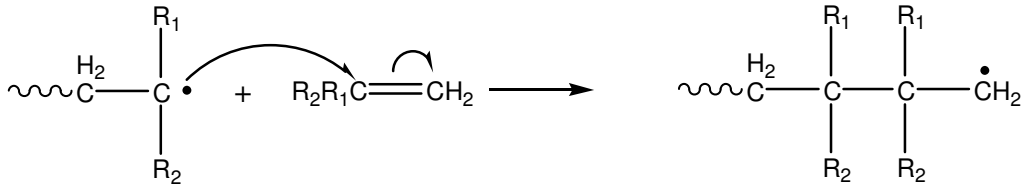

b) Head-to-Tail:

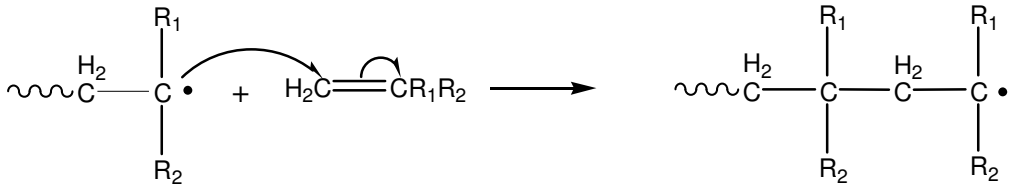

Figure 1.3: a) head-to-head, b) head-to-tail addition of monomer to a propogation free radical chain.

Termination of the propagating chain can occur via two different mechanisms. The first mechanism is the combining of two propagating chains to form a single chain- this is known as combination. The second mechanism is known as disproportionation and occurs when two propagating chains come together and one abstracts a hydrogen from the other producing two terminated polymer chains with different end groups. These two mechanisms are outlined in Figure 1.2. It has been shown that propagating chains of MMA at temperatures of 273K terminate mainly through combination, whereas at temperatures above 330K termination mainly occurs through disproportionation[24].

As the reaction proceeds, it would be expected that the rate of reaction would decrease due to the depletion of monomer and initiator species. Unexpectedly Norrish, Schulz and Trommsdroff all reported an increase in reaction rate towards the end of a free radical polymerisation reaction for undiluted free radical polymerisation[25]. This phenomenon is referred to by several names including, autoacceleration, Trommsdroff-Norrish or the gel effect.

As a free radical reaction propagates, the chain length becomes increasingly longer causing a gradual increase in viscosity. The increase in viscosity will not directly affect the initiation or propagation stages as the monomer and initiator molecules are small,

but the termination step will be greatly affected. Termination relies on diffusion to bring two chain ends together, so as the viscosity increases the rate of diffusion of the propagating chains decreases. This causes a decrease in the rate of termination. As the termination becomes hindered, the number of propagating radicals present in the reaction will increase and since the propagating step is exothermic, the amount of heat evolved will also increase. The increase in the reaction temperature will speed up the formation of radicals from initiator molecules, which will in turn cause a further increase in propagating radicals and of the heat released. As these conditions continue, autoacceleration will occur and if the build up of heat is not dispersed adequately (e.g. through dilution) then the reaction may become explosive.

There are several ways in which free radical polymerisations can be carried out: bulk, solution, suspension and emulsion. In bulk free radical reactions, the initiator is dissolved in the monomer and no dilution of the monomer is required. Although this is the simplest form of free radical polymerisation, the effect of autoacceleration can complicate this method. As with the bulk reactions, in solution polymerisations the initiator is dissolved into the monomer phase, but a solvent is used to dilute the reaction mixture. The solvent will decrease the effect of autoacceleration by reducing the viscosity of the solution and providing a more effective medium to transfer heat through convection. A problem with solution polymerisation is that the solvent must be chosen carefully so that chain termination to the solvent does not occur.

Emulsion polymerisation[26] is carried out in an aqueous medium and the monomer is held in small droplets through the use of a colloidal agent such as sodium lauryl sulphate ($CH_3(CH_2)_{11}SO_4^-Na^+$). Above the critical micelle concentration (CMC), the colloidal agent will form spherical micelles with the hydrophobic tails pointing towards the centre surrounded by the monomer and the polar head groups pointing outwards in contact with the water phase. The initiator is water soluble (usually a persulphate $S_2O_8^{2-}$) and will react with any residual monomer in the aqueous phase and eventually will diffuse into the micelles propagating the polymerisation reaction. Emulsion polymerisations are more controlled than bulk reactions, however the resulting emulsion polymer will be contaminated by the colloidal agent. Examples of emulsion polymers are emulsion paints where the polymers are used in their latex form [27].

1.3.2.1 Chain Transfer

During the free radical polymerisation, radicals can be lost or transferred to either monomer, initiator or solvent molecules. The propagating chain will be terminated but if the species to which the molecule has been transferred is reactive enough then it will initiate another polymer chain. Often the addition of a chain transfer agent is used to control the molecular weight. The most common form of chain transfer agents (CTA) are thiols as the S-H bond ($363 KJmol^{-1}$)[28] is weaker and hence more reactive than the C-H bond ($411 KJmol^{-1}$)[28]. The reaction scheme for the chain transfer process is shown in Figure 1.4. The hydrogen from the thiol will be abstracted by a propagating chain, leaving a sulphur radical which will initiate a new chain.

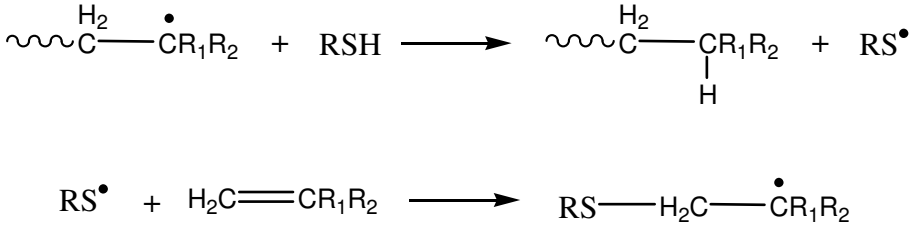

Figure 1.4: Chain transfer mechanism using a thiol CTA.

Chain transfer to the polymer backbone can also take place as the radical at the propagating chain end can abstract a hydrogen from the polymer backbone terminating the polymer chain and creating a new active centre on the polymer backbone. The new radical can then react with monomer leading to chain branching. This is often referred to as back biting and is known to take place in the polymerisation of ethylene in particular.

1.3.2.2 Suspension Polymerisation

Suspension polymerisations[29-31] are most commonly carried out in water with the monomer being insoluble in the aqueous phase. The mixture undergoes a high degree of agitation, usually through the use of a high speed overhead stirrer causing the monomer phase to be broken up into small droplets due to the shear forces induced by

the stirrer. The droplets constantly break up and then coalesce due to collisions with other droplets but eventually equilibrium is reached and an average particle size will be seen. One of the advantages of suspension polymerisation is the production of a uniform particle size typically between 10μm–5mm. The particle size produced will be affected by the degree of agitation, the reactor design and the ratio of water to monomer used[29, 32, 33].

During the polymerisation, the monomer phase will become increasingly viscous as the chain length increases making the droplets "sticky". This increases the risk of the particles aggregating together. To prevent this from occurring, a suspending agent (stabilizer) such as a polyvinyl alcohol[34] or a polyelectrolyte[35] is added, which is absorbed onto the droplet surface and forms a protective barrier preventing the coalescence of the droplets.

The reaction occurs via a free radical polymerisation and it has been found that the kinetic mechanism in a droplet is the same as that of a bulk polymerisation[36]. Initiation and propagation occur in the monomer phase so the initiator therefore needs to be soluble in the monomer phase, so within each monomer droplet a mini bulk polymerisation is occurring. One of the common initiators used in suspension polymerisation is 2,2 azobisisobutyronitrile (AIBN). As the AIBN is heated it will decompose generating two 2-cyanopropyl radicals which are then able to attack the monomer and produce the initiating species. The addition of monomer to the initiating species will occur and the propagation stage will commence.

Autoacceleration can occur during the propagation stages in free radical polymerisation. Unlike bulk reactions, where the increased heat energy cannot be easily dissipated, in suspension polymerisation the water can dissipate some of the heat released, reducing the effects of autoacceleration. If the droplets coagulate together through poor dispersion, then one large bulk reaction will be formed and auto acceleration will occur. The reaction will become uncontrollable and potentially explosive.

The advantages of suspension polymerisation include the production of uniform particles and the diminished effect of autoacceleration. However, there are also several

disadvantages of suspension polymerisation including impurities in the polymer from the suspending agent and the problem caused by the aggregation of the droplets.

1.3.3 Ionic Polymerisation

Ionic polymerisation is another example of chain growth polymerisation but unlike conventional free radical processes, ionic polymerisation techniques can lead to well defined polymers with a low polydispersity. Ionic polymerisations are more experimentally challenging and are extremely sensitive to trace amounts of impurities[37]. There are two types of ionic polymerisation, cationic and anionic. The choice between the two techniques depends on the electrochemistry of the monomer. Monomers with electron donating groups which can stabilize a positive charge are polymerised using cationic polymerisation, whereas electron withdrawing groups on the monomer would lead to stabilization of a negative charge and therefore anionic polymerisation is used.

1.3.3.1 Anionic

Anionic polymerisation[38] can be used to synthesise polystyrene, polybutadiene and can also be used to ring open ethylene oxide to produce poly(ethylene oxide). The initiation of anionic polymerisation commences via the addition of an anion to the monomer which usually contains strong electro negative groups. Some of the more common initiators include sodium naphthalene and butyl lithium ($CH_3(CH_2)_3Li$). Once the active chain carrier is produced then propagation of the chain occurs by the attack of the carbanion on the monomer. Anionic polymerisations have been shown to be a form of living polymerisation[39, 40]. Living polymerisations have no termination step, so the reaction will continue until all the monomer has been consumed. When all the monomer has been consumed and a fresh supply is added then the reaction will continue. This process has lead to the production of well-defined block copolymers[40]. To terminate the reaction, the addition of an acid or a proton donor is required to bind to the propagating chain.

When the solvation effect of the ions are negligible, the strength of the counter ion interaction with the propagating chain will decrease as the alkali metal group is

descended, for example $K^+ > Na^+ > Li^+$. This is due to the increase in the size of the atom and the distance of the electrons from the nucleus which increases the shielding of the outer electrons. However Szwarc[39] studied the effect of the counter ion in the presence of a polar solvent and found that the opposite was true ($Li^+ > Na^+ > K^+$). This is due to a solubility effect; smaller ions can be solvated easier than larger ions such as cesium (Cs^+). The various states of solvation are shown in Figure 1.5. The further to the right of the diagram the ion pair lies, the faster the rate of reaction will be.

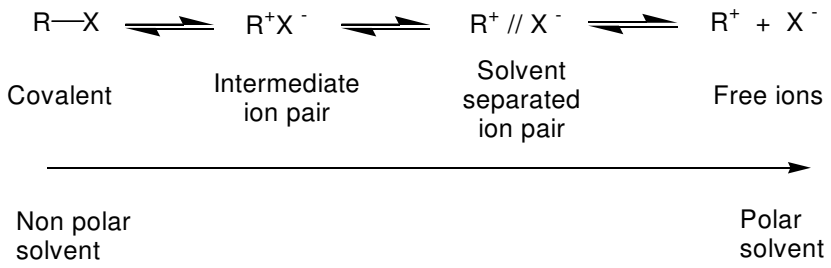

Figure 1.5: an illustration of the effect of polarity on the separation of ions.

As the reaction is living, impurities such as water will terminate the propagating chains causing an increase in the polydispersity or even "killing" the reaction completely. This makes the reaction more experimentally challenging as high purity reactants and solvents are required both of which need to be rigorously dried. The reaction also needs to takes place under vacuum or in an inert atmosphere (e.g. N_2 or Ar) to exclude the moisture from the air.

1.4 Polymer Dynamics

Dynamics concerns the motion of objects. For example, small particles in a liquid will move around in a random fashion due to collisions between other particles. This random motion has become known as Brownian motion. Einstein showed that the diffusion (D) of the particles is inversely proportional to the friction coefficient (ζ) between the particle and the medium as shown in equation(1.1) where k is the Boltzmann constant and T is the temperature.

$$D = \frac{kT}{\zeta} \qquad (1.1)$$

The friction coefficient of a particle will depend on both the size (radius of the particle R) and the viscosity η of the medium it is moving through. Stoke found that the friction coefficient is proportional to ηR. This relationship is known as Stoke's law (equation(1.2)),

$$\zeta = 6\pi\eta R \tag{1.2}$$

Stoke's law and the Einstein equation can be combined to give the Stokes-Einstien relation which enables the diffusion coefficient of a particle of radius R through a medium of viscosity η to be calculated (equation(1.3)).

$$D = \frac{kT}{6\pi\eta R} \tag{1.3}$$

1.4.1 Unentangled Polymers

The Rouse model proposed by P.E. Rouse[41] in 1953 can be used to predict relaxation spectra of unentangled viscoelastic polymer chains. A polymer chain can be divided into N beads each containing n monomers. These N beads are then connected by springs as show in Figure 1.6.

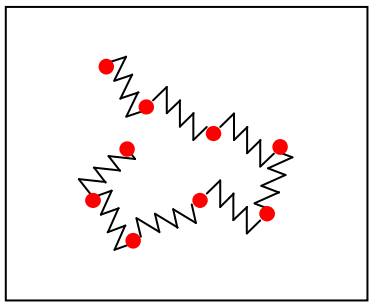

Figure 1.6: A polymer chain represented in the form of the spring bead model.

A single relaxed polymer chain will adopt the most stable conformation: the conformation with the lowest energy. By applying an external force, the polymer chains can be forced to adopt an unfavourable conformation. The polymer chain will then relax via a range of relaxation modes back to its most stable conformation lowering the energy of the system. As polymers possess a self-similar quality the relaxation of one monomer will be the same as the relaxation of N beads but with a different time scale. The dynamics of the unentangled chain can be described by N different relaxation modes. A pictorial representation of these modes is shown in Figure 1.7. These modes are given an index of p=1,2,3,……..,N.

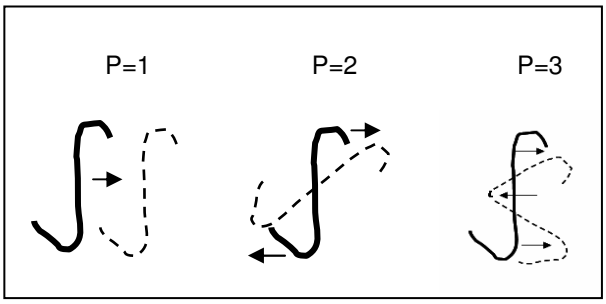

Figure 1.7: An illustration of the Rouse relaxation modes.

In relaxation mode p=1 the chain relaxes by coherent motion of all N beads. Similarly, relaxation mode p=2 involves the coherent motion of N/2 beads. In mode p=1, all N beads move coherently and therefore this mode will have the slowest relaxation time which is known as the Rouse relaxation time τ_R. The fastest relaxation time, which is equal to the relaxation time of a monomer τ_0, corresponds to the relaxation time of mode p=N.

To calculate the diffusion coefficient of a Rouse chain (D_R) with the relaxation mode p=1 the Einstein equation (equation(1.1)) relating diffusion to the monomer friction coefficient ζ can be used. Since there are N segments, the friction coefficient of the whole chain is $N\zeta$ and D_R can be calculated (equation(1.4)),

$$D_R = \frac{kT}{N\zeta} \tag{1.4}$$

The Rouse relaxation (τ_R) requires the diffusion (movement) of the whole chain by a mean squared distance equal to that of the square of its radius of gyration R. Using D_R and the radius of the chain, the relaxation time is given by,

$$\tau_R \approx \frac{R^2}{D_R} = \frac{\zeta N}{kT} R^2 \tag{1.5}$$

The radius of gyration R of an ideal linear chain can be related to the number of monomers, N, of length b in the chain.

$$R = b\sqrt{N} \tag{1.6}$$

Substituting equation(1.6) into equation(1.5) τ_R becomes,

$$\tau_R = \frac{\zeta b^2}{6\pi^2 kT} N^2 \tag{1.7}$$

where the factor $1/(6\pi^2)$ arises from the exact solution of the Rouse dynamics.

1.4.2 Entangled Polymers

In an entangled polymer any individual chain will be surrounded by a network of interconnecting polymer chains, as illustrated in Figure 1.8a. These entanglements around the chain will form constraints which restrict the motion of the chain. P.G. de Gennes[42] proposed that the constraints placed along the length of the polymer chain gives the illusion of the chain being inside a tube. In the tube, the polymer motion is not influenced by any interactions from surrounding chains, but the path is restricted by the tube diameter a. The tube diameter can be calculated from equation(1.8),

$$a \approx b\sqrt{N_e} \tag{1.8}$$

where N_e is the number of monomers (of length b) in an entangled chain segment. The average contour length of the tube $< L >$ is given by equation(1.9), where N/N_e represents the number of sections of size a.

$$\langle L \rangle \approx a\frac{N}{N_e} \approx \frac{b^2 N}{a} \approx \frac{bN}{\sqrt{N_e}} \tag{1.9}$$

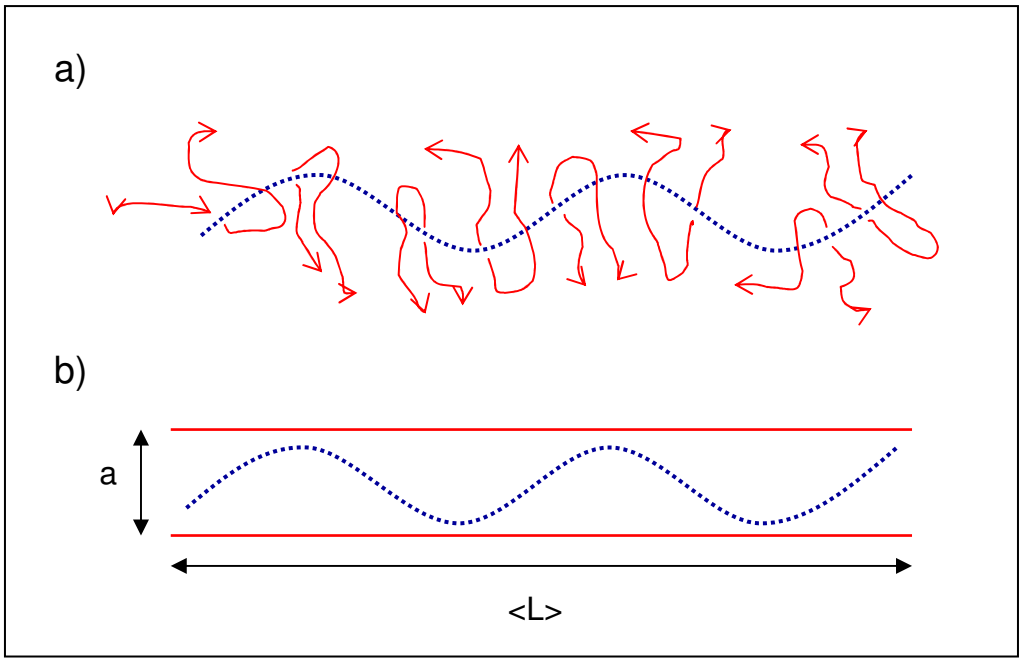

Figure 1.8: a) An entangled polymer chain b) An illustration of a chain within a theoretical tube.

P.G. de Gennes[42] used the tube model to help describe the diffusion of an entangled polymer chain and developed the reptation theory which was later developed by Doi and Edwards[43]. A polymer chain inside a tube is unable to move through the tube walls, but is able to move within the boundary of the tube. The motion of the chain inside the tube is described as being snake like, hence the name of the model, reptation. This movement allows the chain to translate along the tube until it escapes at the tube end. The time required for the chain to diffuse out of a tube of length <L> can be calculated using the Rouse diffusion coefficient D_R, (equation(1.4)). D_R can be used as the entangled chain motion along the tube as the motion is not affected by the surrounding chains, hence the chain behaves as an unentangled chain in its motion along the tube. The reptation time τ_{rep} is given by equation(1.10),

$$\tau_{rep} \approx \frac{\langle L \rangle^2}{D_R} \qquad (1.10)$$

Substituting in values of < L > and D_R from equation(1.9) and equation(1.4) respectively gives,

$$\tau_{rep} \approx \frac{\zeta b^2}{kT} \frac{N^3}{N_e} \approx \frac{\zeta b^2}{kT} N_e^{\,2} \left(\frac{N}{N_e} \right)^3 \qquad (1.11)$$

This gives the principle result of the reptation model, which is that the relaxation time is proportional to the molar mass (M) cubed since $M=NM_{mon}$. However experimental values show the power to be 3.4,

$$\tau_{rep} \approx M^{3.4} \qquad (1.12)$$

The discrepancies in the power have been considered in the literature[43]. The difference between theory and experimental data can be attributed to different modes of relaxation which are not included in the reptation model. These additional relaxation processes include constraint release and contour length fluctuations. In the reptation model the constraint of the tube is defined as being fixed. However, realistically the polymer chains which make up the constraints of the tube are also undergoing relaxation. This means that a chain which makes up part of the reptation tube is free to relax away from the tube. The constraint imposed by that chain will now be lost, allowing the reptating chain inside the tube an extra degree of freedom which it was previously denied. This is known as constraint release and is illustrated in Figure 1.9.

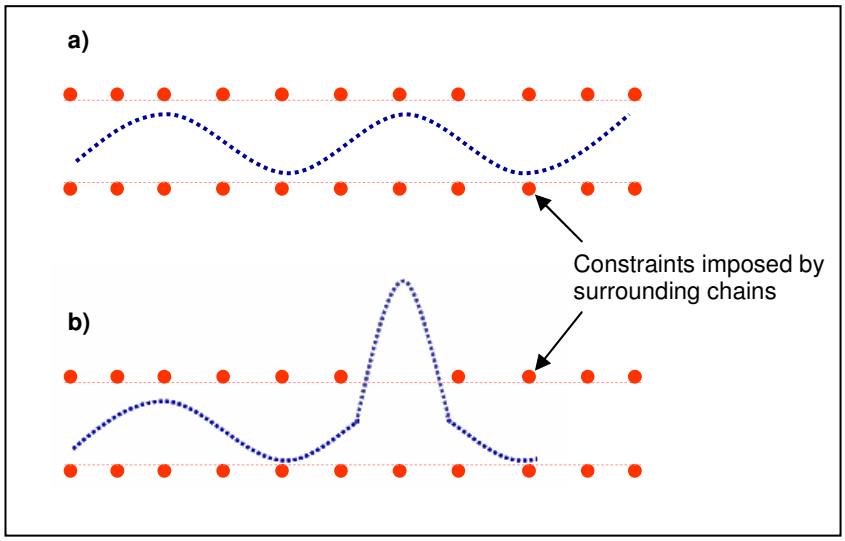

Figure 1.9: Schematic diagram of the constraint release process. Figure a) shows the chain within its theoretical tube and figure b) shows the extra degree of freedom allowed when a constraint is released.

Another additional relaxation process is contour length fluctuations which are caused by fluctuations of the tube length. The tube model assumes that all chains are of the same length, which is the average end-to-end distance of a chain. However the true end-to-end distance of a chain is continually fluctuating about the root mean squared distance. If a chain fluctuates to a smaller distance, the size of the tube will decrease as shown in Figure 1.10b. As the chain fluctuates back to the root mean square distance, the chain ends can relax the stress outside of the tube (Figure 1.10c).

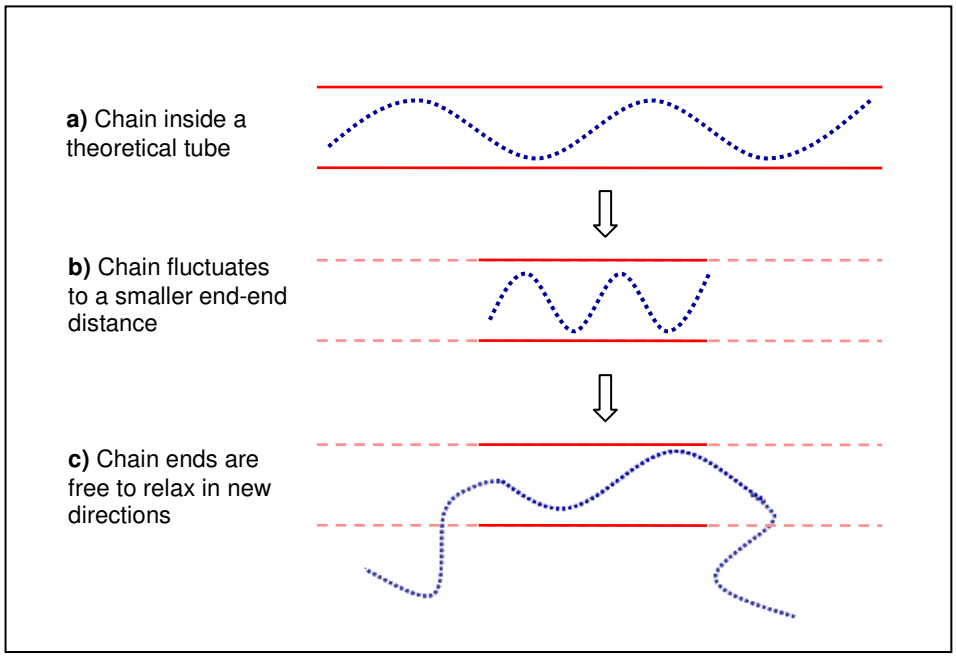

Figure 1.10: Schematic diagram of the contour length fluctuation process.

A.E. Likhtman and T.C.B.McLeish[44] have modified the reptation model to include the effects of contour length fluctuations and constraint release providing a more accurate prediction of the relaxation of entangled polymer chains in the melt.

1.5 Introduction to Clays

1.5.1 Structure

A glossary of clay terms can be found in Appendix D. The majority of naturally occurring clays consist of platelet shaped crystals usually containing oxygen, silica, aluminium and magnesium. The platelets are approximately 1nm in thickness and can be anything up to 2000nm in diameter. This gives a large surface area producing a large clay to polymer interface. Clay platelets are found to stack together face to face producing aggregates. These platelets are held together by electrostatic forces which are generally weak forces, making it theoretically possible to split the clays up into individual platelets leaving nanometer size particles. The most common dimensions used when discussing clays are its d001 spacing and its gallery (or interlayer) spacing. The gallery spacing is the gap between two parallel clay platelets within a clay aggregate, and the d001 spacing is the distance from the top of one clay platelet to another. These dimensions are demonstrated in Figure 1.11.

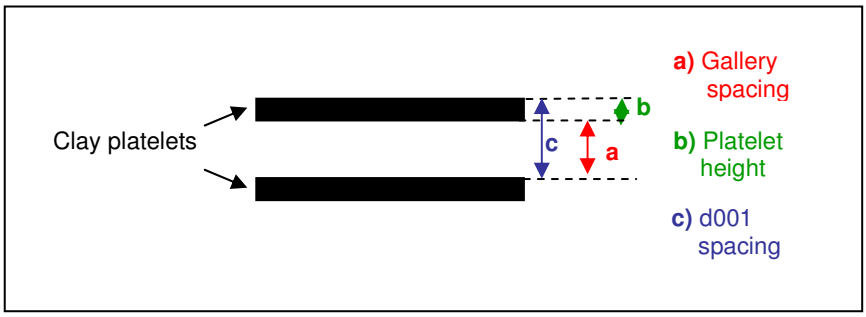

Figure 1.11: Illustration of the d001 and gallery spacing's

Clays are inorganic compounds composed of a combination of tetrahedral and octahedral crystal structures. The tetrahedral layer is illustrated in Figure 1.12 and is composed of SiO_4. The SiO_4 tetrahedral are arranged to form a continuous hexagonal

network through the sharing of an oxygen atom with a neighbouring Si [45]. The shared oxygens form a plane of atoms along the base of the tetrahedral structure and are referred to as the basal oxygens, and form the surface of the clay platelet. The apical oxygens lie at the other end of the clay and they are used to bind to other octahedral or tetrahedral layers.

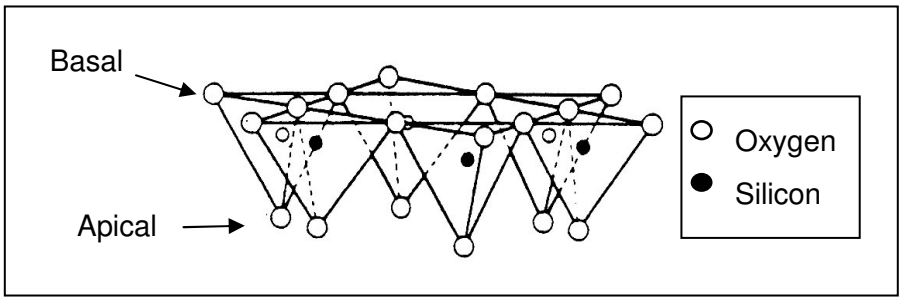

Figure 1.12: Structure of the tetrahedral clay layers.

The octahedral layers are composed of cations such as Mg^{2+} or Al^{3+} which are coordinated to six oxygens or hydroxyl units as shown in Figure 1.13. The octahedral structures are also linked together through the sharing of oxygen atoms to form a layered structure[45]. The clay platelets are made up from different arrangements of the tetrahedral (T) and octahedral (O) structures. Most common clays have either a tetrahedral-octahedral-tetrahedral (TOT) arrangement or a Tetrahedral-octahedral (TO) arrangement. Clays are classified according to the type of layered structure and also by the type of cation present. Table 1.1 shows some common clay types.

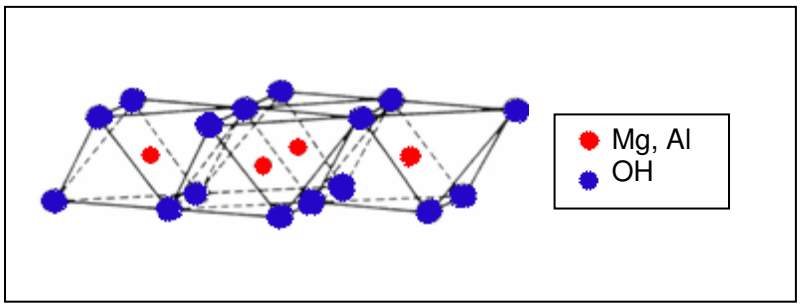

Figure 1.13: Structure of the octahedral clay layers.

Table 1.1: Summary of the structure of some typical clays. (T=tetrahedral, O=octahedral and CEC= cation exchange capacity)

	Kaolinite	**Illites**	**Smectites**	**Vermiculites**
Layer Structure	T O	T O T	T O T	T O T
Natural gallery cations	none	K	Ca, Na	Mg
CEC (meq/g)	0.02	0.2-0.3	0.8-1.2	-
Gallery spacing (nm)	0.71	1.0	~1.5	~1.44

Clays formed by nature contain impurities in their crystal structure which will cause a charge imbalance. The main impurities occur due to the substitution of the Al^{3+} ions in the octahedral layer by a divalent ions such as Fe^{2+} or Mg^{2+} or alternatively from the substation of Mg^{2+} by a monovalent ion. This leaves an excess negative charge in the clay platelets which is neutralised by Na^{+}, K^{+}, Ca^{2+} and other naturally occurring cations which sit at the surface of the clay platelets. The number of ions present on a clay surface can be given by the cation exchange capacity (CEC). The CEC measures the quantity of ions present by the charge (in milliequivalents) which is found to be attached to 100g of dried clay. The degree of impurity present in each platelet will differ from one platelet to another as the clays are formed naturally and there is no control over the extent of impurities present. Synthetic clays such as Laponite contain a known quantity of dopant, therefore a more even charge distribution is expected.

The clays to be used in this project are montmorillonite (MMT) which is a natural smectic clay and Laponite which is a synthetic clay. The reason smectite clays are used is because of their large basal spacing (approximately 1.5nm) which is important in helping to promote exfoliation (the separation of clay platelets) and also the large CEC which allows polymer clays to be easily modified. The basal spacing is important as it needs to be large enough to allow the chains to enter so that the platelets can be successfully exfoliated. The smectite clays such as MMT, bentonite and hectorite have a TOT structure as shown in Figure 1.14. Laponite has the same TOT structure. However because it is a synthetic clay the type and quantity of dopent can be controlled. This leads to a more defined structure which has a whiter appearance making the resulting PCN more appealing to industry as it can be used for a wider range of applications.

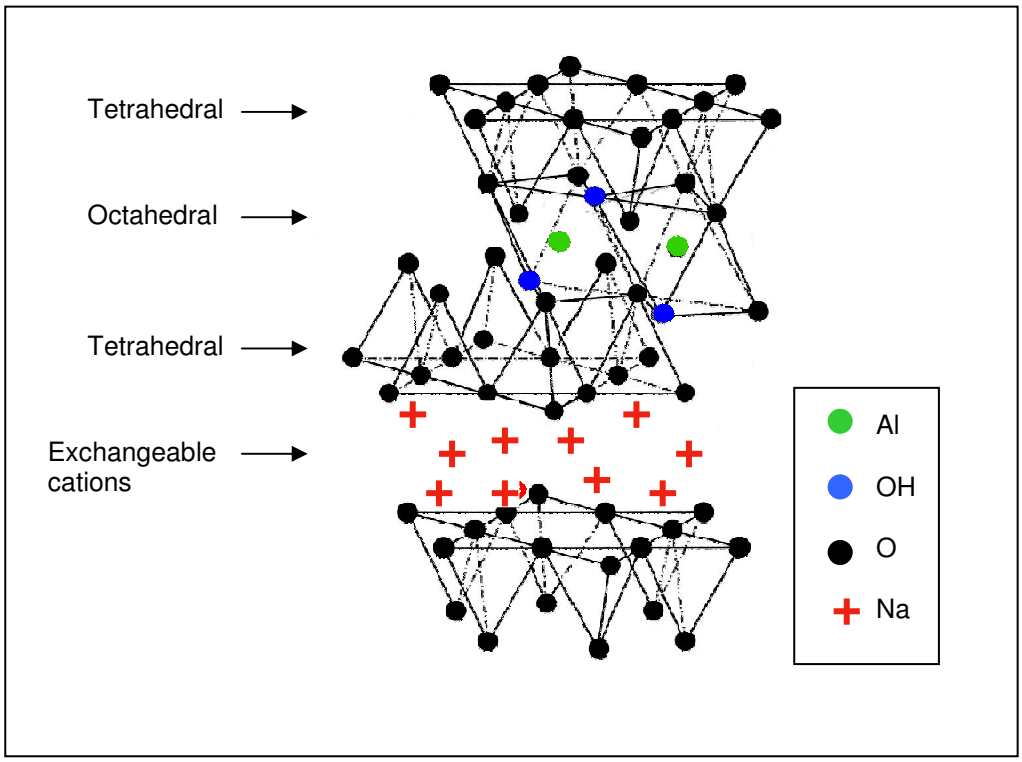

Figure 1.14: Illustration of the TOT structure.

1.5.2 Reactivity of Clays

The chemistry of the clay platelets can sometimes be overlooked. MMT contains three different active sites yielding the potential for both reduction and oxidation of appropriate organic molecules. The first active site can be found on the surface of the MMT and is of an acidic nature. The acidic sites are caused by impurities in the crystal structure producing an overall negative charge, as explained earlier. These active sites are usually charge balanced by the addition of a cation for example H_3O^+, Na^+. When the negative charge is neutralized by a proton (H^+) then the clay surface acts as a Brønsted acid site, since the proton is only loosely bound it can be easily donated to other molecules.

The second active site is found on the edge or rim of the clay platelet and is of a basic nature (electron pair acceptor). The positive rim charge arises from the octahedral Al^{3+} located at the rim or edge of the platelet. The reactive plate rims can be used to react

with organic molecules (anions) to make clay more organophilic, but will not result in an increase of the interlayer spacing. The third active site can be observed in the presence of water or moisture as hydroxyl groups become attached to the rim. The hydroxyl groups can also participate in hydrogen bonding.

1.5.3 Dispersion

Aggregation is the term used when two or more platelets are attracted together face to face. The dispersion of clay platelets involves the breaking up of the clay aggregates leaving individual clay platelets dispersed in the surrounding medium. The extent of exfoliation is important when carrying out cation exchange reactions or when producing PCN, as the degree of dispersion can alter the final physical properties of the PCN.

When clay particles are in solution there are two competing forces which act upon the surface cations: the first is the attraction of the cation to the negatively charged surface (electrostatic) and the second is the effect of diffusion. The result of these two forces sets up an electrical double layer where the cations are no longer tightly held on the surface of the clay but form a partially diffuse layer just above the clay surface[46]. When two platelets approach each other face to face in solution then it is their diffuse double layers which will come into contact first and they will repel each other. If an electrolyte (or salt) is added to the clay water solution then the degree of flocculation and aggregation will increase dramatically[47]. The electrolyte will increase the number of ions present in solution and hence decreases the diffusion tendencies of the cations. This means the cations will sit closer to the platelet surface allowing approaching platelets to get closer together.

Upon modification of clay with an organic cation, a larger degree of aggregation may be observed. This is due to the large organic cations which will be held close to the surface of the clay with their hydrocarbon tails pointing into the solution. This prevents the formation of the electrical double layer by shielding the approaching clay platelets from the surface charge and making it easier for flocculation/aggregation to occur. Another reason for this increase in aggregation is due to the inferior solubility of the organic cations in the polar solution causing them to preferentially aggregate together.

Clay platelets don't always approach each other face to face (FF); edge to edge (EE) and edge to face (EF) attractions can also occur. As mentioned above, FF attractions are referred to as aggregations, but EE and EF attractions are referred to as flocculation. EF attractions were first observed by Van Olphen[48] who named them "house of card" structures because of their appearance, Figure 1.15.

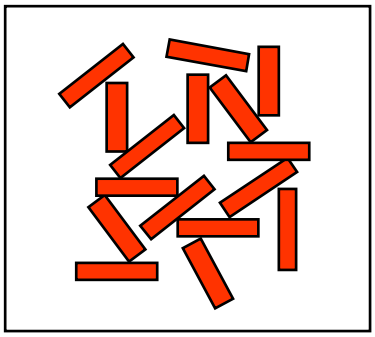

Figure 1.15: The face to edge structure of clay aggregates.

Unlike the faces of the clay platelets, the edges are found to be positively charged due to the hydroxyl groups which become dissociated in solution. Flocculation can occur between the positively charged edges and the negatively charged faces. The amount of flocculation can be reduced by neutralizing or reversing the charge of either the faces or the edge. Generally the edge charge is neutralized by increasing the pH of the solution. Tawari et al[49] studied the effect of pH and temperature on the dispersion of Laponite. It was concluded that as the pH is increased, the positive rim charge decreases, hence decreasing the rate of flocculation. The rate of aggregation was also found to increase with an increase in temperature, which was attributed to the increase in thermal energy present in the system.

1.5.4 Organically Modified Clays

Natural clays are hydrophilic which causes a problem when it comes to dispersing them into polymers since the majority of polymers are hydrophobic and generally a phase separated morphology is produced rather than the desired exfoliated state. To encourage exfoliation of the clay platelets the unfavourable interations between the polymer and the clay need to be reduced. This can be achieved by cation exchange

which substitutes the small inorganic cations with long chain organic cations. The long hydrocarbon chains will increase the hydrophobicity and make the interactions between the clay and polymer more favourable. The most widely used are the alkyl quaternary ammonium cations, such as trimethyl dodecyl ammonium chloride, as such ions are believed to have high bonding strength to the clay[50]. As well as improving the miscibility between the clay and the polymers, long chain organic cations will also increase the gallery spacing making it easier for polymer chains to enter. The main disadvantage of using alkyl quaternary ammonium cations is that they start to degrade at around 200^{o}C[21, 31] which is below the typical processing temperature of many PMMA polymers (230^{o}C).

The cation exchange process has been shown to be diffusion controlled[51]. The diffusion process is believed to start at the platelet edges and moves uniformly towards the centre, so if the platelet diameter was reduced then the exchange time will also be reduced. The diffusion time t is proportional to the square of the distance l, equation(1.13).

$$t \propto l^2 \qquad \textbf{(1.13)}$$

The chain length of the organic cations can affect the intercalation process[18, 52]. Pinnavaia et al [53] used van der Waals radii to calculate the length of the organic cations and then compared it to the basal space of the exchanged montmorillonite measured by x-ray diffraction enabling them to predict the orientation of the cation within the gallery. It was observed that CEC carried out with organo cations of lengths C_4-C_{10} initially adopt a monolayer structure, whereas C_{12}-C_{18} adopts a bilayer structure. On swelling of these structures in epoxy, the montmorillonite containing cations of C_8-C_{18} adopt a vertical orientation[53].

Clay can also be modified so as to incorporate a functional group which will react with the monomer during polymerisation and produce a polymer chain tethered onto the cation[13, 19] so that the extent of exfoliation increases.

1.6 Morphology

The morphology of PCN can be categorised into three possible phases depending on the degree of separation between the clay platelets. These are phase separated, intercalated and exfoliated morphologies, and are illustrated in Figure 1.16.

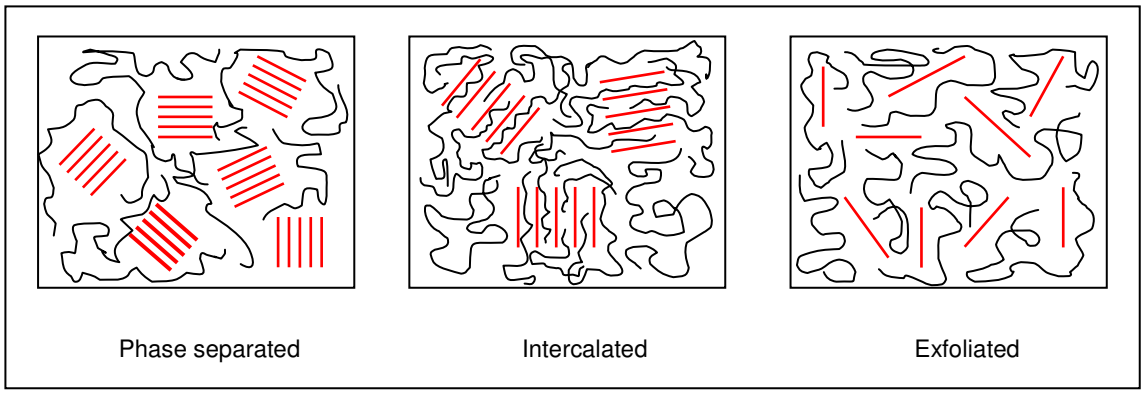

Figure 1.16: Illustration of the phase separated, intercalated and exfoliated PCN phases.

Phase separation occurs when the polymer clay interactions are unfavourable or when the clay layers are bound tightly together, resulting in large clusters of clay aggregates surrounded by a 'sea' of polymer. If the clay layers are forced further apart due to a more favourable polymer-clay interaction then it is possible for the polymer chains to enter into the gallery spacing and intercalation occurs. In an intercalated phase the clay will become 'swollen' by the polymer causing an increase in the gallery spacing although the clay will still retain the layered structure of the aggregate. If the layers are continued to be forced apart then eventually the clay will lose its layered structure and form the exfoliated phase. Here the clay platelets no longer have a d001 or gallery spacing and will take on a random orientation. Alignment of the clay platelets may be possible if a strong directional force is applied to the PCN when the polymer is above its glass transition temperature.

1.7 References

1. Crespy, D.; Bozonnet, M.; Meier, M. *Angewandte Chemie-International Edition* **2008,** 47, (18), 3322-3328.
2. Baughman, R. H.; Zakhidov, A. A.; de Heer, W. A. *Science* **2002,** 297, (5582), 787-792.
3. Hu, J. T.; Odom, T. W.; Lieber, C. M. *Accounts of Chemical Research* **1999,** 32, (5), 435-445.
4. Tallury, P.; Payton, K.; Santra, S. *Nanomedicine* **2008,** 3, (4), 579-592.

5. Chen, B.; Evans, J. R. G.; Greenwell, H. C.; Boulet, P.; Coveney, P. V.; Bowden, A. A.; Whiting, A. *Chemical Society Reviews* **2008,** 37, (3), 568-594.
6. Kawasumi, M.; Hasegawa, N.; Kato, M.; Usuki, A.; Okada, A. *Macromolecules* **1997,** 30, (20), 6333-6338.
7. Ray, S. S.; Maiti, P.; Okamoto, M.; Yamada, K.; Ueda, K. *Macromolecules* **2002,** 35, (8), 3104-3110.
8. Weimer, M. W.; Chen, H.; Giannelis, E. P.; Sogah, D. Y. *Journal of the American Chemical Society* **1999,** 121, (7), 1615-1616.
9. Essawy, H.; Badran, A.; Youssef, A.; Abd El-Hakim, A. E. *Polymer Bulletin* **2004,** 53, (1), 9-17.
10. Zanetti, M.; Camino, G.; Thomann, R.; Mullhaupt, R. *Polymer* **2001,** 42, (10), 4501-4507.
11. Noh, M. W.; Lee, D. C. *Polymer Bulletin* **1999,** 42, (5), 619-626.
12. Jang, B. N.; Wilkie, C. A. *Polymer* **2005,** 46, (9), 2933-2942.
13. Zhu, J.; Start, P.; Mauritz, K. A.; Wilkie, C. A. *Polymer Degradation and Stability* **2002,** 77, (2), 253-258.
14. Gilman, J. W. *Applied Clay Science* **1999,** 15, (1-2), 31-49.
15. Sahoo, P. K.; Samal, R. *Polymer Degradation and Stability* **2007,** 92, 1700-1707.
16. Agag, T.; Koga, T.; Takeichi, T. *Polymer* **2001,** 42, (8), 3399-3408.
17. Rao, Y. Q.; Pochan, J. M. *Macromolecules* **2007,** 40, (2), 290-296.
18. Lan, T.; Pinnavaia, T. J. *Chemistry of Materials* **1994,** 6, (12), 2216-2219.
19. Huang, X. Y.; Brittain, W. J. *Macromolecules* **2001,** 34, (10), 3255-3260.
20. Meneghetti, P.; Qutubuddin, S. *Thermochimica Acta* **2006,** 442, (1-2), 74-77.
21. Li, Y.; Zhao, B.; Xie, S. B.; Zhang, S. M. *Polymer International* **2003,** 52, (6), 892-898.
22. Potschke, P.; Fornes, T. D.; Paul, D. R. *Polymer* **2002,** 43, (11), 3247-3255.
23. Colombani, D. *Progress in Polymer Science* **1997,** 22, (8), 1649-1720.
24. Cowie, J. M. G., *Polymers : chemistry and physics of modern materials*. 2nd ed.; CRC: 1991.
25. Flory, P. J., *Principles of Polymer Chemistry*. Cornell University Press: 1953.
26. Chern, C. S. *Progress in Polymer Science* **2006,** 31, (5), 443-486.
27. Asua, J. M. *Progress in Polymer Science* **2002,** 27, (7), 1283-1346.
28. Huheey, J. E.; Keiter, E. A.; Keiter, R. L., *Inorganic Chemistry: Principles of Structures and Reactivity*. 4 ed.; HarperCollinsCollege Publishers: 1993.
29. VivaldoLima, E.; Wood, P. E.; Hamielec, A. E.; Penlidis, A. *Industrial & Engineering Chemistry Research* **1997,** 36, (4), 939-965.
30. Arshady, R. *Colloid and Polymer Science* **1992,** 270, (8), 717-732.
31. Hedley, C. B.; Yuan, G.; Theng, B. K. G. *Applied Clay Science* **2007,** 35, (3-4), 180-188.
32. Santos, A. F.; Lima, E. L.; Pinto, J. C. *Journal of Applied Polymer Science* **2000,** 77, (2), 453-462.
33. Horak, D.; Pelzbauer, Z.; Svec, F.; Kalal, J. *Journal of Applied Polymer Science* **1981,** 26, (10), 3205-3211.
34. Gupta, D. C. *Journal of Applied Polymer Science* **1985,** 30, (10), 4187-4191.
35. Georgiadou, S.; Brooks, B. W. *Chemical Engineering Science* **2005,** 60, (24), 7137-7152.
36. Kalfas, G.; Ray, W. H. *Industrial & Engineering Chemistry Research* **1993,** 32, (9), 1822-1830.
37. Hadjichristidis, N.; Iatrou, H.; Pispas, S.; Pitsikalis, M. *Journal of Polymer Science Part a-Polymer Chemistry* **2000,** 38, (18), 3211-3234.
38. Baskaran, D.; Muller, A. H. E. *Progress in Polymer Science* **2007,** 32, (2), 173-219.
39. Szwarc, M. *Journal of Polymer Science Part a-Polymer Chemistry* **1998,** 36, (1), IX-XV.
40. Hadjichristidis, N.; Iatrou, H.; Pitsikalis, M.; Mays, J. *Progress in Polymer Science* **2006,** 31, (12), 1068-1132.
41. Rouse, P. E. *Journal of Chemical Physics* **1953,** 21, (7), 1272-1280.
42. Degennes, P. G. *Journal of Chemical Physics* **1971,** 55, (2), 572-&.
43. Doi, M.; Edwards, S. F., *The Theory of Polymer Dynamics*. Clarendon: 1986.
44. Likhtman, A. E.; McLeish, T. C. B. *Macromolecules* **2002,** 35, (16), 6332-6343.
45. Yariv, S.; Cross, H., *Organo-clay complexes and interactions / edited by Shmuel Yariv, Harold Cross.* New York: 2002.
46. http://www.scprod.com/product_bulletins/PB%20Laponite%20XLS.pdf, In.
47. Mongondry, P.; Tassin, J. F.; Nicolai, T. *Journal of Colloid and Interface Science* **2005,** 283, (2), 397-405.
48. Van Olphen, H. *Discussions of the Faraday Society* **1951**, (11), 82-84.
49. Tawari, S. L.; Koch, D. L.; Cohen, C. *Journal of Colloid and Interface Science* **2001,** 240, (1), 54-66.

50. Utracki, L. A., *Clay-Containing Polymeric Nonocomposites*. RAPRA: 2004; Vol. 1.
51. Mackinto.Ee; Lewis, D. G.; Greenlan.Dj. *Clays and Clay Minerals* **1971,** 19, (4), 209-&.
52. Shi, H. Z.; Lan, T.; Pinnavaia, T. J. *Chemistry of Materials* **1996,** 8, (8), 1584.
53. Lan, T.; Kaviratna, P. D.; Pinnavaia, T. J. *Chemistry of Materials* **1995,** 7, (11), 2144-2150.

Chapter 2 Characterisation Techniques

2.1 X-ray Diffraction (XRD)

2.1.1 Experimental Technique

X-ray diffraction (XRD) is a useful technique for characterising the morphology of the PCN as it enables the average basal spacing (distance between two clay platelets) to be calculated The basal spacing is often referred to as the d001 spacing where d refers to the spacing between the planes in an atomic lattice and 001 refers to the principle reflection. An increase in the basal spacing indicates an increase in the extent of intercalation and at the point where the XRD peak can no longer be observed, the clay is thought to have become fully exfoliated within the polymer matrix. In an exfoliated PCN the clay platelets will be at larger distances from each other with random orientation. This means that there will be no average distance between the platelets and therefore no XRD peak will be observed.

XRD will only probe a small area (few mm^2) of the sample at one time, so the disappearance or a decrease in the peak intensity may not necessarily be due to exfoliation[1, 2]. The intensity of the peak will decrease in areas where less clay (or even no clay) is present. Similarly, a broadening and consequently the decrease in intensity of the XRD peak may occur due to a wide distribution of d001 spacings.

X-rays are created by firing a beam of high speed electrons at a metal target, usually copper. The produced x-rays cover a wide spectra of wavelengths consisting of a strong k_α (λ = 1.5Å) component and a weaker k_β (λ = 1.4Å) component. X-ray diffraction requires a monochromatic x-ray source which is obtained by removing the k_β component and allowing the k_α component to pass through to the sample.

When the X-rays are diffracted off an object, there are two possible outcomes - the two waves can be in phase, and hence constructive interference occurs, or the waves can be out of phase and destructive interference occurs. The detected X–ray beam consists mainly of in phase waves as the out of phase waves will cancel each other out. Constructive interference occurs when waves are scattered from atoms which are a whole number of wavelengths apart. This forms the basis of Bragg's law[3]. Figure 2.1 shows two incoming waves, 1 and 2, at an angle of θ and these waves are scattered by atoms A and B respectively. The extra distance wave 2 travels can be calculated using simple trigonometry as shown in equation(2.1). For the diffracted rays 1' and 2' to be in phase with each other, the extra distance travelled by wave 2 has to equal a whole number of wavelengths (λ) giving equation(2.2) where n is an integer.

$$xB + yB = d\sin\theta + d\sin\theta = 2d\sin\theta \qquad (2.1)$$

$$n\lambda = 2d\sin\theta \qquad (2.2)$$

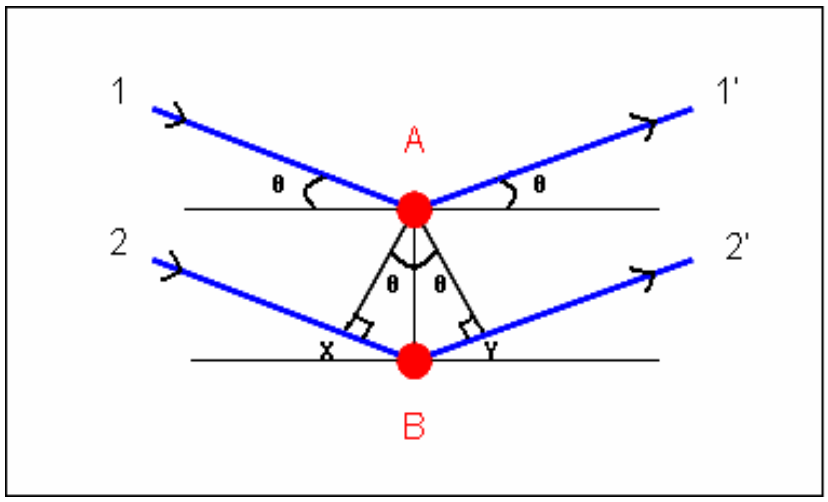

Figure 2.1: Diffraction of x-rays.

2.1.2 Method

The x-ray diffraction was carried out on a Siemens D5000 diffractometer which uses a voltage of 40 kV and a current of 40 mA. The monochromatic X-ray source has a wave length of λ=1.54 Å. X-ray diffraction was performed on the clay samples to determine the initial d001 spacing and also on the PCN to discover the extent of intercalation or exfoliation. XRD was carried out on PCN which had been heat pressed, samples were prepared by heat pressing at 200°C for 15 minutes.

2.2 Transmission Electron Microscopy (TEM)

2.2.1 Method

In TEM, an electron beam is passed through a very thin section of the sample and an image is obtained using the differences in electron density of the materials. Since there is sufficient difference in electron density between the PMMA and the clay to provide a contrast between the two materials, no staining was required. TEM was carried out at Intertek using a Philips CM12 TEM with an accelerating voltage of 120kV and images were captured using a Gatan 2500 camera. 65nm thick samples were cut at room temperature using a Reichert Ultracut-E ultra microtome and placed onto copper grids.

2.3 Differential Scanning Calorimetry (DSC)

2.3.1 Experimental Technique

Differential scanning calorimetry (DSC) can detect changes in the heat capacity caused by chemical or physical transitions. In a polymer system, transitions such as the glass transition (T_g), melting points (T_m), crystallizations (T_{crys}) and rate of cure can be seen. T_g occurs in the amorphous and semi-crystalline polymers and T_m occurs in semi-crystalline polymers. However, semi-crystalline polymers can undergo all three transitions T_g, T_{crys} and T_m. A polymer in a rubbery state has a larger amount of free volume than in its glassy state and as the rubbery material is cooled its free volume will be reduced. When the free volume becomes sufficiently low to restrict chain motion, the chains will become "frozen" and the material becomes glassy. The temperature at which this occurs is known as the T_g. The glass transition temperature will depend upon the architecture, molecular weight, chemical composition and thermal history (e.g. cooling rate) of the polymer chains. There are several equations which relate the T_g to the molecular weight of the polymer[4, 5], which will be discussed in more detail in Chapter 4.5.

DSC works by measuring the heat flow (the heat supplied per unit time) required to either heat the sample at a constant rate (non-isothermal) or to maintain a sample at a constant temperature (isothermal). A schematic diagram of the experimental set up is shown in Figure 2.2.

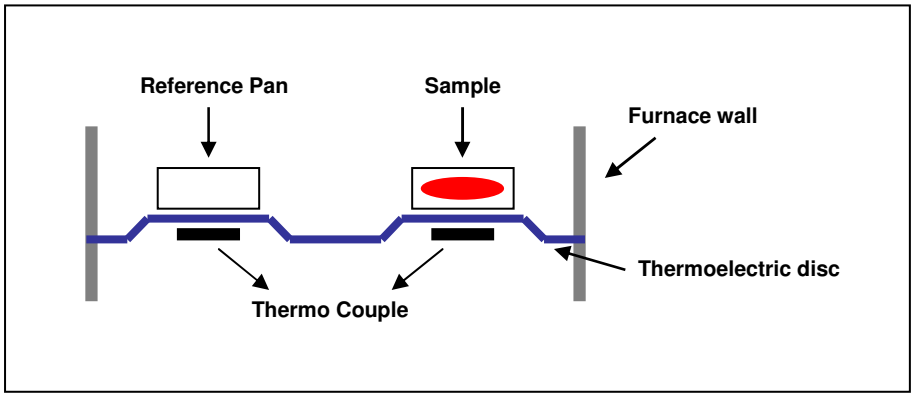

Figure 2.2: A schematic representation of the DSC set up.

In a non-isothermal run, both the sample pan and the reference pan are heated at the same rate. However the sample pan may require more (or less) heat than the reference pan to maintain the same constant heating rate due to endo/exo thermal transitions in the material. It is the difference in energy required to heat the two pans which is measured. An example of a DSC trace is given in Figure 2.3 showing T_g, T_{crys}, and T_m.

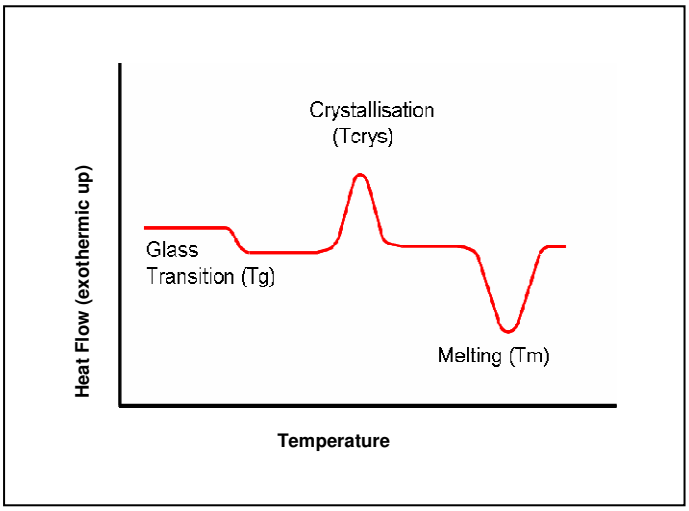

Figure 2.3: DSC trace showing various transitions found within a polymeric material.

2.3.2 Method

DSC on the PCN samples were run on the beads produced by suspension polymerization. Samples of clay and PMMA were also run for comparison. Since good contact with the DSC pan is required in order to gain an accurate T_g, the beads were annealed in the DSC pans at 200^{o}C for 30 minutes allowing them to melt into the pan. Approximately 17 mg of sample was used.

The samples were run on the Thermal Analysis (TA) Q1000 instrument with a purge gas of N_2. The samples were heated from 30^{o}C to 200^{o}C at 20^{o}C per minute and then cooled at 50^{o}C per minute to 30^{o}C. The heat cycle was repeated and the T_g was taken from the second heat cycle to ensure all samples had undergone the same thermal history. The T_g was taken to be at the half height of the step change and the onset temperature was also recorded for comparison. The temperature was calibrated using Indium.

2.4 Thermogravimetric Analysis (TGA)

2.4.1 Experimental Technique

Thermal Gravimetric analysis (TGA) is used to monitor the in-situ weight loss with respect to temperature. There are two modes in which TGA can be used, isothermal and non-isothermal. Isothermal mode involves holding a sample at a constant temperature and measuring the weight loss with time. Non-isothermal mode involves measuring the weight loss as a function of temperature. Also from the non-isothermal data the rate of weight loss with respect to temperature can be calculated and information about the degradation method of the polymer can be obtained[6, 7].

2.4.2 Method

TGA was carried out on the clay and PCN beads. PMMA traces were also recorded for comparison. The temperature corresponding to 5, 10, 30, 50 and 70% weight loss was recorded. The samples were analysed from 30^{o}C to 600^{o}C at a heating rate of 10^{o}C per

minute under nitrogen on a Pyris 1 TGA instrument. Isothermal measurements were carried out to determine the effect of degradation over a 30 minute time period. Temperatures of 100 and 230^{o}C were used.

2.5 Micro Calorimetry

2.5.1 Experimental Technique

The fire properties of a material are extremely important and any method of reducing the flammability of a material is greatly valued as it will decrease the human and financial costs that fire causes. Fire requires three components- fuel, heat and oxygen and if one of these components is missing then the fire will be extinguished. A review of fire hazards in some common polymers can be found in reference[8].

Most polymeric materials will burn but require a source of ignition to do so. Once the polymer is burning it will decompose to give a solid char and volatile gases. These volatile gases will act as a fuel to the fire, for when they are heated in the presence of oxygen they will combust and release heat. This heat will contribute towards the heating of the polymeric material.

Micro calorimetry can be used to measure the rate of heat release (HRR) and the temperature at which maximum HRR occurs for a given material. The rate of heat release is calculated from the mass loss rate of the sample during heating multiplied by the effective heat of combustion of the volatiles released as show in equation(2.3), where dm/dt is the rate of mass loss and H_c is the heat of combustion. The equation is based on the assumption that complete combustion of the volatiles takes place. The heat of combustion for PMMA has been calculated to be 24.96MJKg^{-1}, as shown in reference[9].

$$HRR = \frac{dm}{dt} H_c \qquad (2.3)$$

Micro calorimetry is carried out on a pyrolysis combustion flow calorimeter (PCFC). The sample is heated in the pyrolyser with a typical heating rate of 1^{o}C per second. As the gaseous degradation products are released, the mass loss of the sample is recorded

and the volatiles are carried towards the combustor by an inert gas such as nitrogen. The combustor is held at 900°C and before entering the chamber the volatiles are mixed with a known quantity of oxygen so that as they enter the combustor they become fully oxidised. The effect of combustion is calculated from the depletion of oxygen. A schematic diagram of the experimental setup is shown in Figure 2.4.

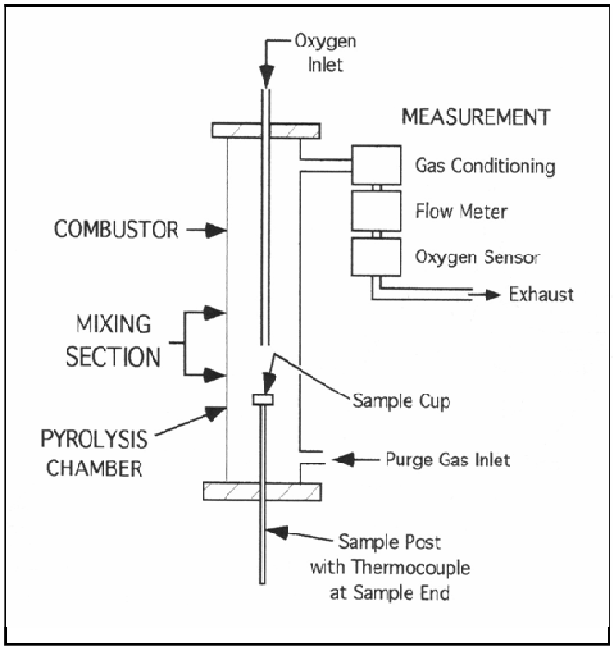

Figure 2.4: Schematic diagram of a micro calorimeter[10].

2.5.2 Method

The measurements were carried out at Intertek on a FAA Micro Calorimeter using an aluminium crucible containing approximately 2.5mg of sample. The samples were run from 75°C to 600°C at 1°C per second; the combustor was held at 900°C with an atmosphere of 80% nitrogen and 20% oxygen. Repeat measurements were taken to ensure reproducibility.

2.6 Rheology

2.6.1 Experimental Technique

2.6.1.1 Stress and Strain

Rheology is the study of deformation of matter resulting from the application of a force[11]. This deformation is generally a result of a shear force which is applied to the sample. Shear is the movement of a layer of material relative to parallel adjacent layers, as opposed to an extensional force which stretches the material without movement between the individual layers. These forces are shown schematically in Figure 2.5.

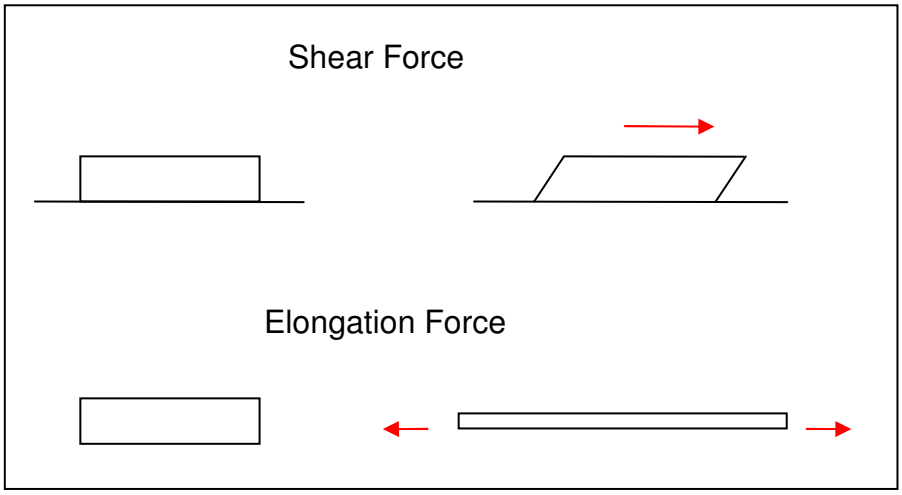

Figure 2.5: Diagram showing shear and elongation forces.

The shear deformation of a sample is shown in Figure 2.6. Shear strain is the response of the material when a shear stress is applied. The stress an object is placed under is the force applied per unit area. Hence when a shear force is applied, the result is a shear stress which is shown in equation(2.4). The strain on a sample is a measurement of deformation relative to a reference height, thus shear strain is when the deformation occurs by a shear force, shown by equation(2.5).

$$\textbf{Shear Stress } \sigma = \frac{\textbf{Shear Force}}{\textbf{Area}} = \frac{F}{A} \qquad (2.4)$$

$$\textbf{Shear Strain } \gamma \textbf{ (unitless)} = \frac{\textbf{Displacement}}{\textbf{Height}} = \frac{\Delta}{H} \qquad (2.5)$$

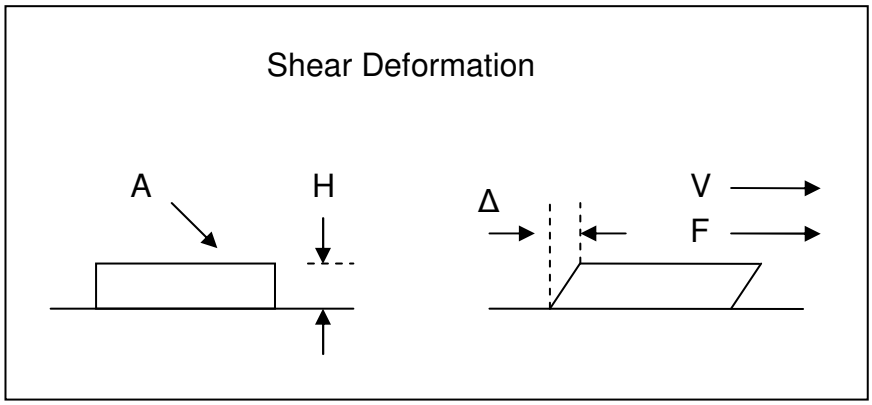

Figure 2.6: Diagram showing shear deformation.

One further variable is the shear rate which is defined as the change in shear strain per unit time and is given by:-

$$\textbf{Shear Rate } \dot{\gamma} = \frac{(\mathrm{d}\Delta/dt)}{H} \qquad (2.6)$$

2.6.1.2 Viscoelastic materials

Polymers are viscoelastic materials, as they contain both solid (elastic) and liquid (viscous) like properties. A perfectly viscous liquid is Newtonian and has no preferred shape, so when a stress is applied it will act equally in all directions, distorting the liquid. The energy used in distorting the liquid will be lost immediately as heat because the liquid has no memory of any previous orientations. The shear strain rate is proportional to the shear stress and the proportionality constant is the shear viscosity η,

$$\sigma(t)=\eta\ \gamma(\mathrm{t}) \qquad (2.7)$$

A perfectly elastic solid is called a Hookean solid and has a fixed shape, so when a stress is applied the material will deform in the direction of the applied stress. The energy produced in distorting the material is stored as elastic energy. The relative deformation or strain that is observed is recoverable on the removal of the stress. This is because unlike the Newtonian oil, elastic solids have memory. The shear strain applied to the Hookean solid is proportional to the shear stress. The proportionality constant is the shear modulus G,

$$\sigma(t)=G\gamma(t) \qquad (2.8)$$

Polymers are considered to be viscoelastic materials, which contain both elastic and viscous properties. Hence when a stress is applied, some of the applied energy will be stored while the rest will be lost. The proportion of the energy stored or lost is dependent on the material studied.

2.6.1.3 Oscillatory Stress Measurements

Using stress controlled oscillatory rheology, the proportion of the energy that is lost and stored in a viscoelastic material can be measured and it is the most commonly used experiment for determining the linear viscoelastic properties of polymer melts. During this experiment an oscillatory stress is applied to the sample and the resulting strain is measured. This resulting strain will also be oscillating as the strain is proportional to the stress, as shown in Figure 2.7. The phase difference between the stress and strain will vary with the frequency at which the stress is applied.

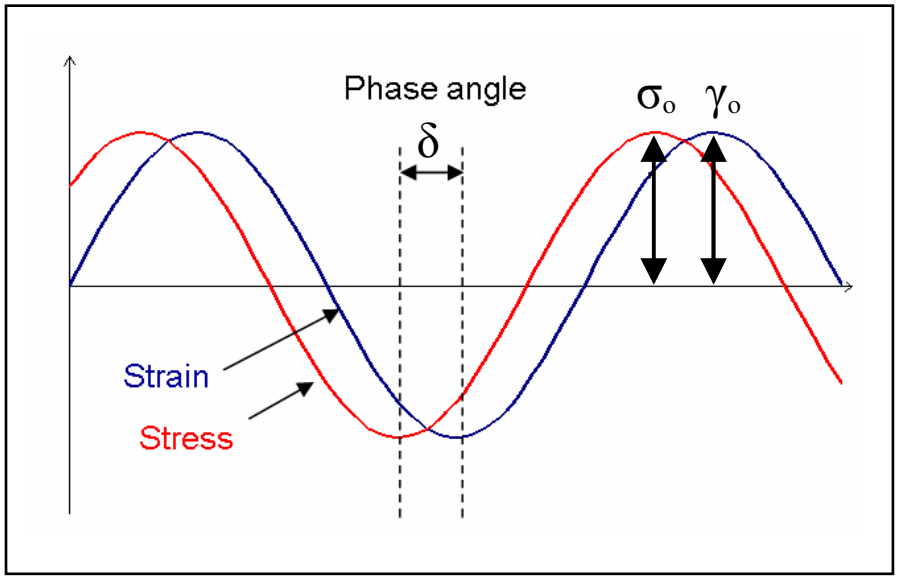

Figure 2.7: The oscillating stress strain response from a viscoelastic polymer.

If an oscillating shear stress is applied then the response is given by equation(2.9)[12]. G' is referred to as the storage modulus which gives the elastic response of the polymer, G" is referred to as the loss modulus which gives the viscous response of the polymer and γ_o represents the strain amplitude and ω represents the frequency.

$$\sigma(t)=\gamma_0\left[G'(\omega)\sin\omega t+G''(\omega)\cos\omega t\right] \qquad (2.9)$$

In a stress controlled oscillatory experiment the stress amplitude is kept constant and the frequency at which the stress is applied is varied. The typical results from a frequency sweep experiment for a high molecular weight linear viscoelastic polymer are shown in Figure 2.8 and is referred to as the master curve.

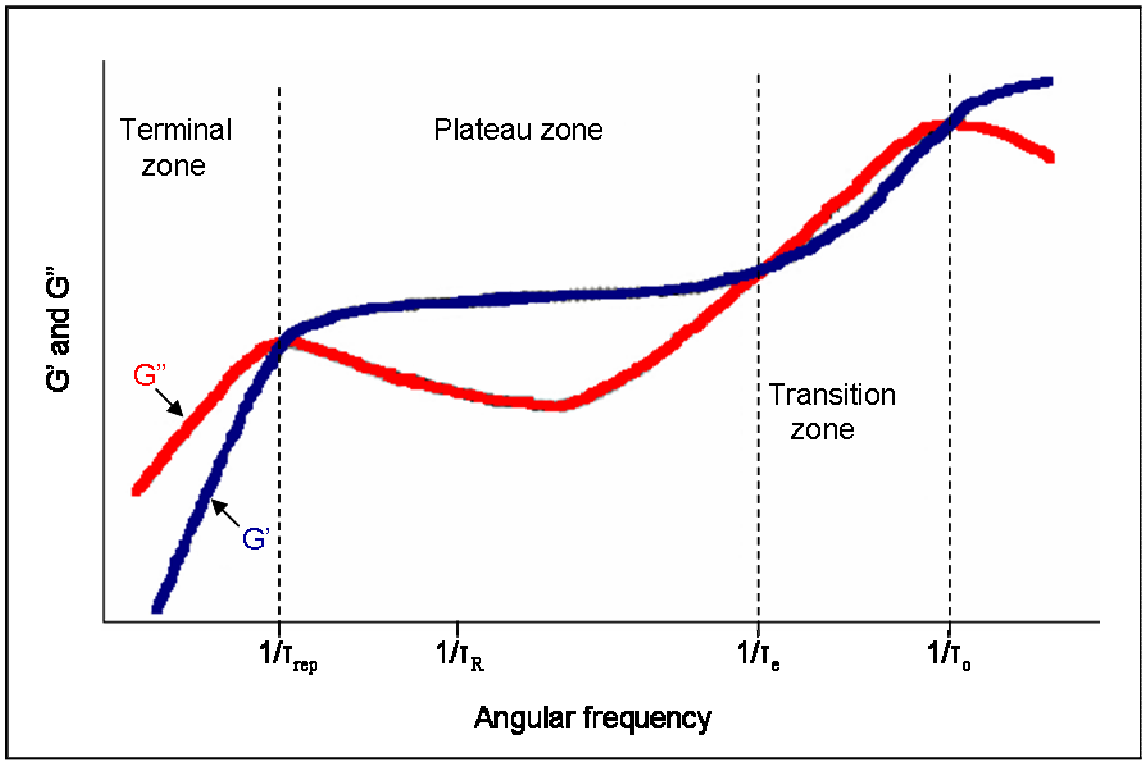

Figure 2.8: Master curve of an entangled polymer. Where τ_{rep} is the reptation relaxation time, τ_R is the Rouse relaxation time, τ_e is the entangled Rouse relaxation time and τ_o is the Kuhn monomer relaxation time.

The region between the Kuhn monomer relaxation time (τ_o) and the entangled Rouse relaxation time (τ_e) is known as the transition zone. This zone appears at a high frequency and therefore involves short relaxation times which are dominated by molecular motions that are independent of the entanglements around them. The lowest frequency region, below the Reptation relaxation time (τ_{rep}), is known as the terminal zone and shows the long relaxation response. This zone is dominated by long range motions which are restricted by the entanglements. The Reptation theory can be used to describe the region[14-16]. The central region of the master curve, between the Reptation relaxation time (τ_{rep}) and the entangled Rouse relaxation time (τ_e), is known as the plateau zone. This is a characteristic region for high molecular weight linear viscoelastic polymers where both short and long relaxation processes occur. The modulus of G' in the plateau zone can be used to calculate the entanglement molar mass M_e,

$$G_e = \frac{\rho RT}{M_e} \qquad (2.10)$$

where R is the gas constant, ρ is the density and G_e is the plateau modulus.

2.6.1.4 Time-Temperature-Superposition

The master curve shown in Figure 2.8 cannot be obtained from one single experiment due to instrumental constraints. Instead the curves are measured in sections carried out at different temperatures which can be shifted together when on a log log plot using the time-temperature-superposition (TTS) theory. This theory was adapted by Williams-Landel-Ferry[17] to give the WLF equation,

$$\log a_T = \frac{C_1(T - T_0)}{C_2 + (T - T_0)} \qquad (2.11)$$

where T_o is the reference temperature, C_1 and C_2 are constants and a_T is the shift factor. The WLF equation works on the assumption that above the T_g of the polymer the fractional free volume increases linearly with respect to temperature. The TTS can be applied to any polymer melt or solution so long as there are no phase transitions or any temperature dependent structural changes. There is also a temperature dependence on the modulus of the sample. This effect is usually small and can even be ignored for most polymers. This shift factor is shown by the symbol b_T and effectively applies a vertical shift to the data.

2.6.2 Method

Oscillatory stress experiments were carried out on the PCN and also on the PMMA, which can be used as a reference. The samples were prepared by heat pressing the beads into a 25 mm disk, with a thickness of 1mm. The samples were pressed at 200^{o}C for 15 minutes and then left to cool to room temperature. Samples were dried in a vacuum oven at 80^{o}C for 24 hours before use to ensure no moisture was present. The samples were run using 25 mm aluminium plates with a frequency range of 0.1 to 100 radians per second. The experiment was carried out between 140^{o}C and 230^{o}C with 15^{o}C temperature intervals. The instrument used was a TA instruments AR2000 rheometer. Viscosity measurements were also carried out using 20 mm 2^o aluminium cone and plate with a truncation gap of 43 μm. 20 mm samples of 0.5 mm thickness were prepared as described previously. Viscosity measurements were carried at 230^{o}C at a shear rate of 5*10^-7 to 50 s^{-1}

2.7 Size Exclusion Chromatography

2.7.1 Method

The molecular weights of the polymer were determined via size exclusion chromatography (SEC). A Viscotek TDA 302 with refractive index, viscosity and light scattering detectors and 2*300 mm PLgel 5 μm mixed C columns was used. An eluent of tetrahydrofuran (THF) was used at a flow rate of 1.0 mL/min at a temperature of 35^{o}C. The detectors were calibrated with a single narrow molecular weight distribution PS standard. The samples were prepared by dissolving 4.5 mg of sample in 3 mL of THF. To prevent blockages to the SEC columns by the clay aggregates the samples were filtered using a 0.2 μm syringe filter. To ensure a fair comparison the pure polymer samples were also filtered. PMMA samples were analysed using triple detection SEC using a dn/dc of 0.085.

2.8 Nuclear Magnetic Resonance (NMR)

2.8.1 Method

^{1}H NMR was used to confirm the structure of organic compounds. However, it can also be used to determine the number average molecular weight (M_n) of polymeric materials from the relative peak intensities. Once the intensities are known then the number of hydrogens in the polymer backbone can be calculated and the M_n can be determined. ^{1}H NMR was carried out on a Varian Inova-500 MHz or Mercury-400MHz spectrometer using $CDCl_3$ as a solvent.

2.9 Matrix Assisted Laser Desorption Ionisation time of flight Mass Spectroscopy (MALDI ToF)

2.9.1 Method

MALDI ToF mass spectroscopy can be used to gain information on the molecular weight of low molecular weight polymers. An Applied Biosystems Voyager DE STR Bio Spectrometry instrument was used with a matrix of alpha-cyano-4-hydroxycinnamic acid (CHCA). The sample and matrix were prepared using a mixture of water and acetonitrile.

2.10 References

1. Meneghetti, P.; Qutubuddin, S. *Chemical Engineering Communications* **2001,** 188, 81-89.
2. Ray, S. S.; Okamoto, M. *Progress in Polymer Science* **2003,** 28, (11), 1539-1641.
3. Hammond, C., *The Basics of Crystallography and Diffraction*. 2 ed.; Oxford University Press: 2001.
4. Binahmad, Z.; Ashby, M. F. *Journal of Materials Science* **1988,** 23, (6), 2037-2050.
5. Odriscoll, K.; Sanayei, R. A. *Macromolecules* **1991,** 24, (15), 4479-4480.
6. Xie, W.; Gao, Z. M.; Pan, W. P.; Hunter, D.; Singh, A.; Vaia, R. *Chemistry of Materials* **2001,** 13, (9), 2979-2990.
7. Kashiwagi, T.; Inaba, A.; Brown, J. E.; Hatada, K.; Kitayama, T.; Masuda, E. *Macromolecules* **1986,** 19, (8), 2160-2168.
8. Irvine, D. J.; McCluskey, J. A.; Robinson, I. M. *Polymer Degradation and Stability* **2000,** 67, (3), 383-396.
9. Robinson, I. M.; McCluskey, J. A. In *Fire Hazards and Flame Retarded Acrylics*, Flame Retardants, 2000; Interscience Communications: 2000; pp 227-238.
10. Lyon, R. E.; Walters, N.; Stoliarov, S. I. In *Thermal Analysis of Flammability*, Flame Retardants, 2006; Interscience Communications: 2006; pp 111-122.
11. Goodwin, J. W.; Hughes, R. W., *Rheology for Chemists : an introduction*. 1 ed.; Royal Society of Chemistry: 2000.
12. Ferry, J. D., *Viscoelastic Properties of Polymers*. 2 ed.; Wiley: 1970.
13. Colby, R. H.; Fetters, L. J.; Graessley, W. W. *Macromolecules* **1987,** 20, (9), 2226-2237.
14. Degennes, P. G. *Journal of Chemical Physics* **1971,** 55, (2), 572-&.
15. Likhtman, A. E.; McLeish, T. C. B. *Macromolecules* **2002,** 35, (16), 6332-6343.
16. Cloizeaux, J. D. *Macromolecules* **1992,** 25, (2), 835-841.
17. Williams, M. L.; Landel, R. F.; Ferry, J. D. *Journal of the American Chemical Society* **1955,** 77, (14), 3701-3707.

Chapter 3 Previous Studies of PMMA Clay Nanocomposites

3.1 Synthesis of PMMA Clay Nanocomposites

3.1.1 Synthetic Techniques

The procedure used to prepare the PCN is expected to influence the outcome of the morphology as the degree of mixing will vary with the technique used. The two main approaches in preparing PCN are melt intercalation[1-3] and in-situ polymerisation[4-9]. There are many examples of both techniques utilising a variety of different polymer matrices, but for the purpose of this project the focus will be on techniques used to synthesise PMMA clay nanocomposites.

The melt intercalation process involves heating the polymer above its T_g and mixing it with clay, usually with the aid of an extruder. There has been little work carried out on melt mixing of PMMA nanocomposites. Venables et al[10] melt mixed PMMA and organically modified clay by use of an extruder and obtained a basal spacing of 3.02nm which did not vary with the clay concentration. Melt mixing has also been carried out by annealing a mixture of clay and PMMA in a vacuum oven[11]. The final morphology was intercalated with a basal spacing of 3.68 nm. A basal spacing of 3.68 nm is large. However the change in basal spacing was only 0.68 nm whereas with the use of an extruder[10] the change was 1.23 nm suggesting that the use of a shear force provides a more efficient mixing process.

In-situ free radical polymerisation of PMMA includes bulk, suspension, emulsion and solution polymerisations. These techniques generally involve the mixing of monomer and clay followed by the free radical polymerisation of the monomer to produce the

PCN. One of the advantages of in-situ polymerisations over melt intercalation is that the process of incorporating the polymer into the gallery of the clay will start with the diffusion of the monomer or even short propagating chains rather than the diffusion of long polymer chains as in the case of melt intercalation. In-situ bulk polymerisation[12-16] has produced intercalated PCN although in some cases large basal spacings of approximately 4 nm were observed[12, 15]. In all cases the clay was mixed with MMA prior to polymerisation.

Suspension polymerisation has been shown to produce both intercalated[15, 17-19] and exfoliated structures[15, 17]. The success in achieving exfoliation appears to depend on the type of cation present on the clay surface. Exfoliation was achieved when the cations contained a functional group which enabled the propagating chain to be tethered to the cation and hence the clay. Such cations include 2,2'-azobis(isobutylamide hydrochloride)[17] in which the azo group was used to initiate the polymerisation, 2-(methacryloyloxy)ethyl trimethylammonium chloride[17] in which the acrylate group will react with a propagating chain, and styryl dimethyl hexadecyl ammonium chloride[15] in which the styryl group will again react with the propagating chain during free radical polymerisation. In the case of suspension polymerisations, if long chain hydrocarbon ammonium salts or even unmodified clays were used, an intercalated morphology was produced.

As for suspension polymerisation techniques, emulsion polymerisation has been shown to produce both intercalated[14, 15, 17, 18, 20-24] and exfoliated[17, 18, 20, 21] morphologies. Brittain et al[17] compared suspension and emulsion techniques and both produced exfoliated morphologies for a tethered surfactant and intercalated morphologies for an alkane surfactant. However, an interesting approach was taken for the emulsion polymerisation of tethered PCN; the surfactant was firstly polymerised into the polymer backbone and then cation exchange was carried out on the clay with the polymer tethered surfactant.

All the examples of reaching exfoliation so far have been with organically modified montmorillonite (MMT). However Sahoo[21] achieved exfoliation using unmodified montmorillonite in an emulsion polymerisation. With clay loadings less then 5 wt%, an

exfoliated morphology was reported, but above 5 wt% only intercalated structures were formed. The 5wt% sample showed no XRD peak and the TEM showed that the clay platelets were still aligned but with large spacings between them. For these samples the clay was dispersed into the aqueous phase and then added to the monomer and stirred for 3 hours at 50^{o}C before the emulsion polymerisation was initiated. This shows that under the right conditions and with sufficient mixing, exfoliation can be achieved without the need to modify the clay prior to the polymerisation.

All the techniques mentioned above are capable of producing both intercalated and exfoliated morphologies although exfoliation is more difficult to achieve. For in-situ polymerisation the morphology is found to be independent of the form of in-situ polymerisation used[15, 17], but it heavily depends on the modification of the clay and the degree of dispersion prior to polymerisation. When using alkyl ammonium cations, dispersion in monomer is more effective than dispersion in water, due to the hydrophobicity of the modified clays, and it was also shown that unmodified MMT dispersed in water can yield exfoliated PMMA clay nanocomposites. It is known that MMT can be fully exfoliated in water suggesting that Sahoo[21] commenced with an exfoliated or partially exfoliated system which was maintained during the polymerisation.

In-situ polymerisation techniques which tether the growing PMMA chains onto the cations of the clay either through the use of a double bond or an azo group (initiator) have a high success rate of producing exfoliated morphologies. When reactive cations cover the clay surfaces there is greater probability of multiple chain growth inside the gallery, as the chain growth will depend on the diffusion of the monomer. With alkyl ammonium cations present, either propagating polymer chains or initiator molecules need to diffuse into the gallery. Once this has occurred, the polymer chain can continue to grow. The probability of another initiator or propagating chain entering the gallery spacing will decrease as the gallery space becomes more crowded.

3.1.2 Effect on Molecular Weight

Previous studies[10, 19, 22, 23] of PCNs created in-situ, have shown changes in the molecular weight for polymerisations carried out in the presence of clay as compared to polymerisations carried out in the absence of clay. Kim et al[19] reported the molecular weights for the polymer matrix of nanocomposites prepared via a suspension polymerisation in the presence of 2-8% of organically modified montmorillonite. The data showed an increase in molecular weight compared to the pure PMMA, with the molecular weight ranging from 333000-638000 $gmol^{-1}$. The molecular weight appeared to have no clear dependence on the clay concentration and Kim concluded that montmorillonite does not affect the kinetics of the polymerisation process. A change in the molecular mass was also observed by Lee et al[22], who used an organically modified bentonite clay. The clay was again seen to cause an increase in molecular mass, however this time a large mass (20-50 wt%) of clay was used.

3.2 Thermal Stability

The thermal stability and fire retardant properties of a material are extremely important and a review of fire hazards in some common polymers can be found in reference[25]. PMMA synthesised via free radical polymerisation has been shown to follow a three step degradation process[26]. As the polymer is heated the first transition observed (165^{o}C) is generally weak and is caused by the scission of the head to head linkages which are formed by the combination of radicals during the termination step of the PMMA synthesis. The second peak at 255^{o}C is degradation initiated by the unsaturated chain ends. The third degradation stage occurs at 360^{o}C which is caused by the random scission of the PMMA chain.

The thermal stability of the organically modified montmorillonite (OMMT) has been investigated by Xie et al[27] and Hedley et al[28]. In both cases it was observed that the degradation of the alkyl ammonium cations occurred at temperatures lower than 200^{o}C. Xie et al[27] studied a variety of organically modified MMT and discovered that the onset of degradation of the alkyl ammonium cations occurred between 150-190^{o}C and that there was no relationship between the structure of the alkyl ammonium cation and the

initial onset temperature. The degradation of the OMMT's were studied using TGA-MS (thermal gravimetric analysis attached to a mass spectrometer), which showed that the degradation products consist of tertiary amines and long chain α-olefins, suggesting that a Hoffman elimination is taking place, as seen in the mechanism outlined in Figure 3.1. Xie et al[27] also found that the onset temperature for degradation of OMMT was on average 15-25^{o}C lower than that of their respective alkyl ammonium salts. It was suggested that the clays were acting as a catalyst due to the close proximity of the alkyl ammonium cations to the Lewis base sites and the basic aluminosilicate clay surface which can lower the activation energy required for the Hoffman reaction to take place.

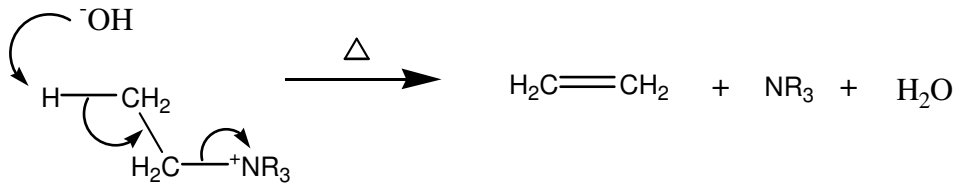

Figure 3.1: Hoffman mechanism.

Despite the low degradation temperature of the OMMT, improved thermal stability of PCN has been observed[29-31]. PCN with a matrix polymer of PMMA was investigated by Zhu et al[8] with both tethered and non tethered composites produced. From TGA analysis a 25-49^{o}C increase in the temperature at 10% weight loss was noticed for the tethered PCN. However, a slight decrease was observed for the untethered PCN. For a 50% weight loss an increase of around 40^{o}C in temperature was observed for both the PCN. Another method of assessing the thermal stability of a polymeric material is through the use of cone calorimetery, which measures the heat release rate (HRR) of a material when it is pyrolised (burned). The lower the HRR rate, the more superior the fire retardency properties of the material. Zhu et al[8] found that both the tethered and untethered PCN produced a lower peak heat release rate (PHRR), and time to ignition for the PCN was equal to or larger than that of pure PMMA, proving that PCN offers an increase in flame retardency.

Samal et al[21] studied PMMA PCN using unmodified MMT. The weight loss vs. temperature traces obtained from TGA showed that PMMA appeared to be more thermally stable than the PCN below 10% weight loss. At a higher percentage weight loss (>30%) the TGA graphs showed that the PCN are found to be more thermally stable, with the temperature increasing with increasing percentage of MMT. The initial decrease in thermal stability at 10% weight loss is surprising since MMT clay displays a significantly higher thermal stability than that of PMMA. The cone calorimetery data also showed that the PHRR (peak heat release rate) decreases with increasing percentage of MMT, but the time to ignition is found to be slightly shorter for the PCN than that of the pure PMMA.

Like the examples seen for PMMA nanocomposites, other polymer matrices such as PS[31, 32], polypropylene[33, 34] and poly(epsilon-caprolactone)[35] also show changes in thermal stability. Reviews into the thermal stability and fire retardency can be found in references[36-40] which discuss the reasons for the changes observed. There are several factors which can cause an increase (or decrease) in the thermal stabilities, and the degree to which these affect the thermal stability will depend on the morphology of the PCN and the nature of the polymer matrix. The main factors are;

- Hindered diffusion of volatile gasses
- Alternate degradation mechanism
- Increased char formation
- Insulating effects of clay

The clay platelets (when well dispersed) generate improved gas barrier properties[41, 42] in PCN. The clay platelets act as physical barriers and force the gas to diffuse via a longer path. This has become known as the labyrinth effect. During thermal degradation the presence of a “labyrinth” of clay platelets slows down the diffusion of the evolved volatile gasses through the material increasing the time it takes for the volatiles to be released and decreasing the rate of mass loss. This effect can occur in any PCN which has a good degree of dispersion such as those in references[19, 43, 44].

Some polymers can degrade via different mechanisms, and the degradation path can affect the thermal stability of the polymer. PS will undergo β chain scission to produce monomer, dimer and trimer molecules[45]. However, Jang et al[46] found that the degradation of PS in the presence of clay produced several additional structures (such as 1,3-diphenylpropane) to those produced by PS. These additional structures are believed to have derived from the recombination of the radicals produced during the initial β chain scission. These recombination products will then undergo random chain scission followed by hydrogen abstraction producing a variety of products. The recombination of radicals can occur more readily in PCN as the clay platelets form physical barriers hindering their diffusion. This consequently brings more radicals together for a longer period of time allowing them to undergo radical transfer and recombine. Changes in degradation products were also observed for a copolymer of poly(ethylene-co-vinyl acetate) (EVA)[47] and polyamide[48] where the clay again acts as either a catalyst or as a diffusion barrier providing the necessary conditions for alternate degradation mechanisms to occur.

The effect of the formation of an insulating char on the surface of the PCN is also discussed in the literature[37, 40, 49]. The formation of char on the surface will act as an insulator and shield the bulk of the material from the heat, reducing the mass loss rate. Gilman et al[37] set up a cone calorimeter containing a thermocouple both at the top and bottom of the sample and a video camera to capture the pyrolysis process. Initially both the Nylon 6 and the PCN showed similar mass loss rates and the temperature at the bottom thermocouple remained the same for both samples. After approximately 180 seconds the mass loss rate for the PCN became lower than that of the Nylon 6 and the temperature at the bottom thermocouple was lower for the PCN than for the Nylon 6. Images from the pyrolysis showed that at 180 seconds over 50% of the PCN surface was covered by char. Whilst there was no char formation for both the Nylon 6 and PCN, the same mass loss rate and thermocouple readings were observed. However the formation of the surface char on the PCN insulated the bulk of the sample and the mass loss rate was reduced.

The last factor in the thermal degradation of PCN is the insulation due to the clay. Unlike Gilman[37], Stretz et al[50] did not observe increased char formation during cone

calorimetry measurements, although improved thermal stabilities were observed. Unmodified MMT is stable above temperatures of 690^{o}C [51] (although any residual water will be released at around 150^{o}C) and it was proposed that the MMT could act as a heat insulator causing a reduction in temperature of the surrounding bulk polymer. The insulating effect of the clay was also observed in references[52, 53].

In conclusion both improvements and reductions of thermal stability were reported. The variation in the data suggests that a combination of factors are working together to alter the thermal stability. There will also be obvious differences arising from the variation in matrix type, the modification of the clay used and the experimental conditions used.

3.3 Glass Transition Temperature

An important property of amorphous polymers is the glass transition temperature (T_g) which is the point at which a polymer goes from a glassy solid to a viscous or rubbery polymer. The glass transition varies with polymer architecture[54] and molecular weight[55]. From past studies of PCN, the T_g has been seen to increase[10, 14, 17] by temperatures up to 20^{o}C, whereas in other cases no change in T_g was observed[56, 57]. There are reports of the glass transition becoming undetectable[11, 18, 22] and that the addition of clay can also decrease the performance of the material[58, 59]. Ober et al[59] studied surface initiated epoxy nanocomposites with clay loadings of 2-15wt% of Cloisite 30B, and a significant decrease in T_g was observed. The decrease is thought to have been caused by the plasticization of the polymer by the surfactant chains.

Lu et al[60] observed a 6^{o}C increase in T_g for epoxy clay nanocomposites with an intercalated morphology, and an increase in T_g was observed with increasing clay content. For a polymer to undergo the transition from glassy to rubbery an increase in segmental motion of the chain is required. As the chains become anchored/confined within the clay layers the segmental motion of the polymer chains will decrease so the temperature required for the polymer to undergo the glass transition will increase.

Increases in T_g for PCN with exfoliated structures have also been observed[17], but since there is no longer any aggregates present then the increase cannot be caused by the confinement of the polymer chains within the clay layers. In order to achieve exfoliation, the clay was modified with a reactive surfactant, allowing the propagating PMMA chains to become tethered to the surfactant. The tethering of the chain ends reduces the number of free chain ends and hence reduces the free volume causing the glass transition to occur at higher temperatures. For a phase separated morphology in PCN systems where there are no or very little interaction between the polymer and clay. It may be expected that the clay will have very little effect on the segmental motion of the polymer chain, allowing the glass transition of the matrix to remain the same. Brittain et al[17] observed a negligible change in T_g of the macrocomposite. However when modified clay was used to produce intercalated/exfoliated structures an increase in T_g was observed.

The loss of the endotherm relating to the glass transition in PCN has again been attributed to the confinement of the polymer chains within the clay layers. One of the differences between observing an increase in T_g and observing no T_g can be related to the percentage of the clay present in the PCN. Generally the disappearance was observed in samples with a higher weight loading of clay (>10wt%). Simon et al[11] used the disappearance of the glass transition to determine the saturation point of PMMA in an organically modified Bentonite. If all the PMMA present resided within the gallery of the clay aggregates then no T_g would be observed. On increasing the amount of PMMA the point at which a T_g is first observed was taken to be the point of saturation. The glass transition was seen to appear above 15% of PMMA. One possible problem with monitoring the disappearance of glass transition with increasing clay content is that the reduction in the amount of PMMA will lead to a gradually weaker change in the heat flow for the T_g.

3.4 Rheology

Thermoplastic materials such as PMMA are melt processed through the use of injection moulding[61, 62], during which the polymer is subjected to shear forces in a molten state. To gain an insight into how materials will behave during processing, rheology can be used to probe the viscosity and shear behaviour of polymers. Differences in rheological behaviour between PCN and their polymer matrices are expected as the platelets could hinder the relaxation of the polymer chains, or the application of a high shear force to the PCN could affect the extent of exfoliation and may even cause alignment of the platelets.

Oscillatory shear rheology provides information on relaxation of the polymer under applied stress. To generate the master curve for oscillatory rheology, the time temperature superposition theory[63] is used, where a_T is the horizontal shift factor used to shift data measured at different temperatures to produce the master curve. It is interesting to note that the value of a_T has been observed to be independent of clay loading and takes on the same value as required for the pure polymer matrix[36, 64, 65], proving the TTS principle is still valid for PCN. From the low frequency (terminal) region of the master curve, PCNs show increases in magnitude of both G' and G''[66-69]. On increasing the weight loading of clay the magnitude of G' (at low frequencies) also increases[36, 65, 66].

On a LOG LOG plot, the gradient of G' and G'' in the terminal region for a linear viscoelastic polymer has the values of 2 and 1 respectively. PCNs show a significant decrease in the gradient compared to that of the polymer matrix[70, 71] and it has been found that as the weight loading of clay increases the gradient of G' decreases[36, 65] which again suggests that the clay is reinforcing the polymer matrix. The increase in gradient of G' is more pronounced than that of G''[70], and eventually the gradient of G' and G'' become equal and the reptation crossover is no longer observed. Solomon et al[64] found that the cross over of G' and G'' at low frequency (corresponding to reptation time[72]) was not observed, indicative of solid like behaviour.

The changes in G' and G'' seen in PCN have been attributed to the presence of a percolated network[70, 71, 73]. The percolated network of clay platelets will produce physical barriers which will restrict the relaxation mechanism of the polymer chains leading to pseudo solid like behaviour. As the change in G' is being caused by the formation of a percolated network, the minimum amount of clay required to form a percolated network can be found from the plot of G' vs. clay loading and the point at which G' starts to increase significantly depicts the threshold for percolation. For polyisoprene and OMMT a volume fraction of greater than 0.02 is required to form a percolated network[73]. The relaxation of the polymer chains is also believed to be affected by adsorption of the polymer chains onto the clay surface. Studies by Lim et al[66] found that as the affinity of the polymer chain towards the clay increases the then relaxation of the polymer chain becomes more hindered.

The effects of mixing and weight loading of clay on the rheology of polystyrene/OMMT nanocomposites were studied by Zhao et al[29]. The changes in the reptation time and the gradient of G' and G'' in the terminal region were recorded. The extent of exfoliation was seen from TEM and x-ray diffraction and related back to the rheology curves. For both low and high clay loadings, the gradient of G' and G'' decreased and the reptation crossover shifted to a lower frequency. When a higher degree of mixing was imposed on the same nanocomposites (through sonication), the lower clay loading showed a further decrease in the gradients and crossover frequency. For the higher clay loading PCN, no crossover was observed, indicating that a fully percolated network had been formed. The percolated network was confirmed from the TEM images which showed that from rheology measurements it is possible to draw conclusions on the morphology of the PCN.

Fornes et al[68] investigated the effect of the matrix molecular weight on the rheology of nylon clay nanocomposites synthesised through the use of an extruder. It was discovered that as the molecular weight of the matrix increased, the gradient of G' decreased, indicating an increase in solid like behaviour. As discussed above, the increase in solid like behaviour is caused by the formation of a percolated network through the exfoliation of the clay platelets, so as the molecular weight is increased then the extent of exfoliation also increases. A higher molecular weight matrix will exert a

higher shear stress for a fixed shear rate on the clay during processing, thus increasing the degree of exfoliation and explaining the differences in the rheology of the terminal region.

The effect of shear forces on the PCN can be investigated using steady state shear viscosity measurements. PCN show an increase in viscosity compared to the pure polymer matrix[68, 74, 75]. However they also show a large degree of shear thinning. Polymers have a large Newtonian plateau region at low shear rates, PCN also show a Newtonian plateau. However this plateau region is smaller as the onset of shear thinning occurs at lower shear rates[68, 76, 77]. The increase in zero shear viscosity observed is caused by the percolated network of the clay platelets[36]. As seen in the oscillatory shear measurements, the clay platelets act as physical barriers preventing the flow of the polymer chains producing a higher modulus material. Above a certain shear rate the clay platelets will gradually be orientated along the direction of the applied shear, breaking up the percolated network and allowing the polymers to flow more freely[76, 78].

Choi et al[79] observed shear thinning in a PEO clay nanocomposite and the onset point of shear thinning was seen to decrease with increasing clay content. To investigate the cause of shear thinning, viscosity measurements were recorded from low to high shear rates and then on the same sample from high to low shear rates. The upward and downward viscosity data were found to be different; with changes seen in the shear thinning region and a slightly lower zero shear viscosity was achieved in the downward measurement. Choi et al[79] also found that the shear thinning is caused by the orientation of the clay platelets and that during the downward viscosity measurements it is thought that the viscous percolated network is being reformed. However the network formation is not quite reaching completion leading to a slightly lower zero shear viscosity than was observed in upward viscosity measurements.

The change in morphology of the PCN can be monitored by performing steady state shear measurements over a range of temperatures. Wang et al[80] plotted viscosity vs. temperature curves for polybutadiene and OMMT intercalated PCNs. The matrix polybutadiene showed a gradual decrease in viscosity with increasing temperature as

expected and the PCN initially followed a similar trend; however above a certain temperature the viscosity increases sharply with temperature. The increase in viscosity indicates a resistance to the relaxation of the polymer chains which can be brought about by a change in morphology from an intercalated to exfoliated state. Aligned and unaligned exfoliated morphologies were produced when the PCN were subsequently cooled and then heated under shear. This again highlights the sensitivity of the PCN morphology to shear.

Similar rheological behaviour has also been observed for other types of nanocomposite systems[81-86]. Du et al[87] studied the rheology of carbon nanotubes (CNT) in a PMMA matrix. G' increased sharply between 0.1 and 0.2 wt% loading of CNT, indicating the formation of a percolated network preventing the motion of the PMMA chains. The existence of the 3D network was confirmed through the use of TEM (transmission electron microscopy). Du et al[87] calculated the threshold of rheological percolation from the plot of G' vs. wt% CNT, the point at which G' started to show large increase indicated the minimum wt% of CNT required to produce a percolated network. For PMMA CNT this was found to be 0.12wt%.

3.5 Objectives

The literature studies highlight some of the successes and failures of polymer clay nanocomposites. As expected the properties of the PCN appear to be dependent on the clay type and the preparation method. In this project free radical suspension polymerisation will be primarily used. It is proposed that clay type and its wt% will be varied in order to determine how it impacts upon the material's physical properties. A natural clay, Cloisite 15a, and a modified and unmodified Laponite clay will be used to investigate the effect of modification on the compatibility of the clay and polymer matrix and hence their impact on the materials properties. It is proposed that both XRD and TEM will be used to characterise the morphology.

It was observed from the literature that in-situ polymerised PCN caused changes in the matrix molecular weight, but no clear correlation between clay loading and the change

in molecular weight was made. It is hoped that this study will provide insight into the effect of clay on the molecular weight. Alterations in the polymer molecular weight will also affect the physical and mechanical properties of the PCN and may mask the effect of the clay. By systematically varying the clay loading it may be possible to distinguish whether changes in the physical and mechanical properties are caused by clay or by changes in matrix molecular weight.

As discussed earlier in this chapter, there are also several different mechanisms believed to cause the increase in thermal stability, including; gas barrier effect and alternate degradation mechanisms. The thermal stability of the PCN will be investigated using TGA and micro calorimetry and the glass transition temperature will be measured using DSC. Any trends in these properties will be investigated and compared to the observations made in the literature. The aim is also to distinguish between changes in T_g which are a result of the addition of clay or are caused by any alterations in the matrix molecular weight.

Rheological measurements provide an insight into how a material will behave during processing and in the case of polymer nanocomposites it has been used to confirm the presence of network structures within the matrix. The effect that the clay type and loading have upon the rheological properties will be studied. If there are significant changes in molecular weight then it is again important to determine its impact on the change in rheological behaviour. Another consideration during the processing of PCN would be the alignment of the clay platelets which may lead to directionality within the material. The extent of the alignment in injection moulded samples can be determined by the use of SAXS measurements.

3.6 Reference

1. Liu, L. M.; Qi, Z. N.; Zhu, X. G. *Journal of Applied Polymer Science* **1999,** 71, (7), 1133-1138.
2. He, C. B.; Liu, T. X.; Tjiu, W. C.; Sue, H. J.; Yee, A. F. *Macromolecules* **2008,** 41, 193-202.
3. Lan, T.; Kaviratna, P. D.; Pinnavaia, T. J. *Chemistry of Materials* **1995,** 7, (11), 2144-2150.
4. Noh, M. W.; Lee, D. C. *Polymer Bulletin* **1999,** 42, (5), 619-626.
5. Lan, T.; Pinnavaia, T. J. *Chemistry of Materials* **1994,** 6, (12), 2216-2219.
6. Kiersnowski, A.; Piglowski, J. *European Polymer Journal* **2004,** 40, (6), 1199-1207.
7. Weimer, M. W.; Chen, H.; Giannelis, E. P.; Sogah, D. Y. *Journal of the American Chemical Society* **1999,** 121, (7), 1615-1616.

8. Zhu, J.; Start, P.; Mauritz, K. A.; Wilkie, C. A. *Polymer Degradation and Stability* **2002,** 77, (2), 253-258.
9. Messersmith, P. B.; Giannelis, E. P. *Chemistry of Materials* **1994,** 6, (10), 1719-1725.
10. Tabtiang, A.; Lumlong, S.; Venables, R. A. *European Polymer Journal* **2000,** 36, (12), 2559-2568.
11. Shen, Z. Q.; Simon, G. P.; Cheng, Y. B. *Journal of Applied Polymer Science* **2004,** 92, (4), 2101-2115.
12. Okamoto, M.; Morita, S.; Taguchi, H.; Kim, Y. H.; Kotaka, T.; Tateyama, H. *Polymer* **2000,** 41, (10), 3887-3890.
13. Stadtmueller, L. M.; Ratinac, K. R.; Ringer, S. P. *Polymer* **2005,** 46, (23), 9574-9584.
14. Meneghetti, P.; Qutubuddin, S. *Thermochimica Acta* **2006,** 442, (1-2), 74-77.
15. Wang, D. Y.; Zhu, J.; Yao, Q.; Wilkie, C. A. *Chemistry of Materials* **2002,** 14, (9), 3837-3843.
16. Meneghetti, P.; Qutubuddin, S. *Chemical Engineering Communications* **2001,** 188, 81-89.
17. Huang, X. Y.; Brittain, W. J. *Macromolecules* **2001,** 34, (10), 3255-3260.
18. Essawy, H.; Badran, A.; Youssef, A.; Abd El-Hakim, A. E. *Polymer Bulletin* **2004,** 53, (1), 9-17.
19. Kim, S. S.; Park, T. S.; Shin, B. C.; Kim, Y. B. *Journal of Applied Polymer Science* **2005,** 97, (6), 2340-2349.
20. Lin, K. F.; Lin, S. C.; Chien, A. T.; Hsieh, C. C.; Yen, M. H.; Lee, C. H.; Lin, C. S.; Chiu, W. Y.; Lee, Y. H. *Journal of Polymer Science Part a-Polymer Chemistry* **2006,** 44, (19), 5572-5579.
21. Sahoo, P. K.; Samal, R. *Polymer Degradation and Stability* **2007,** 92, 1700-1707.
22. Lee, D. C.; Jang, L. W. *Journal of Applied Polymer Science* **1996,** 61, (7), 1117-1122.
23. Meneghetti, P.; Qutubuddin, S. *Langmuir* **2004,** 20, (8), 3424-3430.
24. Kiersnowski, A.; Trelinska-Wlazlak, M.; Dolega, J.; Piglowski, J. *E-Polymers* **2006**.
25. Irvine, D. J.; McCluskey, J. A.; Robinson, I. M. *Polymer Degradation and Stability* **2000,** 67, (3), 383-396.
26. Kashiwagi, T.; Inaba, A.; Brown, J. E.; Hatada, K.; Kitayama, T.; Masuda, E. *Macromolecules* **1986,** 19, (8), 2160-2168.
27. Li, Y.; Zhao, B.; Xie, S. B.; Zhang, S. M. *Polymer International* **2003,** 52, (6), 892-898.
28. Hedley, C. B.; Yuan, G.; Theng, B. K. G. *Applied Clay Science* **2007,** 35, (3-4), 180-188.
29. Zhao, J.; Morgan, A. B.; Harris, J. D. *Polymer* **2005,** 46, (20), 8641-8660.
30. Wang, G. H.; Zhang, L. M. *Applied Clay Science* **2007,** 38, 17-22.
31. Doh, J. G.; Cho, I. *Polymer Bulletin* **1998,** 41, (5), 511-518.
32. Bourbigot, S.; Gilman, J. W.; Wilkie, C. A. *Polymer Degradation and Stability* **2004,** 84, (3), 483-492.
33. Bertini, F.; Canetti, M.; Audisio, G.; Costa, G.; Falqui, L. *Polymer Degradation and Stability* **2006,** 91, (3), 600-605.
34. Tang, Y.; Hu, Y.; Song, L.; Zong, R. W.; Gui, Z.; Chen, Z. Y.; Fan, W. C. *Polymer Degradation and Stability* **2003,** 82, (1), 127-131.
35. Lepoittevin, B.; Devalckenaere, M.; Pantoustier, N.; Alexandre, M.; Kubies, D.; Calberg, C.; Jerome, R.; Dubois, P. *Polymer* **2002,** 43, (14), 4017-4023.
36. Ray, S. S.; Okamoto, M. *Progress in Polymer Science* **2003,** 28, (11), 1539-1641.
37. Gilman, J. W. *Applied Clay Science* **1999,** 15, (1-2), 31-49.
38. Pandey, J. K.; Reddy, K. R.; Kumar, A. P.; Singh, R. P. *Polymer Degradation and Stability* **2005,** 88, (2), 234-250.
39. Leszczynska, A.; Njuguna, J.; Pielichowski, K.; Banerjee, J. R. *Thermochimica Acta* **2007,** 453, (2), 75-96.
40. Leswzynska, A.; Njuguna, J.; Pielichowski, K.; Banerjee, J. R. *Thermochimica Acta* **2007,** 454, (1), 1-22.
41. Osman, M. A.; Rupp, J. E. P.; Suter, U. W. *Journal of Materials Chemistry* **2005,** 15, (12), 1298-1304.
42. Osman, M. A.; Mittal, V.; Morbidelli, M.; Suter, U. W. *Macromolecules* **2004,** 37, (19), 7250-7257.
43. Zanetti, M.; Camino, G.; Reichert, P.; Mulhaupt, R. *Macromolecular Rapid Communications* **2001,** 22, (3), 176-180.
44. Burnside, S. D.; Giannelis, E. P. *Chemistry of Materials* **1995,** 7, (9), 1597-1600.
45. McNeill, I. C.; Zulfiqar, M.; Kousar, T. *Polymer Degradation and Stability* **1990,** 28, (2), 131-151.
46. Jang, B. N.; Wilkie, C. A. *Polymer* **2005,** 46, (9), 2933-2942.
47. Costache, M. C.; Jiang, D. D.; Wilkie, C. A. *Polymer* **2005,** 46, (18), 6947-6958.

48. Jang, B. N.; Wilkie, C. A. *Polymer* **2005,** 46, (10), 3264-3274.
49. Gilman, J. W.; Jackson, C. L.; Morgan, A. B.; Harris, R.; Manias, E.; Giannelis, E. P.; Wuthenow, M.; Hilton, D.; Phillips, S. H. *Chemistry of Materials* **2000,** 12, (7), 1866-1873.
50. Stretz, H. A.; Wootan, M. W.; Cassidy, P. E.; Ko, J. H. *Polymers for Advanced Technologies* **2005,** 16, (2-3), 239-248.
51. Olphen, H. V.; Fripiat, J. J., *Data handbook for clay materials and other non-metallic minerals* 1st ed.; Pergamon Press: 1979.
52. Chang, J. H.; Seo, B. S.; Hwang, D. H. *Polymer* **2002,** 43, (10), 2969-2974.
53. Chang, J. H.; Kim, S. J.; Joo, Y. L.; Im, S. *Polymer* **2004,** 45, (3), 919-926.
54. Young, R. J.; Lovell, P. A., *Introduction to Polymers*. 2 ed.; Chapman and Hall: 1991.
55. Odriscoll, K.; Sanayei, R. A. *Macromolecules* **1991,** 24, (15), 4479-4480.
56. Zerda, A. S.; Caskey, T. C.; Lesser, A. J. *Macromolecules* **2003,** 36, (5), 1603-1608.
57. Miwa, Y.; Drews, A. R.; Schlick, S. *Macromolecules* **2006,** 39, (9), 3304-3311.
58. Zilg, C.; Mulhaupt, R.; Finter, J. *Macromolecular Chemistry and Physics* **1999,** 200, (3), 661-670.
59. Chen, J. S.; Poliks, M. D.; Ober, C. K.; Zhang, Y. M.; Wiesner, U.; Giannelis, E. *Polymer* **2002,** 43, (18), 4895-4904.
60. Lu, H. B.; Nutt, S. *Macromolecules* **2003,** 36, (11), 4010-4016.
61. D.H.Morton-Jones, *Polymer Processing*. Chapman and Hall: 1995.
62. Kalpakjian, S.; Schmid, S. R., *Manufacturing Processes for Engineering Materials*. Pearson Education International: 2003.
63. Williams, M. L.; Landel, R. F.; Ferry, J. D. *Journal of the American Chemical Society* **1955,** 77, (14), 3701-3707.
64. Solomon, M. J.; Almusallam, A. S.; Seefeldt, K. F.; Somwangthanaroj, A.; Varadan, P. *Macromolecules* **2001,** 34, (6), 1864-1872.
65. Krishnamoorti, R.; Giannelis, E. P. *Macromolecules* **1997,** 30, (14), 4097-4102.
66. Kim, H. B.; Choi, J. S.; Lee, C. H.; Lim, S. T.; Jhon, M. S.; Choi, H. J. *European Polymer Journal* **2005,** 41, (4), 679-685.
67. Sepehr, M.; Utracki, L. A.; Zheng, X. X.; Wilkie, C. A. *Polymer* **2005,** 46, (25), 11569-11581.
68. Fornes, T. D.; Yoon, P. J.; Keskkula, H.; Paul, D. R. *Polymer* **2001,** 42, (25), 9929-9940.
69. Galgali, G.; Ramesh, C.; Lele, A. *Macromolecules* **2001,** 34, (4), 852-858.
70. Hoffmann, B.; Kressler, J.; Stoppelmann, G.; Friedrich, C.; Kim, G. M. *Colloid and Polymer Science* **2000,** 278, (7), 629-636.
71. Hoffmann, B.; Dietrich, C.; Thomann, R.; Friedrich, C.; Mulhaupt, R. *Macromolecular Rapid Communications* **2000,** 21, (1), 57-61.
72. Degennes, P. G. *Journal of Chemical Physics* **1971,** 55, (2), 572-&.
73. Jeon, H. S.; Rameshwaram, J. K.; Kim, G. *Journal of Polymer Science Part B-Polymer Physics* **2004,** 42, (6), 1000-1009.
74. Wooster, T. J.; Abrol, S.; MacFarlane, D. R. *Polymer* **2005,** 46, (19), 8011-8017.
75. Krishnamoorti, R.; Vaia, R. A.; Giannelis, E. P. *Chemistry of Materials* **1996,** 8, (8), 1728-1734.
76. Hyun, Y. H.; Lim, S. T.; Choi, H. J.; Jhon, M. S. *Macromolecules* **2001,** 34, (23), 8084-8093.
77. Swain, S. K.; Isayev, A. I. *Polymer* **2007,** 48, (1), 281-289.
78. Wagener, R.; Reisinger, T. J. G. *Polymer* **2003,** 44, (24), 7513-7518.
79. Choi, H. J.; Kim, S. G.; Hyun, Y. H.; Jhon, M. S. *Macromolecular Rapid Communications* **2001,** 22, (5), 320-325.
80. Wang, X. L.; Gao, Y.; Mao, K. M.; Xue, G.; Chen, T. H.; Zhu, J. J.; Li, B. H.; Sun, P. C.; Jin, Q. H.; Ding, D. T.; Shi, A. C. *Macromolecules* **2006,** 39, (19), 6653-6660.
81. Li, G.; Mai, K. C.; Feng, K. C. *Journal of Applied Polymer Science* **2006,** 99, (5), 2138-2143.
82. Wang, Z. B.; Chen, K. Z.; Zhang, Z. K. *Journal of Macromolecular Science Part B-Physics* **2007,** 46, (2), 295-303.
83. Gelves, G. A.; Lin, B.; Sundararaj, U.; Haber, J. A. *Nanotechnology* **2008,** 19, (21).
84. Ceccia, S.; Ferri, D.; Tabuani, D.; Maffettone, P. L. *Rheologica Acta* **2008,** 47, (4), 425-433.
85. Ma, H. Y.; Tong, L. F.; Xu, Z. B.; Fang, Z. P. *Nanotechnology* **2007,** 18.
86. Potschke, P.; Fornes, T. D.; Paul, D. R. *Polymer* **2002,** 43, (11), 3247-3255.
87. Du, F. M.; Scogna, R. C.; Zhou, W.; Brand, S.; Fischer, J. E.; Winey, K. I. *Macromolecules* **2004,** 37, 9048-9055.

Chapter 4 PMMA/Cloisite 15a Nanocomposites

4.1 Experimental

PMMA/Cloisite 15a nanocomposites are synthesised in-situ using a free radical suspension polymerisation technique. The advantage of suspension polymerisation over bulk reaction is that it reduces the build up of heat and viscosity but the reaction inside each droplet still follows a bulk reaction mechanism. Alongside emulsion polymerisation and cast sheet, suspension polymerisation is one of the main techniques employed by Lucite International for the synthesis of PMMA. The experimental set up is outlined in Figure 4.1. A high speed overhead stirrer (1500 rpm) is required in suspension polymerisation to maintain the suspension of monomer in the water phase and could also be advantageous towards the dispersion of the clay.

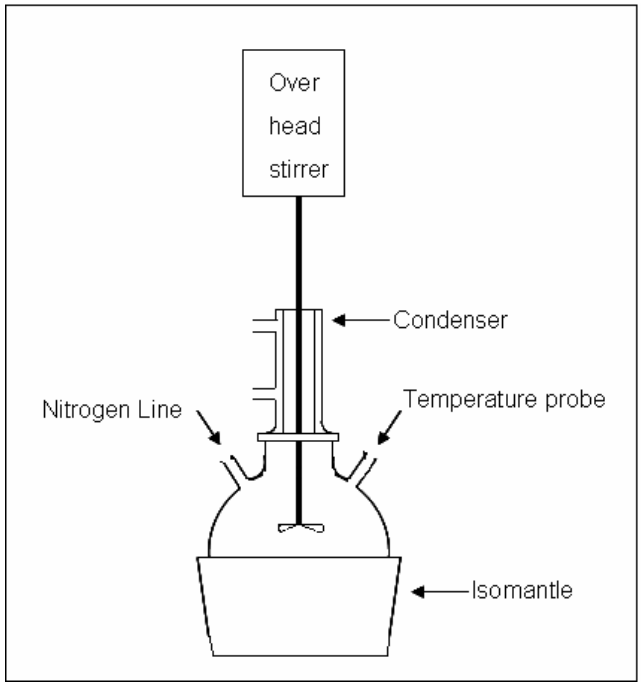

Figure 4.1: Experimental set up used for suspension polymerisation.

4.1.1 Materials

Cloisite 15a (C15a) is a montmorillonite clay which has been organically modified with dimethyl dehydrogenated tallow quaternary ammonium salt and was purchased from Southern Clay. Methylmethacrylate (MMA), the suspending agent 1% aqueous solution of poly(2-methyl-2-propenoic acid) sodium salt (PMA) and initiator, 2,2-azobis(2-methylpropionitrile) (AIBN) were kindly supplied by Lucite International, and used as received. A co-monomer of ethyl propenoate was used in the suspension polymerisation and was purchased from Sigma Aldrich. To control the molecular weight a chain transfer agent (CTA) of 1-dodecanethiol purchased from Fluka was used. All chemicals were used as received.

4.1.2 Suspension Polymerisation of PMMA

4 mol (400 g) of MMA monomer was dispersed in 2 L of deionised water in a three necked round bottom flask. 9.9 mmol (2 g) CTA was added along with 0.12 mol (12 g) ethyl propenoate, 100 g of suspending agent and 6.1 mmol (1 g) of AIBN. The pH of the aqueous phase was maintained at pH 10 through the use of a buffer solution[1]. The suspension was then vigorously stirred using an overhead mechanical stirrer and was heated to reflux (83^{o}C) under a blanket of nitrogen. Once the reflux had receded (approximately 30 minutes) the reaction was stirred at 90^{o}C for 2 hours to consume any residual monomer and then cooled to ambient temperature. The PMMA beads were filtered off and washed with deionised water and then dried in a vacuum oven at 80^{o}C for 24 hours.

4.1.3 Suspension Polymerisation of PMMA nanocomposites

4 wt% (16 g) of Cloisite 15a was added to 4.0 mol (400 g) of MMA monomer in a three necked round bottom flask and was stirred vigorously using an overhead mechanical stirrer for 15minutes, after which 2 L of deionised water was added. 9.9 mmol (2 g) CTA was added along with 0.12 mol (12 g) ethyl propenoate, 100 g of suspending agent and 6.1 mmol (1 g) of AIBN. The pH of the aqueous phase was maintained at pH 10 through the use of a buffer solution[1]. The suspension was vigorously stirred using an

overhead mechanical stirrer and was heated to reflux (83^{o}C) under a blanket of nitrogen. Once the reflux had resided (approximately 30 minutes) the reaction was heat treated at 90^{o}C for 2 hours to remove any residual monomer and then cooled to ambient temperature. The PMMA beads were filtered off and washed with deionised water and then dried in a vacuum oven at 80^{o}C for 24 hours.

PMMA nanocomposites containing 0.05, 0.1, 0.25, 0.5, 1 and 2 wt% Cloisite 15a were also synthesised as above. To help understand the change in molecular weight discussed below, 0.25%C15a samples were also prepared with 0 and 19.8 mmol (4 g) of CTA.

4.2 Preliminary Experiments

The degree of dispersion of C15a in MMA and water was tested by mixing 1wt% solutions of C15a. Immediately after dispersion the samples appeared cloudy, after leaving to stand for 24hr the clay was seen to sediment to the bottom of the vials as shown in Figure 4.2. The clay appeared to have poor solubility in water as expected due to the surface treatment of the clay with hydrophobic cations. The presence of the long chain organic surfactants also proved to produce poor solubility in MMA. The last solubility test was carried out in a 1:1 mixture of MMA and water as shown in Figure 4.2. Water has a higher density (1.0 g.cm^{-3}) than MMA (0.93 g.cm^{-3}) indicating that the top phase will consist of MMA and the lower phase of water. Clay has affected the miscibility between the water and monomer. Equal volumes of MMA and water were used. The image in Figure 4.2 shows that the top MMA layer is approximately a quarter of the size of the bottom layer, the remaining MMA must be present in the bottom layer. The bottom layer is coloured suggesting the clay is also held in suspension within this layer. The colour is uniform throughout this layer with no sedimentation occurring as in the individual mixtures of MMA, water and Cloisite 15a clay. It was seen that C15a clay is not soluble in either water or MMA however it appears possible for C15a clay to be held in suspension by a mixture of the two.

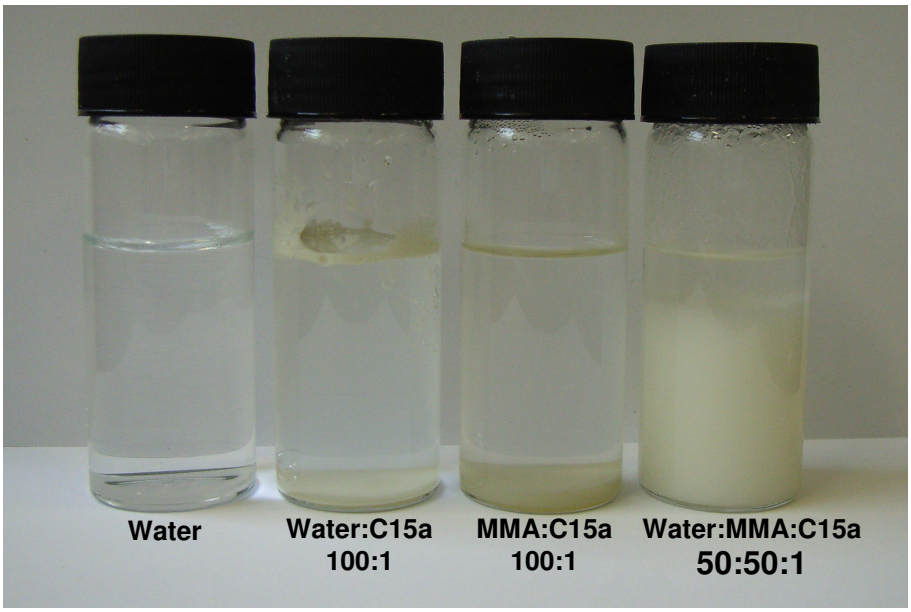

Figure 4.2: Image showing the dispersion of 1%C15a in water, MMA and a 50/50 water MMA mix after 24hr of standing.

Preliminary experiments were carried out using four weight percent (wt%) of C15a clay with dispersion in either water or monomer prior to suspension polymerisation. For predispersion in MMA the method outlined in Chapter 4.1.3 was followed. For predispersion in water the clay was added to 2 L of deionised water in the reaction flask and stirred for 15 minutes using the reaction stirrer. The monomer and remaining reactants were then added and the reaction was carried out as described in section 4.1.3.

Both PCN were tested via XRD to examine the extent of exfoliation and the resulting spectra are shown in Figure 4.3. The XRD peak of both 4%C15a dispersed in water and monomer occur at the same 2θ value giving a d001 spacing of 3.7 nm. The d001 spacing suggests that an intercalated structure was formed in both cases and that the medium used for pre-dispersion has no impact on the outcome. Any premixing may be undone when the remaining reactants are added as the stirring during the reaction would allow the clay to reach its preferred state in either (or both) the monomer or water phase.

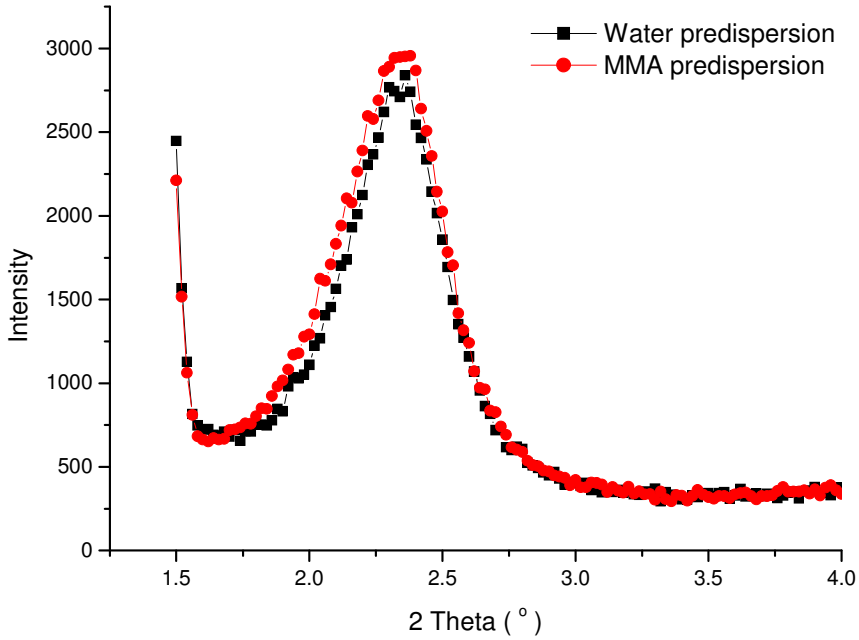

Figure 4.3: XRD spectra of 4%C15a with predispersion in monomer and water.

Although there was no visible difference in the extent of exfoliation produced, pre-dispersion in MMA was undertaken. This would ensure each sample had experienced the same degree of mixing and could also increase the probability of uptake of monomer between the clay layers which would be beneficial to the resulting morphology.

4.3 Effect of Clay on the PMMA Molecular Weight

The molecular weight data of the PCNs are shown in Table 4.1 and Figure 4.4. The PMMA prepared in the absence of clay had a weight average molecular weight of 97000 $gmol^{-1}$, whereas that prepared in the presence of 4% C15a was found to have a M_w of 806000 $gmol^{-1}$ – approximately a 830% increase. There appears to be a trend between the wt% of clay and the molecular weight of the matrix PMMA which can be seen clearly in Figure 4.4. The graph shows that as the wt% of clay increases so does the molecular weight until a clay loading of 0.5 wt% is reached. Above 0.5 wt% the molecular weight plateaus at around 800000 $g.mol^{-1}$. This plateau is unusual as one might expect that the clay would continue to affect the molecular weight of PMMA

matrix as the clay loading is increased. This suggests that there is a limiting factor preventing any further increase in the molecular weight.

Table 4.1: Molecular weight data obtained from GPC of PMMA and PMMA/Cloisite 15a nanocomposites.

	Wt% Clay	CTA (mmol)	M_w(g·mol^{-1})	M_n(g·mol^{-1})	PDI
PMMA	0	9.9	97000	54000	1.8
0.05% C15a	0.05	9.9	137000	60000	2.3
0.1% C15a	0.1	9.9	313000	127000	2.5
0.25% C15a	0.25	9.9	660000	234000	2.8
0.5% C15a	0.5	9.9	802000	206000	3.9
1% C15a	1	9.9	800000	209000	3.8
2% C15a	2	9.9	803000	220000	3.7
4% C15a	4	9.9	806000	257000	3.1

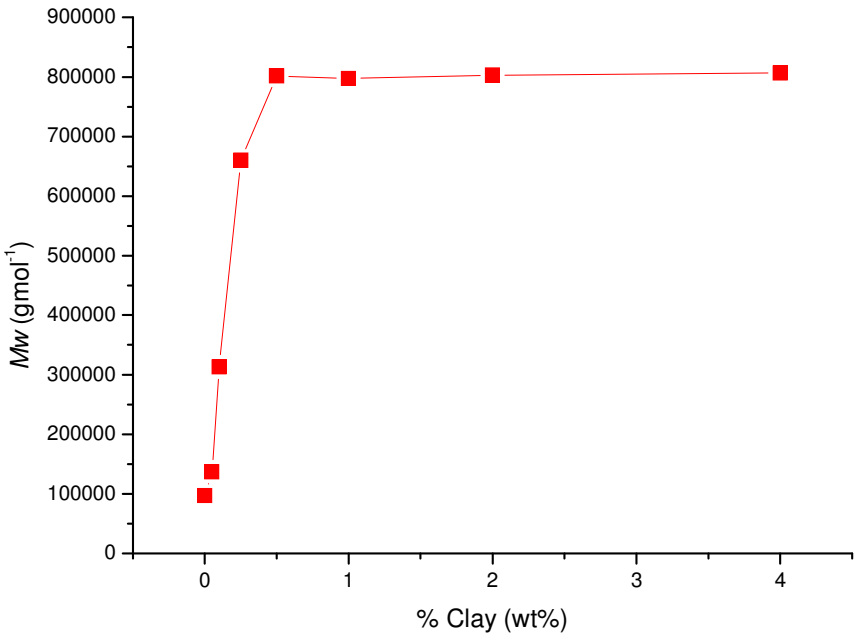

Figure 4.4: Plot of wt% clay vs. molecular weight showing the plateau effect in the molecular weight.

Solomon et al[2] carried out an investigation into the effect of various mineral types (including montmorillonite) in the chain termination of the free radical polymerisations. They found that in the presence of the mineral there was an increase in molecular

weight of the polymer and suggested that this was caused by the preferential absorption of the initiating or propagating free radicals onto the Lewis acid sites found on the rim of the clay. Once absorbed by the Lewis acid site, termination is thought to occur via an electron transfer mechanism. Although montmorillonite was not the most reactive of the minerals studied it was still found to have a significant effect on the molecular weight.

Such a termination of the radicals of the propagating PMMA chains by the clay could account for an increase in the molecular weight. However this does not explain why in our case the molecular weight plateaus at 0.5 wt% clay. Furthermore, whilst termination by the clay might explain the molecular weight increase seen by Solomon et al[2], it cannot account for the large increase associated with the addition of much smaller amounts of clay observed in the present study. Solomon reported a 220% increase in molecular weight on addition of 7 wt% of unmodified montmorillonite. We observed an 830% increase on the addition of 0.5 wt% of modified Cloisite 15a, suggesting that the change in molecular weight may not be due to the termination of the PMMA chains. As an alternative explanation, we investigated whether the CTA was reacting preferentially with the clay, resulting in the large increase in molecular weight and explaining the plateau effect seen. Polymerisations of 0, 0.25, and 2wt% of clay in the absence of CTA were carried out and the resulting molecular weights are shown in Table 4.2 along with the data from the analogous reactions carried out with CTA.

Table 4.2: The effect of CTA upon the molecular weight of PMMA and PMMA/Cloisite 15a nanocomposites.

	Wt% Clay	**CTA (mmol)**	M_w(g·mol^{-1})	M_n(g·mol^{-1})	**PDI**
PMMA	0	9.9	97000	54000	1.8
PMMA(noCTA)	0	0	855000	243000	3.5
2%C15a(noCTA)	2	0	807000	239000	3.4
2%C15a	2	9.9	803000	220000	3.7
0.25%C15a(noCTA)	0.25	0	783000	329000	2.4
0.25%C15a	0.25	9.9	660000	234000	2.8
0.25%C15a(4gCTA)	0.25	19.8	458000	165000	2.8

A molecular weight of 855000 g.mol^{-1} was obtained from the polymerisation of MMA in the absence of clay and CTA. This is much higher than the molecular weight observed for PMMA with CTA and shows the large influence that the CTA has on the molecular weight. Furthermore the molecular weight obtained for PMMA polymerised in the absence of CTA (and clay) is very similar to the plateau value of molecular weight obtained for the PCNs. The 2%C15a (no CTA) sample had a molecular weight of 806000 g.mol^{-1} which was almost identical to that of the 2%C15a (with CTA) signifying that in this case the presence of CTA appears to have no effect. This suggests that the presence of the CTA is somehow negated by the clay. As postulated above we believe that the Lewis acid sites on the clay rim are reacting with the thiol radicals from the CTA and terminating the radical. Furthermore it would appear that at low loadings of clay (below 0.5 wt%) there is insufficient clay present to remove all of the CTA. Figure 4.4 clearly shows that as the clay concentration increases there is a gradual increase in molecular weight suggesting a decreasing amount of active CTA. Eventually a point is reached where there is sufficient clay (0.5 wt%) to react with all of the CTA and the molecular weight plateaus. A closer look at the molecular weight values shows that there is a slight increase of molecular weight from 0.5 to 4wt%. This smaller increase may be caused by termination of the propagating PMMA chains by remaining Lewis acid sites on the clay after reaction with the CTA.

To further investigate the relationship between molecular weight, clay loading and CTA and with a view to lowering the molecular weight of the PMMA in the PCN, a polymerisation with clay loading of 0.25 wt% was carried out with double the usual amount of CTA. 0.25 wt% of clay was chosen as this amount of clay results in a PMMA molecular weight just below the plateau – so the effect of CTA concentration could be most clearly seen. The resultant molecular weights are given in Table 4.2. As expected there is a linear relationship between the amount of CTA and the molecular weight. The 0.25%C15a without CTA had a molecular weight of approximately 800000 g.mol^{-1}, bringing it into line with those of higher clay loadings. With 9.9 mmol CTA the molecular weight dropped to 660000 g.mol^{-1} and with 19.8 mmol CTA the molecular weight was further reduced to 460000 g.mol^{-1}.

4.4 Morphology of PMMA/Cloisite 15a Nanocomposite

Characterisation of the PCN morphology was carried out by XRD and TEM with the aim of relating the morphology to the physical properties. The literature showed that the morphology of the clay appeared to have a large influence on the resulting properties of the material as discussed in Chapter 3.

C15a is "off white" in colour and as a consequence of this the PCN produced are also expected to be coloured. Figure 4.5 is an image of 1mm thick heat pressed samples of varying loading of C15a, a sample of clay is shown on the left hand side for comparison. As the wt% of C15a is increased the colour of the samples becomes more enhanced compared to PMMA confirming that increased amounts of clay have been incorporated during the in-situ polymerisation. PMMA is known for its good optical properties hence it is often used as an alternative to glass. On this scale the PCN remain transparent as indicated by the visibility of the sample names shown in Figure 4.5. However it is believed that as the thickness of the sample is increased, the presence of the clay will reduce the transparency due to its colour. The difference in the colour and transparency of the PCN due to the C15a clay will limit its use as a commercial material.

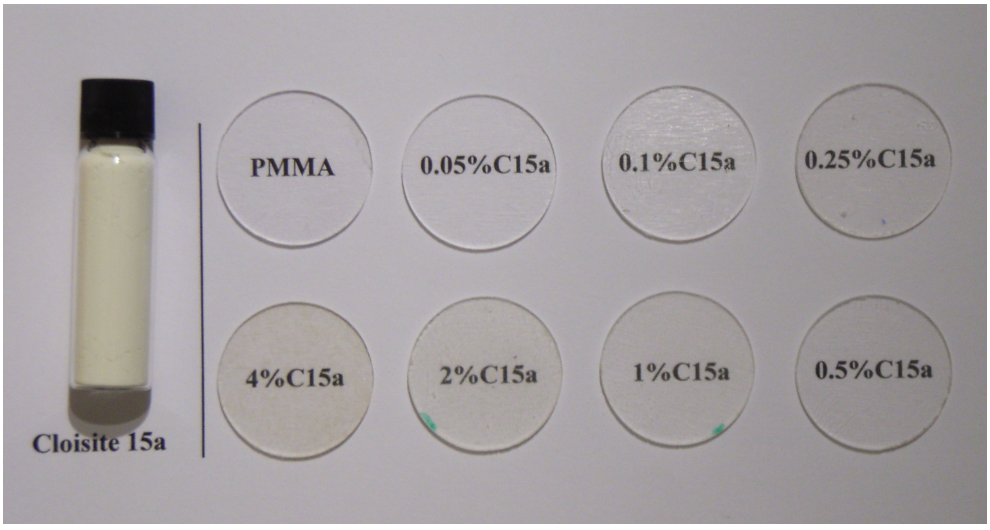

Figure 4.5: Colour changes of the 0.05-4%C15a heat pressed samples. Left hand side shows a sample of Cloisite 15a clay

The basal spacing or the d001 values for the PCN were obtained by XRD and the resulting XRD traces are given in Figure 4.6. The PMMA trace is flat as expected and

both 0.1 and 4%C15a show a scattering corresponding to the d001 peak caused by the basal spacing of the clay. The intensity of the scattering peak is weaker for 0.1%C15a than 4%C15a due to the lower clay loading. Bragg's law (equation(2.2)) can be used to convert the 2θ values into average basal spacings which are given in Table 4.3. An average basal spacing of up to 3.7 nm was seen, which corresponds to an increase of 0.55 nm compared to Cloisite15a clay (3.15 nm). This indicates that polymer chains are entering the clay gallery and are swelling the clay producing an intercalated morphology. The chains in the clay gallery are expected to be in an unfavourable conformation since the increase in basal spacing is less than the radius of gyration (R_g) which is approximately 8 nm for PMMA with a molecular weight of 100000 g.mol^{-1}. Again, by comparing the basal spacing with the clay loading it can be seen that it initially increases with increasing clay loading but plateaus off at 3.7 nm above 0.5 wt%. The reason for the increase in d001 spacing is unknown, but since it follows the same trend as that of the molecular weight it may be attributed to the increase in size of the chains found inside the clay gallery.

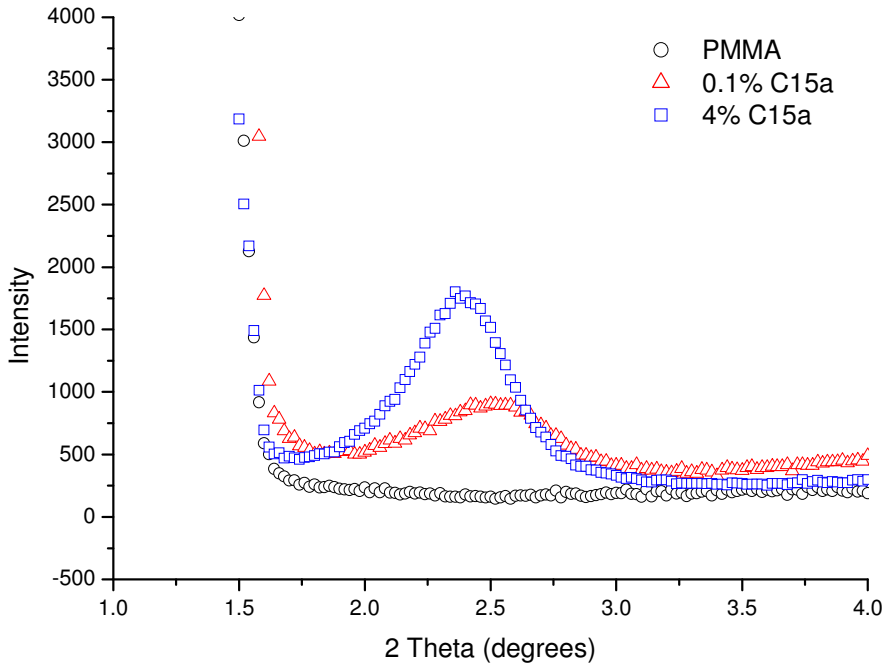

Figure 4.6: XRD traces of PMMA, 0.1%C15a and 4%C15a.

Table 4.3: The basal spacings and aggregate sizes calculated from XRD of PMMA/Cloisite 15a nanocomposites containing different wt% clay.

	wt% Clay	**d001 (nm)**	***B* (rad)**	***t* (nm)**	***m***
C15a	-	3.2	0.0204	7.5	3
0.05%C15a	0.05	3.4	0.0083	18.7	6
0.1%C15a	0.1	3.5	0.0116	13.3	5
0.25%C15a	0.25	3.6	0.0110	13.9	5
0.5%C15a	0.5	3.7	0.0086	18.0	6
1%C15a	1	3.7	0.0070	21.9	7
2%C15a	2	3.7	0.0066	23.4	7
4%C15a	4	3.7	0.0066	23.4	7

Further structural information can be obtained from the distribution and intensity of the XRD peak. Scherrer's formula, equation(4.1), uses the peak broadening caused by diffraction scattering at angles that differ slightly from the Bragg angle to calculate the size of the crystal[3]. In this instance it is used to calculate the thickness of the clay aggregate (t), where B is the full width at half maximum intensity (FWHM) in radians, θ is the diffraction angle and k is a constant with value of 1 (taken from reference[4]). Since both the thickness of the clay aggregate and the basal spacing is known then the number of clay platelets (m) in the aggregate can be calculated from equation(4.2).

$$t = \frac{k\lambda}{B\cos\theta} \qquad (4.1)$$

$$m = \frac{t}{d001} + 1 \qquad (4.2)$$

The XRD traces were fitted to a Gaussian distribution to obtain B, enabling values t and m to be calculated which are given in Table 4.3. The number of clay platelets per aggregate remains similar for all weight loadings of clay, although the slightly larger aggregate size of 0.05%C15a may be due to the weak intensity of the XRD signal obtained which would increase the signal to noise ratio. The values of t and m were also calculated for C15a clay and the average number of clay platelets in the aggregate was found to be 3. This is approximately half the number than that observed from the PCN (m=5-7). As the size of the aggregates appear to be larger in the PCN, the compatibility between the clay and the PMMA is poor. The poor compatibility is

forcing the clay to undergo further aggregation, which appears to be more preferential than dispersing throughout the PMMA matrix. Care must still be taken in interpreting these results too quantitatively because broadening of the XRD peak can also arise from imperfections in the crystal structure, surface roughness and the presence of a range of similar d001 spacings.

To gain further understanding of the morphology, TEM images were taken from small sections of the PMMA/Cloisite 15a nanocomposite. Figure 4.7a and Figure 4.7b are the micrographs of 0.05%C15a and 4%C15a respectively and confirm that the nanocomposites have an intercalated morphology. Figure 4.7b shows that the aggregates themselves appear to be collected together leaving areas of unmodified PMMA matrix, giving the material a two phase appearance. The two phase structure indicates a poor compatibility between the clay and polymer which confirms the findings from the XRD data where the aggregate size also suggests poor compatibility. Due to this poor compatibility, a stronger degree of dispersion is required to force the break up of the clay phase. Further magnification of 4%C15a (Figure 4.7c) shows that in the clay PMMA phase, the aggregates are in fact well dispersed with aggregate sizes ranging from 3-10 and some individual platelets are also clearly visible. The technique used to synthesise PMMA nanocomposites produces good dispersion of clay in the PMMA clay phases. However, further mixing is required in order to achieve good dispersion throughout the whole material in order to achieve a fully exfoliated material.

The TEM images of the 0.1, 0.25, 0.5 and 2%C15a samples can be found in Appendix A.1. These samples also show that the clay is clustered together leaving large areas of unmodified PMMA, giving a similar two phase structure where the size of the clay phase increases with increasing clay content. From the TEM images, t and m can be measured using an image analysis program. By rearranging equation(4.2) the basal spacing or d001 value can be obtained. The calculated d001 values given in Table 4.4 show that the basal spacings are similar for all clay loadings. These spacings are approximately 1 nm smaller than values obtained from XRD and the trend of the initial increase in d001 with clay followed by a plateau between 0.5-4%C15a is no longer seen. Differences in the two values may arise from the measurements taken from TEM which are limited to the resolution of the image and the accuracy of setting the scale bar.

Although there are slight differences between the d001 values obtained from XRD and TEM, the average number of clay platelets in an aggregate are in good agreement and this further emphasises the poor compatibility between PMMA and C15a.

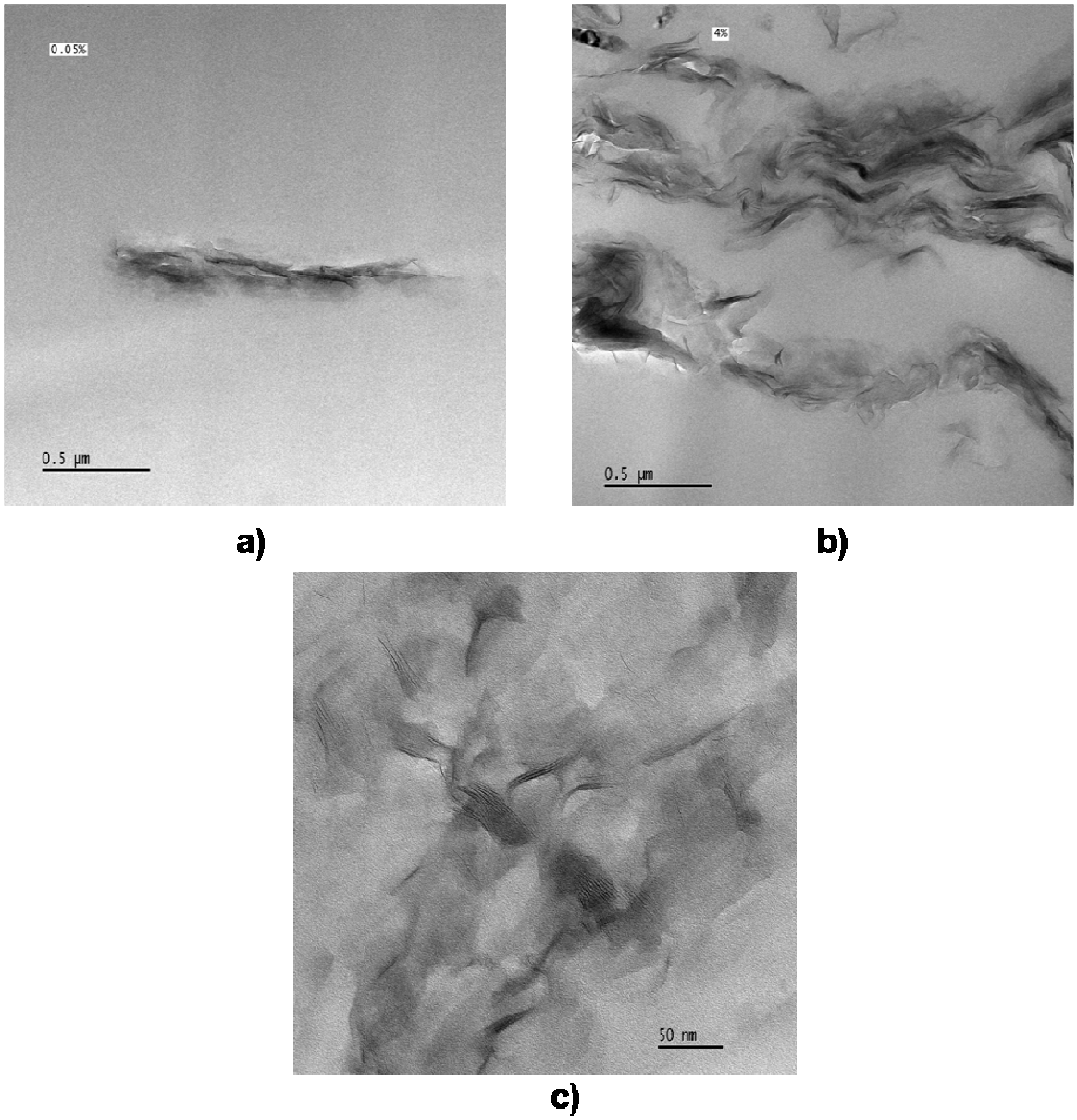

Figure 4.7: TEM images of a) 0.05%C15a, b) 4%C15a on a 0.5 µm scale and c) 4%C15a on a 50 nm scale.

Table 4.4: The basal spacing and aggregate sizes calculated from TEM of PMMA/Cloisite 15a nanocomposites.

	d001 (nm)	***t* (nm)**	***m***
0.05%C15a	2.42	12.91	6
0.1%C15a	2.45	9.32	5
0.25%C15a	2.50	8.10	4
2%C15a	2.37	13.89	7
4%C15a	2.49	14.76	7

4.5 Effect of Clay on the Thermal Properties of PCN

4.5.1 Differential Scanning Calorimetery

Table 4.5 shows the T_g of the resulting PMMA/Cloisite 15a nanocomposites taken from the second heat cycle with a temperature ramp of 20^{o}C per minute between 30-200^{o}C. A selection of DSC traces can be found in Appendix A.2. An increase in T_g for all PCN compared to PMMA was observed suggesting that the clay is beneficial to the physical properties of the matrix. The data shows that the maximum increase in T_g is 3^{o}C and occurs at 0.5 wt% of C15a. At high weight loadings the T_g decreases to 116.4^{o}C (an increase of 1.1^{o}C) and remains constant between 1-4%C15a. The initial increase in T_g for 0.05%C15a suggests that only small quantities of clay are required to produce changes in the physical properties of PCN.

The sample mass and heating rate are both important parameters in running DSC as they can influence the temperature gradient within the sample. Slower heating rates can reduce the temperature gradient within a sample allowing longer time for rearrangements to occur. To investigate the effect of the heating rate upon the T_g of the PCN, DSC measurements were run at the slower heating rate of 5^{o}C per minute. The resulting T_g data is tabulated in Table 4.5. The first observation is the 1-2^{o}C decrease in T_g with the reduction of heating rate. This can be attributed to the lower temperature gradient within the sample caused by a slower heating rate. When comparing values

from the two heating rates, the same trend with respect to the clay loading can be seen. This confirms that the variation of T_g with wt% C15a is real and that it is not a consequence of changes in the temperature gradient.

Table 4.5: T_g for PMMA/Cloisite 15a nanocomposites at heating rates of 5 and 20^{o}C per minute, where Stand dev is the standard deviation of the results.

		Heating rate 20^{o}C per minute		**Heating rate 5^{o}C per minute**	
	% Clay	**Ave T_g (^{o}C)**	**Stand dev**	**Ave T_g (^{o}C)**	**Stand dev**
PMMA	0	115.3	0.2	114.1	0.1
0.05%C15a	0.05	117.7	0.3	115.9	0.3
0.1%C15a	0.1	117.6	0.1	115.4	0.1
0.25%C15a	0.25	117.8	0.1	116.7	0.1
0.5%C15a	0.5	118.4	0.4	116.8	0.2
1%C15a	1	116.5	0.1	114.5	0.3
2%C15a	2	116.4	0.2	114.8	0.2
4%C15a	4	116.5	0.2	114.6	0.4

The trend seen in the T_g maybe related back to the measured basal spacing of the clay. The basal spacing is smaller for 0.05-0.25%C15a samples whereas 1-4%C15a samples have the same slightly larger basal spacing. If changes in T_g are the result of the confinement of the polymer chains within the basal spacing, then a smaller basal spacing would suggest the chains are more tightly confined leading to a higher T_g than those which are more loosely bound. This is what is observed in the PCN samples, 0.05%C15a has a higher T_g than 4%C15a. However if the confinement of the polymer chains is the only factor affecting the T_g then it may be expected that the T_g will increase with increase wt% of clay as a larger proportion of the polymer chains will be partially bound between clay platelets. As this is not the case for the data presented it may suggest that other factors are contributing towards the changes in T_g observed.

Another factor which should be taken into consideration is the effect of the molecular weight upon the T_g. It was seen in Chapter 4.3 that the molecular weight varies with

increasing clay and plateaus above 0.5%C15a. The Flory and Fox model[5] can be used to predict the changes of T_g with respect to molecular weight and is shown in equation(4.3), where $T_{g\infty}$ is the T_g of the polymer at an infinite molecular weight, k is a polymer specific constant and X_n is the number average degree of polymerisation. For PMMA the literature values for $T_{g\infty}$=387 K and k=2902 were taken from reference[5].

$$T_g = T_{g\infty} - \frac{k}{X_n} \qquad (4.3)$$

The predicted T_g for each wt% clay loading was calculated taking into account the degree of polymerisation of each sample. The plot of T_g vs. wt% clay for the PCN along with the predicted values from the Flory and Fox model are shown in Figure 4.8.

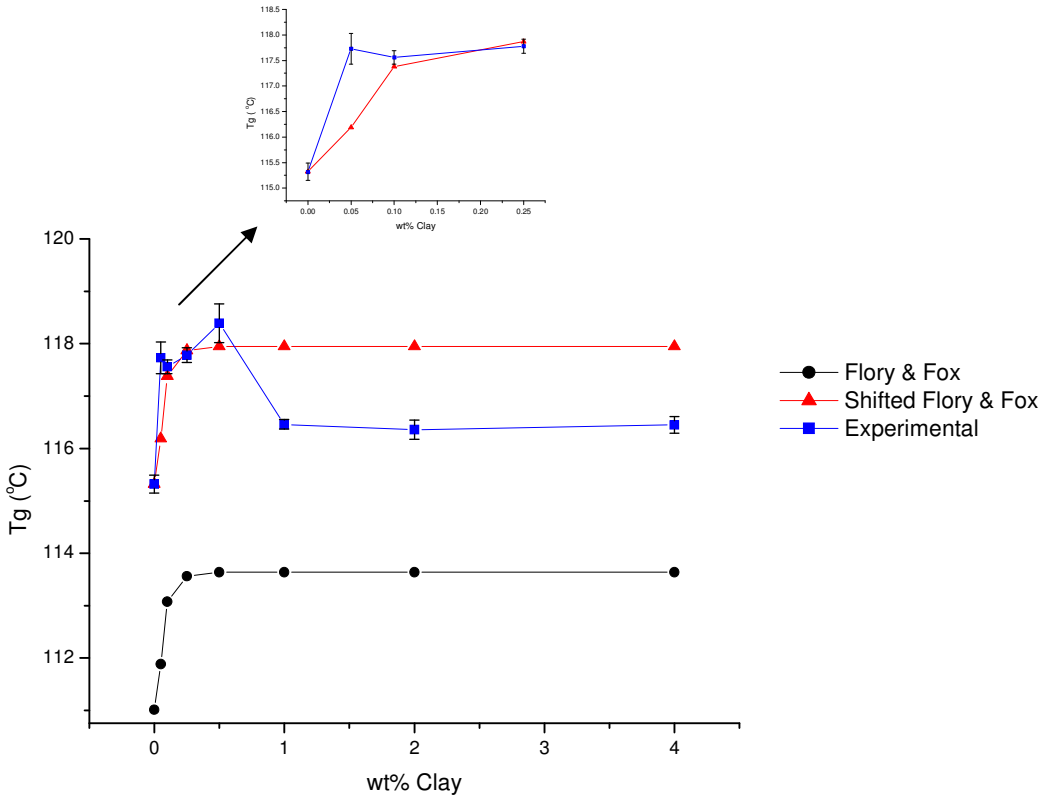

Figure 4.8: Plot of T_g vs wt% showing experimental data and predicted T_g from the Flory and Fox model using the molecular weight of the PCN. The insert shows a close up of the 0-0.25wt% clay region.

The difference between the experimental and predicted values for pure PMMA is believed to be caused by the heating rate used. As the value of T_g obtained is dependent

upon the heating rate then the predicted values obtained from the Flory and Fox model will also depend on the heating rate. This effect is not included in the model and it may be assumed that the effect is included within the constant k. In order to compare the effect of Mw vs. T_g with the experimental data the Flory and Fox model was shifted vertically so that the values for 97 $Kgmol^{-1}$ PMMA agree.

From the shifted Flory and Fox model good agreement between the 0.25-0.5%C15a PCN predicted and experimental values was observed. This suggests that the presence of clay has no direct effect upon the T_g. The 0.05%C15a sample shows a large increase in T_g compared to PMMA and is highlighted in the insert of Figure 4.8. The error bar is smaller than the difference between the experimental and predicted values suggesting that the change is real; although negligible the origin of it is unknown. At higher weight loadings the experimental values fall below the predicted values, indicating the clay is causing a detrimental effect on the T_g. If the Flory and Fox model has accurately predicted the change in T_g with respect to molecular weight then the 1-4%C15a samples fall 1.2^oC lower than the predicted values. This would suggest that the clay is acting as a plasticizer to the PMMA. C15a is organically modified with a dimethy dehydrogenated tallow quaternary ammonium salt, the cations maybe acting as spacers and increasing the free volume within the PCN. The increased free volume would lead to the reduction in the T_g.

4.5.2 Thermogravimetric Analysis

TGA was carried out to investigate the effect of clay on the thermal stability of the material. The PCN were heated from 30 to 500^oC at a rate of 10^oC per minute and the mass loss recorded as a function of temperature. The TGA traces for PMMA, C15a clay and 4%C15a are shown in Figure 4.9. The onset of degradation for C15a clay is lower than that of PMMA and the onset of degradation of 4%C15a lies between that of PMMA and C15a clay. The clay present in the 4%C15a material lowers the onset of degradation due to the less thermally stable organic cations, but above 360^oC the degradation of PMMA and 4%C15a are similar. To gain quantitative measurements the

data was analysed by recording the temperature at which 5, 10, 30, 50 and 70% weight loss had occurred. The results are tabulated in Table 4.6.

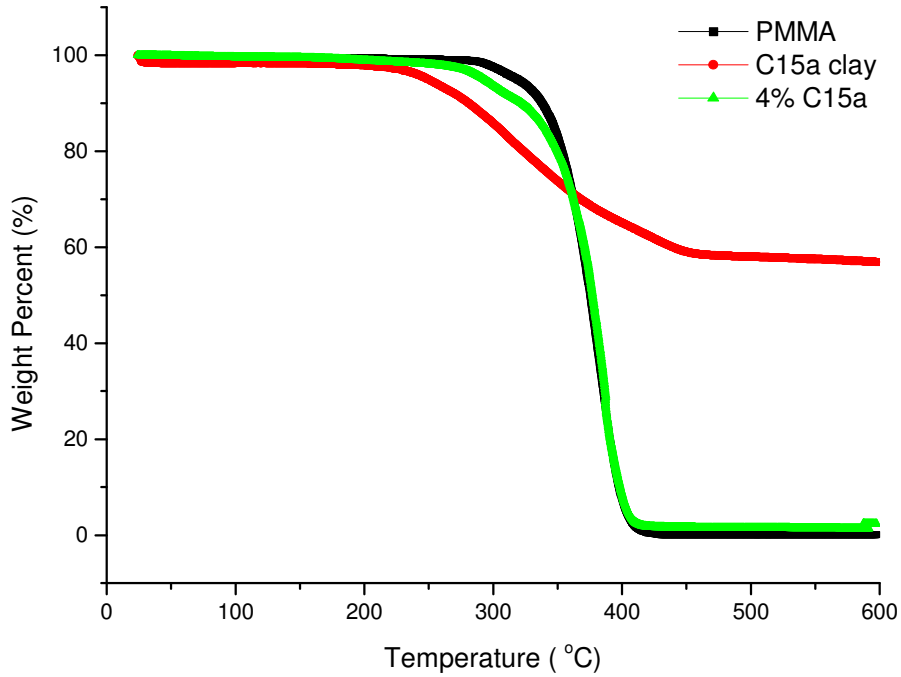

Figure 4.9: TGA traces of PMMA, Cloisite 15a clay and 4%C15a.

Table 4.6: Temperature for 5, 10, 30, 50 and 70% weight loss for PMMA and PMMA/Cloisite 15a nanocomposites.

	Temperature for x% weight loss				
	5% wt loss	**10% wt loss**	**30% wt loss**	**50% wt loss**	**70% wt loss**
PMMA	319	338	362	375	385
0.25%C15a	290	314	353	367	378
0.5%C15a	291	315	358	373	382
1%C15a	293	318	361	376	386
2%C15a	290	316	358	372	382
4%C15a	293	322	363	377	387
C15a clay	250	281	368	-	-

Table 4.6 shows that the temperature at which 5% weight loss occurs is lower for all PMMA/Cloisite 15a nanocomposites compared to PMMA, with a decrease of up to 29°C. This can be expected as 5% weight loss of C15a clay occurs at 250°C, 69°C lower than that of PMMA. As mentioned above the TGA trace of C15a clay confirms the poor thermal properties of the cation which was seen in Figure 4.9.

The temperature at which 5, 10, 30, 50 and 70% weight loss occurs was plotted against wt% clay and is shown in Figure 4.10. By comparing the graphs it can be seen that the PCN show a similar trend at all weight loss percentage with 0.25%C15a occurring at the minimum point. For weight loss greater than 10% there is aproximetly a 10°C increase in temperature going from 0.25%C15a to 4%C15a. It was believed that 4%C15a would show a lower degradation temperature than that of 0.25%C15a as there is a larger percentange of organic cations present. This shows that the degradation of the organic cation is not the only influence on the change in TGA and it is thought that the increase in temperature arises from the hindered diffusion caused by the clay platelets which slows down the release of volatile gases and increases the temperature at which the weight loss occurs. This effect has also been referred to as the labyrinth effect[6].

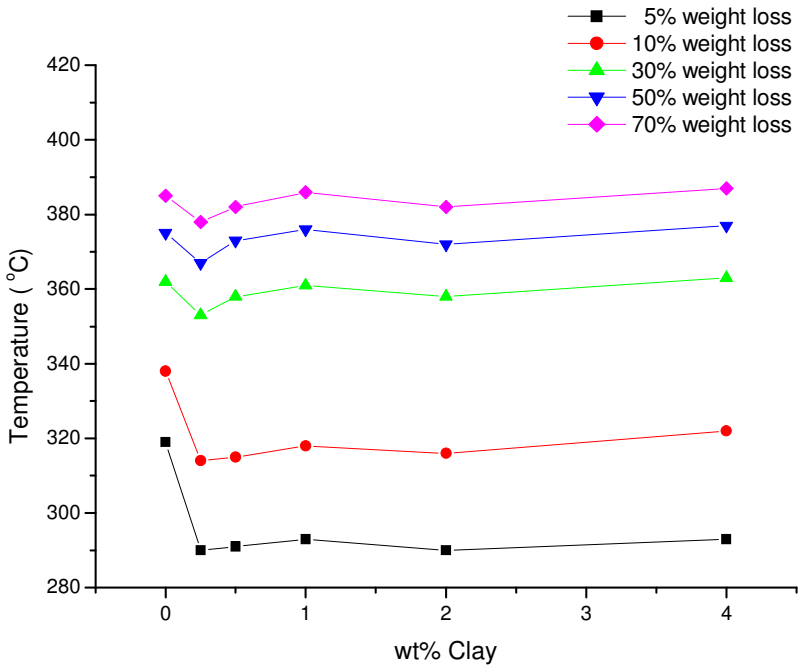

Figure 4.10: Temperature at which 5%, 10%, 30%, 50% and 70% weight loss occurs.

The change of temperature between the PMMA and PCN decreases with increasing percentage weight loss. After the initial decrease in thermal stability due to the cation instability, the weight loss of the PCN must occur slower than that of PMMA for the two materials to show the same thermal stability at higher temperatures. The decrease in the rate of mass loss is caused by the increasing influence of the labyrinth effect of the clay platelets. Above 30% weight loss, the PCN and PMMA exhibit the same thermal stability suggesting that at higher temperatures C15a clay has very little influence on the thermal stability of PMMA.

The degradation of the organic cations present in C15a was investigated using isothermal TGA measurements, where the samples were heated to the desired temperature and held for 30 minutes whilst the mass loss was recorded. Isothermal measurements were carried out on PMMA and 4%C15a at temperatures of 100 and 230^{o}C. The results are shown in Figure 4.11. The gradient of weight loss vs. time gives an indication of rate of weight loss within the sample. At a low temperature (100^{o}C) both PMMA and 4%C15a showed the same rate of weight loss. The initial changes in mass loss could be caused by moisture residing within the sample, and as the weight loss after this point is close to zero for both samples it can be concluded that both these materials are stable at this temperature.

Measurements taken at the processing temperature of PMMA, 230^{o}C, show that the rate of mass loss for 4%C15a is significantly greater than that of PMMA. PMMA was found to have a rate of weight loss of 3.6×10^{-3} wt% per minute, whereas 4%C15a has a rate of weight loss of 6.9×10^{-2} wt% per minute which is approximately 19 times greater than PMMA. This difference arises due to the presence of the cations on the C15a. Degradation of the PMMA/Cloisite 15a nanocomposite at its processing temperature leads to discolouration and weaker physical properties of the material making it less attractive for industrial use.

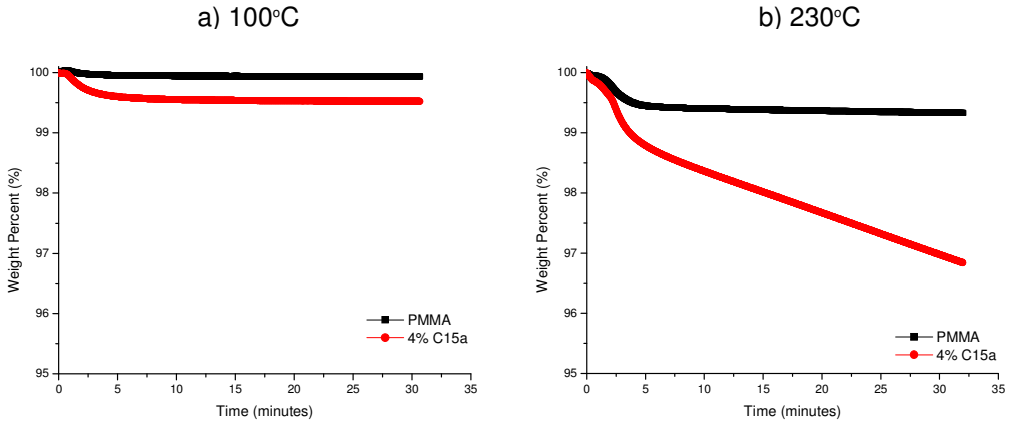

Figure 4.11: Plot of weight loss vs. time for PMMA and 4%C15a at temperatures of 100^{O}C and 230^{O}C.

4.5.3 Micro calorimetry

HRR is the heat release rate which is the rate of mass loss multiplied by the effective heat of combustion. The plot of HRR vs. temperature for C15a, PMMA and 0.1, 0.5 and 4%C15a is given in Figure 4.12. The PMMA trace exhibits two peaks- the lower peak is caused by end initiated depolymerisation from unsaturated chain ends[7] and the higher peak is caused by the random scission of the PMMA chain[7]. The C15a trace shows multiple transitions which will include the degradation of the organic cations and the release of trapped interlayer water molecules. Two important values which can be obtained from these graphs are the maximum HRR and that of T_{max}. T_{max} is the temperature at which the maximum HRR occurs. These values are given in Table 4.7. It can be seen that all PCN have a lower HRR than pure PMMA, with the minimum HRR found for 0.5%C15a (317.14 W.g^{-1}).

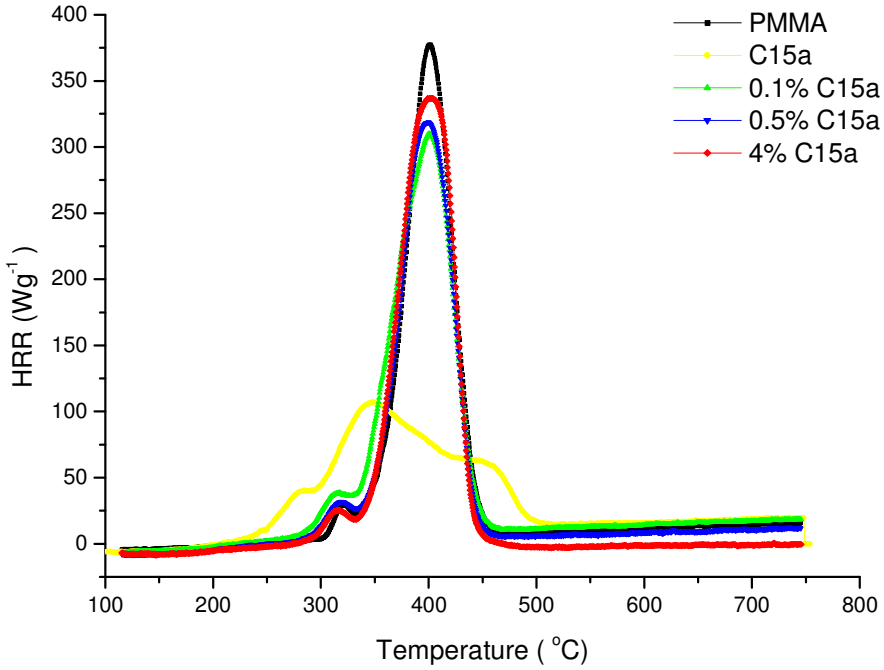

Figure 4.12: Plot of rate of heat release vs. temperature for PMMA, Cloisite 15a clay and 0.1, 0.5 and 4%C15a.

Table 4.7: Experimental and predicted values for T_{max} and rate of heat release for PMMA and PMMA/cloisite 15a nanocomposites.

	Experimental data				RoM data	
	T_{max} (°C)	Stand dev	HRR ($W.g^{-1}$)	Stand dev	T_{max} (°C)	HRR ($W.g^{-1}$)
PMMA	396	7	371	6	396.3	370.9
0.05%C15a	405	3	368	10	396.3	370.8
0.1%C15a	399	2	321	15	396.3	370.6
0.25%C15a	394	6	320	11	396.2	370.2
0.5%C15a	397	3	317	19	396.1	369.6
1%C15a	390	3	347	8	395.9	368.3
2%C15a	391	3	367	22	395.4	365.7
4%C15a	403	2	335	6	394.4	360.4
C15a	348	1	109	4	347.7	109.0

To predict the properties of T_{max} and HRR a rule of mixtures (RoM) approximation was used. RoM combines the physical properties of two materials but it assumes there are no interactions between the two materials. RoM can be seen in equation(4.4) where *f* is the volume fraction of filler, E_m and E_f are the physical properties of the matrix and filler respectively and E_c is the resulting physical property of the composite.

$$E_c = fE_f + (1-f)E_m \qquad \textbf{(4.4)}$$

The HRR as a function of wt% C15a is shown in Figure 4.13, where the red line represents the predicted values obtained using RoM. There is a 20-50 $W.g^{-1}$ decrease in HRR between 0.1-1%C15a from the predicted values. Any decrease seen in the HRR is beneficial as it indicates a lower rate of mass loss and therefore a more thermally stable material. RoM predicts that the HRR should decrease slightly (>2 $W.g^{-1}$) in this region due to the lower HRR of C15a, but it is smaller than the rate of heat release observed. As the heat of combustion was kept constant, the change in HRR is caused by a decrease in the rate of mass loss. In Chapter 3.2 several factors for increased thermal stability were discussed, these included barrier properties[6], char formation[8] and alternate degradation mechanism[9]. An alternative degradation mechanism was investigated by Jang et al[10] who observed no difference in the evolved gas during the degradation of PMMA and PMMA/clay nanocomposites. Both materials underwent β chain scission to produce MMA monomer. This is to be expected as the PMMA radicals produced are not stable enough to form alternate degradation products. Hence the differences observed are due to the hindered diffusion of the volatile gasses, caused by the clay platelets acting as physical barriers.

The values for T_{max} are given in Table 4.7 along with their standard deviation. T_{max} of the PCN all occur at a similar temperature to that of PMMA confirming that C15a does not affect the degradation mechanism of PMMA. This was observed in the TGA data where despite the initial mass loss caused by the clay, the bulk of the mass loss took place at the same temperature as that of PMMA.

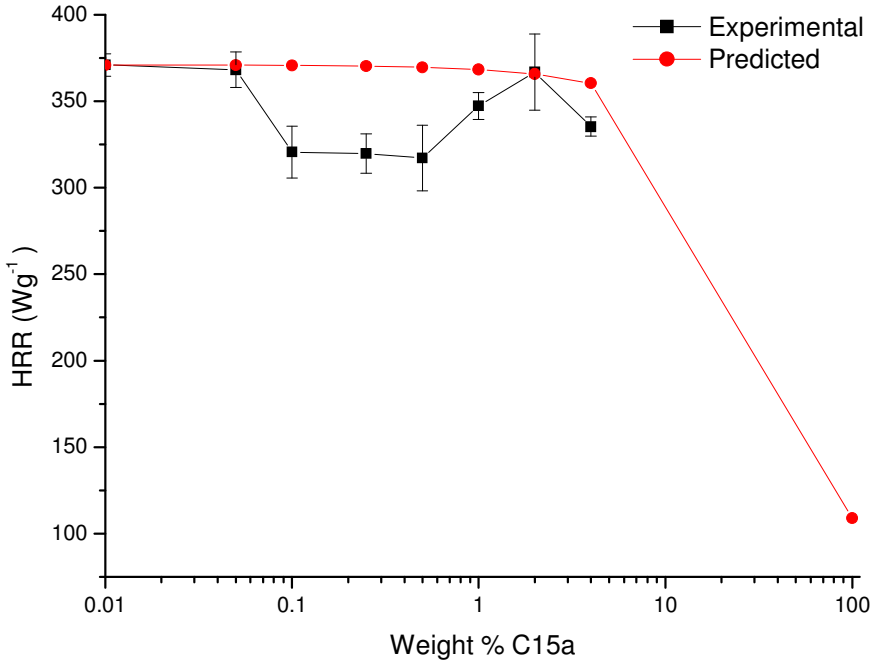

Figure 4.13: Plot of rate of heat release vs. wt% clay along with the predicted values from RoM.

4.6 Effect of Clay on the Rheology of PCN

The linear rheology curves are shown in Figure 4.14. There is little difference between the PCNs containing 0.5, 1, 2 and 4 wt% clay. However 0.1 and 0.05 wt% clearly shows different behaviour from those of the higher clay loading, but even for these low clay loadings there is an increase in *G'* and *G''* compared to unfilled PMMA. The additional rheology curves of 0.5, 1 and 2%C15a can be found in Appendix A.3-5.

The high frequency range of the rheology data for all the samples overlap and the high frequency crossover point is referred to as the entangled rouse relaxation time. This crossover and subsequent higher frequency data points are the result of relaxations on a sub-chain level, and are unaffected by the molecular weight. The crossover of *G'* and *G''* in the lower frequency region corresponds to the reptation relaxation time. Figure 4.14 shows the increase in τ_{rep} upon the addition of clay which may have been caused by the restriction of reptation due to the clay or by the increase in molecular weight.

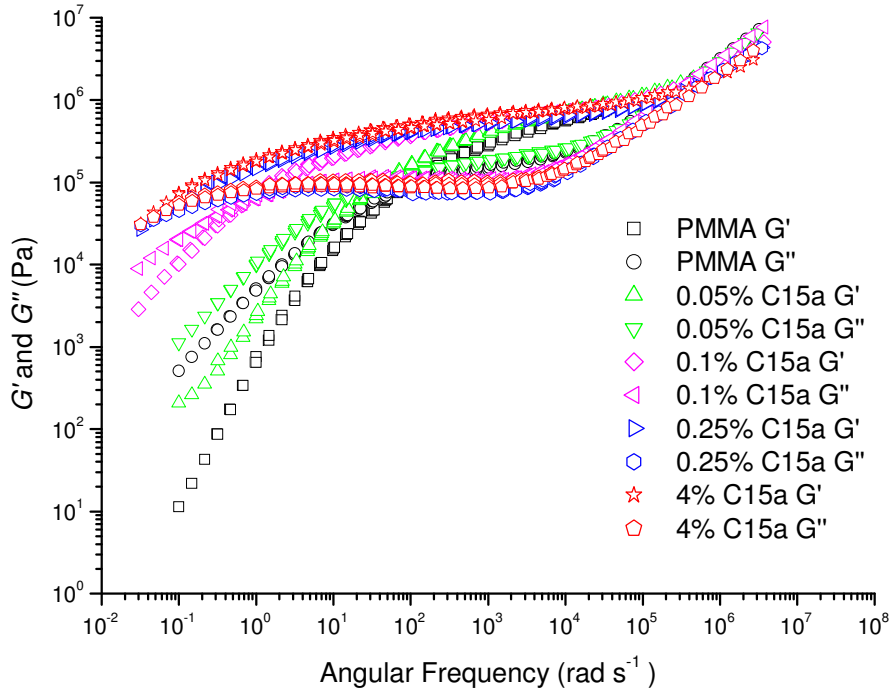

Figure 4.14: Oscillatory shear rheology plots of PMMA and PMMA/Cloisite 15a nanocomposites after TTS has been applied. A reference temperature of 230^{o}C was used.

The Predicted rheological data can be obtained to distinguish between the two possible causes suggested for the observed changes in the rheology. In order to model the rheology of polymers produced by free radical polymerisation the polydispersity of the material needs to be considered. Van Ruymbeke et al[11] predicted the rheology for monodisperse, bidisperse and polydisperse polystyrene samples with the use of experimentally determined molecular weight distribution obtained by size exclusion chromatography. Van Ruymbeke found that a model by des Cloizeaux[12] provided the best fit to the experimental data. This model is based on a time dependent process, with a relaxation function given by,

$$F_{TDD}(t,M)=\frac{8}{\pi^2}\sum_{n=0}^{\infty}\frac{1}{(2n+1)}\exp\left\{-(2n+1)^2\left[\frac{t}{\tau_{rep}(M)}+\frac{\tau_i(M)}{\tau_{rep}(M)}\left(\sum_{n=1}^{\infty}\left[\frac{1-\exp\left(-n^2\frac{t}{\tau_i(M)}\right)}{n^2}\right]\right)\right]\right\} \quad (4.5)$$

where M is the molecular weight, t is the time, τ_{rep} is the reptation relaxation time and τ_i is an intermediate relaxation time which lies between τ_{rep} and the Rouse relaxation time

(τ_R)[12]. In order to include the effects of polydispersity, the relaxation function would need to be calculated for a number of different values of *M* and the relaxation modulus *G(t)* can be then obtained using the double reptation concept as a mixing rule. Double reptation was derived independently by des Cloizeaux[13] and Tsenoglou[14] as shown in equation(4.6), where *w(M)* is equal to *W(M)/dlog(M)* and *dW(M)* is the weight fraction of chains with molecular weight below *M*, G_N^o is the plateau modulus and β is a constant typically assumed to have the value of 2.0[13-15], although some studies have shown that for highly entangled melts the value of β may in fact be larger[11, 16].

$$G_{rep}(t)=G_N^0\left(\int_{\log M_e}^{\infty}\left(F(t,M)w(M)d\log M\right)\right)^{\beta} \qquad (4.6)$$

The Rouse region is modelled using the Rouse relaxation for an entangled polymer melt as shown in equation(4.7) in a similar fashion to van Ruymbeke et al[11]. The final issue to consider is the calculation of the storage (*G'*) and loss (*G''*) modulus from the relaxation function. The usual method of calculating *G'* and *G''* is by carrying out a Fourier transform, but in this case Fourier transform would be computationally intensive and unnecessary, therefore the Schwarzl relation[17] is used.

$$G_{Rouse}(t)=G_N^0\sum_{p=N}^{\infty}\frac{1}{N}\exp\left(\frac{-p^2t}{\tau_R(M)}\right)+\frac{1}{3}G_N^0\sum_{p=1}^{N}\frac{1}{N}\exp\left(\frac{-p^2t}{\tau_R(M)}\right) \qquad (4.7)$$

The model by des Cloizeaux[12] as used by van Ruymbeke et al[11] was used to predict the rheology of the polymer clay nanocomposites based on their molecular weight distributions. The three relaxation times (τ_{rep}, τ_i, τ_R) are related to molecular weight by,

$$\begin{aligned}\tau_{rep} &= K_{rep}M^3\\ \tau_i &= K_iM^2\\ \tau_R &= K_RM^2\end{aligned} \qquad (4.8)$$

where K_{rep}, K_i and K_R are all constants and for PMMA at 230°C were found to take on the following values; K_{rep} = 8.0×10^{-17} sDa^{-3}, K_i = 6.6×10^{-13} sDa^{-2} and K_R = 8.6×10^{-13} sDa^{-2}.

The other parameter required in the model is the plateau modulus G_N^0. The literature values for M_e, the entanglement molecular weight that is related to the plateau modulus,

range from 5000 to 10000 g.mol^{-1} [12, 15, 18, 19] for PMMA. Carrot et al[19] suggested such variation in M_e and G_N^0 was due to thermal variations and molecular weight differences. Due to these factors the G_N^0 value used was found from our experimental data for PMMA to have a value of 7.6×10^5 Pa.

The predicted rheology data for PMMA is shown in Figure 4.15. The model shows good agreement with the experimental data especially around the plateau region with the reptation crossover points aligning. The model starts to fail in the lower terminal region and this is believed to be caused by the failure of the Schwarzl relation[17]. The model was also applied to the 4%C15a and 0.1%C15a samples. All the parameters were kept constant but the molecular weight data of the respective samples, obtained via SEC, was fed into the model. The comparison between the model and experimental data for 4%C15a and 0.1%C15a can be seen in Figure 4.16 and Figure 4.17 respectively.

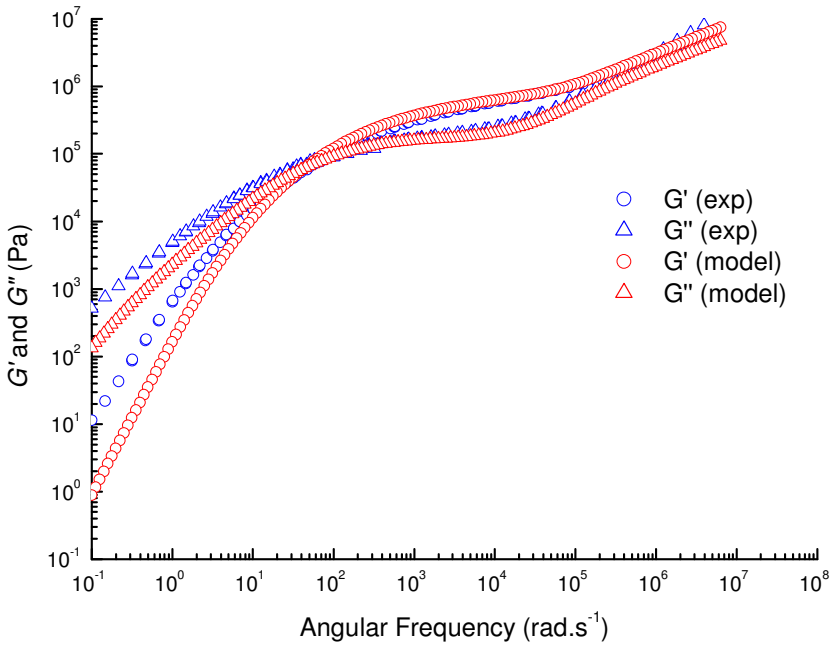

Figure 4.15: Comparison of model (red) and experimental (blue) rheology data for PMMA.

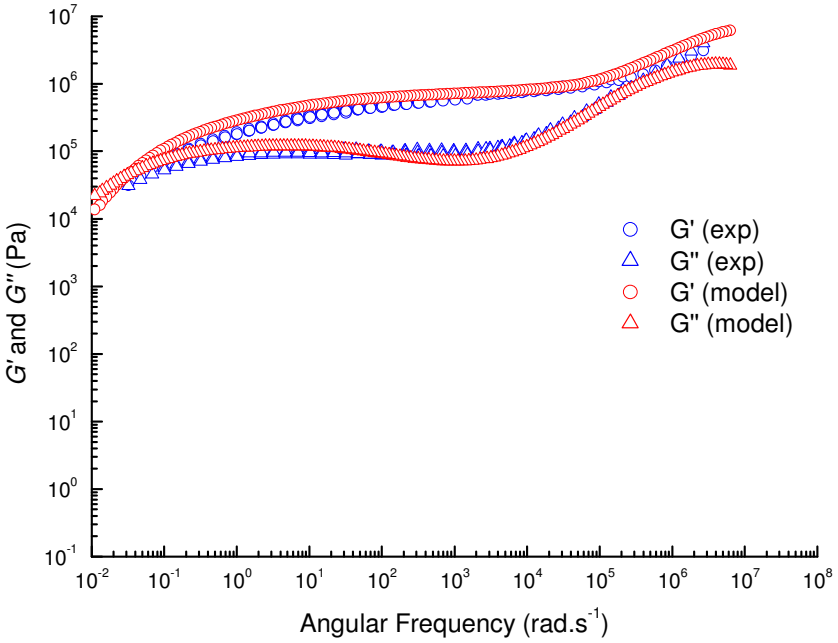

Figure 4.16: Comparison of model (red) and experimental (blue) rheology data for 4%C15a.

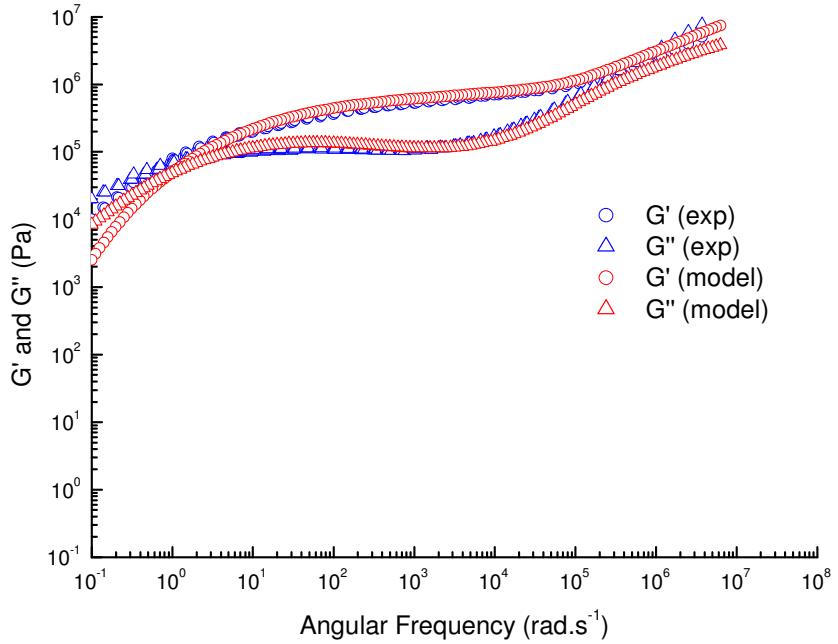

Figure 4.17: Comparison of model (red) and experimental (blue) rheology data for 0.1%C15a.

Again the model shows good agreement with 0.1 and 4% experimental data. For the 4%C15a the model shows a large plateau region and the long reptation relaxation time which was present in both the experimental data. The value of the modulus is in good agreement with the experimental; however the theoretical modulus starts to fall away at the low frequency end which is again believed to be caused by the failure of the Schwarzl relation. As there are no significant differences between the experimental and predicted rheological data it can be concluded that the changes in the rheological properties upon addition of C15a clay can be justified by the changes in *Mw* and PDI alone and that the clay is not contributing to the changes in the rheology seen between PMMA and the PMMA C15a samples.

4.7 Alignment of Clay Platelets during Processing

Suspension polymerisation results in small beads of polymer and for these to be used commercially they need to be processed in order to produce the required shape needed for a specific task. One of the most common methods for processing plastics is injection moulding. Injection moulding involves the injection of a molten polymer into a mould usually under high pressure. This process induces stress on the material which in turn can affect the morphology of the PCN through the alignment of the clay with the flow direction.

Small angle x-ray scattering (SAXS) was carried out on the PMMA/Cloisite 15a nanocomposites in order to investigate the effect of processing on the alignment of clay platelets. The PCN and PMMA were processed using a Battenfeld Microsystem 50 micro moulding instrument from Bradford University. The materials were passed through a fixed extruder at a temperature of 230^{o}C and injected into a mould held at a temperature of 80^{o}C producing samples of size 20 mm in length, 0.5 mm in thickness and 1.5 mm wide (Figure 4.18). Measurements were taken at four different points along the sample at 4 mm intervals with position 1 being closest to the injection gate as illustrated in Figure 4.18.

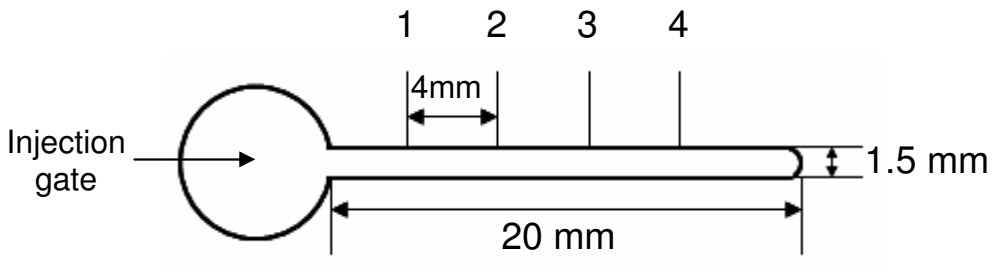

Figure 4.18: Illustration of the dimensions of injection moulded sample.

The experiments were carried out on the DUBBLE beam line at the European Synchrotron Radiation Facility (ESRF) in Grenoble. A sample to detector distance of 3.7 m, and an x-ray beam of wavelength of 0.83 Å was used. The main advantage of using synchrotron radiation as the x-ray source is that the intensity of the x-rays received are greater than those received from conventional x-ray sources. This decreases the exposure time required during the experiment.

SAXS measurements were first carried out on heat pressed PCN to obtain the basal spacing prior to injection moulding as shown in Figure 4.19. The scattering pattern of heat pressed PCN shows two concentric circles, the outer circle is the scattering from the clay and corresponds to a length scale of 7.9 nm. This peak corresponds to the second scattering peak of the clay or the d002 spacing and relates to a basal spacing of 3.95 nm, 0.25 nm larger than the XRD measurement. The concentric circle shows that the scattering is isotropic and that there is no orientation of the clay. The inner scattering ring is caused by both the amorphous PMMA and the beam stop. The confirmation of this is seen in the scattering of PMMA (Figure 4.19) as the inner scattering ring can still be seen.

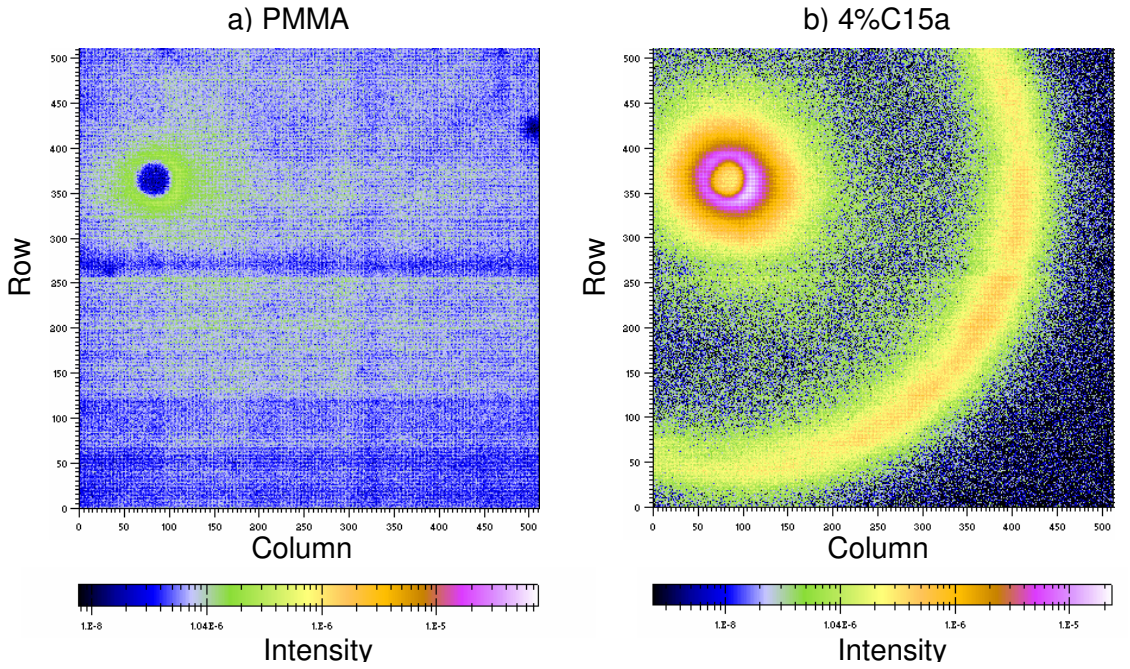

Figure 4.19: SAXS scattering patterns of heat pressed a) PMMA and b) 4%C15a.

After injection moulding the concentric circles are no longer visible and the scattering occurs only in the horizontal plane (Figure 4.20). The anisotropy or orientation indicates that the basal spacing is only present along the horizontal direction meaning that the clay is aligned with the direction of flow (vertical direction). This is illustrated in Figure 4.21. A varying injection speed between 50-800 mm per second was used in processing 4%C15a in order to obtain information on the effect of injection speed on the alignment of the clay. From the scattering patterns of 4%C15a with injection speeds of 200 and 800 mm per second, figures a and b respectively, it can be observed that the scattering from 800 mm per second occurs over a larger area than that of the scattering of 200 mm per second. The width of the peak is an indication of the degree of anisotropy within the material. A narrow full width half maximum (FWHM) indicates a high level of anisotropy as the basal spacing occurs in one direction and conversely a large FWHM is an indication of a larger degree of isotropy. As the clay loading in the PCN is decreased the intensity of the scattering due to the basal spacing becomes weaker as seen in Figure 4.20c. The peak intensity decreases with lower clay loadings and it becomes difficult to obtain accurate measurements unless a larger exposure time is used.

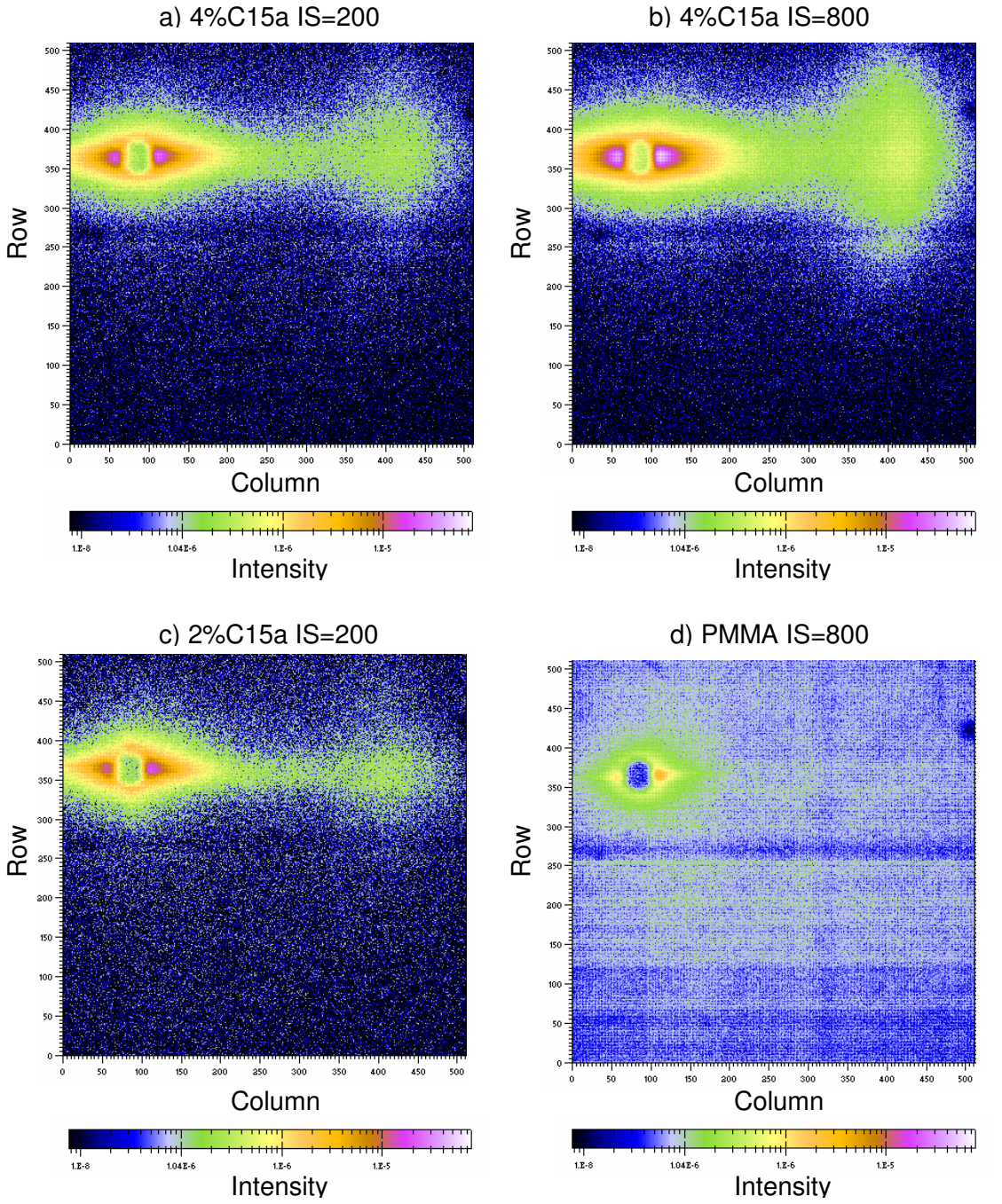

Figure 4.20: SAXS scattering of injection moulded samples at position 3 for a) 4%C15a injection speed of 200 mm per second, b) 4%C15a injection speed of 800 mm per second, c) 2%C15a injection speed of 200 mm per second and d) PMMA injection speed of 800 mm per second

The basal spacing was calculated by radial averaging between -90 and 90° with the beam stop taken as the centre as shown in Figure 4.22. A typical result is shown in Figure 4.23, and it can be seen that the second peak is weak compared to the amorphous scattering of the PMMA. The maximum of the second peak corresponds to the basal spacing of the clay. To obtain the width and hence the extent of anisotropy of the basal spacing the data at a distance corresponding to the basal spacing is plotted against the corresponding angle θ as shown in Figure 4.24, and a value for the FWHM was obtained via Gaussian fit to the experimental data. Equation(4.9) displays the Gaussian equation used to obtain the fit where, y_o is the offset in the y direction, x_c and y_c are the coordinate of the peak centre, A is the area of the peak and w is the width of the peak. The width is related to FWHM by a constant ($1/\sqrt{\ln 4}$) and as the relation is constant for all samples, the value of w along with its corresponding error will be used to assess the peak width. An example of a typical Gaussian fit is shown in Figure 4.24, the Gaussian distribution produces a good fit to the experimental data. The symmetry of the distribution of the angle of orientation of the clay suggests that the disordering occurs equally in all directions.

$$y_C = y_O + \frac{A}{w\sqrt{\pi/2}}\, e^{\left(\frac{-2(x-x_C)^2}{w^2}\right)} \qquad \textbf{(4.9)}$$

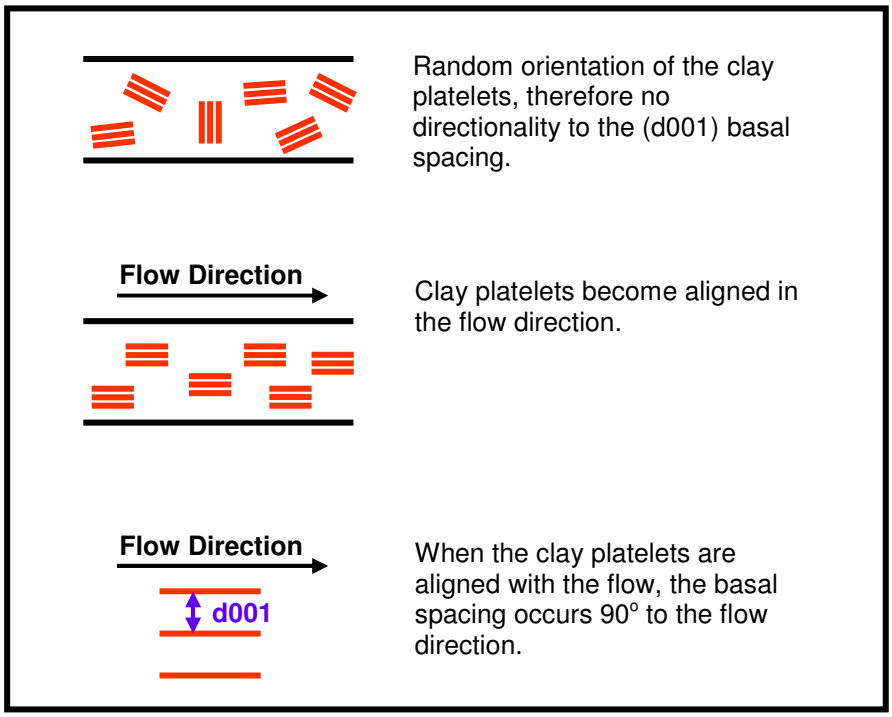

Figure 4.21: Alignment of clay platelets with the flow direction.

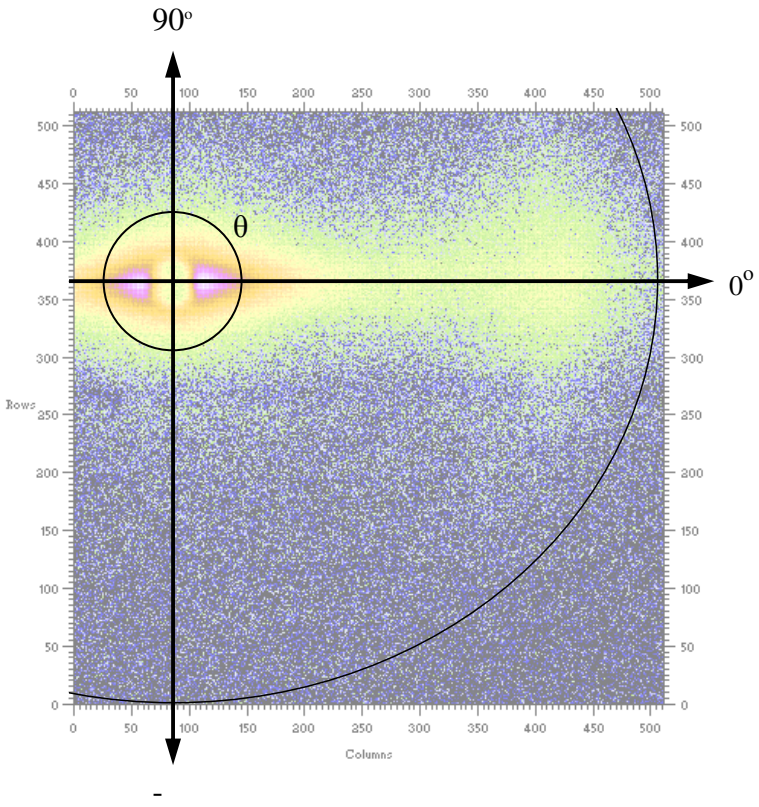

Figure 4.22: Illustration of SAXS scattering axis.

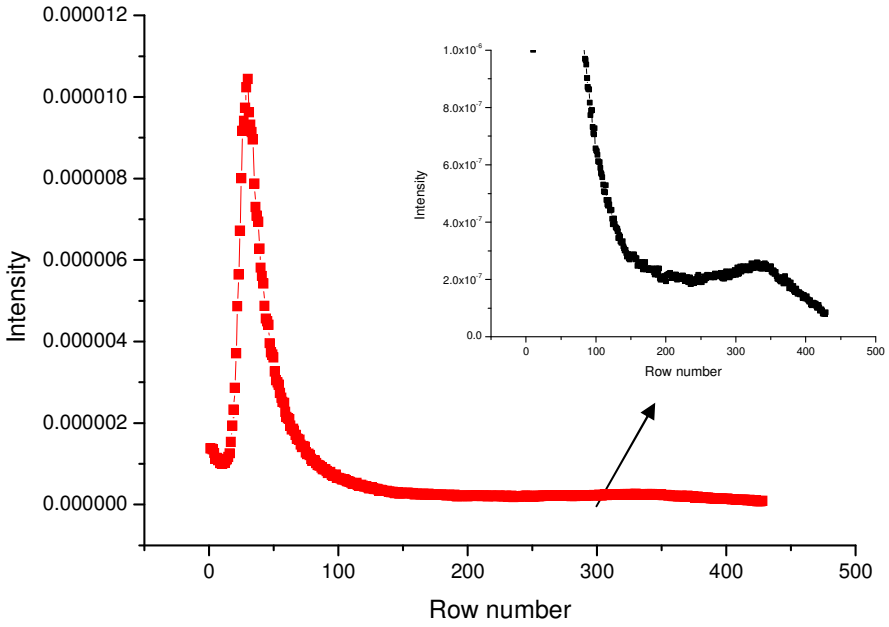

Figure 4.23: Radial average data for 4%C15a at an injection speed of 200 mm per second (position 3). The insert is set at a smaller scale showing the weak basal spacing peak.

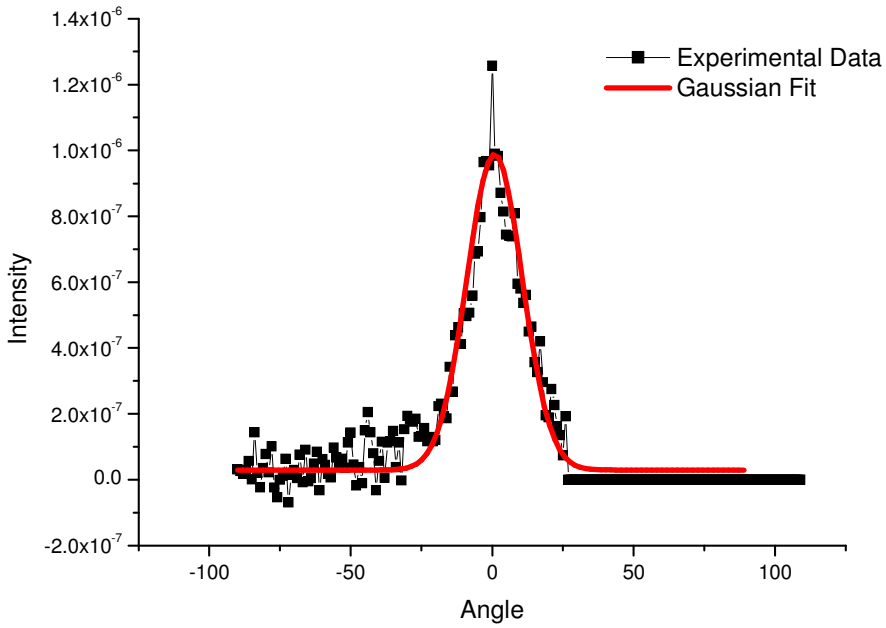

Figure 4.24: Gaussian fit to the basal spacing peak of 4%C15a at an injection speed of 200 mm per second (position 3)

The calculated FWHM for 4%C15a along with their associated errors are plotted in Figure 4.25. As we move away from the injection gate (move from position 1-4) the width of the peak increases from 12.6° – 19.3° and indicates that the clay loses anisotropy. The force applied to the material during the injection process will be at its strongest at the injection gate and as the material moves into the mould, resistance from the walls will reduce the force giving the polymer a greater chance of relaxation as the distance from the injection gate is increased. The relaxation of the PMMA chains will allow the clay platelets to adopt a more disordered orientation giving rise to the decrease in anisotropy as the distance from the injection gate increases.

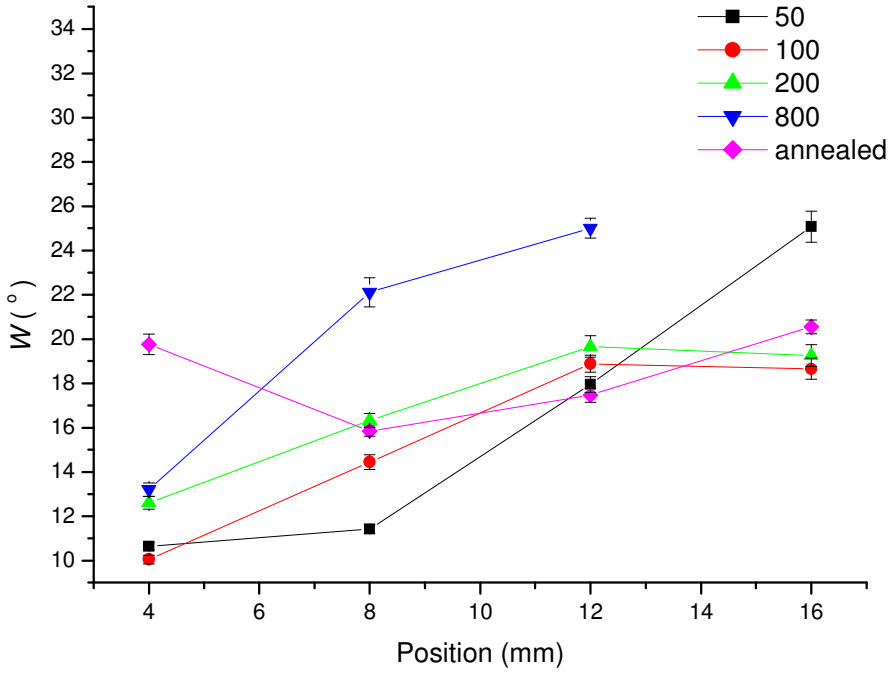

Figure 4.25: Graph showing the width of the basal spacing peak with respect to the position along the 4%C15a sample. The legend shows the different injection speeds (mm per second).

By increasing the injection speed the peak width increased showing a decrease in the degree of orientation. It was initially thought that an increase in injection speed would increase the extent of anisotropy as a higher injection speed would lead to a large injection force and a quicker injection time (less time for relaxation). From Chapter 4.8 the rheology data showed that at 230°C 4%C15a still have a large reptation time making

the material melt stiff at this temperature. The high viscosity of the material means that either a very large force or a smaller force applied for a longer period of time is required to orientate the clay platelets. The decrease in orientation with increasing injection speed leads to the conclusion that due to the high viscosity there is insufficient time to allow the platelets to reach the same extent of orientation reached at lower injection speeds.

4%C15a samples were annealed at 150^{o}C for 50 minutes inside the injection mould to see if the anisotropy can be removed. The changes in the peak width with position is plotted in Figure 4.25. The data shows that an average degree of anisotropy has been reached along the length of the sample, although a large extent of orientation can still be observed. The annealing of the samples will allow the PMMA chains to relax allowing the clay platelets the freedom to realign; the remaining anisotropy can be a result of the PMMA chains not fully relaxing. As seen from the rheology data in Chapter 4.8 the PCN have large relaxation times due to their increased molecular weight, so the time the samples were annealed may not have been long enough to fully relax the samples at that temperature. For example the reptation relaxation time for 4%C15a at 230^{o}C is greater than 30 minutes, however if the temperature was dropped to 150^{o}C the relaxation time for this material would be greater than 707 hours according to the principle of time temperature superposition. Another possible reason for the remaining anisotropy is the insufficient degree of interaction between the clay and PMMA chains. As the clay platelets are not physically attached to the polymer chains it may be possible for the polymer chains to relax around the clay platelets leaving behind a large degree of anisotropy. If there was tethering or a degree of interaction between the clay and the PMMA chains then a greater extent of isotropy may be expected.

4.8 Conclusion

A series of polymer clay nanocomposites (PCN) were prepared from poly(methyl methacrylate) (PMMA) and an organically modified clay, Cloisite 15a using an in-situ suspension polymerisation technique. By increasing the amount of Cloisite 15a present in the suspension polymerisation an increase in the molecular weight of the PMMA

matrix was observed and the molecular weight was found to plateau with a value of approximately 800000 $g.mol^{-1}$ with loadings of > 0.5 wt% of Cloisite 15a. The polymerisation of the matrix PMMA carried out in the absence of CTA produced similar molecular weights suggesting that the CTA had been made "inactive" during the polymerisation. The cause of the increase in the PMMA molecular weight is reaction of the CTA with the Lewis acid sites situated on the rim of the clay. Above 0.5 wt% clay there is sufficient clay to react with all the CTA resulting in the plateauing of molecular weight. On closer inspection of the "plateau" region (Figure 4.4) a slight increase in the molecular weight was seen which is possibly caused by the termination of the PMMA chains by the clay.

XRD measurements showed an increase of 0.55 nm of the basal spacing for 1-4%C15a compared to C15a clay showing that an intercalated morphology has been achieved. Also through the analysis of the d001 peak broadening the average number of clay platelets in an aggregate was obtained. The aggregate size was found to be approximately double that of C15a clay confirming that dispersion within the PMMA matrix is unfavourable. The XRD data was found to be in good agreement with the TEM images.

The TEM showed a good degree of dispersion was obtained during the suspension polymerisation process, although there are still regions where no clay is present which is preventing the formation of percolated networks. The shifting of the reptation time to lower frequencies as seen by oscillatory shear rheology might have been an indication of a reinforcing effect caused by the formation of a network of clay platelets. However modelling the rheology data for the matrix PMMA of the PCN and including the polydispersity effects showed a good agreement between the predicted rheology and experimental data. This agreement demonstrated that the shift in the reptation time is caused by changes in the molecular weight of PMMA matrix rather than the partial formation of a percolated network in the PCN.

The changes in molecular weight also played a part in the changes in T_g observed. The PCN showed a 1-3^oC increase in T_g compared to PMMA, but through the use of the

Flory and Fox model it was seen that an increase in T_g was expected due to the increase in molecular weight of the matrix PMMA. TGA data showed a lower onset temperature due to the presence of the lower thermal stability of the organic cation. Despite the lower onset the degradation of the cation was not seen to have a detrimental effect on the bulk of the degradation process. Isothermal TGA measurements also highlighted a potential problem in processing this material as a significant mass loss of 4%C15a was observed at the processing temperature (230^{o}C) of PMMA. Potential consequences of processing PMMA/Cloisite 15a nanocomposites were also seen from the SAXS data of micromoulded 4%C15a. SAXS measurements showed that the clay platelets orientated along the direction of the flow, adding directionality to the physical properties of the material. Although alignment imposes limits on the range of applications of the material, it is believed that alignment of the clay can be used to give enhanced barrier properties and mechanical strength along one direction.

Although PMMA/Cloisite 15a nanocomposites showed no beneficial properties over PMMA, this work highlights the need for thorough characterisation of PCN. This work showed that possible side reactions during the polymerisation of the matrix polymer caused by the reactivity of the clays should be considered when contemplating the preparation of PCNs with the clays present during the polymerisation. This work also demonstrates the need for thorough characterisation of such PCNs. Rheology is often used to suggest the positive effects of clays in nanocomposites. Whilst we had anticipated a demonstrable benefit from the inclusion of clay into the PMMA matrix, the careful combination of size exclusion chromatography, theoretical and experimental rheology has shown unequivocally that in this instance the clays are not responsible for the changes in rheology.

4.9 Reference

1. Georgiadou, S.; Brooks, B. W. *Chemical Engineering Science* **2005,** 60, (24), 7137-7152.
2. Solomon, D. H.; Swift, J. D. *Journal of Applied Polymer Science* **1967,** 11, (12), 2567-&.
3. Cullity, B. D.; Stock, S. R., *Elements of X-ray Diffraction*. 3 ed.; Prentice Hall: 2001.
4. Tabtiang, A.; Lumlong, S.; Venables, R. A. *European Polymer Journal* **2000,** 36, (12), 2559-2568.
5. Odriscoll, K.; Sanayei, R. A. *Macromolecules* **1991,** 24, (15), 4479-4480.

6. Zanetti, M.; Camino, G.; Reichert, P.; Mulhaupt, R. *Macromolecular Rapid Communications* **2001,** 22, (3), 176-180.
7. Kashiwagi, T.; Inaba, A.; Brown, J. E.; Hatada, K.; Kitayama, T.; Masuda, E. *Macromolecules* **1986,** 19, (8), 2160-2168.
8. Gilman, J. W. *Applied Clay Science* **1999,** 15, (1-2), 31-49.
9. Jang, B. N.; Wilkie, C. A. *Polymer* **2005,** 46, (9), 2933-2942.
10. Jang, B. N.; Costache, M.; Wilkie, C. A. *Polymer* **2005,** 46, (24), 10678-10687.
11. van Ruymbeke, E.; Keunings, R.; Stephenne, V.; Hagenaars, A.; Bailly, C. *Macromolecules* **2002,** 35, (7), 2689-2699.
12. Cloizeaux, J. D. *Macromolecules* **1992,** 25, (2), 835-841.
13. Descloizeaux, J. *Europhysics Letters* **1988,** 5, (5), 437-442.
14. Tsenoglou, C. *Macromolecules* **1991,** 24, (8), 1762-1767.
15. Leonardi, F.; Majeste, J. C.; Allal, A.; Marin, G. *Journal of Rheology* **2000,** 44, (4), 675-692.
16. den Doelder, J. *Rheologica Acta* **2006,** 46, (2), 195-210.
17. Schwarzl, F. R. *Rheologica Acta* **1971,** 10, 166.
18. Wu, S. *Journal of Polymer Science Part B-Polymer Physics* **1989,** 27, (4), 723-741.
19. Carrot, C.; Guillet, J. *Journal of Rheology* **1997,** 41, (5), 1203-1220.

Chapter 5 PMMA/Laponite RD Nanocomposites

5.1 Experimental

In this chapter, the synthesis using Laponite RD clay (purchased from southern clay) will be discussed. Laponite RD (LRD) is a synthetic clay so unlike the natural clay Cloisite 15a, control over the chemical composition and particle size is achieved. This means that there are fewer impurities present to cause the discolouration of the clay, giving Laponite RD a white appearance. Laponite RD is also smaller in size than Cloisite 15a with a platelet diameter of ~25 nm compared to ~2000 nm for Cloisite 15a. The surface of the Cloisite 15a clay platelets was organically modified with dimethyl dehydrogenated tallow quaternary ammonium salt, whereas Laponite RD is unmodified and the negative surface charge is neutralised by sodium cations (Na^+). Organic modification of the clay is believed to promote mixing in the organic phase and helps to increase the basal spacing. It is known that unmodified Laponite RD can be fully exfoliated in water leaving a high clarity solution[1] and it is hoped that the exfoliation can be maintained during the polymerisation procedure.

PMMA/Laponite RD nanocomposites are synthesised in-situ using a free radical suspension polymerisation technique. The synthetic method used to produce the PCN was previously described in Chapter 4.1, with pre dispersion carried out in deionised water rather than the MMA phase. PMMA nanocomposites containing 0.05, 0.25, 0.5 and 1%LRD were synthesised.

5.2 Effect of Laponite on Suspension Polymerisation

From the comparison of the dried suspension beads, it was noted that the PMMA/LRD nanocomposites appeared to have a smaller particle size than that of unfilled PMMA. To quantify this difference the particle sizes were measured using a Beckman Coulter LS 13 320 Laser Diffraction Particle Analyzer. The measurements were carried out in water and a refractive index of 1.49 for PMMA was used[2]. The particle distribution for 1%LRD is shown in Figure 5.1. There are two different methods of analysing the data. The first is the volume percent, which is the volume of particles of size x as a percentage of the total volume (as shown in black on the graph). The second method is the number percent which is the number of particles of size x as a percentage of the total number of particles (as shown in red on the graph).

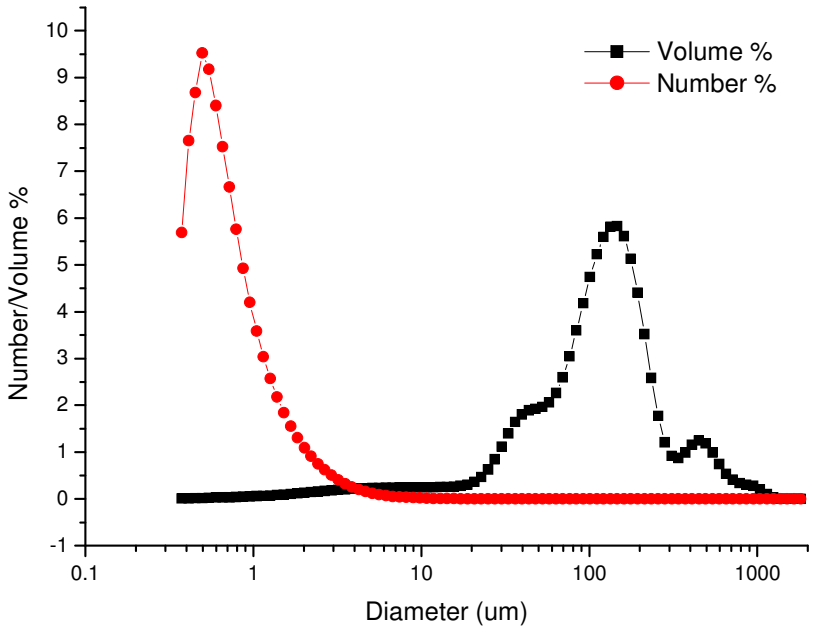

Figure 5.1: Graph illustrating the difference in number and volume% for 1%LRD.

The difference between the two values indicates that there are relatively few particles of large diameter which consequently take up a larger percentage volume than the smaller diameter particles. The number percentage data shows that there are a large number of particles with only a small diameter, but due to their small size only make up a small

percentage of the total volume. It is also interesting to note that the volume percentage data shows a multi mode distribution.

Table 5.1 shows both the volume and number percent of particle size for PMMA and PMMA/Laponite RD nanocomposites. Measurements from both volume and number percent have a large standard deviation associated with their values indicating that a wide particle size distribution is present in all samples. The samples are usually sieved (or separated) before they are used for industrial applications to ensure a uniform particle size. 0.25 and 0.5%LRD exhibit a similar particle size, but despite this there appears to be a decrease in particle size with increasing wt% clay. This trend is present in both the number and volume percentage data. From volume percent, PMMA has an average particle diameter of 777 μm and 1%LRD has an average particle size of 170 μm, 607 μm less than PMMA. Particle size in suspension polymerisation can be affected by monomer concentration, surfactant levels and stirrer speed (as reported in the literature[3-5]), all of which were kept constant for each of the reactions.

Table 5.1: Number and volume % particle diameters for suspension beads of PMMA and PMMA/Laponite RD nanocomposites, where Stand dev is the standard deviation of the results.

	Volume%		**Number%**	
	Diameter(μm)	**Stand dev**	**Diameter(μm)**	**Stand dev**
PMMA	777.4	490	6.8	7.7
0.05%LRD	446.1	440	1.4	1.9
0.25%LRD	212.3	150	1.7	2.9
0.5%LRD	235.3	190	1.8	1.9
1%LRD	169.8	170	0.8	0.9

It was expected that the presence of the clay would cause a small increase in particle size as each droplet would have to contain the additional volume of the clay, so the decrease in particle size observed was unexpected. The droplet size is determined by the equilibrium between the break up and coalescence of the monomer droplets in the water phase. The surfactant is used to coat the monomer droplets to prevent them from sticking/coalescing during the polymerisation. Increasing surfactant levels was seen to decrease the droplet size[6, 7], as an average particle size will be obtained when there is

enough surfactant present at the particle surface to prevent coalescence. An increase in surfactant concentration will allow a larger surface coverage and hence smaller particle size. Since the surfactant level is kept constant for all reactions the decrease in droplet size suggests that a smaller equilibrium size is preferred in the presence of the clay.

Gupta[8] discusses alternate surfactants for suspension polymerisation and mentions the use of talc (a type of clay mineral ($[Si_8(Mg_{5.45}Li_{0.4})O_{20}(OH)_4]Na_{0.7}$)) as a stabilizer in suspension polymerisation. Clay acting as a surfactant could be a possible cause of the decrease in particle size seen in these experiments. The particle size appeared to decrease with increasing clay content; the more clay present the greater the surface coverage and the smaller the particle size. The use of Laponite clay as a stabilizer has also been reported in the literature[9, 10]. Bon et al[9] used Laponite RD as a stabilizer in pickering miniemulsions of styrene and acrylates. Pickering miniemulsions are miniemulsions which are stabilized by solid particles (such as clay). The term is named after Ramsden[11] and Pickering[12] who first carried out the work. In order for the Laponite particles to sit at the water/oil interface, Cauvin et al[10] added sodium chloride to the suspension with the aim of reducing the electrical double layer between the clay platelets resulting in flocculation.

Although our suspension system does not contain a salt such as sodium chloride, sodium ions from the suspending agent and the presence of the buffer could cause a similar effect on the electrical double layer of the Laponite particles. This makes it favourable for them to sit at the water/MMA interface and act as a suspending agent in addition to the PMA suspending agent already added. The excess suspending agent will cause a decrease in particle size with the highest clay loading producing the smallest diameter beads.

The time-temperature profile of the PMMA and 1%LRD suspension reactions are shown in Figure 5.2. The profile for both PMMA and 1%LRD initially follow the same trend as both are heated at the same rate and contain approximately the same volume. However above 70^{o}C the two traces differ. The temperature profile for PMMA levels off at 83^{o}C for 30 minutes. This stage indicates that steady state kinetics have been reached as the rate of termination equals the rate of initiation so that the overall

concentration of free radicals is constant. At a time of 70 minutes there is a sharp increase in the temperature indicating the end of the steady state conditions. For the 1%LRD suspension, the increase in temperature at the end of the reaction occurs after 55 minutes, 15 minutes quicker than that of PMMA. Since the 1%LRD reaction is occurring over a shorter period of time then either a faster rate of reaction or an earlier onset of gel effect may be taking place.

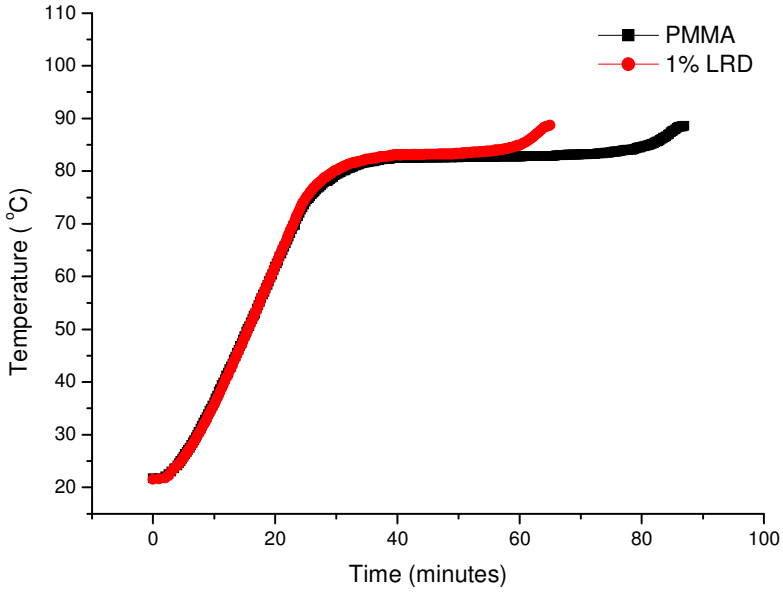

Figure 5.2: Time-temperature data from the suspension polymerisation reaction of PMMA and 1%LRD.

5.3 Morphology of PMMA/Laponite RD Nanocomposite

As for the PMMA/Cloisite 15a nanocomposites, the morphology of the PMMA/Laponite RD samples has been characterised using both XRD and TEM. Heat pressed samples of all LRD nanocomposites were colourless and transparent in appearance resembling that of unfilled PMMA. A comparison of PMMA, 1%LRD and 1%C15a from 1 mm heat pressed samples are shown in Figure 5.3. It can be seen that 1%C15a has a yellow tint to its appearance and is less transparent compared to the samples of PMMA and 1%LRD. This difference is caused by the colouration of the clay- Laponite clay is whiter in appearance than Cloisite 15a producing the more

transparent/colourless material. This gives the Laponite RD nanocomposites potential to be used in a wider range of products.

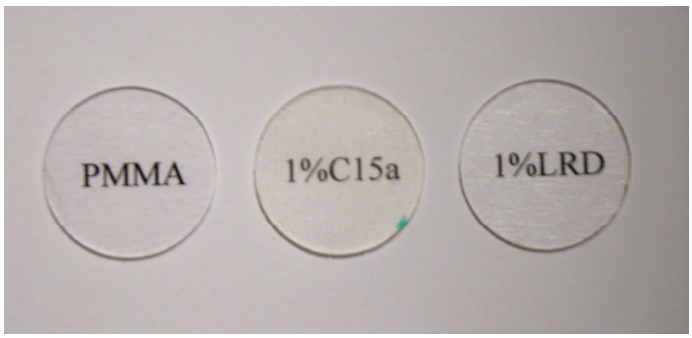

Figure 5.3: Colour changes of the PMMA, 1%LRD and 1%C15a heat pressed samples.

The XRD traces of PMMA, Laponite RD and 1%LRD are shown in Figure 5.4. The Laponite RD clay shows a broad peak at 7.3^{o} corresponding to a basal spacing of 1.2nm. This is 2 nm smaller than the basal spacing of Cloisite 15a. Cloisite 15a is modified with an ammonium salt containing carbon eighteen chains which prevent the clay platelets from stacking close together. Laponite RD is unmodified and the surface negative charge is neutralised by Na^{+} ions which are small, allowing the clay platelets to stack more closely.

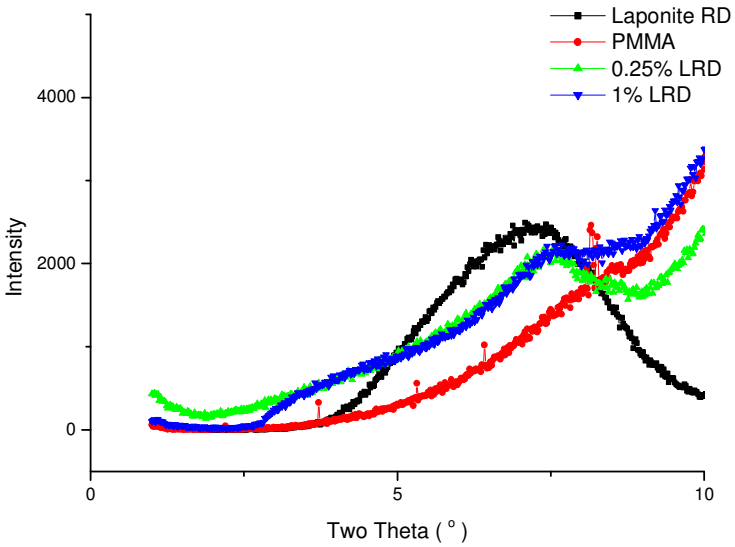

Figure 5.4: XRD traces of Laponite RD, PMMA and 1%LRD

The XRD trace of PMMA exhibits a large increase in intensity at higher two theta values. This peak is believed to arise from the amorphous scattering from the PMMA chains (which was also seen in the SAXS data presented in Chapter 4.9) and occurs in the same two theta region as the diffraction peak of the Laponite RD. As a result of this, the XRD traces of PMMA/Laponite RD nanocomposites show the diffraction peak caused by basal spacing occurring as a shoulder on the side of the PMMA amorphous scattering. This makes the interpretation of the basal spacing by XRD difficult. If the peak on the shoulder corresponds to the d001 peak then the basal spacing for 1%LRD occurs at 7.6^{o} a distance of 1.16 nm, 0.04 nm smaller than pure Laponite RD clay. The basal spacing for 0.25%LRD occurred at a slightly higher value of 1.18 nm which is still smaller (0.02 nm) than the pure Laponite RD clay.

The subtraction of the PMMA trace from that of the PCN leaves a weak broad peak making the peak maximum difficult to define. The lack of a definite peak could imply a high extent of exfoliation or a board distribution of d001 spacing. However the accuracy of the basal spacing obtained from XRD is unknown as the positions of the d001 peaks may not be accurate due to the distortion of the peak maximum caused by PMMA. If the basal spaces calculated from the original XRD data are correct then it indicates that a lesser degree of dispersion was achieved compared to the PMMA/Cloisite 15a nanocomposites which showed an increase in basal spacing of 0.55 nm compared to the C15a clay.

To verify the degree of dispersion and basal spacing, TEM images were taken of the heat pressed PMMA/Laponite RD nanocomposites. Figure 5.5 shows that the PCN exhibit an unusual network structure consisting of inter connecting circles. The clay structure appears to be uniform throughout the PMMA matrix, the presence of long range connectivity suggesting the formation of a percolated network. This structure is present in 0.25, 0.5 and 1%LRD. However the structure does not appear in the 0.05%LRD as there is insufficient clay present to form the continuous structure. The percolated network appears to be made up of individual and small aggregates of clay platelets but because of the small size of the individual platelets the aggregate size and the basal spacing could not be measured.

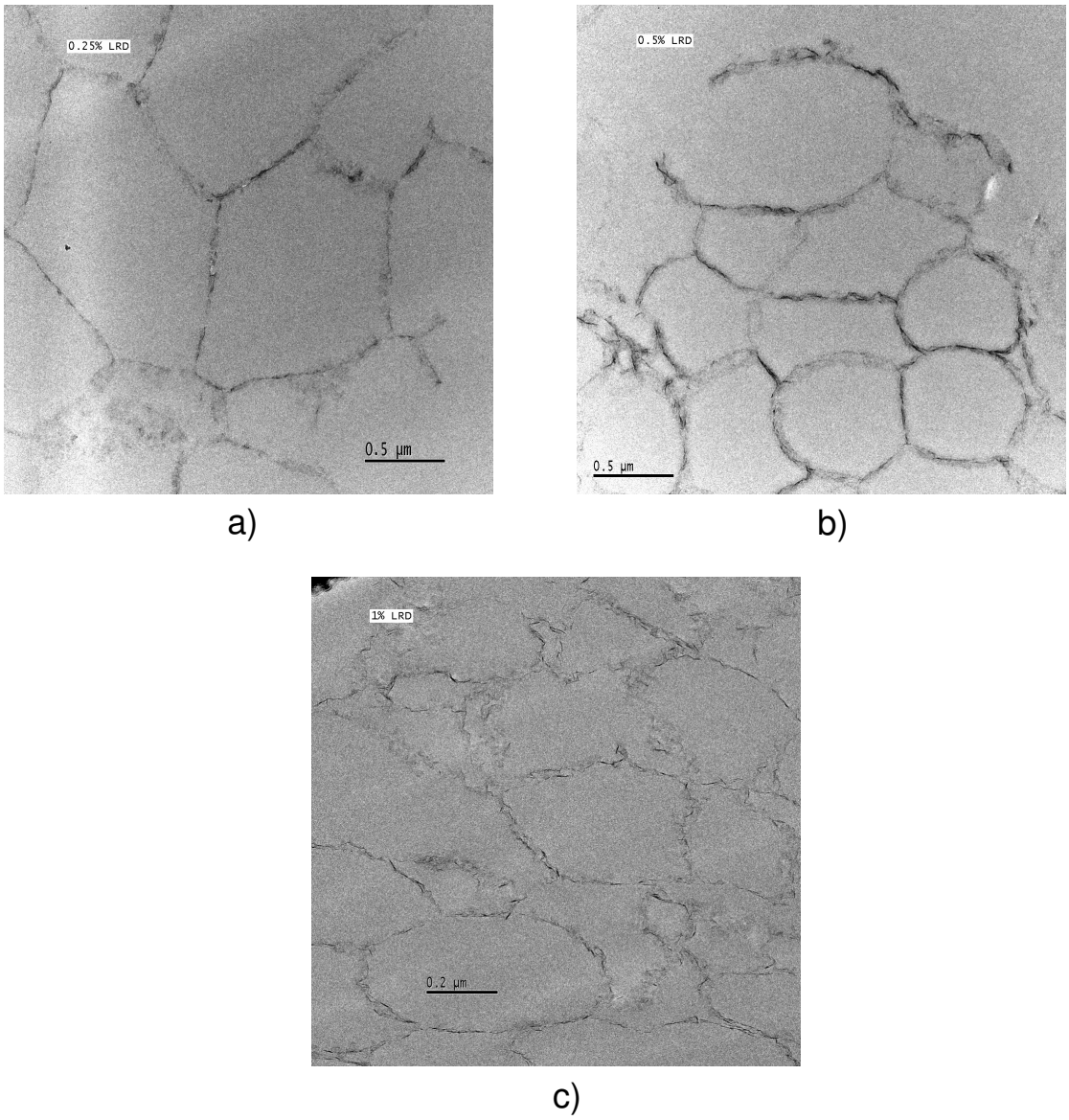

Figure 5.5: TEM images of a) 0.25%LRD at 0.5 µm, b) 0.5%LRD at 0.5 µm and c) 1%LRD at 0.2 µm.

Figure 5.5 shows that the size of the structure appears to decrease with increasing clay content. To quantify this observation the size of the structures were obtained by measuring adjacent points across the structure using image analysis software. The results are tabulated in Table 5.2. The size of the structure decreased from 1470 nm to 421 nm with increasing clay content. It is interesting to note that the ratio of the structure size between samples follows that of the weight percent clay present. For example as the amount of clay doubles from 0.5 to 1 wt% the structure size halves and similarly quadrupling the wt% of clay causes the structure size to quarter indicating that the clay is controlling the structure size.

Table 5.2: Structure size measured by TEM for 0.25, 0.5 and 1%LRD.

	Diameter of Structure (nm)	STDEV	Ratio
1%LRD	421	86	1.0
0.5%LRD	843	117	2.0
0.25%LRD	1470	148	3.5

To confirm the presence of the network throughout the sample, ESEM imaging was used to view the samples at a larger length scale. As for the TEM samples, the ESEM samples were heat pressed and the bulk was microtomed and imaged. Figure 5.6 shows the SEM images of 1%LRD. ESEM imaging was carried out on a Philips FEI XL30 ESEM using gaseous secondary detector. Images show the difference in height of the surface, light areas being higher (closer to detector) than that of the dark areas.

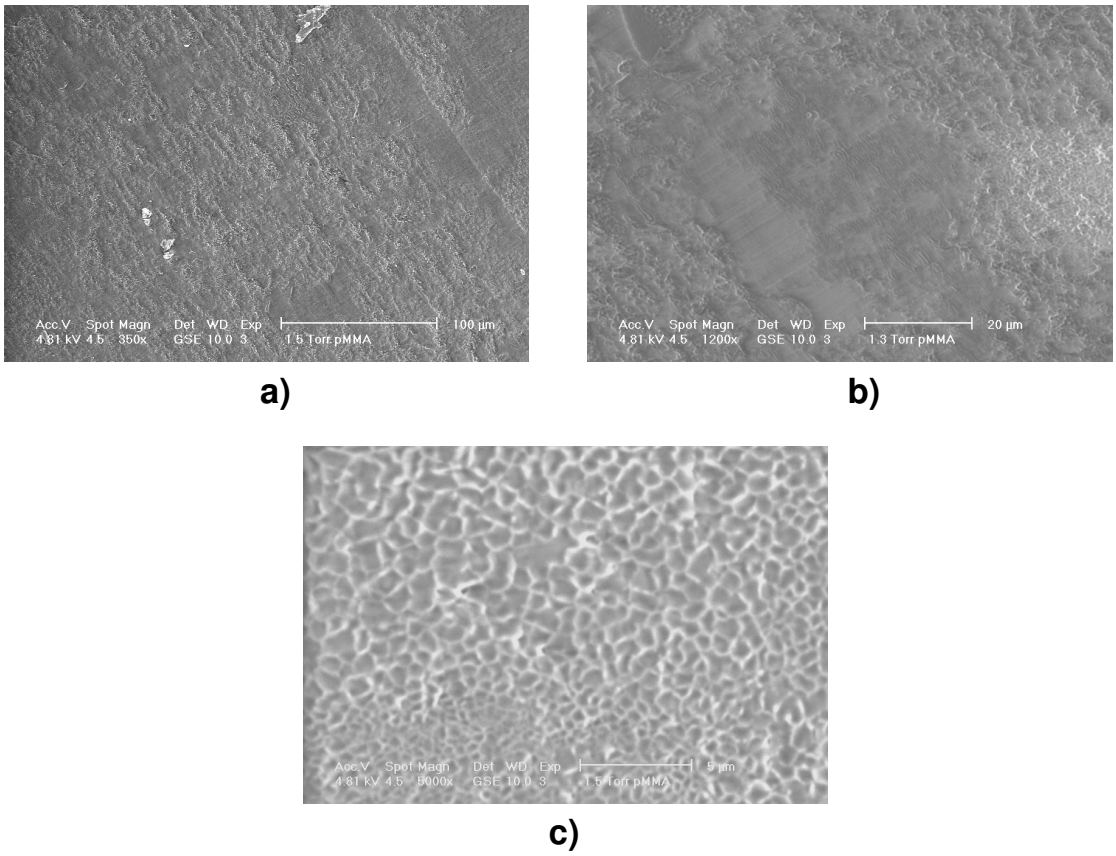

Figure 5.6: ESEM images from the bulk of a beat presses sample of 1%LRD. Image a) has a length scale of 100µm, b) 0f 20µm and c) of 5µm.

The network structure appeared to be present throughout the sample indicating good dispersion of the clay (Figure 5.6c). However there are still small areas where the

network is not present as seen in Figure 5.6b. These areas are in the minority and the bulk of the sample contained the network structure. For comparison with the TEM images the size of the structures were measured. The dark areas had an average size of 706±110 nm and the light areas 138±24 nm in diameter. These sizes are larger than those measured by TEM and are of a similar length scale as the particle size.

There are two possible causes for the formation of a percolated network of clay platelets. The first is phase separation between the clay and PMMA and the second is the surface coverage of the suspension beads by LRD clay. The latter is believed to be the cause of the network. As discussed in section 5.2 it is believed that the Laponite clay platelets are acting as a surfactant and forming a protective coating around the suspension beads. When the Laponite coated beads are heat pressed, the result is a percolated network with a structure diameter similar to that of the size of the bead diameter. Analysis of the average structure size showed that the 1%LRD structure is 420 nm which is approximately half the size of the beads (820 nm). The pressure applied during heat pressing may cause the compression of the beads, producing the smaller structure size.

Assuming that the Laponite RD forms a mono layer around each PMMA bead the surface area that x wt% of LRD can cover and hence the size of the PMMA particles can be calculated using the densities and volume of MMA and Laponite RD. An example calculation is given in Appendix B for 1%LRD and the calculated structure sizes are given in Table 5.3. The calculated structure sizes are still smaller than the average particle size, but are larger than the TEM measurements. The size of the calculated structures suggests that there is enough clay present to maintain the structure throughout the material, but also indicates that the clay surrounding each bead is rarely more than a nanolayer thick.

Table 5.3: The calculated structure size assuming continuous network throughout the material.

	Mass of clay (g)	**Calculated Structure size (nm)**
1%LRD	4	504
0.5%LRD	2	1008
0.25%LRD	1	2017

The theory of the Laponite RD being present only at the surface of the clay was confirmed by carrying out TEM on the 1%LRD beads. To gain TEM images of the suspension beads, the beads were first imbedded into an epoxy resin and microtomed sections of the beads were imaged. The images are shown in Figure 5.7. Figure 5.7a shows a collection of 1%LRD beads, which again highlights the presence of the variety of particle sizes. An average size of 0.8±0.3 μm was calculated confirming the values from the particle sizer. The dark line outlining the beads confirms the presence of clay around the surface of the suspension beads (Figure 5.7b). It can be seen that the clay is not just present on the very outer edge but has penetrated a short distance inside the PMMA bead where there also appears to be small scale structures present which take on a spherical appearance, Figure 5.7c.

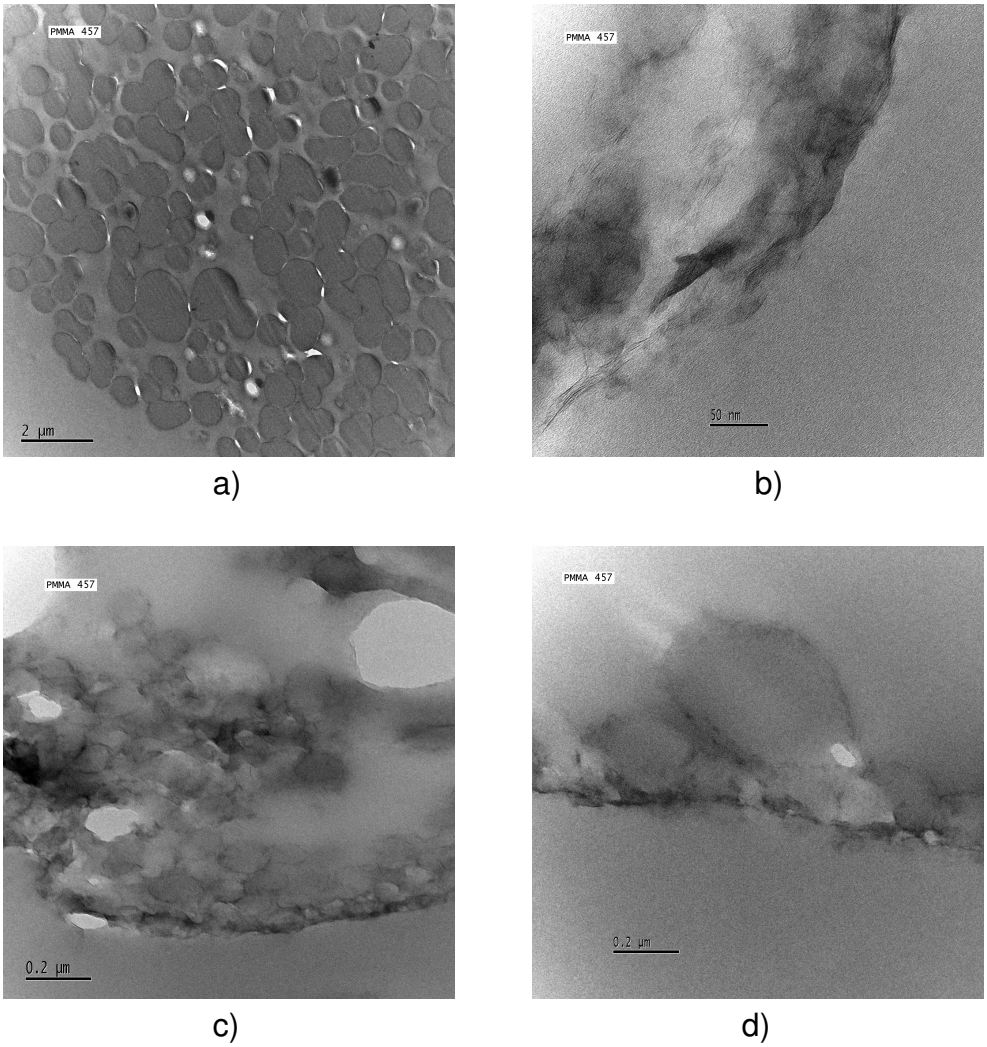

Figure 5.7: TEM images of 1%LRD beads embedded in epoxy resin.

5.4 Effect of Clay on the PMMA Molecular Weight

The effect of Laponite RD on the PMMA molecular weight was investigated using SEC. Values of M_w, M_n and PDI for PMMA and PMMA/Laponite RD nanocomposites are tabulated in Table 5.4. M_w was seen to increase with increasing clay content accompanied by a large increase in PDI. The PDI increases from 1.8 for PMMA to 8.8 for 1%LRD. The molecular weight (Figure 5.8) showed a bimodal distribution, with the main peak appearing at 76000 g.mol^{-1}. The low molecular weight peak remained constant for PMMA, 0.05, 0.25 and 0.5%LRD. However for 1%LRD the peak shifted to lower molecular weight (60000 g.mol^{-1}). As the wt% of LRD increased a high molecular weight peak appears at 1000 kg.mol^{-1} which increases in size as wt% of LRD increases.

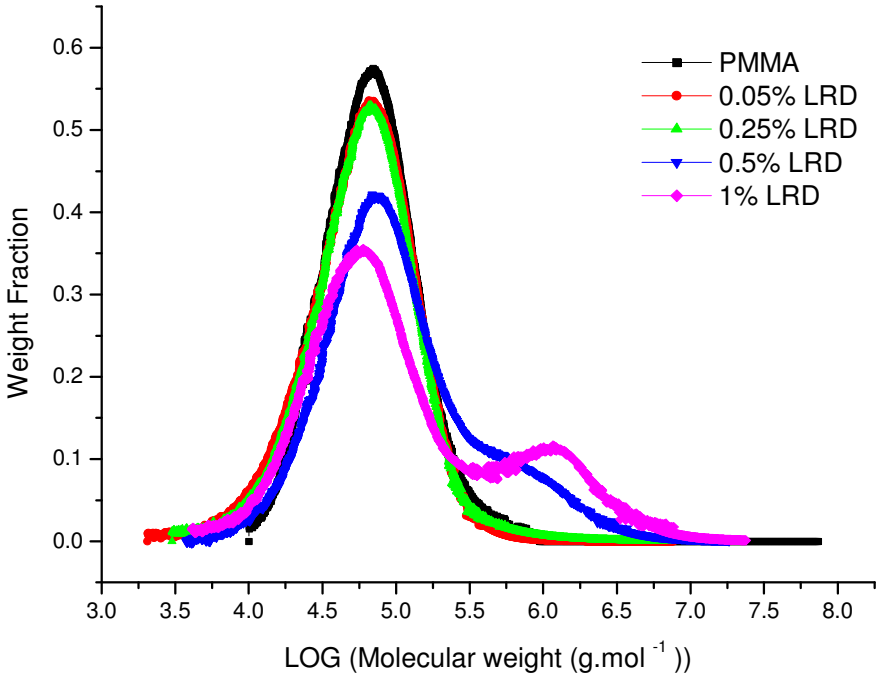

Figure 5.8: Weight fraction vs. molecular weight graphs for PMMA and PMMA/Laponite RD nanocomposites.

Table 5.4: Molecular weight data obtained from SEC of PMMA and PMMA/Laponite RD nanocomposites.

	wt% Clay	**M_w (g.mol^{-1})**	**M_n (g.mol^{-1})**	**PDI**
PMMA	0	75000	45000	1.8
0.05%LRD	0.05	76000	36000	2.1
0.25%LRD	0.25	89000	38000	2.3
0.5%LRD	0.5	230000	53000	4.4
1%LRD	1	380000	43000	8.8

From work carried out on PMMA/Cloisite 15a nanocomposites it was seen that the Lewis acid sites present on the rim of the montmorillonite clay platelets causes the termination of free radicals. It was found that the chain transfer agent (1-dodecanethiol) was being removed from the reaction by the clay. The molecular weight increased with increasing clay content until a plateau occurred above 0.5% due to the number of available Lewis acid sites being greater than that required to remove all of the CTA.

In the PMMA/Laponite RD nanocomposites the increase in M_w (or the percentage of high molecular weight polymer present) increases with increasing wt% clay, suggesting that the clay is involved in this change. The presence of the bimodal distribution suggests that the cause of the change in M_w is either different to that seen in the Cloisite 15a clay or the effect has become isolated as the bulk of the material appears to have a molecular weight distribution similar to that of unfilled PMMA. It was observed from the morphology studies that the clay was found to reside at the edges/boundary of the PMMA beads. The failure of the clay to be incorporated into the centre of the suspension droplets during the free radical polymerisation means that the polymerisation occurring at the core of the suspension beads will be unaffected by the presence of the clay. The removal of the CTA by the clay platelets should not lead to a bimodal distribution. Viscosity inside the droplet will be low enough to allow diffusion of monomer so one average M_w should be achieved throughout the sample which would be larger than that of unfilled PMMA. Also if the viscosity is low then the CTA could easily diffuse to the surface of the droplet to be consumed by the clay.

For polymerisation of MMA in the presence of clay, Solomon[13] suggested that the increase in molecular weight was caused by the decrease in the number of free radicals present through the termination or disproportionation of the radicals at the Lewis acid sites. It is believed that if the CTA is not involved in the reaction then the change in molecular weight may be caused by the reaction of propagating chains with the Lewis acid sites. Solomon[13] did not study the polydispersity of the molecular weight distribution, but since propagating chains are being prematurely terminated and higher molecular weight polymer chains are being produced a broader distribution should be observed.

There are several other reports in the literature where bimodal distributions in PMMA clay nanocomposites were observed. Venables[14] synthesised PMMA clay nanocomposites via solution polymerisation and observed a decrease of approximately 200,000 $g.mol^{-1}$ on increasing clay content (0-23 vol%). Little change in molecular weight was seen at low clay loading (4-7 vol%). The bimodal distribution was assigned to the heterogeneous reaction conditions present during the polymerisation, as reactions occurring near the clay surface would react with the clay giving rise to low molecular weight fraction. This ties in with the observations made by Solomon and could also be occurring in our PMMA/Laponite RD suspension system. The slight decrease in the low M_w peak for 1%LRD could be an indication of early termination of the PMMA chains by the clay. As the number of free radicals is reduced the remaining chains will be of higher M_w.

Qutubuddin[15] also observed a bimolecular weight distribution in both the unfilled PMMA and PMMA clay nanocomposites. The average molecular weight for 10% clay was larger than PMMA, for both bulk and emulsion in-situ polymerisation methods. The bimodal distribution seen in the PMMA is caused by the increase in viscosity during the gel effect. The enhancement of the bimodal distribution was thought to be due to the clay inhibiting the free radical polymerisation. The time-temperature profile of PMMA and 1%LRD in Figure 5.2 showed that the early stages of polymerisation followed a similar reaction profile. However 1%LRD shows the end of the steady state kinetics occurs quicker than in PMMA. This suggests that either a faster rate of

reaction or the onset of gel effect occurs earlier possibly leading to the high molecular weight fraction.

The molecular weight distribution of a polymer synthesised via free radical polymerisation can also be affected by the reaction kinetics during the polymerisation, especially during the gel effect. It is postulated that three different molecular weight steps can occur during a free radical polymerisation[16]. The first is under the steady state conditions where the rate of initiation is equal to the rate of termination leading to a constant number of propagating free radicals. A change in molecular weight is believed to occur at the onset of the gel effect. The gel effect exhibits a lower rate of termination as the increase in viscosity hinders the diffusion of the long polymer chains. This allows a greater extent of monomer addition and hence an increase in molecular weight. A further change in molecular weight is thought to occur when the glass effect is reached. The glass effect is when the T_g of the polymer becomes higher than the polymerisation temperature. When this occurs the polymer will become glassy, decreasing the rate of monomer diffusion. This will cause a decrease in the average rate of increasing molecular weight.

It is also interesting to note that the molecular weight was seen to increase with decreasing particle size. A sample of 1%LRD was passed through a series of sieves ranging from 177 μm to <63 μm and SEC measurements were made on each fraction. The particle sizes and corresponding molecular weights are tabulated in Table 5.5. Both M_w and M_n increases with decreasing particle size but the PDI remains similar for all sizes. The bimodal distribution is present for all particle sizes, however the magnitude of the high molecular weight peak increases with decreasing particle size (Figure 5.9). The ratio between the two peaks is given in Table 5.5 where peak 1 is the low molecular weight peak.

Table 5.5: Molecular weight data obtained via SEC for varying particle sizes of 1%LRD.

Sieve size(µm)	M_w(g.mol^{-1})	M_n(g.mol^{-1})	PDI	Peak1:Peak2
177	280000	48000	5.8	3.4 : 1
125	370000	60000	6.2	3.2 : 1
63	480000	71000	6.6	3.1 : 1
<63	590000	107000	5.5	2.3 : 1

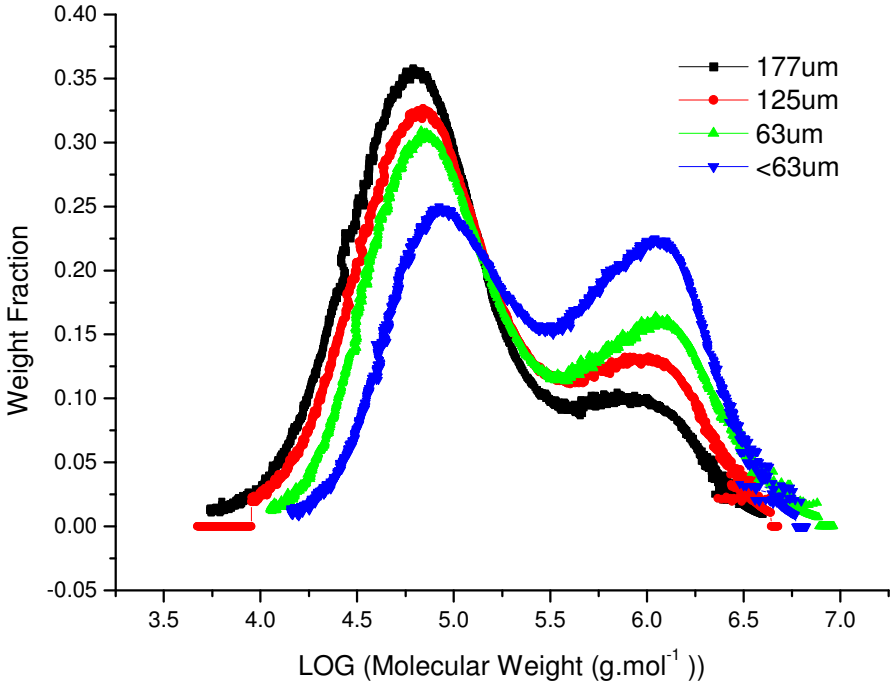

Figure 5.9: Plot of weight Fraction vs. molecular weight for varying particle sizes of 1%LRD.

The reason behind the change in molecular weight distribution with decreasing particle size is unknown. It was however observed that the increase in the high molecular weight peak could be related to an increase in the amount of clay present. Smaller beads will have a larger effective surface area than that of the larger sized beads and hence will contain a greater number of clay platelets relative to the amount of monomer.

5.5 Effect of Clay on the Thermal Properties of PCN

5.5.1 Differential Scanning Calorimetery (DSC)

DSC measurements allow an investigation into the temperature at which materials undergo phase transitions e.g. melting point and glass transition temperature, since these transitions are either exothermic or endothermic and are accompanied by a change in heat flow. The glass transition temperatures for PMMA/Laponite RD nanocomposites are given in Table 5.6, where a heating rate of 20°C per minute was used. The T_g was found to be an average of 2°C higher than that of PMMA which has a T_g of 115.3°C. The T_g for 0.05, 0.5 and 1%LRD was constant (117.3°C) suggesting that increasing amounts of clay had no further affect on the T_g. This again illustrates that only small quantities of clay are required to cause changes in the physical properties of nanocomposites. However 0.25%LRD has a glass transition temperature of 119°C which is 4°C higher than PMMA. The measurements were repeated four times and the standard deviation was found to be 0.5°C suggesting that the increase is real, although the cause is unknown.

Table 5.6: T_g with Standard deviations for PMMA and PMMA/Laponite RD nanocomposites.

	wt% Clay	Ave T_g (°C)	Stand dev
PMMA	0	115.3	0.2
0.05%LRD	0.05	117.3	0.8
0.25%LRD	0.25	119.1	0.5
0.5%LRD	0.5	117.3	0.2
1%LRD	1	117.4	0.4

Comparison of PMMA/Laponite RD and PMMA/Cloisite 15a nanocomposites shows that the T_g for lower loadings of C15a (between 0.05 and 0.25%) is similar to that of the Laponite RD nanocomposites (117.7°C). However, unlike Cloisite 15a nanocomposites, the Laponite RD samples did not exhibit the same extent of increase in molecular weight. These changes in glass transition are not believed to be related directly to the

changes in molecular weight. As the wt% of Cloisite 15a was increased above 0.5% a decrease in T_g was observed. 1%C15a has a glass transition temperature of 116.5^oC which is 0.9^oC lower than the T_g observed for 1%LRD. It was concluded in Chapter 4.5 that a decrease in glass transition was caused by a plasticization effect from the organic cations present on the surface of Cloisite 15a. As Laponite RD has not been organically modified, this effect is not present making Laponite RD more effective in increasing the T_g than Cloisite 15a.

Changes in the glass transition are usually related to changes in free volume, when the free volume of the system decreases the temperature required to undergo the T_g increases. The PMMA/Laponite RD nanocomposites showed an increase in T_g which would suggest either a decrease in free volume or confinement of the polymer chains[17, 18]. If the clay is directly involved in the process then one would expect the T_g to continue to increase with increasing clay content as a larger fraction of polymer chains will become restricted/confined by the clay. Studies of the morphology showed that the clay platelets were mainly present on the surface of the beads. The clay will only be able to influence the T_g of the chains in contact with its surface so the bulk of the beads will not be affected by the clay.

A possible reason for the change in T_g could be a thermal barrier or heating effect. It was shown earlier in the chapter that the clay covers the surface of the PMMA beads, with the particle size decreasing as more clay is available to create larger surface areas. For DSC measurements, contact between the pan and the sample is very important to ensure efficient transfer of heat from the pan to the sample[19]. If the beads are covered by a layer of clay then the contact between the pan and the sample will no longer be between the pan and PMMA but between the pan and Laponite RD clay. The beads will create an uneven sample/pan contact and if the clay prevents the polymer chains from relaxing into the pan then there would be a reduction in the efficiency of the heat transfer. Also clays are believed to be thermal insulators[20] and since the heat will now have to be passed through the clay to the polymer a delay in the temperature of the T_g will occur.

5.5.2 Thermogravimetric Analysis

PMMA/Laponite RD nanocomposites beads were heated from 30-500°C at a rate of 10°C per minute and the thermal stability of these composites were studied by plotting mass loss vs. temperature. TGA traces of Laponite RD, PMMA and 1%LRD are shown in Figure 5.10. 1%LRD follows a similar mass loss during heating as that of PMMA. Laponite RD only showed a small decrease in mass as the only loss in this region is caused by the loss of residual water found in the clay structure[21].

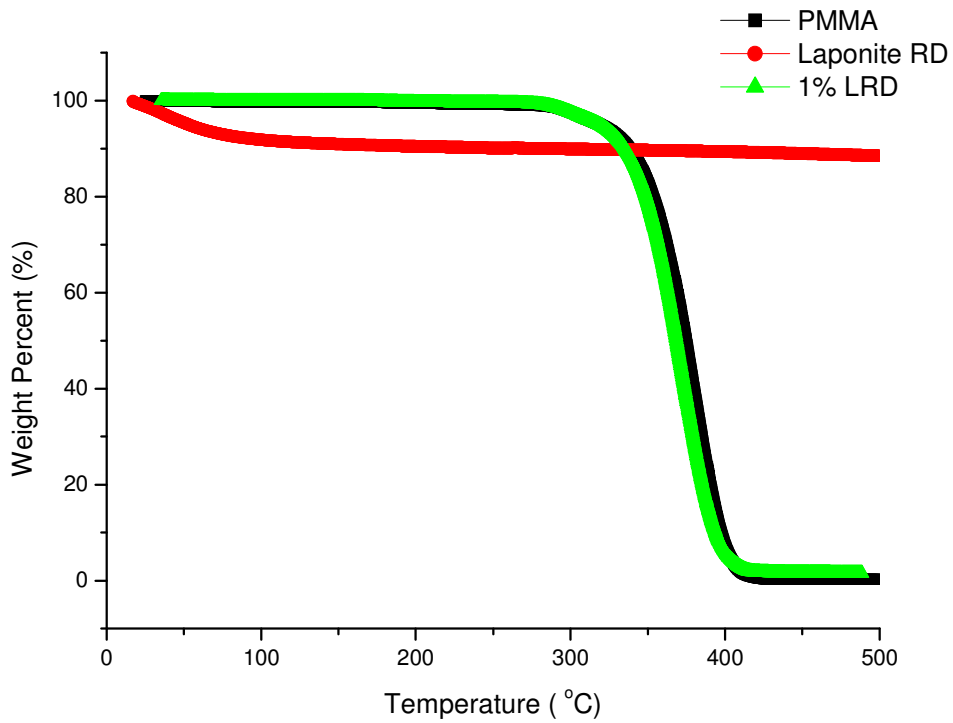

Figure 5.10: TGA traces for PMMA, Laponite RD and 1%LRD.

The temperature at which 5, 10, 30, 50 and 70 wt% loss occurred for PMMA and the PCN are recorded in Table 5.7. The data shows that the weight loss for nanocomposites containing 0.05-1%LRD all occur at approximately the same temperature as that of unmodified PMMA. This suggests that the clay does not affect the degradation mechanism of PMMA and has no effect on the diffusion of the volatile gases. Studies of the morphology led to the conclusion that the clay platelets were located at the surface of the suspension beads leaving the bulk (or core) of the beads unmodified. The degradation of the PMMA will proceed as for the unfilled PMMA[22] and as the

degradation temperature remains the same it suggests that there is insufficient clay to provide a large enough barrier to slow down the evolution of the volatiles. Laponite RD consists of platelets which are smaller in size than those of Cloisite 15a, causing a further reduction in the barrier effect.

Table 5.7: Temperature for 5, 10, 30, 50 and 70% weight loss for PMMA and PMMA/Laponite RD nanocomposites

	Temperature for x% weight loss (^{o}C)				
	5% wt loss	**10% wt loss**	**30% wt loss**	**50% wt loss**	**70% wt loss**
PMMA	319	338	362	375	385
0.05%LRD	317	337	362	374	385
0.25%LRD	311	333	357	369	379
0.5%LRD	315	332	357	370	381
1%LRD	319	335	357	369	379

Despite the TGA of the laponite RD nanocomposites remaining the same as unfilled PMMA, the Laponite RD clay is advantageous compared to Cloisite 15a clay as described in Chapter 4.6. Weight percentage loss of 5, 10 and 30 wt% occurred at lower temperature (29^{o}C) for Cloisite 15a nanocomposites than that of PMMA and was believed to be caused by the presence of the alkyl ammonium cation present on the surface of the clay. Laponite RD has not been organically modified hence this effect was not observed and initial degradation temperatures remained similar to that of PMMA.

As with the Cloisite 15a nanocomposites, isothermal measurements at 230^{o}C were carried out on 1%LRD for 30 minutes. The rate of weight loss can be calculated from the gradient of weight loss vs. time plot. A rate of weight loss was found to be 7.7×10^{-3} wt% per minute for 1%LRD compared to 3.6×10^{-3} wt% per minute for unfilled PMMA. Although this is still significantly larger than that of PMMA it is nearly a factor of ten lower than that of Cloisite 15a, indicating that significantly less degradation in Laponite RD than Cloisite 15a nanocomposites would occur during the processing of the materials.

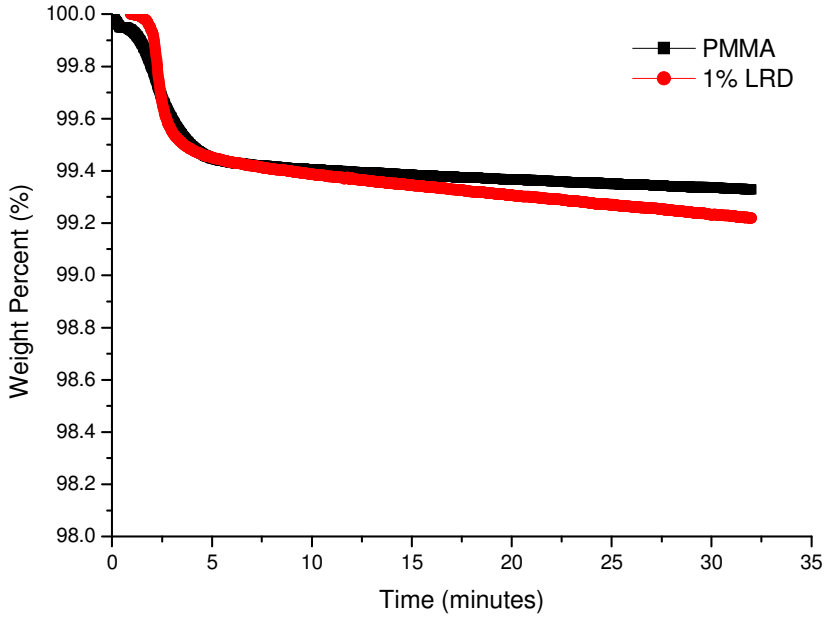

Figure 5.11: Isothermal TGA data at 230°C for PMMA and 1%LRD.

5.5.3 Micro calorimetry

Unlike the TGA data, the micro calorimetry data shows the beneficial properties of the Laponite RD clay in the PMMA matrix. Values for T_{max} and HRR are tabulated in Table 5.8 and the HRR data shows that there is a 55 $W.g^{-1}$ decrease for the 1%LRD compared to PMMA. The decrease in HRR is an indication of the presence of a slower rate of mass loss as it is believed that the degradation mechanism and hence the heat of combustion will be unaltered (Chapter 4.7). The slower rate of mass loss should have also been detected in the TGA data by the increase in temperature for a given wt% loss. However it was seen that the TGA data remained similar to that of unfilled PMMA. Both micro calorimetry and TGA were carried out on the suspension beads, however the rate of heating between the two techniques was different. The TGA was carried out at a much faster heating rate of 20°C per minute whereas micro calorimetry was carried out at 1°C per minute, which could potentially lead to the differences in observed results. The decrease in HRR is beneficial to a material as a slower mass loss leads to a slower release of energy/heat from a material, making the material safer in a potential fire.

Table 5.8: Measured values for rate of heat release (HRR) and the temperature at maximum HRR (Tmax) of PMMA and PMMA/Laponite RD nanocomposites, where Stand dev is the standard deviation of the results..

	wt% Clay	Tmax(°C)	Stand dev	HRR($W.g^{-1}$)	Stand dev
PMMA	0	403.1	0.5	346.2	18.1
0.05%LRD	0.05	406.4	0.6	311.2	7.1
0.25%LRD	0.25	406.7	0.4	346.8	15.3
0.5%LRD	0.5	406.7	1.5	356.0	17.2
1%LRD	1	406.9	0.6	292.0	2.8

Table 5.8 also shows that Laponite RD is advantageous for the temperature at which maximum HRR occurs (T_{max}), with an increase of 3°C compared to PMMA. After the initial jump in T_{max} there is only a slight increase in T_{max}, of 0.5°C, with increasing clay content. As the increase is so small the calculated standard deviation (approximately 0.6) is larger than the increase suggesting that this trend might not be real. This trend in data was also seen in the DSC data where it was suggested that the jump in T_g was caused by the thermal properties of the clay which surrounds the polymer beads. A similar phenomenon could be the cause of the increase in T_{max}.

5.6 Effect of Clay on the Rheology of PCN

Figure 5.12 shows the master curves of 0.05 and 0.25%LRD alongside unfilled PMMA. The master curves were shifted using time temperature superposition to a reference temperature of 230°C. The high frequency entangled rouse crossover occurs at the same frequency as that of PMMA and they also exhibit the same reptation crossover. Similar reptation times were expected as the 0.05 and 0.25%LRD nanocomposites are of similar molecular weights to that of the unfilled PMMA and as seen in Chapter 1.4, τ_{rep} increases with increasing molecular weight. In the terminal region; G' and G'' of 0.25%LRD have a higher gradient than that of 0.05%LRD and unfilled PMMA. Figure 5.13 shows the master curves of 0.5% and 1%LRD alongside PMMA. The lower frequency region of both 0.5% and 1%LRD are different to that of PMMA and 0.05 and

0.25%LRD. For 0.5%LRD both G' and G'' appear to meet at lower frequencies and then run parallel. For 1%LRD there is no crossover in G' and G'' in this region and they are seen to be parallel to each other.

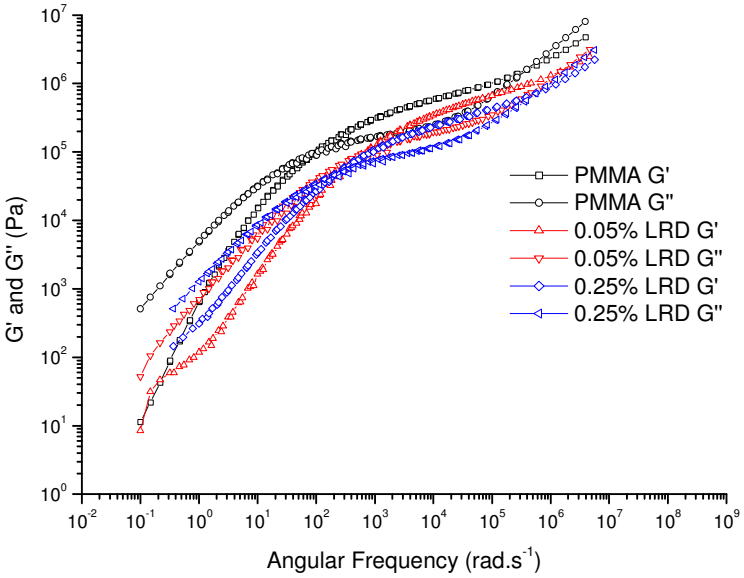

Figure 5.12: Oscillatory shear Rheology plots of PMMA and 0.05 and 0.25%LRD after TTS was applied. A reference temperature of 230^{o}C was used.

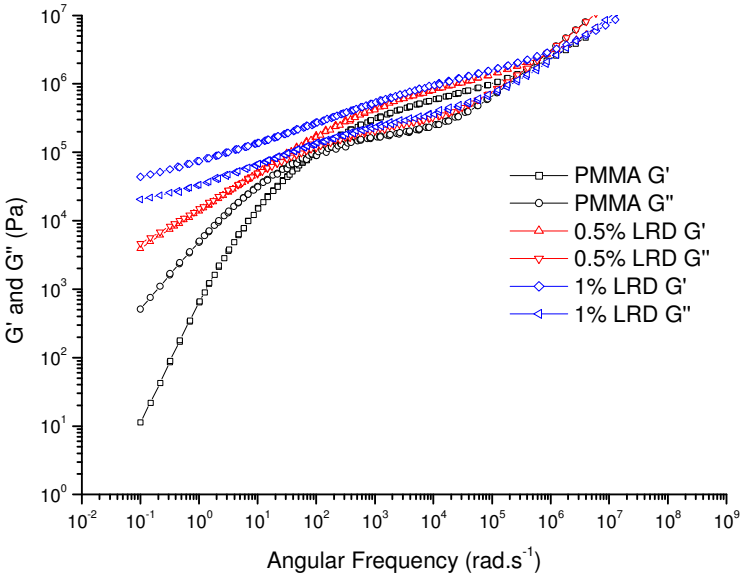

Figure 5.13: Oscillatory shear Rheology plots of PMMA and 0.5 and 1%LRD after TTS was applied. A reference temperature of 230^{o}C was used

G' being parallel to G'' is a signature of the formation of a network structure throughout the material and was seen in the 0.5% and 1%LRD samples. The characterisation of the morphology through the use of TEM and SEM showed the presence of a percolated network which is believed to be caused by the LRD clay covering the surface of the MMA droplets during suspension polymerisation. This is expected to be the cause of the network behaviour seen in the rheological measurements.

Molecular weight measurements for 1%LRD showed the presence of a high molecular weight shoulder (~1000 kg.mol^{-1}) and as seen in Chapter 4.8 differences in rheology can be masked by changes in molecular weight. The molecular weight data for 1%LRD was used in the time dependent diffusion model by des Cloizeaux[23] along with double reptation[24], as described in Chapter 4.8, to predict the rheology for polydisperse samples. Values of K_{rep}, K_i, K_R, β and G_N^o were kept constant and the same values were used as given in Chapter 4.8. The predicted rheology for 1%LRD alongside the experimental data can be seen in Figure 5.14.

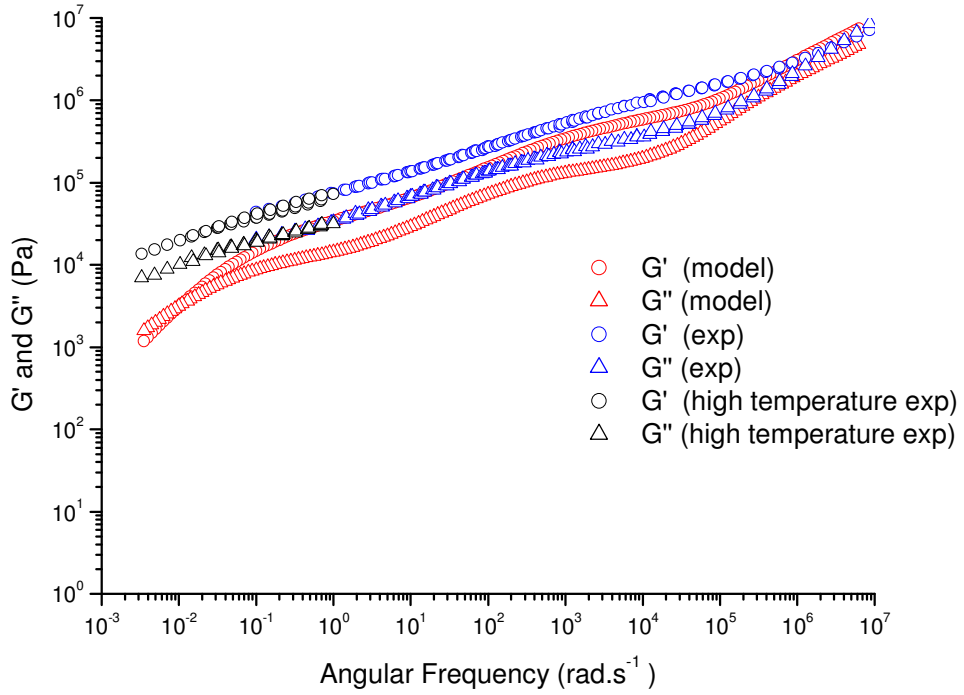

Figure 5.14: Comparison of model (red) and experimental (blue) rheology data for 1%LRD, with the high temperature 1%LRD given in black. A reference temperature of 230^{o}C was used.

The plateau region of the predicted rheology shows two different transitions- the plateau at high frequency is caused by the low molecular weight peak, whereas the plateau at low frequency is the result of the molecular weight fraction at 1000 $kg.mol^{-1}$. Due to the high molecular weight the model predicted that the material will have a high relaxation time, which occurs at a lower frequency than that which can be measured experimentally at 230°C. To reach these lower frequencies, measurements at higher temperatures need to be made. Figure 5.14 also shows the high temperature experimental data of 1%LRD for measurements between 245-275°C. The experimental data of G' and G'' appear to be running parallel to each other in the region where the predicted data shows the reptation crossover. Unfortunately higher temperature measurements cannot be undertaken as this would cause significant degradation of the PMMA chains.

In the terminal region of a viscoelastic material $G' \propto \omega^2$ and $G'' \propto \omega$ so on a LOG LOG plot G' and G'' exhibits gradiants of 2 and 1 respectively. The experimental values for PMMA were found to be G' = 1.77 and G'' = 0.97. The change in gradient of the terminal region can be used as an indication of the extent to which reptation is the dominant relaxation mechanism. Table 5.9 shows the gradients of G' and G'' for PMMA and PMMA/Laponite RD nanocomposites.

Table 5.9: Terminal gradients of G' and G'' for PMMA and PMMA/Laponite RD nanocomposites.

	G' Gradient	**G'' Gradient**
PMMA	1.77	0.97
0.05%LRD	1.20	0.91
0.25%LRD	0.85	0.93
0.5%LRD	0.44	0.35
1%LRD	0.22	0.21
1%LRD (after shear)	0.78	0.65

The gradients of both G' and G'' decrease with increasing clay content. For 1%LRD both G' and G'' have a gradient of 0.2, which is indicative of solid-like behaviour and can be related back to the presence of the percolated network. The changes in gradient

of G' are larger than those observed in G'' which was previously noted in the literature[25]. The decrease in gradient of G' appears to occur gradually as the wt% clay increases indicating an increase in the strength of the network. The most significant change in gradient occurs between 0.25 and 0.5%LRD and referring to the master curves (Figure 5.12 and Figure 5.13) it can be seen that there is also a large increase in the magnitude of G' between 0.25 and 0.5%LRD. This suggests that the amount of clay required to produce a fully percolated network occurs between these two values. The amount of clay required to produce a percolated network in this system may be larger than literature values (a value 0.02 vol% was seen in reference[26]) as there is little penetration of the clay inside the PMMA beads so that the network is confined/restricted to being formed around the suspension beads.

The nature of the network can be tested through the use of stress sweeps. The application of a large shear force through the use of a stress sweep could potentially lead to the break up of the network structure. If the network is physical in nature then the application of a shear force will destroy the network by aligning the clay platelets such that they do not form a percolated network. This would then allow the polymer chains to relax via reptation and the reptation relaxation time will be observed in the following frequency step. If the network is chemical in nature then the application of shear force will not alter the network structure and the frequency data will remain unchanged. The application of shear stress will also help to rule out the effect of the high molecular weight present as again the frequency data will remain unchanged if this was the cause of the change in rheology. The experiments were carried out as follows; first a frequency sweep was carried out at 230^{o}C between 0.1-100 radians per second followed by two stress sweeps (also at 230^{o}C) between 1-50 kPa. Then to confirm any changes or similarities in the frequency data, the frequency sweep is repeated. The stress sweeps and frequency data for PMMA can be seen in Figure 5.15.

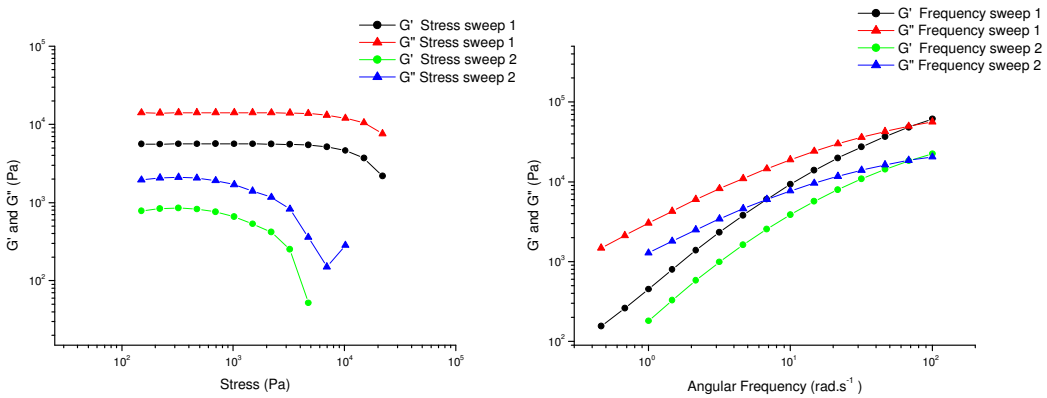

Figure 5.15: First and second, stress and frequency sweeps for PMMA.

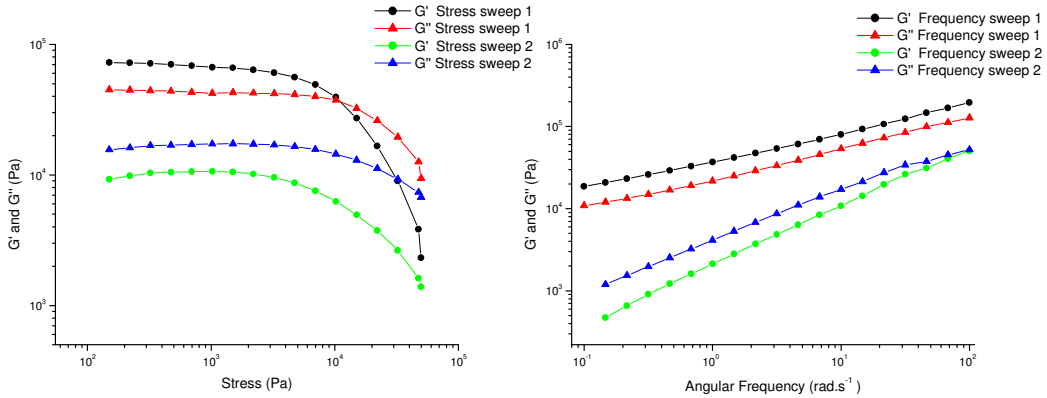

Figure 5.16: First and second, stress and frequency sweeps for 1%LRD

The frequency data in Figure 5.15 shows no change in the reptation crossover or in the gradients of G' and G'' before and after the stress sweep as expected. However for the second frequency sweep, G' and G'' are lower than during the first although the overall shape remains the same, which is caused by the loss of material between the plates during the high oscillatory shear. The experiment was also carried out on the 4%C15a sample and again there was no change in G' and G'', which further confirms that the change was caused by the high molecular weight rather than the formation of a network. The graphs for 4%C15a can be seen in Appendix A.6. Figure 5.16 shows the stress and frequency sweeps for 1%LRD. Unlike PMMA, G' starts off higher than G'' but when a stress of 10 KPa was reached during the first stress sweep, G' and G'' crossed over and in the following stress sweep G'' remained higher than G'. This suggests that the network can be permanently destroyed at shear stresses above 10 KPa. The frequency data shows G' higher than G'' and both are parallel to each other. However after the

stress sweeps, G'' starts higher than G' and the reptation relaxation time can be seen by the crossover of G' and G''. The crossover occurs at an angular frequency of around 10^{-2} s^{-1}, which roughly corresponds to that of the pure PMMA. The predicted rheology data for 1%LRD (as seen in Figure 5.14) shows a low frequency crossover (~10^{2} s^{-1}) due to the presence of the high molecular weight. This indicates that the effect of high molecular weight is not seen in the linear rheology, implying that the high molecular weight fraction is not interacting (not mixed) with the matrix PMMA. A possible reason for this would be if the high molecular weight PMMA fraction was covering or confined by the Laponite RD platelets. The stress experiments confirm the presence of a physical network within the 1%LRD material. Similar changes in the network structure for 0.5%LRD were also observed after the application of shear stress. The stress and frequency graphs for 0.5%LRD can be found in Appendix A.7.

For 1%LRD; after the stress sweep a cross over in G' and G'' was seen. The gradient of G' was also seen to increase form 0.22 to 0.78. This suggests that the percolated network has been broken (or weakened). Therefore the network is only physical and unlike Closite 15a nanocomposites, the changes in the rheology of Laponite RD nanocomposites are caused by the presence of a network rather than changes in molecular weight.

5.7 Effect of Extrusion Upon the Morphology of PCN

As discussed in Chapter 4.9, injection moulding is one of the commercial techniques used to produce the required shape of material needed for a specific task. The first step in injection moulding is to convert the suspension beads into larger pellets of material. This is done by passing the material through a twin screw extruder at 230^{o}C and then out through a die. The extrudate is stretched and cooled before being cut into pellets. There are several ways polymeric materials can behave on leaving the die. Ideally, the material will remain a similar diameter to that of the die, but the material is often seen to swell in size or even to produce a rugged shark skin (stick-slip) structure. The behaviour of the material as it leaves the die is a common problem in processing.

The swelling in size of a polymeric material as it leaves a die is known as die swell and is the ratio of the maximum diameter of the extrudate (D2) to the size of the die (D1) as shown in Figure 5.17. This is caused by the polymer chains relaxing and returning to a portion of their former conformation which results in an increase in cross sectional area. As the polymer is forced through the die it is subjected to shear stress which causes the polymer chains to stretch out in the direction of the flow. If the die is of sufficient temperature and length then the polymer chains will have time to relax the applied stress so upon leaving the die the material will be of similar size to that of the die. If there is insufficient time for the polymer chains to relax within the die then upon exiting the die the imposing stresses are released causing die swell. This is illustrated in Figure 5.17.

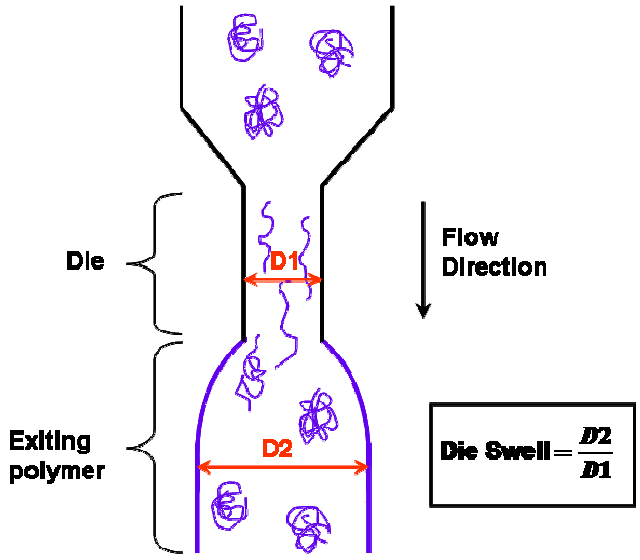

Figure 5.17: The die swell of a polymer as it exits a die.

1%LRD suspension beads were passed through a Clextral twin screw extruder at a temperature of 230°C and forced out through a die with a diameter of 6mm. The 1%LRD material produced a large die swell of 1.8-2. For comparison a 97 $Kgmol^{-1}$ PMMA produced a die swell of approximately 1.1-1.4. An increase in die swell is the consequence of a larger entanglement relaxation time as a greater proportion of the chains will have insufficient time to relax out the stresses imposed on them whilst passing through the die. As discussed in Chapter 4.8, the relaxation of polymers can be seen from rheology and changes in reptation relaxation time can be related to changes in molecular weight. SEC measurements of 1%LRD showed that the matrix PMMA had a

bimodal molecular weight distribution. The main peak was similar to that of the standard PMMA. However a small fraction of chains were found to have M_w of approximately 1000 Kg.mol^{-1}. The increase in M_w is expected to cause an increase in the relaxation time and hence the die swell. The rheology of 1%LRD showed no reptation crossover due to the presence of the network structure which dominated the rheology. After the network structure was broken, the rheology showed that 1%LRD behaved similar to PMMA. Although the presence of the high molecular weight was not seen in the rheology, it clearly influenced the die swell.

Studies into the die swell of PCN have shown that the presence of clay reduces the extent of the die swell. Muksing et al[27] observed a decreasing die swell of polypropylene with increasing clay content (1-7%). The clay platelets which become aligned with the flow direction provide an additional barrier preventing the recovery of the original chain conformation. This effect was also seen in references[28-30]. In the case of 1%LRD, Laponite RD has a smaller platelet diameter than that of bentonite and montmorillonite which were used in the above references. The smaller diameter particles are expected to have a smaller effect on reducing the die swell. The clay platelets may be causing a reduction in the die swell but the effects of this are masked by the presence of the high molecular weight fraction.

To obtain an injection moulded sample of 1%LRD the amount of die swell needs to be reduced. This was achieved by mixing the 1%LRD (50:50) with a standard PMMA of M_w 97 Kg.mol^{-1}. Initial mixing took place in the barrel where the 1%LRD pellets were mixed with similar sized pellets of PMMA. The mixture of pellets was then passed down the extruder, through the die, and re-pelletised. The die swell was significantly reduced to 1.3 allowing the injection moulding of the material to take place.

The 1%LRD suspension beads were seen to be coated on the outside with Laponite RD clay (Chapter 5.3). When these beads were heat pressed a percolated network structure was formed which could be weakened on the application of shear stress as seen in the rheology data. The network structure is expected to be destroyed by the shear forces imposed on the material by the extruder. TEM was used to view these structural

changes. Figure 5.18a shows the network structure is no longer present and instead small clusters of clay are seen throughout the material. This indicates that the shear force provided during the extrusion process was sufficient to break up the clay structure. The image also shows that the clay clusters are well dispersed throughout the material. By starting with the clay platelets surrounding the suspension beads it ensured that the clay was dispersed evenly throughout the material. This also suggests that extrusion is a useful method in dispersing clay platelets. Figure 5.18c is a magnification of a clay cluster and both individual clay platelets and aggregates containing 2-5 platelets are present.

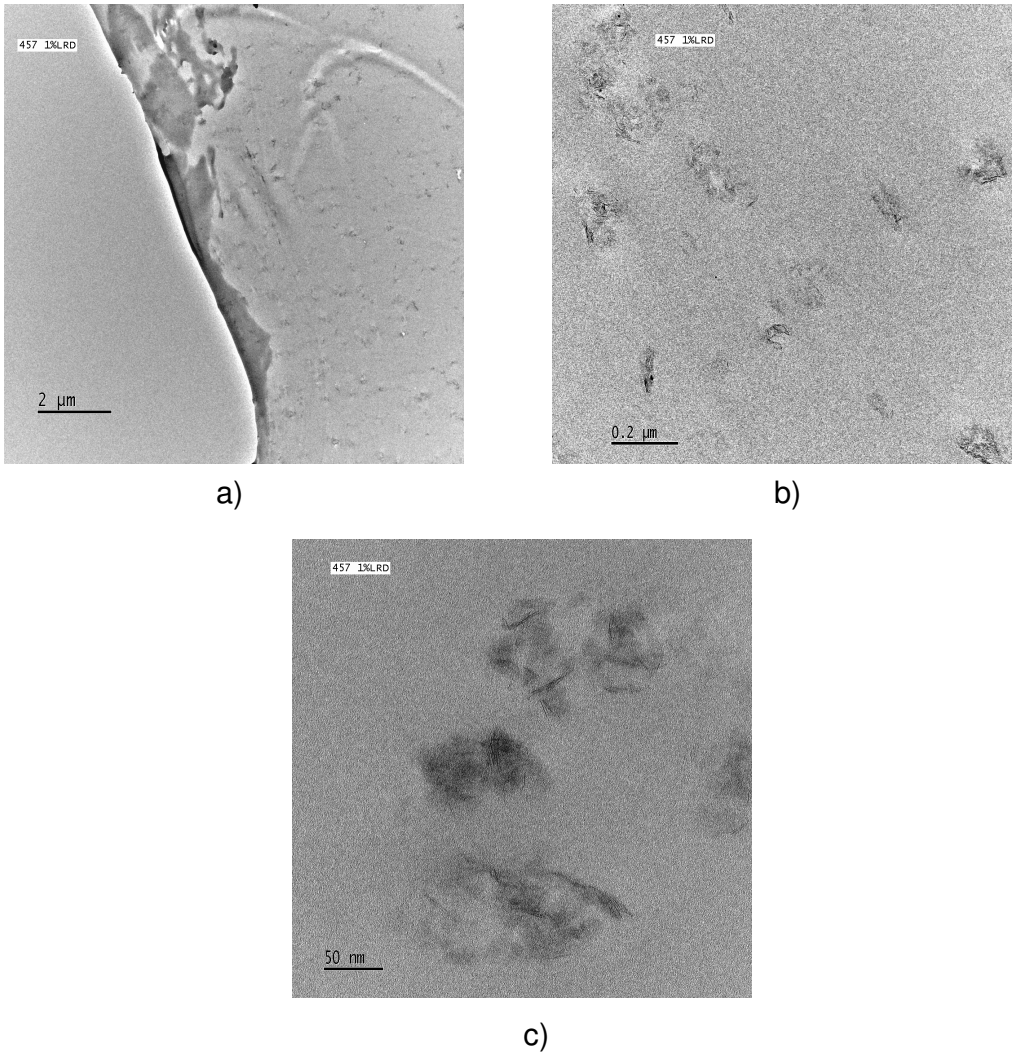

Figure 5.18: TEM images of pelletised 1%LRD at scales of a) 2µ m, b) 0.2 µm and c) 50 nm.

The blending of PMMA and 1%LRD was expected to produce a similar clay structure to that seen in 1%LRD but with the clay aggregates being more spaced apart. Figure

5.19a shows a similar dispersion of clusters of clay aggregates. However the presence of a network structure was also seen. Figure 5.19b shows the network structure on the left hand side of the image, with the remaining image showing the presence of dispersed clay aggregates. The network structure has a diameter of 1µm which is similar to the size of the structures seen in the heat pressed samples of 1%LRD suggesting that some of the 1%LRD suspension beads remained intact during the extrusion process. Magnification of the network structure (Figure 5.19d) shows that the network does not appear as intact as that of the heat pressed morphology (Figure 5.5) suggesting that weakening of the structure has occurred. Additional TEM images can be seen in Appendix A.8

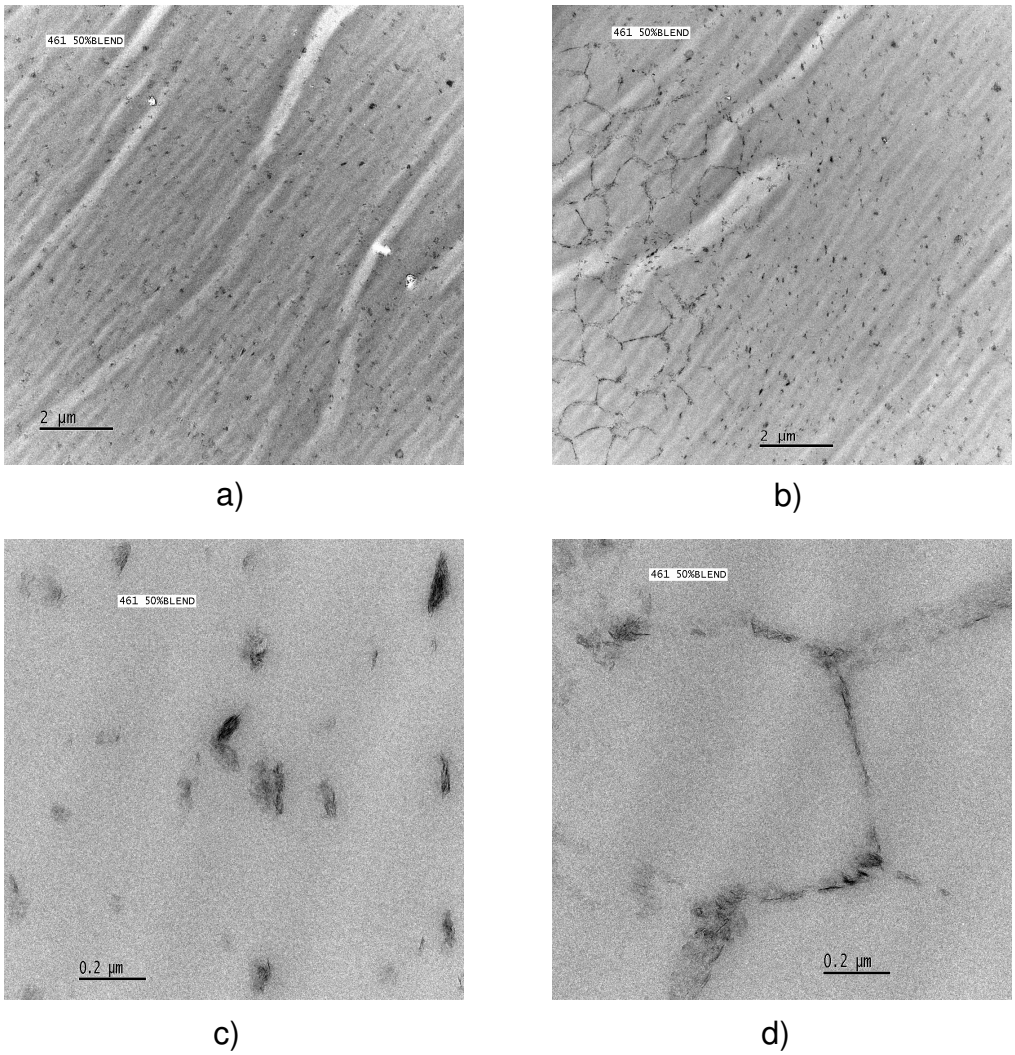

Figure 5.19: TEM images of pelletised 50:50 PMMA:1%LRD at scales of a) 2µ m, b) 2µ m, c) 0.2 µm and d) 0.2 µm.

The presence of the remaining network structure after two passes through an extruder is surprising but the reason for this is unknown. It is reasonable to suggest that since a portion of the network remains in the 50:50 PMMA:1%LRD blended material then it can be expected that some structure remains within the pelletised 1%LRD. One explanation of the remaining structure is that not all beads were destroyed on the first pass through the twin screw extruder. Some of the beads may have passed a non-mixing zone. However it is questionable as to how so many beads were not mixed yet remained in a large cluster. It was also surprising that the clusters of beads remained intact during the second pass through the twin screw extruder.

Another possible reason for the remaining network is that the network structure may be stronger than first believed. Strong interactions or chemical bonds between the clay and PMMA chains may be present which are capable of withstanding the shear forces applied during the extrusion process. This was initially ruled out through the use of rheology as changes in rheology after shear suggested the break up of the network. However the extent to which the network was broken is unknown. The network may have simply been weakened sufficiently to allow the relaxation of the polymer chains to be detected. In both 1%LRD and 50:50 PMMA:1%LRD there was no sign of individual bead structures, which suggests that the shear force supplied by the extruder was sufficient to break up the majority of the beads.

To gain a better understanding of the effect of extrusion on the break up of the LRD coated beads, further investigations need to be made. Further samples should be submitted for TEM to discover how common the presence of the remaining network structure is within the 50:50 PMMA:1%LRD. Additional TEM should also be carried out on the extruded 1%LRD to see if the network structure is still present within this material.

5.8 Conclusion

In this chapter the PMMA/Laponite RD nanocomposites were investigated. The nanocomposites were synthesised in-situ using free radical suspension polymerisation. The presence of clay affected the outcome of suspension polymerisation and produced changes in both molecular weight and particle size. Through TEM imaging of the cross section of suspension beads it was seen that the clay was coating the outside of the beads. Previous studies found in the literature[9, 10] showed that Laponite RD could be used as a suspending agent in miniemulsion polymerisation and it is believed that this is occurring in our suspension system yielding the Laponite coated PMMA beads. The action of the Laponite platelets as a surfactant would mean an increase in the level of surfactant compared to that used in PMMA suspension. The increase in surfactant levels caused a decrease in bead size which was shown through particle size measurements. 1%LRD showed a 6 μm decrease in particle size compared to PMMA.

Heat pressed samples of PMMA/Laponite RD nanocomposites were imaged via TEM and ESEM. The images showed an interconnecting structure which appeared to be present throughout the material. The structures appear to be made up of individual and small aggregates of platelets indicating that an intercalated/exfoliated material was produced. As the structures were present throughout the material a good degree of dispersion was also achieved. The structure represents the boundaries of the beads as they are forced together during heat pressing which produced a percolated network. The size of the structure was seen to decrease with increasing clay content. This can be related back to the suspension polymerisation where a larger amount of clay is the equivalent of a large concentration of surfactant and hence small beads are formed. The images also show that there is little clay present within the core of the suspension beads. So although there appears to be good dispersion throughout the material, the dispersion is limited to the outside of the PMMA beads indicating poor miscibility between MMA and Laponite RD.

The presence of the percolated network led to unusual rheological behaviour. The gradient of G' in the terminal region was found to decrease with increasing clay content. This pseudo solid like behaviour is caused by the restriction of the reptation relaxation

process by the percolated network. The type of network (chemical or physical) in the PCN was investigated by placing the materials under a large stress to see if the network could be broken. For 1%LRD, the frequency data at 230^{o}C showed no reptation crossover and G' remained higher than G''. However after a stress sweep, the frequency data for 1%LRD showed a reptation crossover in the G' and G'' data. The crossover observed occurred at a similar angular frequency to that of PMMA suggesting that the linear rheology was not influenced by the high molecular weight. The presence of the crossover after the stress sweep led to the conclusion that the network structure is physical in nature as it can be broken under stress. The stress sweep also confirmed that the change in molecular weight was not attributing to the change in rheology as was seen in Chapter 4 for PMMA/Cloisite 15a nanocomposites.

The molecular weight was seen to increase with increasing clay content accompanied by a large increase in polydispersity (PDI). The plot of normalised weight fraction vs. molecular weight showed the presence of a bimodal distribution for 1%LRD. The lower molecular weight peak appeared in the same position for 0.05, 0.25 and 0.5%LRD, but a slight decrease in this peak was observed for 1%LRD. With increasing wt% clay a larger molecular weight peak grew more predominant. The increase in the high molecular weight peak with increasing clay content was an indication that the clay is again involved in the change. The cause of the change in molecular weight is unknown, but it was noted that for 1%LRD the high molecular weight peak was seen to increase with decreasing particle size.

The thermal properties of PMMA/Laponite RD nanocomposites were also investigated. From DSC measurements an average 2^{o}C increase in T_g was achieved. The reason for the increase in T_g is unknown. It was suggested that it could be caused by the clay coating the bead surface, either acting as a thermal barrier or by preventing good contact between the sample and the pan. The mass loss of PMMA and PMMA/Laponite RD nanocomposites measured via TGA during a temperature ramp were similar for all wt% clay loadings. This suggests that the clay did not provide any barrier effect against the diffusion of the volatile gasses. Isothermal measurements for 1%LRD show a slightly larger rate of mass loss than PMMA. However the rate of mass loss for 1%LRD is

nearly a factor of ten lower than that of PMMA/Cloisite 15a making the PMMA/Laponite RD nanocomposites more suitable for processing.

This work showed that the clay influences the suspension polymerisation and alters the molecular weight (distribution) of the PMMA matrix. The cause of this is unknown and further investigation into this area is required. Despite this, the clay coated PMMA beads could have uses in nano-templating as it may be possible to tailor the reaction conditions to produce particles of a particular size, which are then heat pressed to give a desired continuous network structure. A colourless and transparent appearance gives them the potential to be used in a wide range of applications, and beneficial changes in thermal properties were also observed.

5.9 Reference

1. http://www.scprod.com/pdfs/Laponite%20brochure%20EN.pdf, In.
2. Brandrup, J.; Immergut, E. H., *Polymer Hand Book*. 3 ed.; Wiley: 1989.
3. Horak, D.; Pelzbauer, Z.; Svec, F.; Kalal, J. *Journal of Applied Polymer Science* **1981,** 26, (10), 3205-3211.
4. VivaldoLima, E.; Wood, P. E.; Hamielec, A. E.; Penlidis, A. *Industrial & Engineering Chemistry Research* **1997,** 36, (4), 939-965.
5. Santos, A. F.; Lima, E. L.; Pinto, J. C. *Journal of Applied Polymer Science* **2000,** 77, (2), 453-462.
6. Georgiadou, S.; Brooks, B. W. *Chemical Engineering Science* **2005,** 60, (24), 7137-7152.
7. Arshady, R. *Colloid and Polymer Science* **1992,** 270, (8), 717-732.
8. Gupta, D. C. *Journal of Applied Polymer Science* **1985,** 30, (10), 4187-4191.
9. Bon, S. A. F.; Colver, P. J. *Langmuir* **2007,** 23, (16), 8316-8322.
10. Cauvin, S.; Colver, P. J.; Bon, S. A. F. *Macromolecules* **2005,** 38, (19), 7887-7889.
11. Ramsden, W. *Proceedings of the Royal Society of London* **1903,** 72, 156.
12. Pickering, S. U. *Journal of the Chemical Society, Transactions* **1907,** 91, 2001.
13. Solomon, D. H.; Swift, J. D. *Journal of Applied Polymer Science* **1967,** 11, (12), 2567-&.
14. Tabtiang, A.; Lumlong, S.; Venables, R. A. *European Polymer Journal* **2000,** 36, (12), 2559-2568.
15. Meneghetti, P.; Qutubuddin, S. *Langmuir* **2004,** 20, (8), 3424-3430.
16. Maschio, G.; Scali, C. *Macromolecular Chemistry and Physics* **1999,** 200, (7), 1708-1721.
17. Shen, Z. Q.; Simon, G. P.; Cheng, Y. B. *Journal of Applied Polymer Science* **2004,** 92, (4), 2101-2115.
18. Tallury, P.; Payton, K.; Santra, S. *Nanomedicine* **2008,** 3, (4), 579-592.
19. Hatakeyama, T.; Quinn, F. X., *Thermal Analysis; Fundamentals and Applications to Polymer Science*. Wiley: 1999.
20. Chang, J. H.; Kim, S. J.; Joo, Y. L.; Im, S. *Polymer* **2004,** 45, (3), 919-926.
21. Olphen, H. V.; Fripiat, J. J., *Data handbook for clay materials and other non-metallic minerals* 1st ed.; Pergamon Press: 1979.
22. Jang, B. N.; Wilkie, C. A. *Polymer* **2005,** 46, (9), 2933-2942.
23. Cloizeaux, J. D. *Macromolecules* **1992,** 25, (2), 835-841.
24. van Ruymbeke, E.; Keunings, R.; Stephenne, V.; Hagenaars, A.; Bailly, C. *Macromolecules* **2002,** 35, (7), 2689-2699.

25. Hoffmann, B.; Kressler, J.; Stoppelmann, G.; Friedrich, C.; Kim, G. M. *Colloid and Polymer Science* **2000,** 278, (7), 629-636.
26. Jeon, H. S.; Rameshwaram, J. K.; Kim, G. *Journal of Polymer Science Part B-Polymer Physics* **2004,** 42, (6), 1000-1009.
27. Muksing, N.; Nithitanakul, M.; Grady, B. P.; Magaraphan, R. *Polymer Testing* **2008,** 27, (4), 470-479.
28. Zhong, Y.; Zhu, Z. Y.; Wang, S. Q. *Polymer* **2005,** 46, (9), 3006-3013.
29. Sadhu, S.; Bhowmick, A. K. *Journal of Polymer Science Part B-Polymer Physics* **2005,** 43, (14), 1854-1864.
30. Chen, D. Z.; Yang, H. Y.; He, P. S.; Zhang, W. A. *Composites Science and Technology* **2005,** 65, (10), 1593-1600.

Chapter 6 Organic Modification of Laponite RD

6.1 Background

In the previous experiments, polymer nanocomposites were formed in-situ using Cloisite 15a and Laponite RD clays. The organic modified clay Cloisite 15a showed poor compatibility with both MMA and water. The resulting PCN were intercalated with a phase separated morphology. Unmodified clays such as Laponite RD can be fully dispersed in aqueous medium which can potentially be used to give exfoliated morphologies as discussed in Chapter 5. Despite fully exfoliating the Laponite RD in the aqueous phase the poor compatibility between the Laponite and MMA left the centre of the PMMA beads unmodified.

In order to achieve fully exfoliated nanocomposites, good dispersion throughout the matrix is required which can be gained through the application of a high shear force or through improving the compatibility between the clay and polymer. Surface modification of Laponite RD will be carried out to promote exfoliation without the need of an additional mixing stage in the processing of the material. It would be ideal to use short chain PMMA for the surface modification; however PMMA is not soluble in water complicating the exchange reaction. Instead a water soluble polymer such as poly(ethylene oxide) (PEO) can be used. This allows the exchange reaction to be carried out in water retaining the exfoliated structure. The increased compatibility between modified LRD and PMMA will help to improve the dispersion within the suspension droplets.

To achieve a fully exfoliated nanocomposite using PEO modified Laponite RD, the PEO and PMMA need to be compatible with each other. The compatibility of two

polymers can be given by the Flory Huggins interaction parameter (χ)[1]. Values of $\chi>0$ suggest that interactions between the two species are unfavourable and could lead to phase separation. When $\chi<0$ the two species are compatible and a miscible system is seen. For PEO/PMMA, χ has been reported as being negative with a small magnitude[2-4]. The value of χ. can be influence by the volume fraction of PMMA present[2, 4-6], the length of the PEO chains[3] and the temperature[4, 6].

Polymer PMMA/PEO blend nanocomposites have been reported in the literature[7, 8]. Lim et al[7] found that the PMMA/PEO blend nanocomposite (Cloisite 25a) produced a similar d001 spacing ($2\theta \sim 2.6^{o}$) to that of PMMA/Cloisite 25a ($2\theta \sim 2.61^{o}$), whereas PEO/Closite 25a had a lower d001 spacing ($2\theta \sim 2.91^{o}$). This showed that for Cloisite 25a clay, PMMA was more effective in incorporating polymer chains between the clay platelets. Surface modification of Laponite with PEO has previously been studied[9, 10]. PEO modified Laponite was incorporated into a PEO matrix through melt blending using an extruder[10]. The rheology of the nanocomposites showed a transition from a viscoelastic liquid to a viscoelastic solid. The critical concentration for this was found to be at 0.5wt% of PEO-Laponite.

In order to be able to carry out a cation exchange on Laponite with PEO, one end of the PEO chain needs to be a functionalized as a cation. To obtain the modified LRD a mono-amine functionalized PEO was synthesised; the presence of difunctionality could lead to tethering of two clay platelets. One possible method of synthesising mono functionalised amino PEO is via the use of ammonia as shown in Figure 6.1. However due to the basic nature of the ammonium, a mixture of products including PEO-NH_2, $(PEO)_2$-NH and $(PEO)_3$-N can be formed. The mechanisms for these reactions are shown in Figure 6.1b and Figure 6.1c respectively.

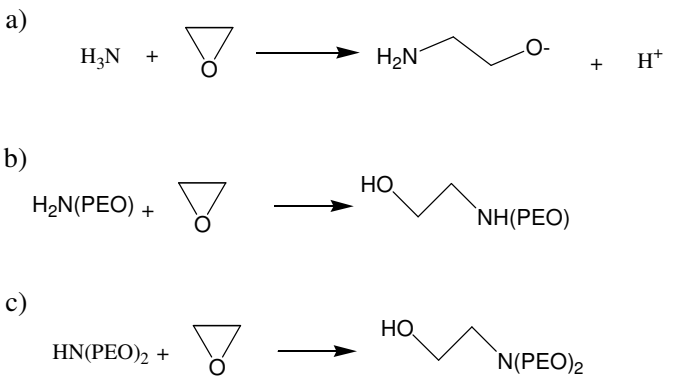

Figure 6.1: Shows the possible side reactions during the addition of EO to ammonia

Several other synthetic methods have been described in the literature for the synthesis of PEO-NH_2. These include functional group conversion of one of the alcohol end groups on a PEO chain, anionic polymerisation using a protected amine as an initiator and the anionic polymerisation initiated with a tertiary amino-alcohol. These three routes are discussed in more detail below.

P. Mangondry et al[9] converted the alcohol end group of the PEO to an amine using Gabriels synthesis. Figure 6.2 outlines the reaction pathway. An α-hydroxy-ω-methoxy-PEO is used rather than the dihydroxyl terminated PEO to prevent the formation of the diamine. From NMR they claim that the conversion to amine is greater than 95%.

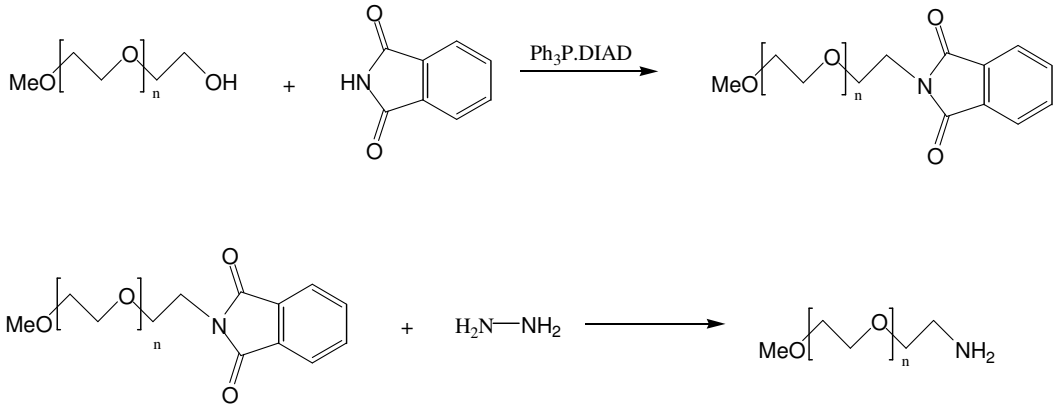

Figure 6.2: Synthesis of amino PEO via Gabriels mechanism.

The second alternative route is anionic polymerisation using a protected primary amine initiator to ensure that the amine could not participate in the polymerisation. After the polymerisation is complete the protecting group can be removed to leave the amine. N.Nagaski et al[11] used an acetonitrile complex to initiate anionic polymerisation.

Acetonitrile is highly acidic due to the electron withdrawing effect of the cyano group, and was converted into the amine using $LiAlH_4$ as shown in Figure 6.3. The PEO-NH_2 was 90% pure, with 10% of the dihydroxyl terminated PEO which is believed to arise due to contamination from water.

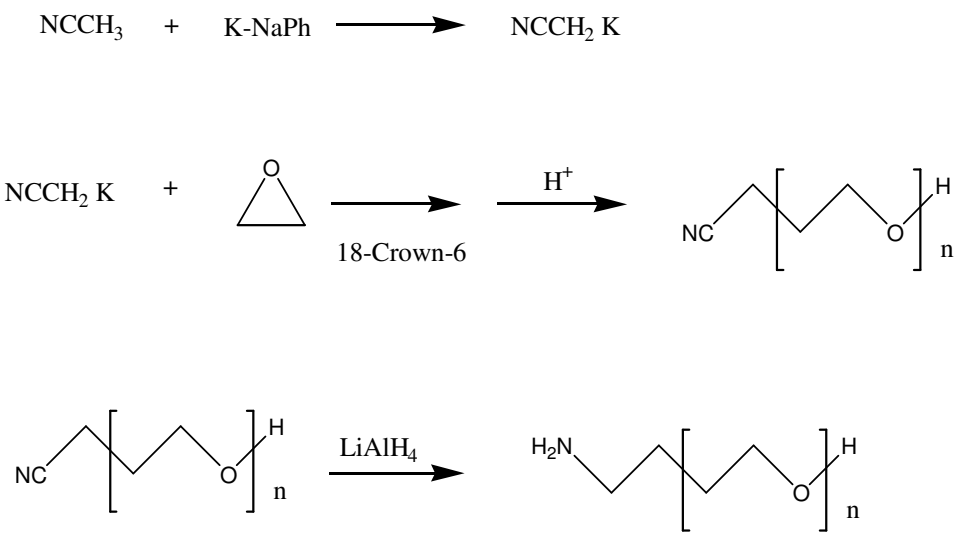

Figure 6.3: The formation of amino PEO through the use of a cyano initiator which is converted to the amine through hydrogenation.

A third alternative method is the anionic polymerisation of an amino alcohol. If the rate of attack on EO from the alcohol is greater than the rate of attack from the amine then PEO-NH_2 should be formed. Mosquek et al[12] investigated this effect and found that by using a base which is strong enough to deprotonate the alcohol (pKa=29-30 in DMSO) but not the amino group (pKa=35-40 in THF) then the reaction will be successful. They used diphenylmethyl potassium (DPMK) (pKa=33.01 in THF). The reaction scheme is shown in Figure 6.4. Secondary alcohols such as 2-(N-methylamino) ethanol were also tried.

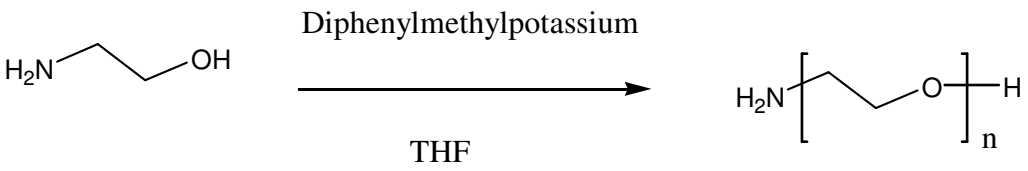

Figure 6.4: Reaction mechanism of amino PEO using an amino alcohol.

The proposed method to synthesise mono-amino PEO is to use a similar approach to that of Mosquek et al[12]. This method is less synthetically challenging than some of the

other proposed methods and by starting with a tertiary amino alcohol the possibility of obtaining $(PEO)_2$-NH and $(PEO)_3$-N should be removed.

6.2 Synthesis of quaternary amino PEO

The reaction scheme for the synthesis of a quaternary mono amino PEO is shown in Figure 6.5. The reaction was carried out in two stages; the first is the synthesis of mono functionalised amino PEO through the anionic polymerisation of ethylene oxide using dimethyl ethanol amine (DMEA) as an initiator. Diphenylmethyl potassium was used to remove the hydrogen from the ethanol of the DMEA enabling the DMEA to initiate the polymerisation of ethylene oxide. The second stage is the quarternisation of the amine end group on the PEO using methyl iodide. The target molecular weights for the PEO were 1600 and 5000 $gmol^{-1}$. These molecular weights were chosen as one lay above and one below the entanglement length of PEO which is 1600-2200 $gmol^{-1}$ [13].

a) Synthesis of mono functionalised amino PEO

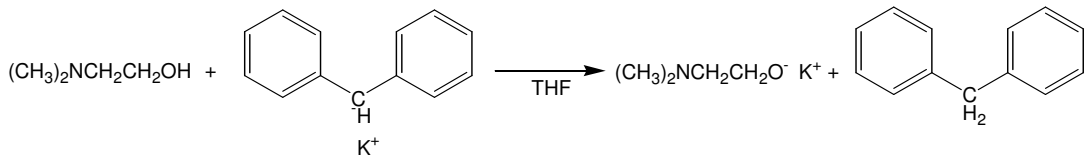

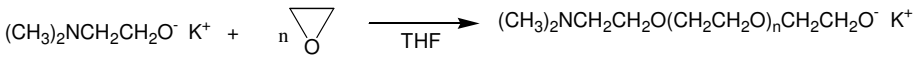

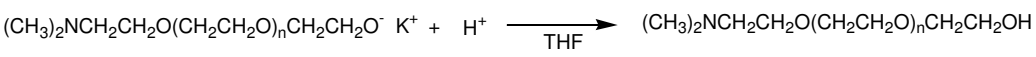

b) Quaternisation of mono functionalised amino PEO

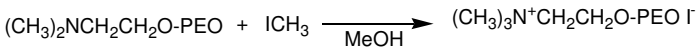

Figure 6.5: The reaction mechanism for the synthesis of quaternary amino PEO.

6.2.1 Anionic Polymerisation of mono functionalised amino PEO

6.2.1.1 Purification of Starting Materials

Mono functionalised amino PEO was synthesised using an anionic polymerisation technique. Anionic polymerisations are extremely sensitive to impurities, in particular water, so all reagents and solvents have to be rigorously dried before the anionic polymerisation can take place. The solvent tetrahydrofuran (THF) was freeze dried on a high vacuum line, in the presence of sodium wire and benzophenone. The benzophenone produces a complex with sodium in the absence of water and indicates when the solvent is dry. The reagents used in the reaction, ethylene oxide (EO), dimethylethanol amine (DMEA) and diphenylmethyl potassium (DPMK) were also vigorously freeze dried on a high vacuum line. Care was taken to ensure that EO remains below its boiling point (10.4^{o}C) at all times.

6.2.1.2 Anionic Polymerisation

Approximately 100mL of dry THF was distilled into a clean Christmas tree (Figure 6.6) and the freeze-degas-thaw process was repeated to ensure all the moisture was removed. The amount of initiator required for the reaction was calculated based on the amount of EO to be used and the target molecular weight as seen in equation(6.1), where M_n is the number average molar mass.

$$M_n = \frac{\text{Mass of Monomer}}{\text{Moles of Initiator}} \qquad \textit{(6.1)}$$

As diphenylmethyl potassium (DPMK) can directly polymerise EO leading to unwanted side products an excess of DMEA is used. A molar ratio of DMEA to DPMK of 1:0.8 was used instead of 1:1, ensuring that all the DPMK reacts with the DMEA without leaving excess DPMK which can react with EO. Another way of checking that there is no excess DPMK is by the disappearance of the deep red colour, as DPMK is red and DPMH is colourless. The appropriate volumes of DMEA and DPMK were transferred into the THF using an air tight syringe and stirred.

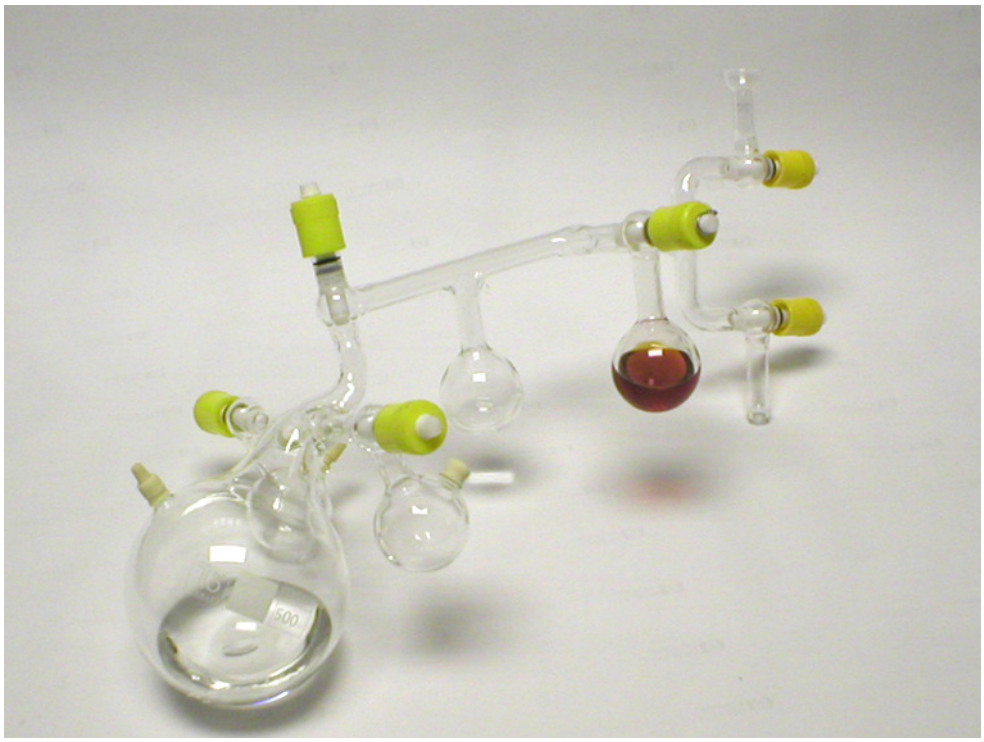

Figure 6.6: Christmas tree reaction flask.

Once the DPMK has reacted with the DMEA, the EO can be distilled into the Christmas tree flask. The reaction mixture was left stirring under vacuum at room temperature for 72 hours. As the reaction is a living polymerisation, there is no termination step, so the propagating chains were terminated by displacing the K^+ ions using a molar excess of acetic acid and generating the alcohol terminated PEO.

After the termination process the reaction mixture was removed from the high vacuum line and the PEO was precipitated from the THF using excess hexane (THF:hexane is 1:10). The white precipitate was collected by filtration using a Buckner funnel and dried in a vacuum oven for 48 hours.

6.2.2 Quaternisation of mono functionalised amino PEO

The reaction of mono amino PEO with methyl iodide (Aldrich) to produce a quaternary amino PEO needs to be carried out under dry conditions. Methyl iodide will react with water to give hydrogen iodide and methanol. The mono amino PEO and solvent (methanol) were purified on a high vacuum line to ensure all residual moisture is removed. Dry methanol (MeOH) (ten times the amount of PEO) was decanted into the

PEO flask and stirred until all the amino PEO was dissolved. Excess methyl iodide (1.5 times the number of amino end groups) was injected into the MeOH amino PEO solution and left to stir for 72 hours. Methyl iodide was used in excess to overcome any residual water which is present.

After 72 hours the reaction mixture was transferred into a round bottom flask and the MeOH was removed by rotor evaporation. The residue was dissolved in deionised water and washed three times with diethyl ether to remove any residual methyl iodide. The aqueous phase was then reduced to dryness using rotor evaporation leaving a cream coloured solid.

6.2.3 Characterisation

6.2.3.1 ^{1}H NMR

The mono functionalised amino PEO and its salt were characterised by ^{1}H NMR. The NMR traces are shown in Appendix A.9-10, the peaks and their corresponding structures are tabulated in Table 6.1. As expected the methyl peak shifts from 2.24 ppm to a higher chemical shift of 3.43 ppm. This is due to the presence of the positive charge on the nitrogen which increases the deshielding of the protons. It can be seen that the peak at 2.24ppm is no longer present in the NMR trace for the salt indicating that the reaction has gone to completion. A similar shift in the adjacent CH_2 peak can be seen from the NMR of PEO and its salt. There are two extra peaks in both the mono amino PEO and its salt, they lie either side of the PEO back bone peak (3.74 and 3.51 ppm). These peaks are the carbon satellites caused by small amounts of ^{13}C present in the PEO back bone.

^{1}H NMR data can also be used to determine the molecular weight of the PEO chains, by using the peak integrals which gives information on the number of protons present. By setting the integration height of a known peak to the corresponding number of protons (for example the integral of the $(N(C\underline{\mathbf{H}}_3)_2)$ peak can be set to six), then the number of protons in the PEO chain can be determined and hence the molecular weight. The calculated molecular weights are given in Table 6.2.

Table 6.1: The chemical shifts and their associated structures from the ^{1}H NMR of 5K PEO and 5K PEO salt. (a) broad peak b) carbon satellites can be seen at 3.51 and 3.74ppm)

	PEO Chemical shift(PPM)	PEO salt Chemical shift(PPM)
$N(C\underline{\mathbf{H}}_3)_2$	2.24 (s)	-
$N^+(C\underline{\mathbf{H}}_3)_3$	-	3.43 (s)
$NC\underline{\mathbf{H}}_2CH_2$	2.49 (t)	4.02[a]
$NCH_2C\underline{\mathbf{H}}_2O$	3.56 (t)	3.97 (t)
$OC\underline{\mathbf{H}}_2C\underline{\mathbf{H}}_2O$	3.62[b]	3.62[b]
$OCH_2C\underline{\mathbf{H}}_2OH$	3.71 (t)	3.71 (t)

6.2.3.2 Molecular Weight

Molecular weight measurements were carried out on the 5K and 1.6K PEO-$N(CH_3)_2$ using SEC. Due to the charges present in the 5K and 1.6K PEO-$N^+(CH_3)_3$ SEC could not be used to measure the molecular weight as the charge will cause the molecules to interact with the column and alter their retention time. The molecular weights for the PEO salt were measured using MALDI-ToF. Table 6.2 shows the molecular weight data for 5K and 1.6K PEO obtained from SEC, MALDI-TOF and NMR. The MALDI-ToF spectra for 1.6K PEO can be seen in Appendix A.11-12.

The target molecular weight is higher than the actual molecular weights; this is due to the presence of impurities such as water which can also cause initiation of PEO chains and reduce the overall molecular weight.

Table 6.2: Molecular weight data for 5K and 1.6K PEO and PEO-salt.

	M_n (g.mol^{-1}) (Target)	M_n (g.mol^{-1}) (NMR)	M_n (g.mol^{-1}) (MALDI)	M_n (g.mol^{-1}) (SEC)	PDI (SEC)
5K PEO	5000	4600	5000	4200	1.1
5K PEO salt	5000	4500	4900	-	-
1.6K PEO	1600		1600	1300	1.13
1.6KPEO salt	1600	1600	1600	-	-

6.3 Synthesis of PMMA/LRD-PEO nanocomposites

The first step in the synthesis of PMMA nanocomposites containing PEO modified Laponite RD (LRD) is the cation exchange between the unmodified LRD and the quaternary amino PEO synthesises in Chapter 6.2. To reduce the number of reaction steps the cation exchange was carried out in the reaction vessel, removing the need for drying the LRD-PEO and increasing probability of keeping an exfoliated structure. The average cation exchange capacity (CEC) for Laponite RD is 0.55meq/g. Tassin et al[10] showed that LRD fully saturated with PEO produced the highest reinforcing effects, so the amount of PEO used was calculated based on a CEC of 0.6meq/g to ensure total coverage of the LRD surface. The cation exchange reaction was carried out at a pH of 10 to prevent the degradation of the Laponite clay[14-16]. Once the cation exchange reaction has completed the free radical suspension polymerisation was carried out as described in Chapter 4.1.

For the synthesis of 0.5wt% 5K PEO-LRD, 1L of deionised water was measured into the polymerisation reaction flask and taken to pH10 using sodium hydroxide (Aldrich). 0.57g of Laponite RD (Southern Clay) was added and stirred using an overhead mechanical stirrer until the mixture became transparent; an indication that the Laponite had become exfoliated. 1.43 g of quaternary amino PEO was dissolved in 50 mL of deionised water in a separate beaker. Once the PEO has fully dissolved it was added gradually to the LRD/water mixture and left to stir for three days to ensure the exchange reaction goes to completion. 950 mL of deionised water and 4mol (400 g) of MMA monomer were added along with 9.9 mmol (2 g) CTA, 0.12 mol (12 g) ethyl propenoate, 100 g of suspending agent and 6.1 mmol (1 g) of AIBN. The pH of the aqueous phase was maintained at pH 10 through the use of a buffer solution[17]. The suspension was vigorously stirred using an overhead mechanical stirrer and was heated to reflux (83^{o}C) under a blanket of nitrogen. Once the reflux had resided (approximately 30 minutes) the reaction was heat treated at 90^{o}C for 2 hours to remove any residual monomer and then cooled to ambient temperature. The PMMA beads where filtered off and washed with deionised water and then dried in a vacuum oven at 80^{o}C for 24 hours.

PMMA nanocomposites containing 0.5 and 1 wt% of 5K PEO-LRD and 0.5wt% of 1.6 K PEO-LRD were synthesised.

6.4 Effect of Clay on the PMMA Molecular Weight

In PMMA nanocomposites containing either Cloisite 15a or Laponite RD clay it was found that the presence of the clay caused changes in molecular weight. The molecular weights of PMMA/PEO-LRD nanocomposites were also measured using SEC and are tabulated in Table 6.3. A 3000-13000 g.mol^{-1} increase in M_w was observed for the PCN accompanied by a slight increase in the PDI. The molecular weight distribution can be seen in the plot of weight fraction vs. molecular weight, Figure 6.7. The distribution is similar to that of PMMA, there was no indication of a bimodal distribution as was observed for PMMA/Laponite RD nanocomposites (Chapter 5.4).

Table 6.3: Molecular weight data obtained from SEC of PMMA and PMMA/PEO LRD nanocomposites.

	M_w(g.mol^{-1})	M_n(g.mol^{-1})	PDI
PMMA	75000	45000	1.8
0.5%1.6KPEOLRD	78000	33000	2.4
0.5%5KPEOLRD	84000	32000	2.6
1%5KPEOLRD	87000	38000	2.3

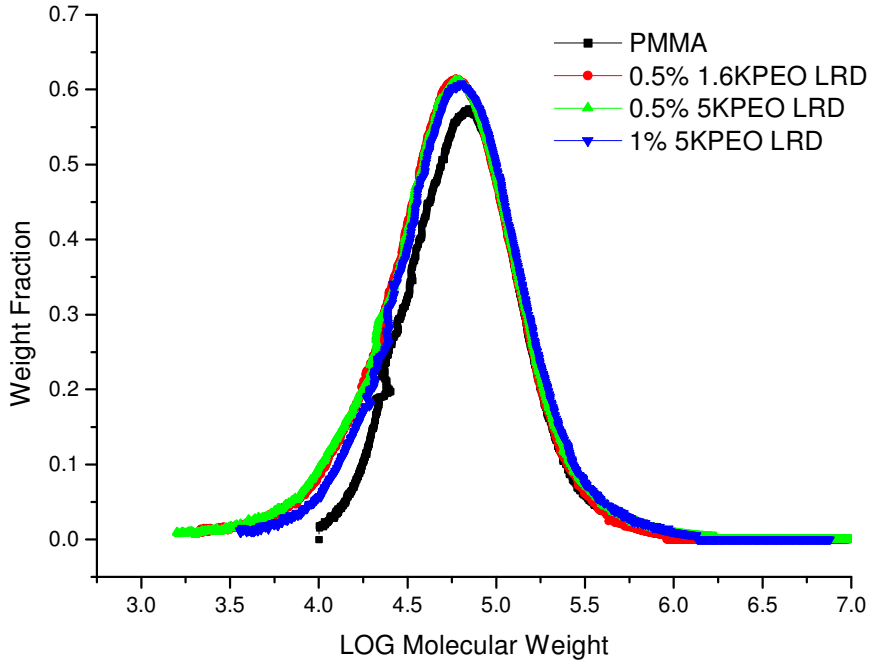

Figure 6.7: Weight fraction vs. molecular weight graphs for PMMA and PMMA/PEO LRD nanocomposites.

Previous studies containing 1 wt% of Cloisite 15a or LRD clay produced molecular weights of 800000 and 380000 $g.mol^{-1}$ respectively. These values are significantly larger than that of PEO-LRD samples. This suggests that the cation exchange with PEO helps reduce the undesired side reactions which were found to occur during the polymerisation process. There is a contradiction in the literature as to whether PEO chains can be found at the Laponite RD rims (edges). Nelson et al[18] proposed that the PEO can wrap or extend from one face to the other which would reduce the number of available lewis acid sites. Zebrowski et al[19] suggests that PEO can be absorbed onto the surface of the Laponite only. If PEO became absorbed around the clay rim the number of sites availed for radical attack will be significantly reduced. With the active sites on the clay blocked by the PEO chains the side reactions which were seen to take place during free radical suspension polymerisation are unable to take place.

The amount of additive used in the polymerisation was calculated based on mass of monomer; however the amount of clay in each will vary due to the presence of the cation. For example 1%5KPEO LRD will contain approximately 0.3wt% of LRD clay

the rest of the mass is made up of the PEO cation. By comparing 1%5KPEO LRD with 0.25-0.5%LRD then a lower molecular weight is still seen for the PEO-LRD nanocomposites suggesting that the PEO modification is useful in reducing the changes in molecular weight.

A closer look at the molecular weight values revels that on increasing the wt% of 5KPEO LRD clay the molecular weight also increased. The increase is small but it may be an indication of the interference of the clay with the suspension polymerisation process. To prove this, higher weight loadings will need to be investigated. The 0.5%5KPEO LRD also exhibit a higher molecular weight (84000 $g.mol^{-1}$) than that of 0.5%1.6KPEO LRD (78000 $g.mol^{-1}$). The difference in molecular weight of the matrix PMMA between the two samples is relatively small (6000 $g.mol^{-1}$) given the large PDI of the samples. It could also be an indication of the coverage of the PEO upon the clay surface. The more free active sites on the clay the larger the expected molecular weight suggesting that the 1.6KPEO provided a better surface coverage of the clay than that of 5KPEO.

6.5 Effect of Clay on the Thermal Properties of PCN

6.5.1 Differential Scanning Calorimetery

PEO has a T_g of approximately -67^oC [20] which is significantly lower than that of PMMA (115^oC). It was suggested in Chapter 4.6 that the dimethyl dehydrogenated tallow ammonium cations present on the montmorillonite surface may be acting as a plasticiser causing a slight decrease in T_g with higher clay loadings. With the glass transition of PEO being lower than that of PMMA a similar effect may be seen here. The average T_g values for PMMA/PEO LRD nanocomposites are tabulated in Table 6.4. The addition of PEO modified LRD clay was beneficial to the glass transition temperature although the increase was only slight (1-2^oC). Again with the changes in T_g being small they may be masked by the changes in molecular weight. So by using the Flory Fox equation (equation(4.3)) as given in reference[21] the glass transition at the

molecular weight values of the nanocomposites were predicted and tabulated in along side their average T_g (Table 6.4).

Table 6.4: Experimental and predicted T_g values for PMMA and PMMA/PEO LRD nanocomposites.

	T_g(^{o}C)	stand dev	Predicted T_g (^{o}C)
PMMA	115.3	0.2	115.3
0.5%1.6KPEOLRD	116.1	0.1	115.5
0.5%5KPEOLRD	116.2	0.2	115.7
1%5KPEOLRD	117.1	0.1	115.9

The Flory Fox equation as described in Chapter 4.6 predicts that an increase in T_g should be observed with increasing molecular weight. The glass transition temperatures of the PCN still appear larger than the predicted values suggesting that the molecular weight is not the only factor attributing to the changes in the glass transition. It was also seen that 1%5KPEO LRD has a higher T_g than 0.5%5KPEO LRD suggesting that at these levels clay is beneficial to the T_g. Higher clay loadings should be run to see if the presence of the cation causes any plasticisation of the material. Increases in T_g for PCN have been attributed to the confinement of the chains within the clay layers or the restriction of the chain motion due to an affinity to the clay surface. As the morphology of these PCN has not yet been studied, the reason of the increase in the T_g is unknown.

It was believed that the length of the PEO chains would affect the extent of its entanglement with the PMMA chains hence altering the materials physical properties. 1.6 Kg.mol^{-1} PEO is below the entanglement molecular weight for PEO, whilst 5 Kg.mol^{-1} PEO lies above the entanglement molecular weight. This provides a possible difference in the enganglement between the two samples. A glass transition of 116^{o}C was observed for both 0.5%1.6k and 0.5%5KPEO LRD. This shows that the length of the PEO chain plays no part in the change in the glass transition.

6.5.2 Thermogravimetric Analysis

TGA was carried out on Laponite RD, 5KPEO, 5KPEO salt and 5KPEO modified LRD and their corresponding traces can be seen in Figure 6.8. Laponite RD clay showed an initial mass loss due to residual water found in the clay structure[22]. A similar mass loss can be seen for 5KPEO-LRD and is also believed to be caused by residual water as both materials are hydrophilic. 5KPEO exhibits the largest mass loss whereas 5KPEO salt has a smaller mass loss due to the presence of the inorganic anions. 5KPEO modified Laponite RD has the smallest mass loss as the clay does not decompose at these temperatures. The reduced mass loss shows that both PEO and Laponite RD clay is present in the sample.

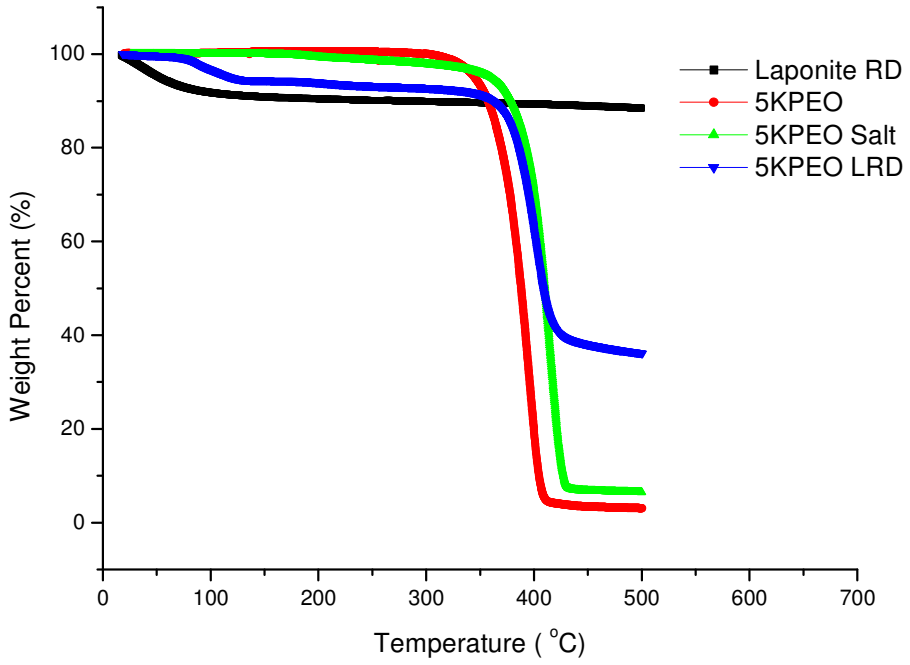

Figure 6.8: TGA traces for Laponite RD, 5KPEO, 5KPEO salt and 5KPEO modified Laponite RD

The cations present on the Cloisite 15a clay were seen to degrade at a lower temperature than that of PMMA causing a slight decrease in the degradation temperature for the PCN at lower mass losses. Unlike Cloisite 15a the PEO cations have a higher thermal stability than that of PMMA with the temperature for 10% mass loss of 362°C. This

means that there will be no interference in the mass loss due to the early onset of the cation degradation as observed for Cloisite 15a.

The TGA traces for PMMA/PEO LRD nanocomposites are shown in Figure 6.9. The temperature profile is the same for all samples, however there is a shift to higher temperature for all PCN. This suggests a slight increase in thermal stability for the PCN. The temperature at which 5, 10, 30, 50 and 70% weight loss occurs are tabulated in Table 6.5. The table shows that all PEO-LRD nanocomposites have a similar temperature for x% mass loss which is approximately 10^{o}C higher than PMMA. The degradation temperatures for PEO-LRD nanocomposites are also higher than that of the PMMA/Laponite RD nanocomposites. For example 1%LRD showed a similar temperature profile to that of PMMA, however 1%5KPEO LRD exhibits approximately a 10^{o}C increase in temperature for the loss of x weight % compared to that of PMMA. The reason for the increase is unknown but could be due to a higher degree of dispersion of the clay or the combined thermal properties of the PEO and LRD clay.

Table 6.5: Temperature for 5, 10, 30, 50 and 70% weight loss for PMMA and PMMA/PEO LRD nanocomposites.

	Temperature for x% Weight Loss (^{o}C)				
	5% wt loss	**10% wt loss**	**30% wt loss**	**50% wt loss**	**70% wt loss**
PMMA	319	338	362	375	385
0.5% 1.6KPEO LRD	327	347	371	383	394
0.5% 5KPEO LRD	334	348	371	385	396
1% 5KPEO LRD	329	347	371	384	394

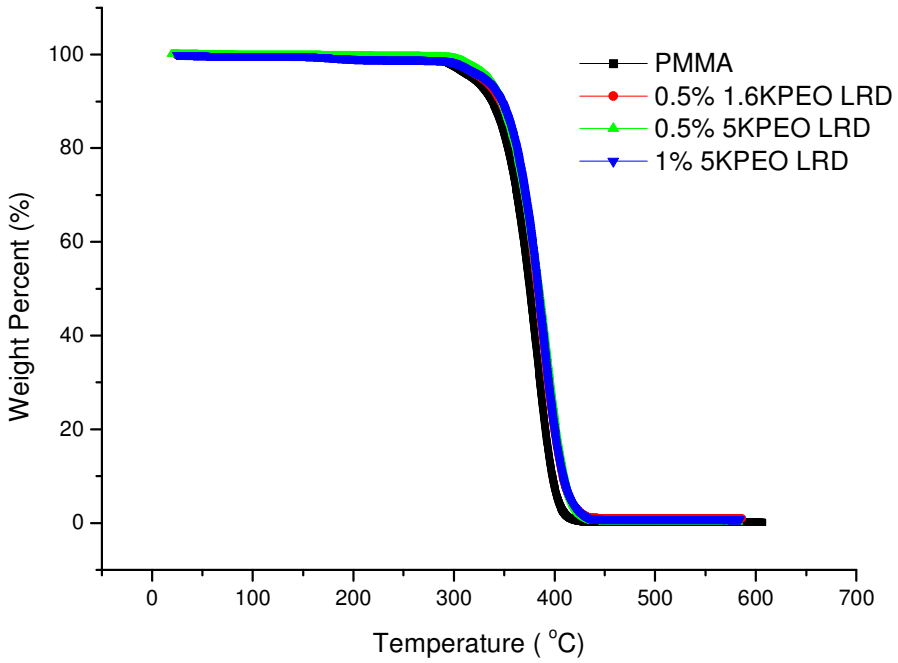

Figure 6.9: TGA traces for PMMA and PMMA/PEO LRD nanocomposites.

6.6 Effect of Clay on the Rheology of PCN

Rheology of the PMMA/PEO LRD nanocomposites was studied to gain insight into the presence of any network structure which may have formed. The master curves for PMMA and PMMA/PEO LRD nanocomposites containing both 1.6K and 5KPEO are shown in Figure 6.10. The lower frequency data for the nanocomposites differ from that of PMMA as the gradients of the PCN appear lower than that of PMMA.

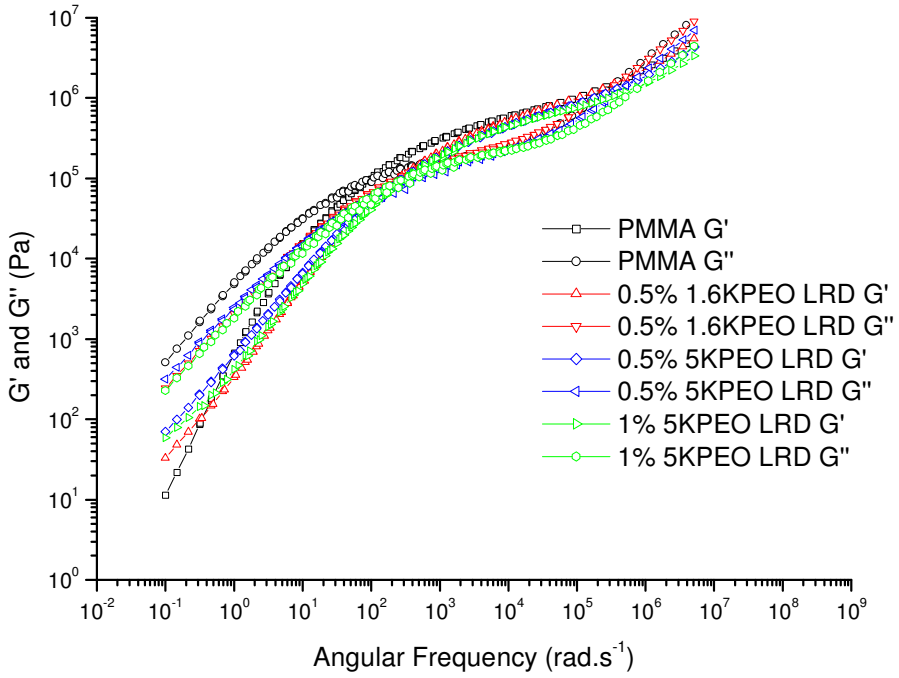

Figure 6.10: Oscillatory shear rheology plots of PMMA and PMMA/PEO LRD nanocomposites.

Table 6.6: Terminal gradients of G' and G'' for PMMA and PMMA/PEO LRD nanocomposites.

	G' gradient	G'' gradient
PMMA	1.70	0.94
0.5% 1.6KPEO LRD	1.08	0.91
0.5% 5KPEO LRD	0.98	0.84
1% 5KPEO LRD	0.96	0.87

The gradients of G' and G'' in the terminal region were measured and their values are tabulated in Table 6.6. All PMMA/PEO LRD nanocomposites exhibited a decrease in the gradient showing the reinforcing effects of the clay. The gradients of 5KPEO samples are smaller than those of the 1.6KPEO LRD indicating that the network effect is more pronounced in the 5KPEO nanocomposites. It was expected that the 1.6KPEO would exhibit the largest change as on a wt% basis it contains a higher percentage of clay. As 5KPEO has the largest network it would suggest that a higher extent of dispersion has been reached, the larger 5KPEO cations may be preventing the aggregation of the clay platelets. As the wt% of 5KPEO was increased from 0.5 to 1%

the gradient was seen to increase further. This was expected as an increase in the amount of clay will increase the extent of network formation within the PMMA matrix.

By comparing the rheology of 1%5KPEO LRD with that of 1%LRD, it was seen that the unmodified LRD produces the lowest gradient and hence the strongest network. Unlike 1%LRD the reptation crossover is still observed in 1%5KPEO LRD suggesting that the network is not significant enough to hide the effects of the reptation process of PMMA chains. As discussed earlier 1%5KPEO LRD contains less clay than 1%LRD for the amount of additive is based on a wt%. For 1%5KPEO LRD there is an equivalent of 0.3 wt% LRD clay, hence a weaker network structure is expected. However when comparing 1%5KPEO LRD with that of 0.25-0.5%LRD the G' gradient of PEO-LRD PCN is still higher. In the PMMA/Laponite RD nanocomposites the suspension droplets provided a template for the Laponite RD clay making it possible to produce a percolated network throughout the material once the beads have been heat pressed together. The weaker network seen in the 1%5KPEO LRD suggests that the templating effect is not as prominent or does not occur as the compatibility between the clay and MMA will have altered on modification with PEO cations. The lack of percolated network could also be an indication of improved dispersion of the PEO-LRD throughout the PMMA matrix.

6.7 Conclusion

This chapter showed the successful synthesis of mono amino PEO using dimethyl ethanol amine as an initiator. The mono amino PEO was converted into a quaternary salt via the addition of methyl iodide to the ammonium end group. The mono amino PEO and its salt was characterised using NMR and a shift in methyl groups on the ammonium was seen, indicating the ammonium had been quaternised. Two different molecular weight PEO chains were synthesised with the target molecular weights of 5000 $g.mol^{-1}$ and 1600 $g.mol^{-1}$. The PMMA/PEO LRD nanocomposites were prepared via free radical suspension polymerisation. The modification of the LRD clay with PEO was carried out in the reaction flask prior to the suspension polymerisation. This

reduces the number of steps required in the synthesis making it more appealing for industrial scale up.

Although a limited number of PMMA/PEO LRD nanocomposites were synthesised beneficial properties in the PCN were observed. Firstly, studies of the matrix PMMA showed no large increase in molecular weight suggesting that the PEO was covering the active sites in the clay preventing the radical attack. The production of high molecular weight polymer will make the processing of the material difficult. Improvements in thermal stability were also observed and the 5KPEO salt was seen to have a higher thermal stability than that of PMMA. This means that the degradation of the cations will not interfere with the degradation of the PMMA matrix as was seen for Cloisite 15a PCN. All PMMA/PEO LRD nanocomposites exhibited similar values for x% weight loss at an average of 10^{o}C higher than those of pure PMMA. This is a significant increase in thermal stability and is believed to be caused by a higher degree of dispersion or the combined thermal stability properties of the PEO and LRD clay.

The frequency sweep master curves of the PMMA/PEO LRD nanocomposites showed similar Rouse relaxation times, but changes in the terminal gradients were observed. All PCN showed a decrease in the G' and G'' gradient, however it was suggested that 5KPEO LRD produced a higher degree of dispersion than that of 1.6KPEO LRD. As the wt% of clay was increased the gradient decreased indicating the presence of a more extended network.

Laponite RD was modified with both 1.6K and 5KPEO and it was believed that differences in physical properties would be observed due to their ability to interact/entangle with the surrounding PMMA chains. Similar physical properties were seen for both PEO chain lengths suggesting an insignificant difference between the ability of the PEO chains to entangle with the matrix or that the covering of the clay surface was more important than entanglement between the PMMA and PEO chains. It was also observed that increasing the wt% of additive improved the physical properties of the PCN as seen in the DSC and rheology data. However further measurements should be made to confirm this.

6.8 References

1. Rubinstein, M.; Colby, R. H., *Polymer Physics*. Oxford University Press: 2003.
2. Ito, H.; Russell, T. P.; Wignall, G. D. *Macromolecules* **1987,** 20, (9), 2213-2220.
3. Hamon, L.; Grohens, Y.; Soldera, A.; Holl, Y. *Polymer* **2001,** 42, (24), 9697-9703.
4. Chen, X.; Yin, J. H.; Alfonso, G. C.; Pedemonte, E.; Turturro, A.; Gattiglia, E. *Polymer* **1998,** 39, (20), 4929-4935.
5. Machado, J. C.; Silva, G. G.; Soares, L. S. *Journal of Polymer Science Part B-Polymer Physics* **2000,** 38, (8), 1045-1052.
6. Hopkinson, I.; Kiff, F. T.; Richards, R. W.; King, S. M.; Farren, T. *Polymer* **1995,** 36, (18), 3523-3531.
7. Kim, H. B.; Choi, J. S.; Lee, C. H.; Lim, S. T.; Jhon, M. S.; Choi, H. J. *European Polymer Journal* **2005,** 41, (4), 679-685.
8. Shen, Z. Q.; Simon, G. P.; Cheng, Y. B. *Journal of Applied Polymer Science* **2004,** 92, (4), 2101-2115.
9. Mongondry, P.; Bonnans-Plaisance, C.; Jean, M.; Tassin, J. F. *Macromolecular Rapid Communications* **2003,** 24, (11), 681-685.
10. Loiseau, A.; Tassin, J. F. *Macromolecules* **2006,** 39, (26), 9185-9191.
11. Nagasaki, Y.; Iijima, M.; Kato, M.; Kataoka, K. *Bioconjugate Chemistry* **1995,** 6, (6), 702-704.
12. Mosquet, M.; Chevalier, Y.; LePerchec, P.; Guicquero, J. P. *Macromolecular Chemistry and Physics* **1997,** 198, (8), 2457-2474.
13. Walkenhorst, R.; Selser, J. C.; Piet, G. *Journal of Chemical Physics* **1998,** 109, (24), 11043-11050.
14. Nicolai, T.; Cocard, S. *Langmuir* **2000,** 16, (21), 8189-8193.
15. Thompson, D. W.; Butterworth, J. T. *Journal of Colloid and Interface Science* **1992,** 151, (1), 236-243.
16. Mongondry, P.; Tassin, J. F.; Nicolai, T. *Journal of Colloid and Interface Science* **2005,** 283, (2), 397-405.
17. Georgiadou, S.; Brooks, B. W. *Chemical Engineering Science* **2005,** 60, (24), 7137-7152.
18. Nelson, A.; Cosgrove, T. *Langmuir* **2004,** 20, (6), 2298-2304.
19. Zebrowski, J.; Prasad, V.; Zhang, W.; Walker, L. M.; Weitz, D. A. *Colloids and Surfaces a-Physicochemical and Engineering Aspects* **2003,** 213, (2-3), PII S0927-7757(02)00512-5.
20. Cowie, J. M. G., *Polymers : chemistry and physics of modern materials*. 2nd ed.; CRC: 1991.
21. Odriscoll, K.; Sanayei, R. A. *Macromolecules* **1991,** 24, (15), 4479-4480.
22. Olphen, H. V.; Fripiat, J. J., *Data handbook for clay materials and other non-metallic minerals* 1st ed.; Pergamon Press: 1979.

Chapter 7 Conclusion

7.1 Conclusion

Free radical suspension polymerisation was used to synthesise (in situ) three different PMMA clay nanocomposites (PCNs) with varying weight fractions of clay. The first PCN system studied contained a natural montmorillonite clay, organically modified with dimethyl dehydrogenated tallow ammonium salt (Cloisite 15a). The resulting nanocomposites were found to have an intercalated structure and an off white appearance caused by the discolouration of the clay. The second system studied used the synthetic clay Laponite RD which contained Na^+ cations on the surface. The clay was found to form an unusual, continuous network structure throughout the material and, unlike Cloisite 15a nanocomposites the material was colourless in appearance. The third system to be studied used a PEO modified Laponite RD. Mono amino PEO was synthesised using dimethylethanol amine as an initiator. The modification of the Laponite RD took place in the reaction flask prior to the suspension polymerisation.

An important property of the PCN is its morphology, as the degree of clay dispersion will dramatically affect the properties of the material. Despite the organic modification of Cloisite 15a to reduce its hydrophilicity, an intercalated structure was observed with large areas of the material containing no clay. A high degree of intercalation was seen with an increase in d001 spacing suggesting that the PMMA was present between the clay platelets swelling the clay. This showed that there was some degree of compatibility between the clay and polymer. Despite this apparent compatibility the resulting areas containing no clay, suggest that only poor mixing was achieved. The suspension polymerisation is constantly stirred, but once the average droplet size has been achieved, there will be minimal shear force on the clay platelets to promote mixing.

The unmodified Laponite RD was initially believed to show a lesser degree of dispersion than that of Cloisite 15a due to its high hydrophilicity, however TEM images of heat pressed samples showed that a percolated network was present throughout the samples. The laponite RD was not fully compatible with MMA but instead acted as a suspending agent during suspension polymerisation. The result was PMMA beads coated with Laponite RD clay giving the appearance of a percolated network when heat pressed. The Laponite RD clay exhibited a lower level of compatibility with the MMA than that of Cloisite 15a, as little clay was observed within the PMMA beads. Further work needs to be carried out on the compatibility between MMA and clay in order to produce a PCN in which the clay shows a higher degree of dispersion. Modification of the clay with an acrylic group could be used to improve compatibility and would also have the advantage of tethering the propagating chains to the surface of clay. This could force the separation of the clay platelets and may lead to improved physical properties[1]. Despite the poor dispersions in the materials studied, the coating of PMMA beads with clay provides an alternate and intriguing route to producing network structures.

Addition of clay to the suspension polymerisation was found to result in changes in the molecular weight of the resulting polymer and it was established that the clay modifies the suspension polymerisation. Nanocomposites containing Cloisite 15a clay had the greatest impact, resulting in increases in molecular weight of up to 830%. The molecular weight was seen to increase with increasing wt% clay reaching a maximum molecular weight with a weight fraction of clay of 0.5 %. The clay was suspected to be reacting with the CTA, which was confirmed by carrying out the suspension polymerisation in the absence of CTA – nearly identical molecular weights were achieved. The maxima in molecular weight was caused by the presence of sufficient clay to react with all the CTA, the addition of higher clay loadings caused little change to the molecular weight.

The presence of Laponite RD clay also caused a change in the molecular weight distribution of the PMMA matrix. Unlike the changes seen in the Cloisite 15a nanocomposites, the presence of Laponite clay resulted in a bimodal molecular weight distribution with the lower molecular weight peak occurring at a similar molecular

weight to that of unmodified PMMA. The molecular weight changes in Laponite RD nanocomposites are not thought to be caused by the reaction of the clay with the CTA. The reason for the bimodality is unknown but suggests the presence of heterogeneous reaction conditions. It was observed that the quantity of high molecular weight present in the PMMA matrix increased with increasing wt% of Laponite RD suggesting the involvement of the clay. Upon the sieving of the 1%LRD suspension beads, the molecular weight increased with decreasing particle size which again can be related to the increasing clay content.

These two different nanocomposites systems showed that different clays will react in different ways during the same suspension polymerisation highlighting the need for careful characterisation of the matrix polymer. A possible way of preventing these changes in molecular weight is by blocking the reaction sites. The modification of Laponite RD with PEO showed only a small increase in molecular weight (< 13000 $g.mol^{-1}$) and it was believed that the PEO may be blocking the active sites on the rim of the clay platelets.

Oscillatory shear rheology of PMMA/Cloisite 15a and PMMA/Laponite RD nanocomposites showed that changes in the relaxation mechanism was occurring with either an increase in reptation time or the disappearance of the crossover point. The change in observed rheology suggests the formation of a network structure within the material. However the increase in molecular weight and polydispersity of the matrix PMMA will also affect the rheological behaviour of the materials. To distinguish between the two effects, the rheology of the PCN was predicted using the time dependent diffusion model by des Cloizeaux, along with double reptation, so that the effects of polydispersity could be included. The results showed that the rheological properties of the PCN with Cloisite 15a were dictated by molecular weight and that the clay appeared to have little effect on the rheology. However the rheology of the 1% LRD PCN resulted from the formation of a percolated network; chains will probably undergo reptation, but the network contribution to the modulus will be much greater. The presence of Laponite RD clay produced beneficial effects on the rheological properties of the resulting PCN in contrast to the PCNs formed with Cloisite 15a. This

highlights the importance of producing PCNs in which the clay is well dispersed in order to achieve the desired enhancements in the rheological properties.

A gradual decrease in the gradient of G' in the lower frequency range was seen with an increasing weight fraction of Laponite RD, illustrating the increasing effect of the network on the restriction of the reptation process with increasing clay content. The loss of the reptation crossover occurred between 0.5 and 1%LRD indicating that greater than 0.5 wt% of Laponite RD clay is required to fully mask the contribution of relaxation by reptation relaxation to stress relaxation. After the 1%LRD underwent stress sweeps, the oscillatory shear data for 1%LRD showed the presence of the reptation crossover. The crossover observed occurs at a similar angular frequency to that of the pure PMMA sample, suggesting that the linear rheology was not influenced by the high molecular weight fraction in the PCN. This was also seen by the differences in the predicted and experimental relaxation times for the 1%LRD calculated using the molecular weight distribution obtained from SEC.

For the materials to be used on a commercial scale the beads will need to be injection moulded into the desired shape. The rheology showed the large relaxation times of the PCN compared to those of unmodified PMMA suggesting higher temperatures and longer relaxation times would be required for the processing of these materials. Preliminary experimental observations for processing of 1%LRD showed that a large die swell occurred making the material difficult to process. However the Cloisite 15a PCN was successfully processed using a micro moulding instrument. The orientation of the clay platelets with the flow field was studied using SAXS. The SAXS measurements confirmed the alignment of the platelets which will consequently introduce directionality to the properties of processed PCN materials.

Although there were mixed results with regards to the enhancement of physical properties in the resulting PCNs, some important observations were made. Clays were found to participate in side reactions during the free radical polymerisation causing changes to the molecular weight and molecular weight distribution. The reactivity of the clay should be considered when contemplating the preparation of PCN especially when using an in-situ polymerisation technique. This work also shows the need for

thorough characterisation of the PCN. Rheology is often used to 'confirm' the positive effects of clay nanocomposites. However rheology in isolation is not capable of substantiating such claims as demonstrated in this work. We have shown through the use of SEC and theoretical predictions of rheology that changes in rheology were due to the changes in the matrix polymer and not the presence of the clay. The rheology of Laponite RD clays showed an increase in the terminal gradients of G' and G'' due to the presence of a percolated network. It was thought that the Laponite RD clay was acting as a suspending agent during the suspension polymerisation. Although the use of Laponite RD as a suspending agent has been previously reported[2, 3] this is the first time (to our knowledge) that this approach has resulted in an effective way of producing a percolated network throughout the material and may have a potential use as a nanotemplate.

7.2 Reference

1. Huang, X. Y.; Brittain, W. J. *Macromolecules* **2001,** 34, (10), 3255-3260.
2. Bon, S. A. F.; Colver, P. J. *Langmuir* **2007,** 23, (16), 8316-8322.
3. Cauvin, S.; Colver, P. J.; Bon, S. A. F. *Macromolecules* **2005,** 38, (19), 7887-7889.
4. Tabtiang, A.; Lumlong, S.; Venables, R. A. *European Polymer Journal* **2000,** 36, (12), 2559-2568.
5. Choi, H. J.; Kim, S. G.; Hyun, Y. H.; Jhon, M. S. *Macromolecular Rapid Communications* **2001,** 22, (5), 320-325.

Appendix A Additional Data

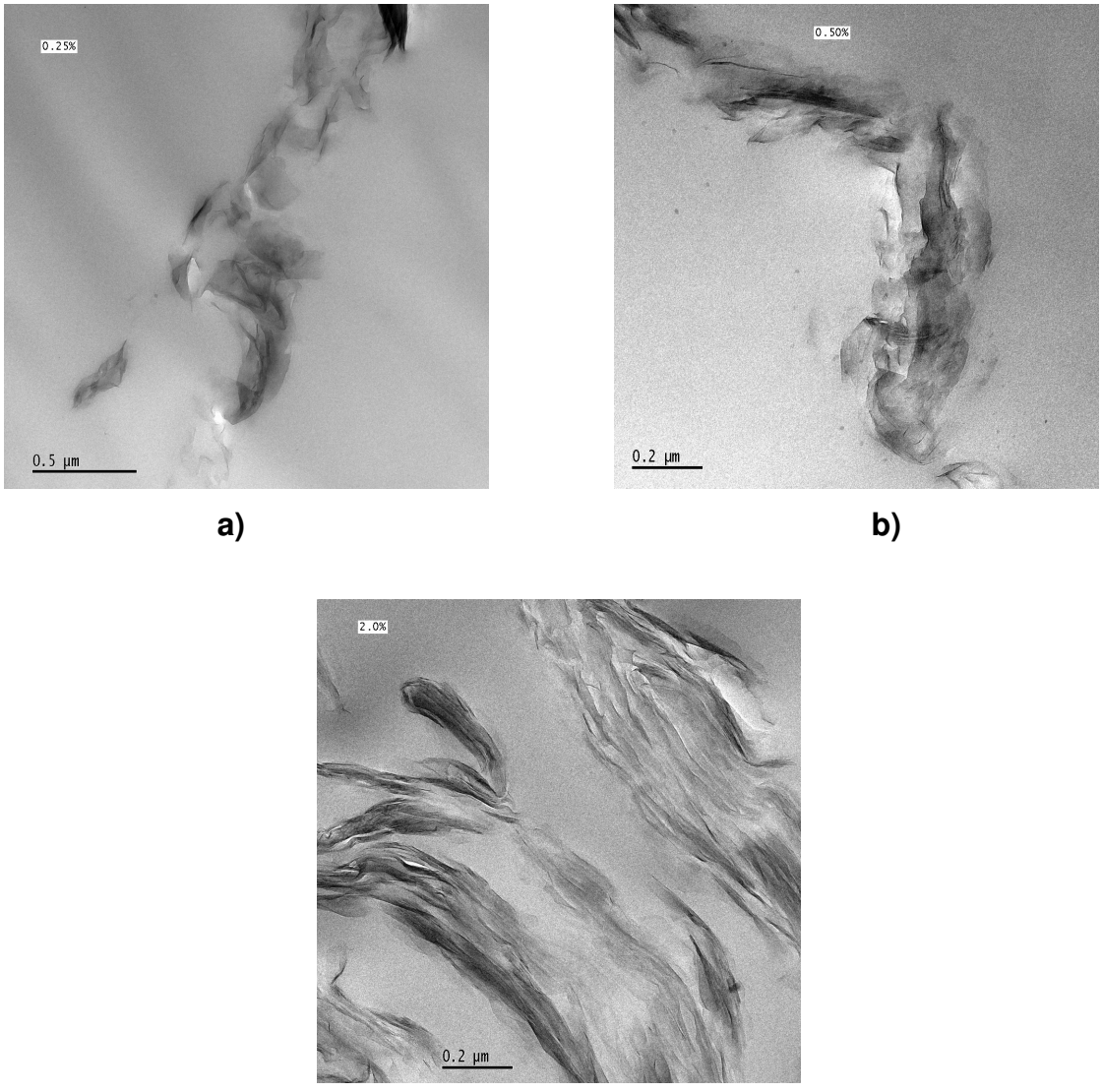

Figure A.1: TEM images of a) 0.25%C15a on a 0.5µm scale, b) 0.5%C15a and c) 2%C15a on a 0.2µm scale.

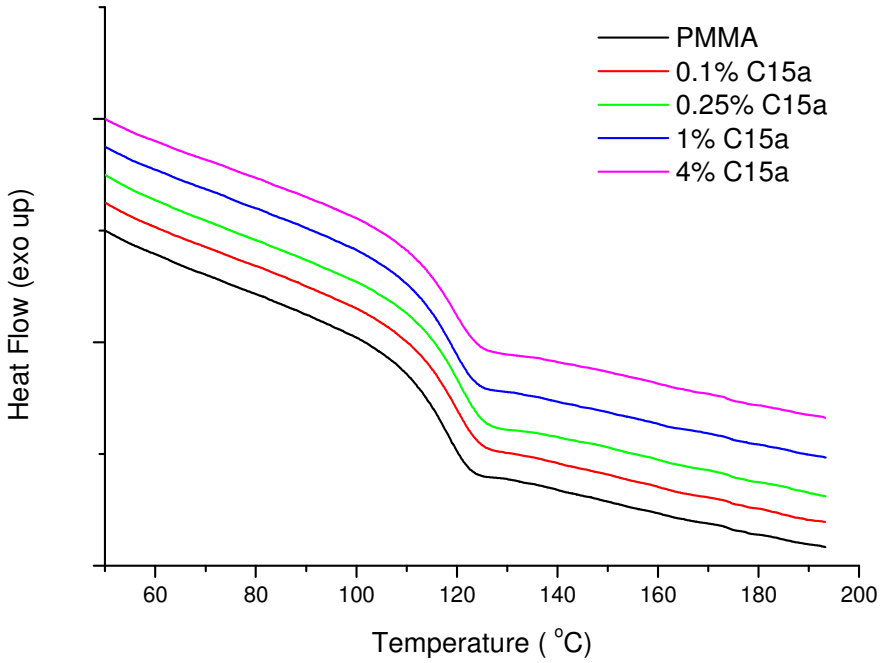

Figure A. 2: DSC traces for PMMA and PMMA C15a nanocomposites.

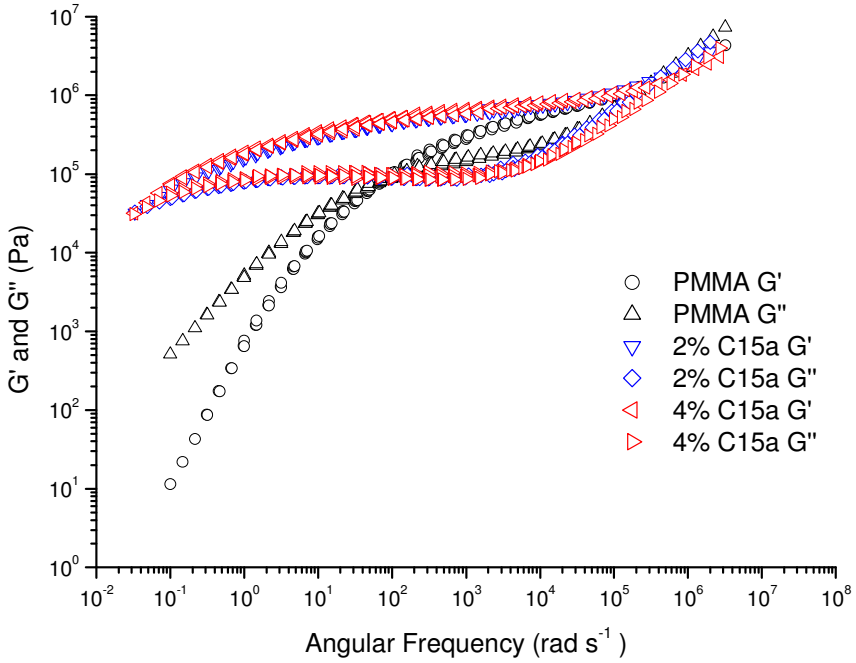

Figure A 3: Oscillatory shear rheology of PMMA, 4%C15a and 2%C15a after TTS has been applied. A reference temperature of 230°C was used.

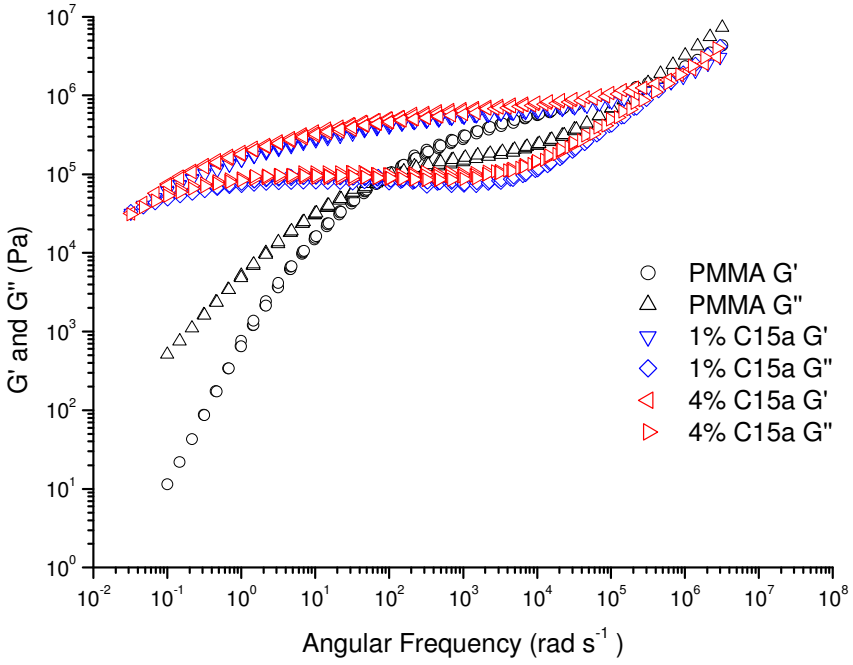

Figure A.4: Oscillatory shear rheology of PMMA, 4%C15a and 1%C15a after TTS has been applied. A reference temperature of 230^{o}C was used.

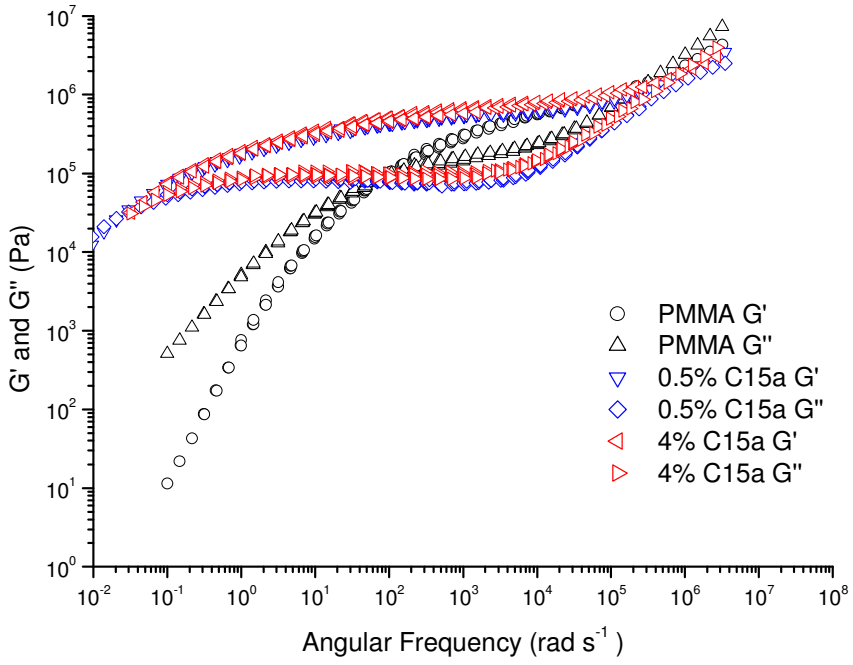

Figure A.5: Oscillatory shear rheology of PMMA, 4%C15a and 0.5%C15a after TTS has been applied. A reference temperature of 230^{o}C was used.

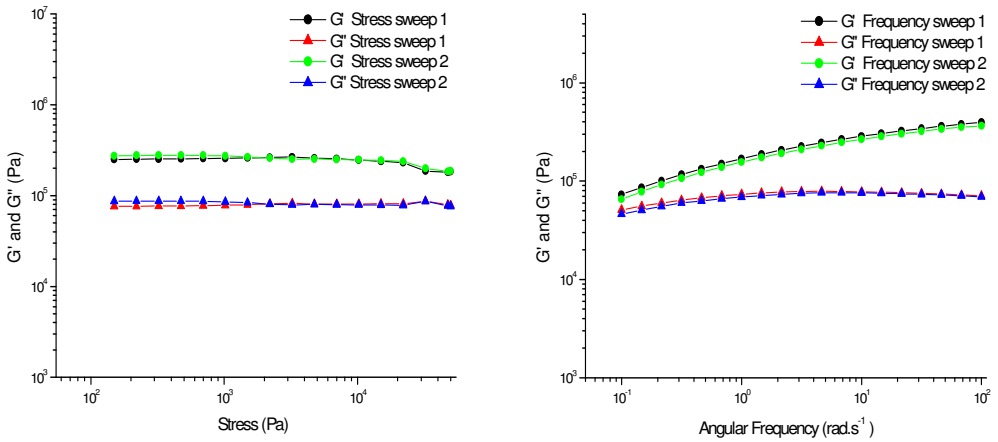

Figure A.6: First and second, stress and frequency sweeps for 4%C15a.

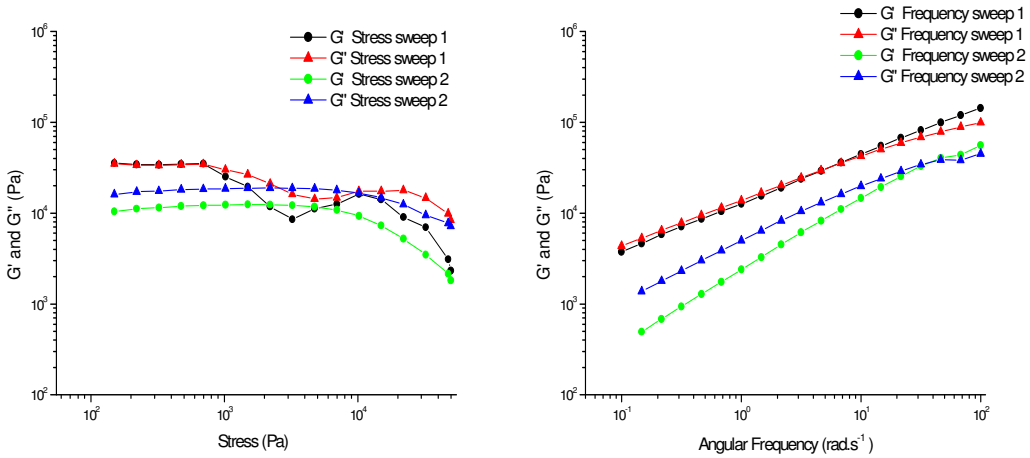

Figure A 7: First and second, stress and frequency sweeps for 0.5%LRD.

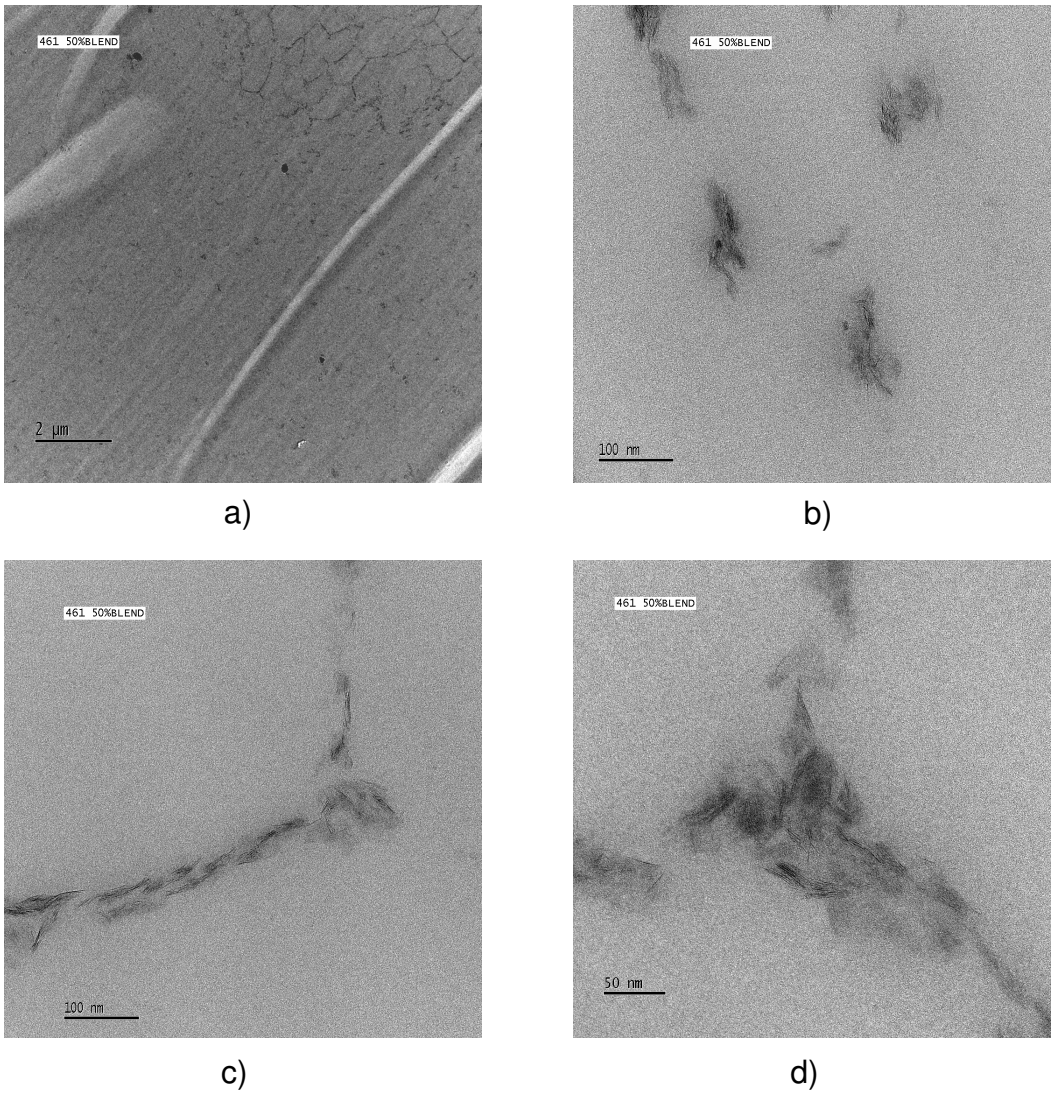

Figure A. 8; TEM images of pelletised 50:50 PMMA:1%LRD at scales of a) 2 µm, b) 2 µm , c) 0.2 µm and b) 0.2 µm

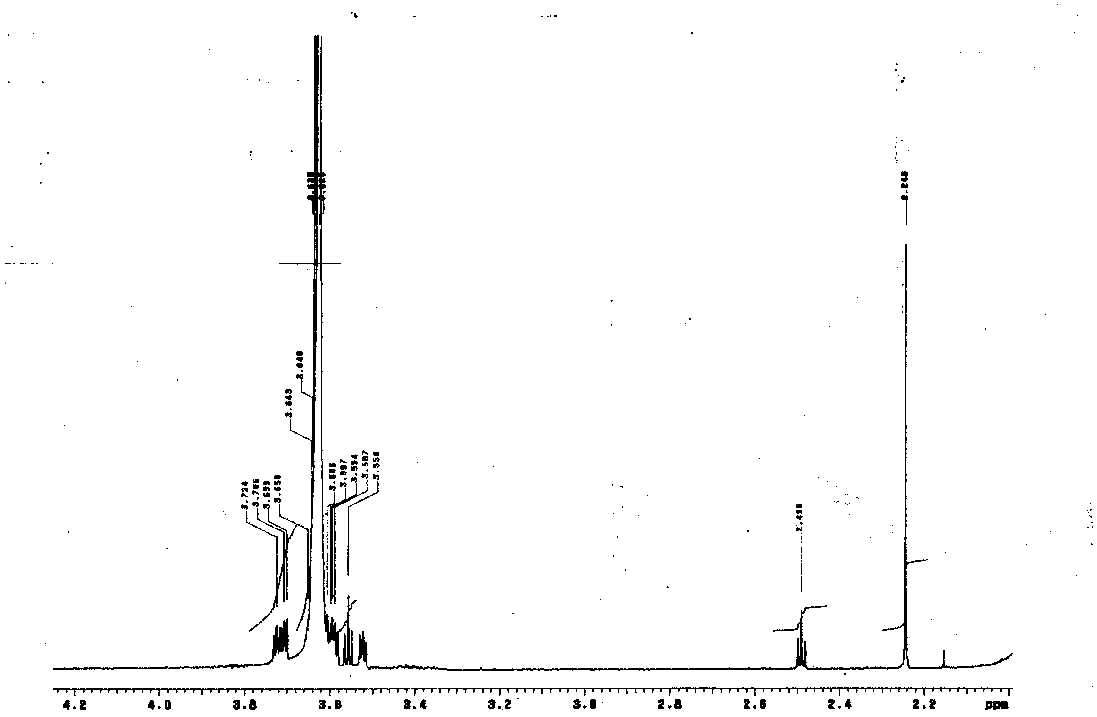

Figure A.9: ^{1}H NMR of 5K mono functionalised amino PEO.

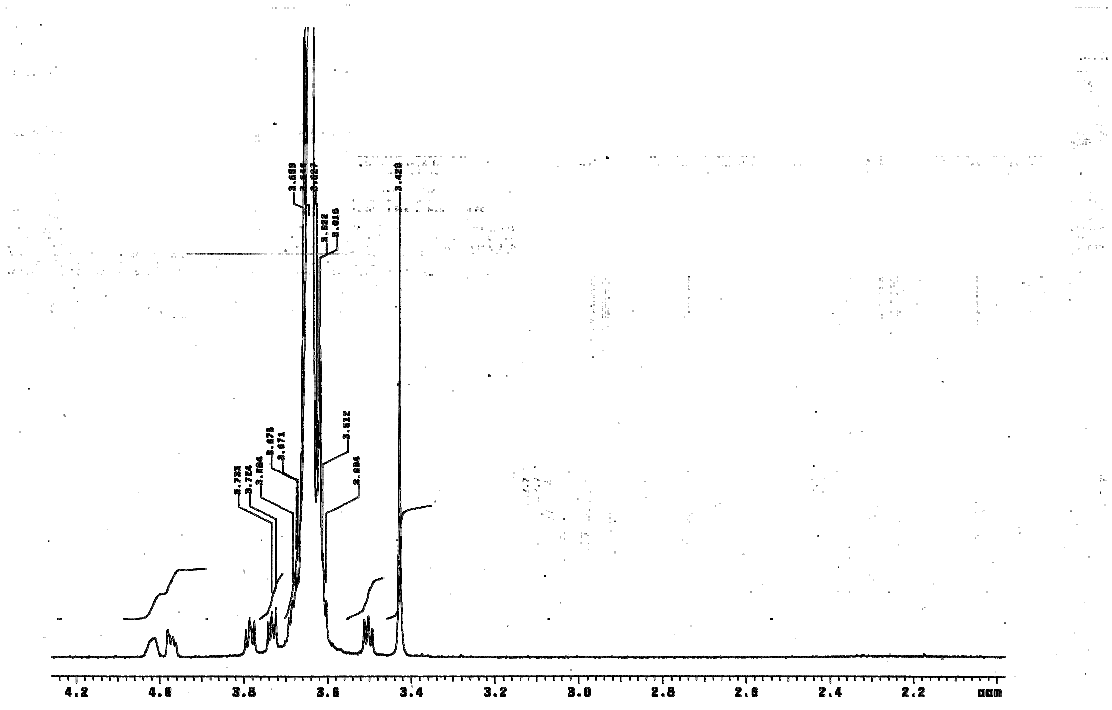

Figure A.10: ^{1}H NMR of 5K mono functionalised quaternary amino PEO.

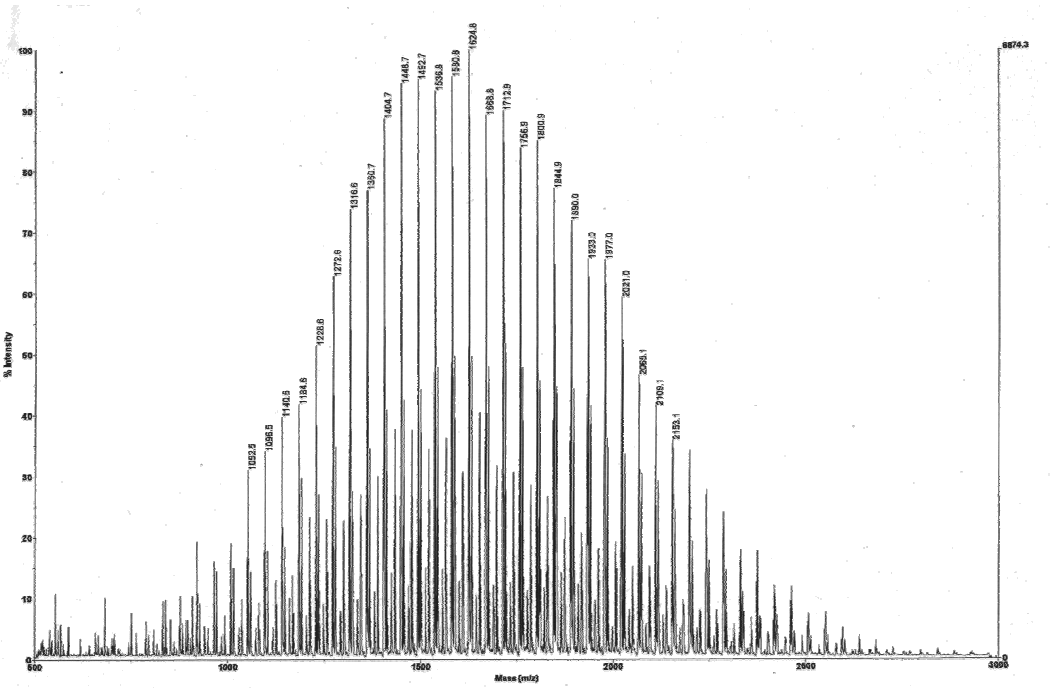

Figure A. 11: MALDI-ToF spectra of 1.6K mono functionalised amino PEO.

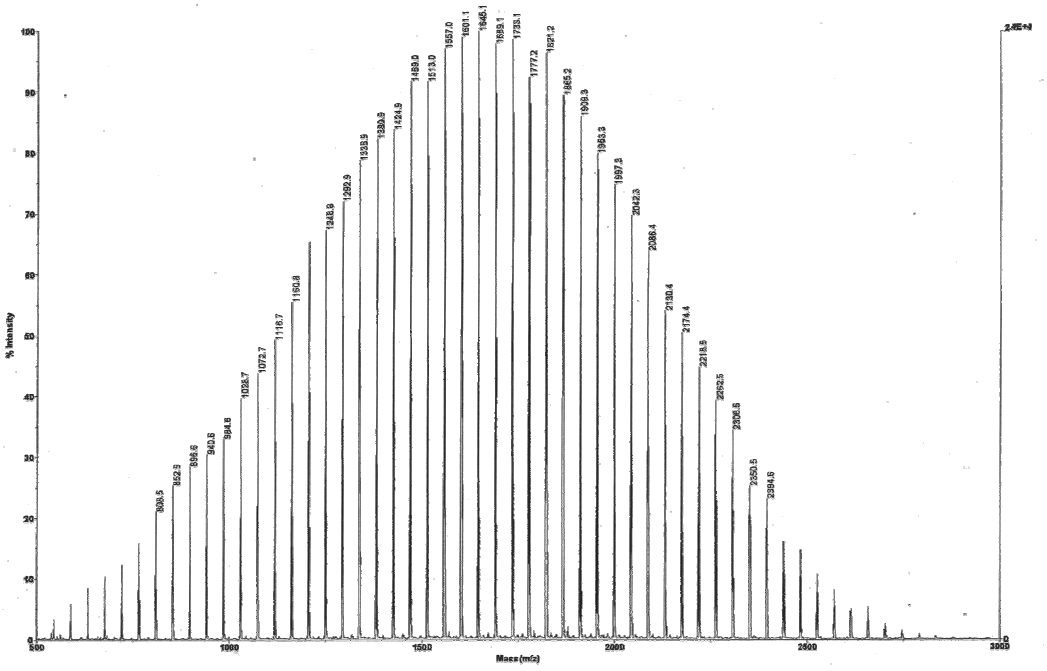

Figure A. 12: MALDI-ToF spectra of 1.6K mono functionalised amino PEO.

Appendix B Bead Size Calculations

It has been suggested that Laponite RD clay is acting as a suspending agent during the suspension polymerisation of PMMA/Laponite RD nanocomposites. The PMMA bead size in the presence of Laponite RD can be calculated by comparing the surface area of PMMA beads and Laponite RD clay, assuming monolayer coverage of the clay. Physical constants used during the calculation are as follows;

Density of PMMA	$1.19E^{3}$ Kgm^{-3}
Diameter of Laponite	$2.50E^{-8}$ m
Height of Laponite	$1.00E^{-9}$ m
Density of Laponite	$1.00E^{3}$ Kgm^{-3}

The number of PMMA beads present during the suspension polymerisation is equal to the total volume of PMMA (V_{PMMA}) divided by the volume of one bead (V_{bead}).

$$\textbf{Number of PMMA beads} = \frac{V_{PMMA}}{V_{bead}}$$

The total surface area of PMMA beads (T_{PMMA}) of radius r is calculated as follows;

$$\begin{aligned} T_{PMMA} &= \textbf{Number of beads} \times \textbf{SA of one bead} \\ &= \frac{V_{PMMA}}{V_{bead}} \times 4\pi r^{2} \\ &= \frac{V_{PMMA}}{\frac{4}{3}\pi r^{3}} \times 4\pi r^{2} \\ T_{PMMA} &= \frac{3V_{PMMA}}{r} \end{aligned}$$

Similarly the number of Laponite RD platelets present during the suspension polymerisation is equal to the total volume of Laponite RD (V_{LRD}) divided by the volume of one platelet ($V_{platelet}$).

$$\textbf{Number of LRD platelets} = \frac{V_{LRD}}{V_{platelet}}$$

Only one surface of the clay platelet (of radius r_l and height h) will be in contact with the PMMA beads. The total surface area of Laponite RD in contact with PMMA beads (T_{LRD}) is calculated as follows;

$$\begin{aligned} T_{LRD} &= \textbf{Number of platelets} \times \textbf{SA of one platelet} \\ &= \frac{V_{LRD}}{V_{platelet}} \times \pi r_l^2 \\ &= \frac{V_{LRD}}{\pi r_l^2 h} \times \pi r_l^2 \\ &= \frac{V_{LRD}}{h} \end{aligned}$$

Assuming the Laponite RD clay forms a monolayer around the polymerising MMA beads, then T_{PMMA} beads will be equal the to T_{LRD} clay. Rearranging will allow the radius of the polymer beads (r) to be obtained;

$$\begin{aligned} T_{LRD} &= T_{PMMA} \\ \frac{V_{LRD}}{h} &= \frac{3V_{PMMA}}{r} \\ r &= \frac{3V_{PMMA} \times h}{V_{LRD}} \end{aligned}$$

Appendix C Hollow PMMA/Laponite RD Beads

An unusual finding was made during the scanning electron microscopy of the PMMA/Laponite RD suspension beads. The beads were imaged using a gaseous secondary detector in order to obtain additional measurements of the particle size. During the mounting of the 1%LRD samples upon the ESEM stubs, the beads were pressed down onto the adhesive tape to ensure good contact. However this caused structural damage to the 1%LRD beads as shown in Figure C.1. The beads have been broken and appear to be hollow shells. As discussed in Chapter 1 suspension polymerisation proceeds via a bulk reaction so each bead should consist of solid PMMA. The structure of PMMA beads was also studied, and were again pressed onto the ESEM stubs in order to attempt to fracture some of the beads. Most of the beads remained intact suggesting a solid structure; however some beads were seen to have fractured as shown in Figure C.2. Unlike 1%LRD, the PMMA beads show that small "air pockets" are present near to the surface of the bead. The PMMA wall around the "air pocket" appeared to be creased or dimpled and is relatively thin in appearance. This was expected as the contraction of the gas during the cooling of the beads will cause the thin outer PMMA wall to collapse as the pressure inside the "air pocket" decreases.

The formation of hollow beads directly from suspension polymerisation has been noted before in reference[1]. Guerreo[1] carried out SEM on suspension polymerised polyacrylamide beads and revealed various internal structures of the beads including porous structures and hollow beads. An explanation for these structures was not presented however it was suggested that they were caused by the evolution of degradation gases such as NH_3.

The hollow beads formed by 1%LRD may be an extension of the "air pockets" seen in the PMMA beads. This suggests that the clay is not directly responsible for the formation of the hollow beads but is enhancing an effect already seen to occur in PMMA. The polymerisation occurs at the temperature of reflux of the MMA and water mixture at 83^{o}C, which is lower than the boiling point of both MMA (100^{o}C) and water (100^{o}C), as MMA and water form a positive azeotrope reducing the boiling point. A temperature of 83^{o}C is too low for the thermal degradation of PMMA but the hollow bead structure could be the result of the evolution of N_2 from the thermal degradation of the initiator azobis(2-methylpropionitrile) (AIBN). AIBN thermally degrades to give two cyanopropyl radicals and N_2. The cyanopropyl radical will initiate the polymerisation and the N_2 will be evolved as a gas from the MMA phase (AIBN is soluble in MMA). If the N_2 is unable to escape from the MMA phase, pockets of N_2 will be polymerised into the PMMA beads. If sufficient build up of N_2 is present then a hollow structure may be formed.

The rate of production of N_2 can be related to the kinetics of free radical polymerisation. From the temperature profiles of PMMA and 1%LRD shown in Figure5.2 it was observed that the reaction for 1%LRD appears quicker than that of PMMA. The faster kinetics of 1%LRD reaction would suggest the faster formation of N_2 and a shorter time to the point at which the beads become glassy. This would give the N_2 gas a shorter time period to escape from the polymerising beads suggesting more N_2 would be trapped within their cores. However as stated in Chapter5.2 the reason for the difference in kinetics is unknown.

The Laponite RD clay could be enhancing the effect of the entrapment of the N_2 gas by its coating of the surface of the suspension droplets. Chapter 5.3 discussed the possibility of Laponite RD clay acting as a suspending agent and the covering of the polymer beads with Laponite RD will introduce a physical barrier which the N_2 would need to diffuse through in order to escape. Another possibility for the formation of the hollow structures is the inclusion of water inside the MMA beads.

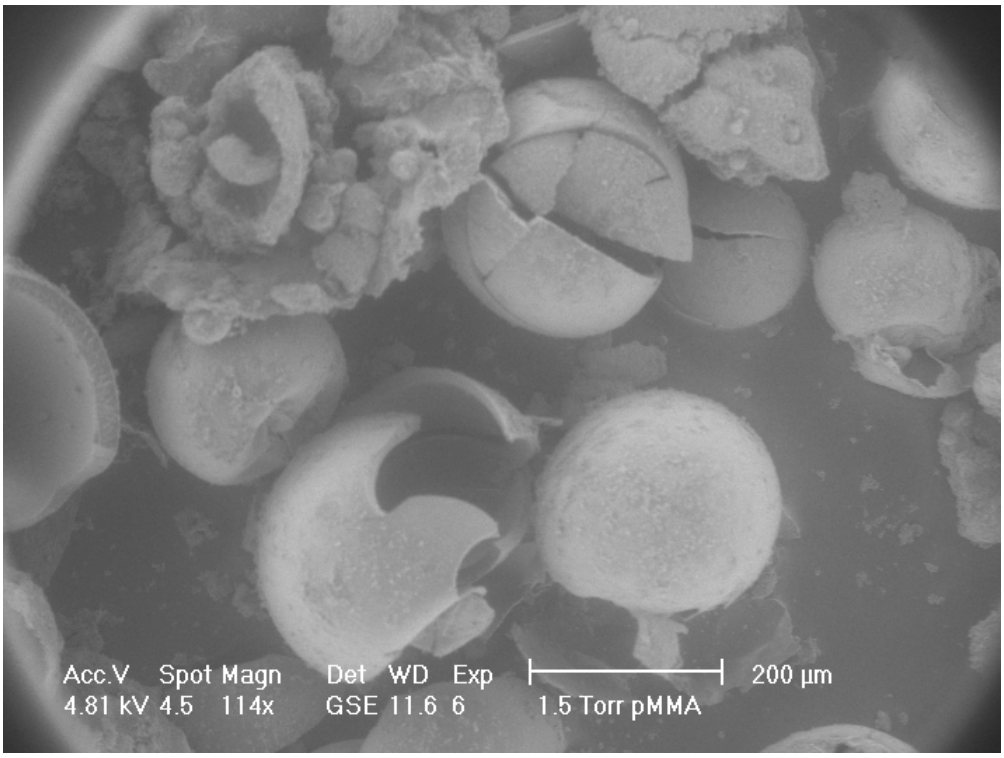

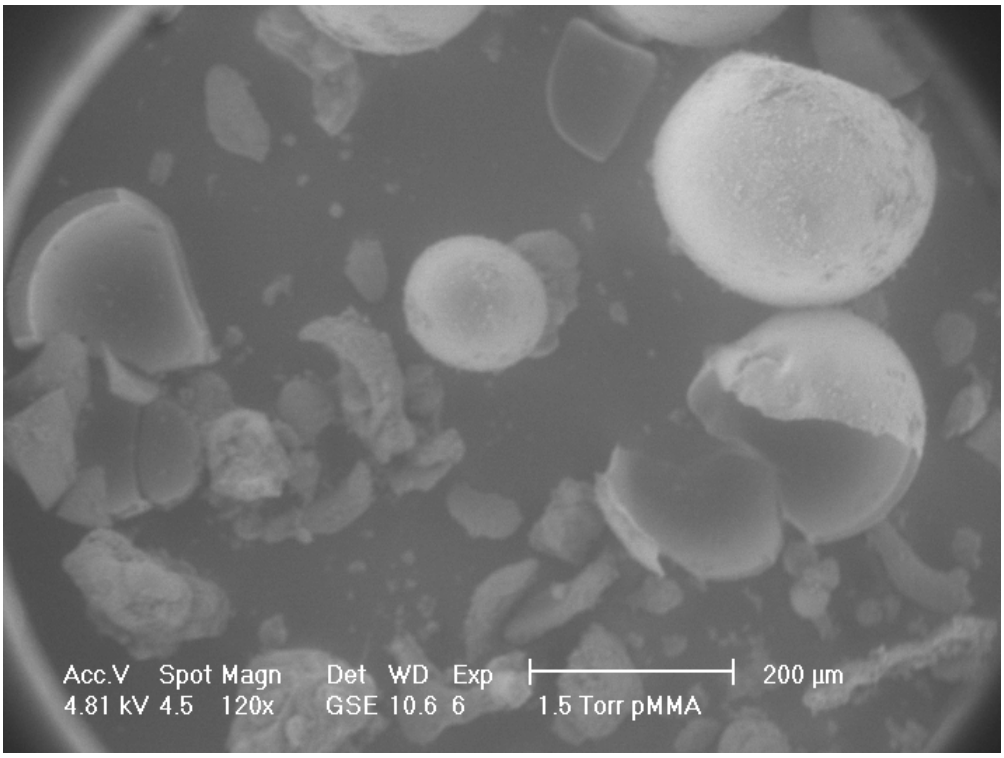

Figure C.1: ESEM images of 1%LRD beads.

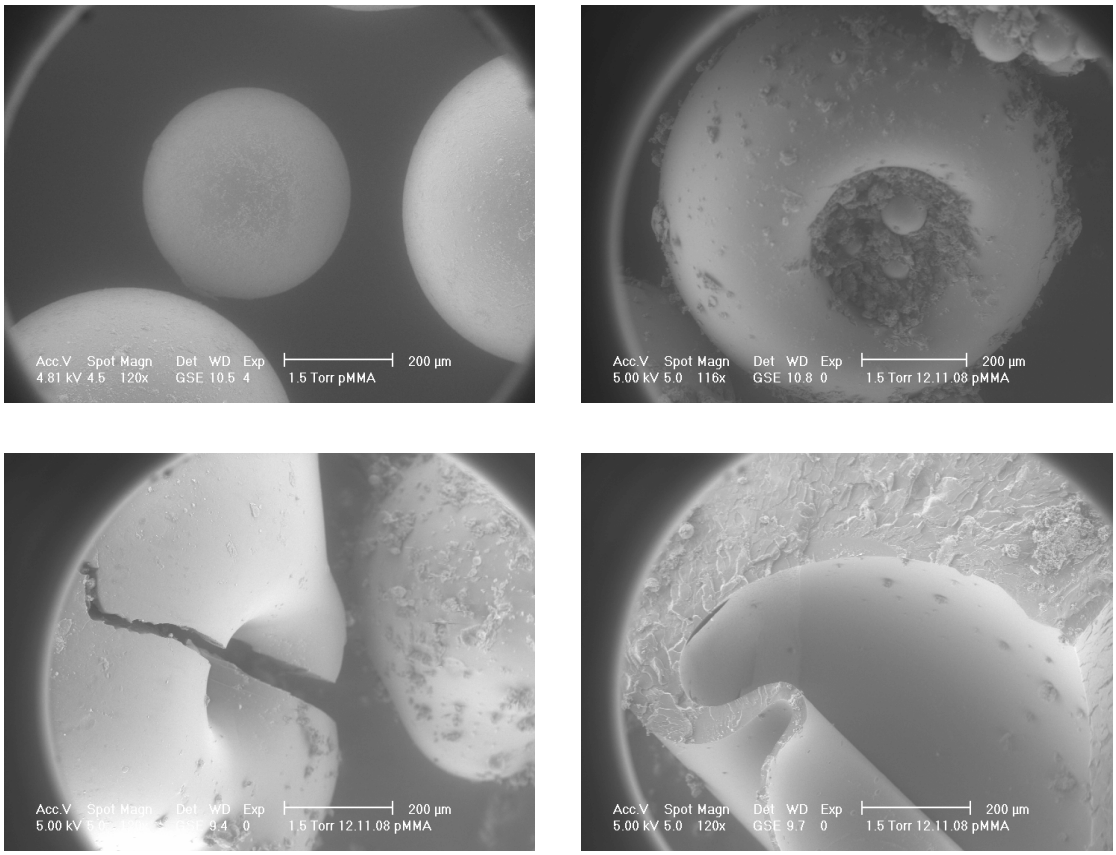

Figure C.2: ESEM images of PMMA beads.

---

1. Guerrero, S. J. *Journal of Materials Science Letters* **1985,** 4, (12), 1481-1484.

Appendix D Glossary of Clay Terms

Aggregation: Stack of clay platelets which are held together by electrostatic forces.

Basal Spacing: The perpendicular distance from the top of one clay platelet to the top of the next parallel clay platelet. The value of Basal spacing differs from the gallery spacing by the subtraction of the platelet height.

Cation Exchange: Involves replacing or exchanging the existing cations found on the clay surface with an alternative cation. This is usually used to improve the compatibility between the clay and polymer.

Cation Exchange Capacity (CEC): Measures the quantity of ions attached to the clay surface and is usually measured in milliequivalents per 100g of clay.

d001 Spacing: The perpendicular distance between diffracting planes. d represents the miller indices used in XRD. d001 spacing is also known as basal spacing.

Exfoliated: Where the clay platelets become individually dispersed within the polymer matrix. The layered structure of the clay platelets has been lost.

Flocculation: The process where platelets come out of the suspension and form larger clusters by aggregating together.

Gallery Spacing: The perpendicular distance or separation between two parallel clay platelets. Also known as interlayer spacing.

Intercalated: An intercalated state has been reached where there is some inclusion of polymer chains within the gallery spacing causing it to swell.

Interlayer Spacing: See gallery spacing.

Percolation: Long range connectivity. In the case of polymer clay nanocomposites a long range network structure throughout the material.

Appendix E Notation

a	tube diameter
A	area of the peak
AIBN	2,2-azobis(2-methylpropionitrile)
a_T	modulus shift factor (horizontal)
b	effective bond length (Kuhn length)
B	full width at half maximum intensity
b_T	modulus shift factor (vertical)
C15a	Cloisite 15a
CEC	cation exchange capacity
CTA	chain transfer agent
D	diffusion coefficient
DEMA	dimethyl ethanol amine
DMSO	Dimethyl sulfoxide
DPMK	diphenylmethyl potassium
D_R	diffusion coefficient of a Rouse chain
DSC	differential scanning calorimetry
dW(M)	weight fraction of chains with molecular weight below M
E_c	physical properties of composite
E_f	physical properties of filler
E_m	physical properties of matrix
EO	ethylene oxide
f	volume of filler
FTDD(t,M)	des Cloizeaux time dependent diffusion function
FWHM	full width at half maximum intensity
G	shear modulus
G'	stroage modulus
G''	loss modulus
G(t)	relaxation modulus
G_e	plateau modulus
G_N^o	plateau modulus
GPC	gel permeation chromotography
H_c	heat of combustion
HRR	heat release rate
IS	injection speed
k	boltzmann constant

L	contour length of the primitive path
l	distance
LRD	Laponite RD
M	molecular weight
m	number of clay platelets in an aggregate
MALDI ToF	matrix assisted laser desorption time of flight mass spectroscopy
M_e	entanglement molar mass
MeOH	methanol
MMA	methyl methacrylate
MMT	montmorillonite
M_n	number average molecular weight
M_w	weight average molecular weight
N	number of beads in a polymer chain
n	number of monomers in a bead
N_e	number of monomers in an entangled chain segment
NMR	nuclear magnetic resonance
OMMT	organically modified montmorillonite
PCN	polymer clay nanocomposites
PDI	polydispersity
PEO	poly ethylene oxide
PMA	poly(2-methly-2-propenoic acid) sodium salt
PMMA	poly(methyl methacrylate)
ppm	parts per million
PS	polystyrene
Q	rate of heat release
R	radius of a sphere
R	gas constant
R_g	radius of gyration
RoM	rule of mixtures
rpm	reverlutions per minute
SAXS	small angle x-ray scattering
SEC	size exclution chromotography
ST DEV	standard deviation
Stand dev	standard deviation
T	temperature
t	aggregate thickness
t	time
T_{crys}	crystalisation temperature
TEM	transmission electron microscopy
T_g	glass transition temperature
TGA	thermogravimetric analysis
$T_{g\alpha}$	Tg of a polymer at an infinate molecular weight
THF	tetrahydrofuran
T_m	melting temperature

T_{max}	temperature at which the maximum HRR occurs
TTS	time teperature superposition
w	peak width
wt%	weight percent
x_c	x coordinate of the peak centre
X_n	number average degree of polymerisation
XRD	x-ray diffraction
y_c	y coordinate of the peak centre
y_o	offset in the y direction
γ	shear strain
$\dot{\gamma}$	shear rate
ζ	friction coefficient
η	viscosity
θ	diffraction angle
θ	scattering angle
λ	wavelength
ρ	density
σ	shear stress
τ_e	entangled Rouse relaxation time
τ_i	intermediate relaxation time
τ_o	relaxation time of monomer
τ_R	Rouse relaxation time
τ_{rep}	reptation relaxation time
χ	Flory Huggins interaction parameter
ω	angular frequency

Appendix F List of Figures